

Some pages of this thesis may have been removed for copyright restrictions.

If you have discovered material in AURA which is unlawful e.g. breaches copyright, (either yours or that of a third party) or any other law, including but not limited to those relating to patent, trademark, confidentiality, data protection, obscenity, defamation, libel, then please read our [Takedown Policy](#) and [contact the service](#) immediately

COALESCENCE OF SECONDARY DISPERSIONS IN
PACKED BEDS

by

SILVYA BAEZ POLEO

A Thesis submitted to
The University of Aston in Birmingham
for the Degree of Doctor of Philosophy.

September

1983

SUMMARY

"COALESCENCE OF SECONDARY DISPERSIONS IN PACKED BEDS"

SILVYA BAEZ POLEO

Ph.D.

SEPTEMBER 1983

A study has been made of the coalescence of secondary dispersions in beds of monosized glass ballotini. The variables investigated were superficial velocity, bed depth, ballotini size and dispersed phase concentration.

Equipment was designed to generate a toluene in water dispersion with phase ratios from 0.1 - 1.0 v/v % and whose mean drop size was determined using a Coulter Counter. The coalesced drops were sized by photography and the mean diameter of the effluent drops was determined using a Malvern Particle Size Analyser.

Previous models describing single phase flow in porous media are reviewed and it was found that the experimental data obtained in this study is best represented by the Carman-Kozeny equations.

Relative permeability correlations were used to predict the saturation profiles across the bed from measured two phase pressure drop data.

Theoretical comparison of drop capture mechanisms indicated that direct and indirect interception are predominant. The total capture efficiency for the bed can also be evaluated using Spielman and Fitzpatrick's correlation. The resulting equation is used to predict the initial, local drop capture rate in a coalescer.

A mathematical description of the saturation profiles is formulated and verified by the saturation profiles obtained by relative permeability. Based on the Carman-Kozeny equation, an expression is derived analytically to predict the two phase pressure drop using the parameters which characterise the saturation profiles. By specifying the local saturation at the inlet face for a given velocity and phase ratio, good agreement between experimental pressure drop data and the model predictions was obtained. An attempt to predict the exit drop size has been made using an analogy for flow through non cylindrical channels.

Key Words: Coalescence
 Porous Media
 Pressure Drop
 Secondary Dispersions
 Relative Permeability

ACKNOWLEDGEMENTS

The author would like to express her gratitude to:

Professor G. V. Jeffreys, my Supervisor, for his invaluable help and guidance throughout the project.

The members of the Technical and Clerical Staff of the Department of Chemical Engineering.

To my parents

CONTENTS

	<u>Page</u>
SUMMARY	
CHAPTER 1 <u>Introduction</u>	1
CHAPTER 2 <u>The Nature, Formation and Occurrence of Secondary Dispersions</u>	
2.1 Introduction	4
2.2 Theory of Dispersion Formation	4
2.2.1 Subdivision of the Bulk Phase	10
2.2.2 Nucleation and Growth	12
2.2.3 Spontaneous Emulsification	12
2.3 Preparation of Secondary Dispersions	13
2.3.1 Emulsification by Dispersion Method	13
2.3.2 Emulsification by Condensation	20
2.3.3 Critical Emulsification	22
2.4 Industrial Occurrence of Secondary Dispersions	23
2.4.1 Effluent from the Oil Industry	23
2.4.2 Other Sources	24
CHAPTER 3 <u>Methods of Separation of Secondary Dispersions</u>	
3.1 Stability of Secondary Dispersions	26
3.2 Treatment of Secondary Dispersions	28
3.2.1 Addition of Chemicals	29
3.2.2 Centrifugal Separation	29
3.2.3 Coalescence by Electrical Methods	30
3.2.4 Air Flotation	30

CONTENTS

		<u>Page</u>
3.2.5	Heat Treatment	31
3.2.6	Coalescence Induced by a Third Body	31
3.2.7	Disadvantages of Separation Methods	33
CHAPTER 4	<u>Coalescence in Packed Beds</u>	
4.1	Effect of Operating Conditions	35
4.2	System Characteristics	39
CHAPTER 5	<u>Mechanisms of Drop Dispersion Coalescence in Packed Beds</u>	
5.1	Introduction	44
5.2	Drop Capture	44
5.2.1.1	Indirect Interception	48
5.2.1.2	Hydrodynamic Retardation	54
5.2.2	Direct Interception	55
5.2.3	Inertial Impaction	56
5.2.4	Sedimentation	58
5.2.5	London - Van de Waal's Forces	59
5.2.6	Electrical Double Layer Forces	61
5.2.7	Diffusion	63
5.3	Coalescence Processes	67
5.3.1	Coalescence Sites	67
5.3.2	Drop Passage through Interstices	69
5.4	Dispersed Phase Flow Regime	72
5.4.1	Drop Redispersion	73
5.4.2	The Travelling Drop Hypothesis	74
5.4.3	Critical Drop Diameter	76
5.4.4	Dispersed Phase Continuum Model	77

CONTENTS

		<u>Page</u>
5.5	Saturation Profiles	78
5.6	Exit Drop Release	82
CHAPTER 6	<u>Experimental Work</u>	
6.1	Equipment Design	86
6.2	Coalescer Design	91
6.3	Packing Selection and Preparation	92
6.3.1	Surface Properties of Glass Ballotini	98
6.4	Liquid System Description	99
6.5	Pressure Drop Measurement	100
6.6	Operating Procedure	102
6.7	Bed Voidage Determination	105
6.8	Experimental Design	106
6.8.1	Operating Conditions	106
CHAPTER 7	<u>Determination of Drop Size Distributions</u>	
7.1	Introduction	110
7.2	Microscopy	110
7.3	Light Reflectance	111
7.4	Light Scattering	111
7.5	Ultrasonics	113
7.6	The Coulter-Counter	113
7.7	Laser Techniques	118
CHAPTER 8	<u>Experimental Results</u>	
8.1	Inlet Drop Size	132
8.2	Coalesced Drop Size	132
8.2.1	Effect of Bed Depth on Exit Drop Size	135

CONTENTS

	<u>Page</u>	
8.2.2	Effect of Ballotini Diameter	135
8.2.3	Effect of Phase Ratio on Coalesced Drop Size.	138
8.3	Drop Release	141
8.4	Effluent Secondary Drops	146
8.5	Separation Efficiency	151
CHAPTER 9	<u>Analysis of Pressure Drop Data</u>	
9.1	Fluid Flow Equations	157
9.1.1	Phenomenological Models	159
9.1.2	Models Based on Conduit Flow	162
9.1.2.1	Geometric Permeability Models	163
9.1.2.2	Statistical Permeability Models	165
9.1.3	Models Based on the Navier-Stokes Equation	166
9.1.4	Flow Models Based on Flow Around Submerged Objects.	168
9.2	Single Phase Flow Pressure Drop	168
9.3	Factors Affecting the Value of the Kozeny Constant.	170
9.3.1	Shape Factor and Tortuosity	170
9.3.2	Wall Effect	172
9.3.3	Effect of Voidage	174
9.3.4	Other Factors	178
9.4	Analysis of Pressure Drop Data	179
9.5	Transient Pressure Drop	183
9.6	Two Phase Pressure Drop	189
9.7	Saturation Profiles	193

CONTENTS

		<u>Page</u>
9.7.1	Relative Permeability Method of Oil Saturation	197
9.7.2	Relative Permeability Calculation from Pressure Drop Data	200
CHAPTER 10	<u>Model of Dispersion Coalescence</u>	
10.1	Prediction of Filter Coefficient	221
10.1.1	Vinson and Churchill Equation	221
10.1.2	Spielman and Goren Equation	224
10.1.3	Sherony and Kintner Equation	226
10.1.4	Rosenfeld and Wasan Equation	227
10.2	Theoretical Comparison of Capture Mechanisms	228
10.2.1	Screening Mechanisms	234
10.3	Rate of Drop Capture	242
10.4	Dispersed Phase Saturation Prediction	246
10.4.1	Preliminary Considerations	246
10.4.2	Mathematical Description of Saturation Profiles	253
10.5	Two Phase Pressure Drop Prediction	263
10.5.1	Previous Models	263
10.5.2	Derivations of Proposed Equations	264
10.6	Testing The Model	268
10.6.1	Evaluation of Parameters from Saturation Data	268
10.6.2	Comparison with Experimental Data	268
10.7	Exit Drop Size Predictions	271
10.7.1	Preliminary Considerations	271

CONTENTS

	<u>Page</u>
CONCLUSIONS	275
RECOMMENDATIONS FOR FURTHER WORK	279
APPENDICES	281
NOMENCLATURE	320
LIST OF REFERENCES	325

APPENDICES

Page No

APPENDIX A	Physical Properties of Liquid System	281
B	Bed Voidage Determination	285
C	Determination of the Hamaker Constant.	286
D	Evaluation of Specific Surface for Coalescer Containing Drops of Dispersed Phase.	287
E	Integration of Pressure Drop Equation	288
F	Calculation of Experimental Error in Pressure Drop Measurement.	290
G	Computer Flowsheet for Calculation of Rate of Drop Capture.	295
H	Regression Analysis Used in the Evaluation of the Decay Factor k	300
I	Computer Program for Evaluation of Capture Mechanism Contributions	301
J	Tabulated Experimental Results	305
K	Prediction of Exit Drop Size	318

LIST OF FIGURES

<u>Figure</u>		<u>Page</u>
Figure 2.1	Schematic Diagram of the Processes Involved in the Production or Destruction of Disperse Systems.	6
Figure 2.2	Mutual Potential Energy of two Colloidal Particles as a Function of the Distance of Separation between their Surfaces.	8
Figure 2.3	Mutual Potential Energy Surface of Two Colloid Particles of a Lyophobic Colloid in a Liquid Medium.	11
Figure 2.4	Mechanical Methods of Emulsification	15
Figure 2.5	Emulsification Using Electro-Magnetic Transducers.	18
Figure 2.6	Emulsification by Condensation.	21
Figure 5.1	Depiction of a Drop Capture Mechanism	47
Figure 5.2	Coalescence Mechanisms in a Packed Bed	68
Figure 5.3	Proposed Droplet Hydrodynamics in a Non-Wetted Packing of Equal Sized Spheres.	71
Figure 5.4	Internal Drop Release Mechanisms	75
Figure 5.5	Pendular and Funicular Saturation Regimes for an Idealised Porous Medium of Packed Spheres.	75
Figure 5.6	Exit Drop Release Mechanisms	83
Figure 6.1	Flow Diagram of Equipment.	87
Figure 6.2	General Arrangement of Equipment	88
Figure 6.3	Coalescer Column for Pressure Drop Measurement	93
Figure 6.4	Stainless Steel Supporting Mesh with Polypropylene Moulding.	94
Figure 6.5	Original Manometry System.	101
Figure 6.6	Modified Manometric System with Pressure Taps.	101

LIST OF FIGURES

		<u>Page</u>
Figure 6.7	Arrangement for Measurement of Pressure Drop with Taps and Pressure Transducers.	103
Figure 7.1	Typical Size Distribution of Inlet Dispersion.	115
Figure 7.2	Microscope Photographs of Calibrating Red Mulbery Pollen in its Dry and Wet State.	117
Figure 7.3	Malvern 2200 Particle Sizer Basic Opto-Electronic System.	121
Figure 7.4	Malvern 2200 Particle Sizer Background Reading Printout.	123
Figure 7.5	Malvern 2200 Particle Sizer Sample Analysis Printout using Two Parameter Models.	126
Figure 7.6	Malvern 2200 Particle Sizer Sample Analysis Printout Using Independent Model.	127
Figure 7.7	Typical Photograph of the Coalesced Dispersion.	130
Figure 7.8	Typical Size Distribution of Coalesced Drops Leaving Exit Face.	131
Figure 8.1	Variation of Inlet Drop Size with Velocity for Toluene/Water System (0.1% v/v Dispersed Phase Concentration)	133
Figure 8.2	Change in Mean Drop Size with Concentration of Dispersed Phase at 3.0×10^{-2} m/s Constant Superficial Velocity.	134
Figure 8.3	Variation of Exit Drop Size with Velocity for Ballotini 486 μm and Bed Depth 20×10^{-2} m	136
Figure 8.4	Variation of Coalesced Drop Size with Bed Depth for Ballotini Size 486 μm .	137

LIST OF FIGURES

	<u>Page</u>
Figure 8.5	Variation of Coalesced Drop Size with Ballotini Size for Bed Depth 5×10^{-2} m and 20×10^{-2} m at Constant Velocity 10×10^{-3} m/s. 139
Figure 8.6	Variation of Exit Drop Size with Phase Ratio for Bed Depth 20×10^{-2} m, 486 μ m, Ballotini Size, Constant Velocity. 140
Figure 8.7	Drop Release of Coalesced Drops at Exit Face. 142
Figure 8.8	"Froth-Flotation" Type Mechanisms Observed at Low Superficial Velocities. 143
Figure 8.9	Coalesced Drops Residing at Exit Face at Low Superficial Velocities. 145
Figure 8.10, 8.11, 8.12	Cine -film Photographs of Coalesced Dispersed Phase Moving Through the Coalescer. 147
Figure 8.13	Variation of Effluent Drop Size with Bed Depth for Ballotini Size 486 μ m 152
Figure 8.14	Variation of Effluent Drop Size with Bed Depth for Ballotini Size 57.5 μ m 152
Figure 8.15	Variation of Effluent Drop Size with Phase Ratio for Ballotini 486 μ m and 5×10^{-2} m Bed Depth. 153
Figure 8.16	Variation of Effluent Drop Size with Phase Ratio for Ballotini 486 μ m and 20×10^{-2} m Bed Depth. 153
Figure 8.17	Variation of Separation Efficiency with Velocity. 154
Figure 8.18	Variation in Separation Efficiency with Phase Ratio for Ballotini Size 486 μ m, 20×10^{-2} Bed Depth, and 0.3×10^{-2} m/s Superficial Velocity. 156
Figure 9.1	Systematic Arrangement of Spheres and Their Porosities. 173
Figure 9.2	Correlations of Single Phase Pressure Drops for Different Ballotini Sizes. 180

LIST OF FIGURES

		<u>Page</u>
Figure 9.3	Two Phase Pressure Drop for 20×10^{-2} m Bed Depth, 486 μ m Ballotini Size, and 0.1 % v/v Dispersed Phase Concentration Transient Behaviour.	184
Figure 9.4	Two Phase Pressure Drop for 20×10^{-2} m Bed Depth, 486 μ m Ballotini Size and 0.1% v/v Dispersed Phase Concentration Transient Behaviour.	187
Figure 9.5	Pressure Drop Vs Bed Depth, for 20×10^{-2} m Bed Depth, 486 μ m Ballotini Size and 0.3×10^{-2} m Velocity, Transient Behaviour.	188
Figure 9.6	Effect of Concentration on Time to Steady State Vs. Superficial Velocity	190
Figure 9.7	Effect of Velocity on Pressure Drop Ratio Vs Bed Depth for 486 μ m Ballotini Size and 20×10^{-2} m Bed Depth.	191
Figure 9.8	Variation of Pressure Drop Ratio with Concentrations of Dispersed Phase. Ballotini 486 μ m, Bed Depth 20×10^{-2} m 0.3×10^{-2} ms ⁻¹ .	192
Figure 9.9	Effect of Ballotini Size on Pressure Drop Ratio Vs. Bed Depth.	194
Figure 9.10	Pressure Drop Ratio Vs Time for Different Bed Depths.	195
Figure 9.11	Pressure Drop Ratio Vs Bed Depth for Increasing Operating Time.	196
Figure 9.12	Relative Permeabilities Vs Saturation Curves.	199
Figure 9.13	Saturation Vs Bed Depth. Ballotini 486 μ m, 20×10^{-2} m Bed Depth, 0.3×10^{-2} m/s, 0.15% v/v Dispersed Phase Concentration.	2C3
Figure 9.14	Saturation Vs Bed Depth. Ballotini 486 μ m, 20×10^{-2} m Bed Depth, 0.3×10^{-2} m/s Velocity, 0.2% v/v Dispersed Phase Concentration.	204
Figure 9.15	Saturation Vs Bed Depth. Ballotini 486 μ m 20×10^{-2} m Bed Depth, 0.3×10^{-2} m/s Velocity and 0.3% v/v Dispersed Phase Concentration.	2C6

LIST OF FIGURES

		<u>Page</u>
Figure 9.16	Saturation Vs Bed Depth, Ballotini 486 μ m. 20 x 10 ⁻² m Bed Depth, 0.3 x 10 ⁻² m/s Velocity and 0.4 % v/v Dispersed Phase Concentration.	207
Figure 9.17	Saturation Vs Bed Depth, Ballotini 486 μ m, 20 x 10 ⁻² m Bed Depth, 0.3 x 10 ⁻² m/s Velocity and 1.% v/v Dispersed Phase Concentration.	209
Figure 9.18	Effect of Concentration of Dispersed Phase on Saturation Vs Bed Depth, Ballotini 486 μ m 20 x 10 ⁻² m Bed Depth, 0.3 x 10 ⁻² m/s Velocity.	210
Figure 9.19	Effect of Velocity on Saturation Vs Bed Depth 486 μ m Ballotini and 20 x 10 ⁻² m Bed Depth.	211
Figure 9.20	Effect of Velocity on Saturation Vs Bed Depth	212
Figure 9.21	Effect of Ballotini Size on Saturation Vs Bed Depth. 20 x 10 ⁻² m Bed Depth, 0.1 x 10 ⁻² m/s Velocity	214
Figure 9.22	Effect of Ballotini Size on Saturation Vs Bed Depth, 20 x 10 ⁻² m Bed Depth, 0.3 x 10 ⁻² m/s Velocity.	215
Figure 9.23	Saturation Vs Bed Depth for Increasing Operating Time.	216
Figure 9.24	Saturation Vs Time for Different Bed Depth	217
Figure 9.25	Comparison of Saturation, Vs Bed Depth, Profiles obtained using $\frac{\Delta P_2}{\Delta P_1} \frac{\mu c_1}{\mu c_2}$ and $\frac{\Delta P_2}{\Delta P_1} \frac{\mu c}{\mu d}$	219
Figure 9.26	Saturation Vs. k_d/k_c	220
Figure 10.1	Variation of Total Capture Efficiency with Velocity for Different Drop Sizes.	225
Figure 10.2	Variation of Capture Efficiencies with Velocities at 0.1 μ m	233
Figure 10.3	Variation of Capture Efficiencies with Drop Size at 0.1 x 10 ⁻² m/s.	235

LIST OF FIGURES

		<u>Page</u>
Figure 10.4	Dimensionless Capture Efficiencies Vs Adhesion Number at Different $k'T/Q$ according to Spielman and Fitzpatrick.	241
Figure 10.5	Effect of Superficial Velocity on the Variation of Volume Fraction of Dispersed Phase Uncaptured with Bed Depth.	245
Figure 10.6	Oil Saturation Regimes.	248
Figure 10.7	Saturation Profiles of Spielman and Su	248
Figure 10.8	Variation of Hold-Up with Bed Depth.	250
Figure 10.9	Variation of Hold-Up with Superficial Velocity.	252
Figure 10.10	Idealised Saturation Profiles	254
Figure 10.11	Experimental and Predicted Dispersed Phase Saturation Vs. Bed Depth for $486\mu\text{m}_2$ Ballotini, 20×10^{-2} m Bed Depth, 0.3×10^{-2} m/s Velocity and 0.2% v/v Dispersed Phase Concentration.	256
Figure 10.12	Experimental and Predicted Dispersed Phase Saturation Vs Bed Depth for $486\mu\text{m}$ Ballotini, 20×10^{-2} m Bed Depth, 0.3×10^{-2} m/s Velocity and 0.4% v/v Dispersed Phase Concentration.	257
Figure 10.13	Experimental and Predicted Dispersed Phase Saturation Vs Bed Depth for $486\mu\text{m}$ Ballotini, 20×10^{-2} m Bed Depth, 4.0×10^{-2} m/s Velocity and 0.1% v/v Dispersed Phase Concentration.	258
Figure 10.14	Experimental and Predicted Dispersed Phase Saturation Vs Bed Depth for $486\mu\text{m}$ Ballotini, 20×10^{-2} m Bed Depth, 5.0×10^{-2} m/s Velocity and 0.1% v/v Dispersed Phase Concentration.	259
Figure 10.15	Average Decay Factor Vs Low Velocity Range. Ballotini $486\mu\text{m}$, 20×10^{-2} m Bed Depth and 0.1% v/v Dispersed Phase Concentration.	261

LIST OF FIGURES

		<u>Page</u>
Figure 10.16	Average Decay Factor Vs High Velocity Range. Ballotini 486 μm , 20×10^{-2} m Bed Depth, 0.1 % v/v Dispersed Phase	261
Figure 10.17	Average Decay Factor Vs Dispersed Phase Concentration for Different Superficial Velocities.	262
Figure 10.18	Predicted Vs. Experimental Pressure Drop Ratio.	269
Figure 10.19	Schematic Representation of the Capillary Area.	273
Figure 10.20	Predicted Vs. Experimental Exit Drop Size.	274

LIST OF TABLES

		<u>Page</u>
Table 5.1	Maximum Values of Dimensionless Groups Encountered in Coalescence Studies.	53
Table 5.2	Comparison of Equations Describing Drop Capture by Diffusion	65
Table 6.1	Properties of Granular Coalescer Media	97
Table 6.2	List of Variables in Secondary Dispersion Coalescence Studies	107
Table 6.3	Experimental Design	109
Table 9.1	Variable K_0 for Streamline Flow in Various Cross Sections	173
Table 9.2	Different Porosity Functions for Low Reynolds Number Flow	177
Table 9.3	Single Phase Pressure Drop Correlations	182
Table 9.4	Comparison of Theoretical Vs. Experimental Single Phase Permeability	202
Table 10.1	Basic Set of Parameters of Capture Mechanisms and Filter Coefficients.	222
Table 10.2	Dimensionless Groups and Equations Used in Capture Mechanisms Evaluation.	230
Table 10.3	Total Capture and Drop Diameters Encountered in Secondary Dispersion Coalescence.	231
Table 10.4	Significance of Different Capture Mechanisms at 5% Contribution Level for Range of Velocities and Drop Diameters Encountered in Secondary Dispersion Coalescence.	232
Table 10.5	Values for $f_1(N_{Ad})$ obtained from Spielman and ¹ Fitzpatrick.	240

CHAPTER ONE
INTRODUCTION

CHAPTER ONE

INTRODUCTION

In recent years, changes in the scale of operations required to find and transport oil have led to a pollution problem of major proportions : oil on the sea. These changes occurred slowly, and the change in magnitude of the possibilities for pollution went unrecognised until a series of dramatic accidents gave the problem widespread public notice.

The changes in the scale of oil operations stem from an ever increasing demand for energy. Oil pollution is the almost inevitable consequence of the dependence of a rapidly growing population on a largely oil-based technology. However, recent concern with oil pollution on the continental shelf and the treatment of acute oil spills near coastal areas has tended to obscure the fact that most of the oil lost to the environment is either spilled at sea in the normal operation of tankers, or is washed out to the sea from coastal areas. These aqueous wastes from petroleum refineries, steel mills, ships, tankers and many other industrial operations, carry finely dispersed oils which can adversely affect the quality of the water into which these wastes are discharged.

For such dispersions, an initial or primary massive separation of oil may be achieved effectively by gravity settling. However, gravity alone is often insufficient for eliminating the residual secondary dispersion which may consist of drops down to 1 μ m diameter constituting

a relatively small volume fraction. The settling velocity for such droplets is very small and thus prohibitively long settler residence times are required for adequate separation of the two phases by gravity.

Accordingly, various auxiliary procedures have been used in conjunction with gravity settling in order to promote more rapid coalescence and separation of the dispersed phase. Such procedures include the addition of chemical coagulants, use of alternating electrical fields and centrifugation. These processes are often expensive and inefficient. The coalescence of the finely dispersed oil drops into large and readily separable drops by passage through porous media is an attractive method since it is a very efficient, continuous and potentially inexpensive process. Drops are captured within the bed, where they are retained to induce coalescence, and eventually after coalescence are released as larger primary drops. Because the drops are not permanently retained, the bed usually operates under steady state conditions except in cases where particulate material present in the feed dispersion, causes rapid deterioration in the efficiency and operating life of the device.

In the literature dealing with coalescence by porous solid contact, little attention has been paid to coalescence by unconsolidated media, such as pebble beds in spite of their ability to be backwashed or fluidised periodically for rejuvenation.

Practical design of coalescers is usually based on trial and error procedures because the mechanisms of

coalescence in porous media are not fully understood. The objective of this investigation was to analyse the mechanisms of drop capture and two phase flow in a coalescer in order to develop a mathematical model for the efficiency, represented by the filter coefficient and the energy requirements measured by the pressure drop across the bed. Since both the filter efficiency and the pressure drop depend on the distribution of held-up oil, the theoretical estimation of the profile of held-up oil in the bed has also been the aim of this study. The effects of the operating conditions and bed properties, and the evaluation of the proposed theoretical models has been accomplished through a series of well-defined experiments using granular porous media of accurately known geometrical characteristics.

CHAPTER TWO

THE NATURE, FORMATION AND OCCURRENCE
OF SECONDARY DISPERSIONS

CHAPTER TWO
THE NATURE, FORMATION AND OCCURRENCE
OF SECONDARY DISPERSIONS

2.1 INTRODUCTION

The dispersion of one liquid phase into another relatively immiscible one by any turbulence-creating devices produces a temporary emulsion which can exhibit very different physical and chemical properties depending upon the drop size of the dispersed phase. Therefore the drop size have been extensively used to classify particular dispersions, generally divided into primary dispersions, secondary dispersions and colloids or emulsions. Although there is no clear division between primary and secondary dispersions in terms of drop size, most previous workers in the field have arbitrarily referred to dispersions of mean droplet diameter less than 100 μm as secondary dispersions. Such arbitrary definition of a secondary dispersion must be considered as an over-simplification especially when a theoretical description of the phenomenon of coalescence is attempted. The reason for this is that before coalescence, the dispersion may behave as a colloidal system and after coalescence of the drops by a selected coalescence medium, the dispersion will behave as a primary dispersion.

2.2 THEORY OF DISPERSION FORMATION

A fundamental understanding of the basic processes of dispersion and coalescence can be gained by a

consideration of colloidal systems. Colloids may be defined as systems in which a significant proportion of the dispersed phase molecules lie in or are associated with interfacial regions. Because of the excess energy associated with the formation of new surfaces, subdivision of a liquid within another liquid always increases the energy of the system and the dispersed phase is thermodynamically unstable (or metastable) with respect to the bulk phase. The energy is also modified by interaction between the surfaces and the phase in which it is immersed. Therefore the state of the dispersion colloids is characterised by the excess free energy. Depending on the magnitude of this energy, the dispersed colloid may become thermodynamically stable with respect to the bulk phase and form a one-phase colloidal system (lyophilic dispersion) or remain unstable (or metastable) with respect to the bulk phase and form a two-phase colloidal system (lyophobic dispersion). The processes occurring in the formation and destruction of colloids are illustrated in the schematic diagram in Fig. 2.1.

When two particles in a lyophobic dispersion collide they may adhere to one another; if the system is metastable only a fraction of the collisions will result in adhesion (flocculation) or completely fusing (coalescence). Thus flocculation-stable and coalescence-stable dispersions may be distinguished. Dispersed particles in a flocculated coalescence-stable state form large aggregates - so-called coagulation structures.

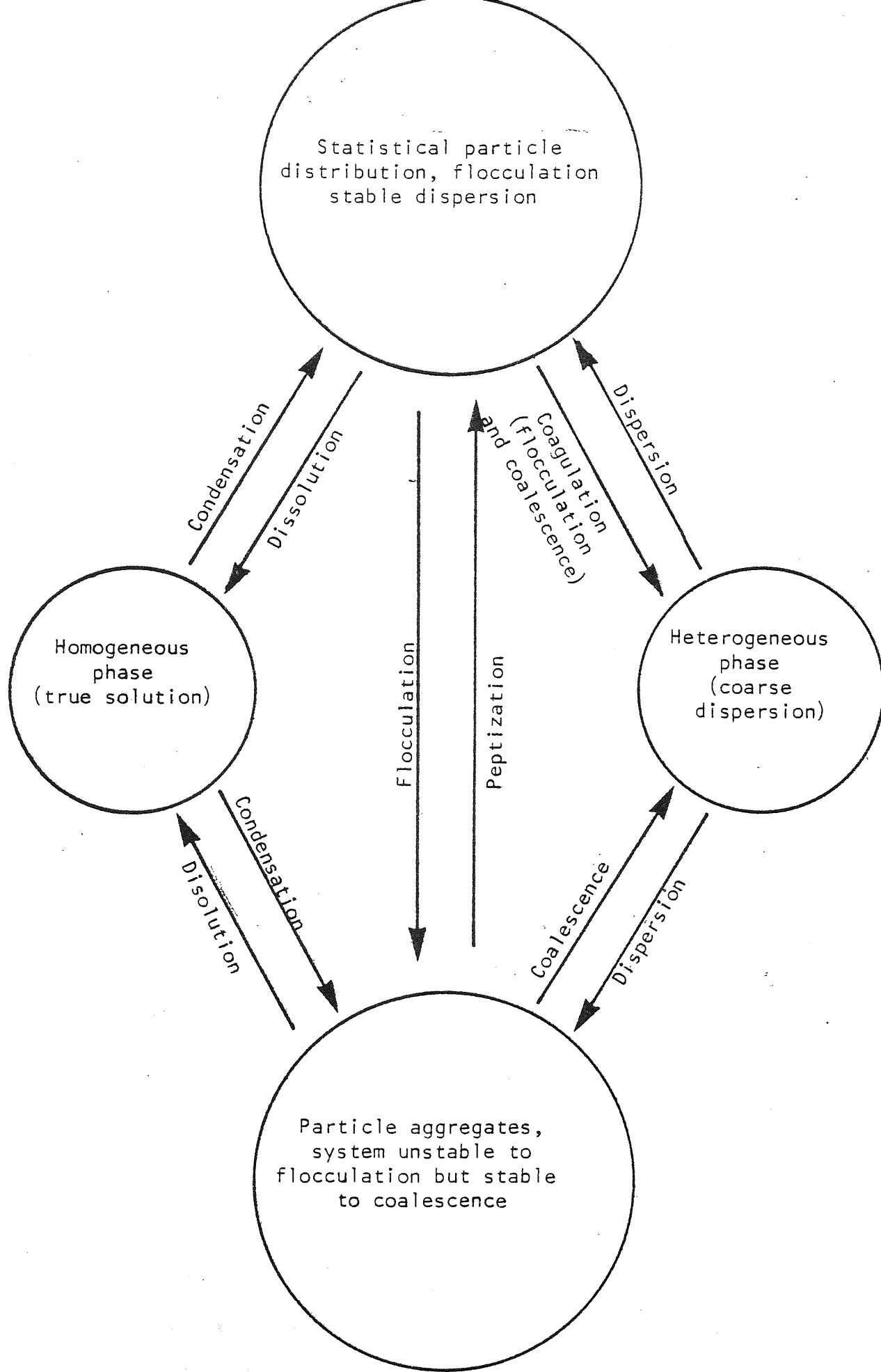


FIG. 2.1 Schematic Diagram of the Processes Involved in the Production or Destruction of Disperse Systems

The particles themselves, however, still behave as individuals separated by thin films of the dispersing medium or by adsorption layers of surface-active (or macromolecular) substances. Destruction of these interlayers leading to particle fusion is termed coalescence. The general term coagulation comprises both flocculation and coalescence.

The metastability of lyophobic colloids arises from the existence of an energy barrier which has to be surmounted before the two particles can adhere. This energy is clearly a function of the distance of separation between the particles decreasing as the distance increases. In keeping with the usual conventions, negative potential energies will be associated with attraction and positive potential energies with repulsion. This convention permits one to speak of the "height" of energy "barriers" and the "depth" of energy minima. Fig. 2.2 (1) is a qualitative sketch of potential energy curves which are resultant of a repulsive and an attractive component. Such curves may show a maximum and two minima although some of these features may be masked if one contribution greatly exceeds the other. The height of the maximum above Energy = 0 is called the height of the energy barrier (P). The deeper minimum is called the primary minimum (M_1); and the more shallow one, the secondary minimum (M_2). Although attraction predominates at large distances - that is, the secondary minimum is generally present - it may be quite shallow, especially in view of the effects of retardation and the medium

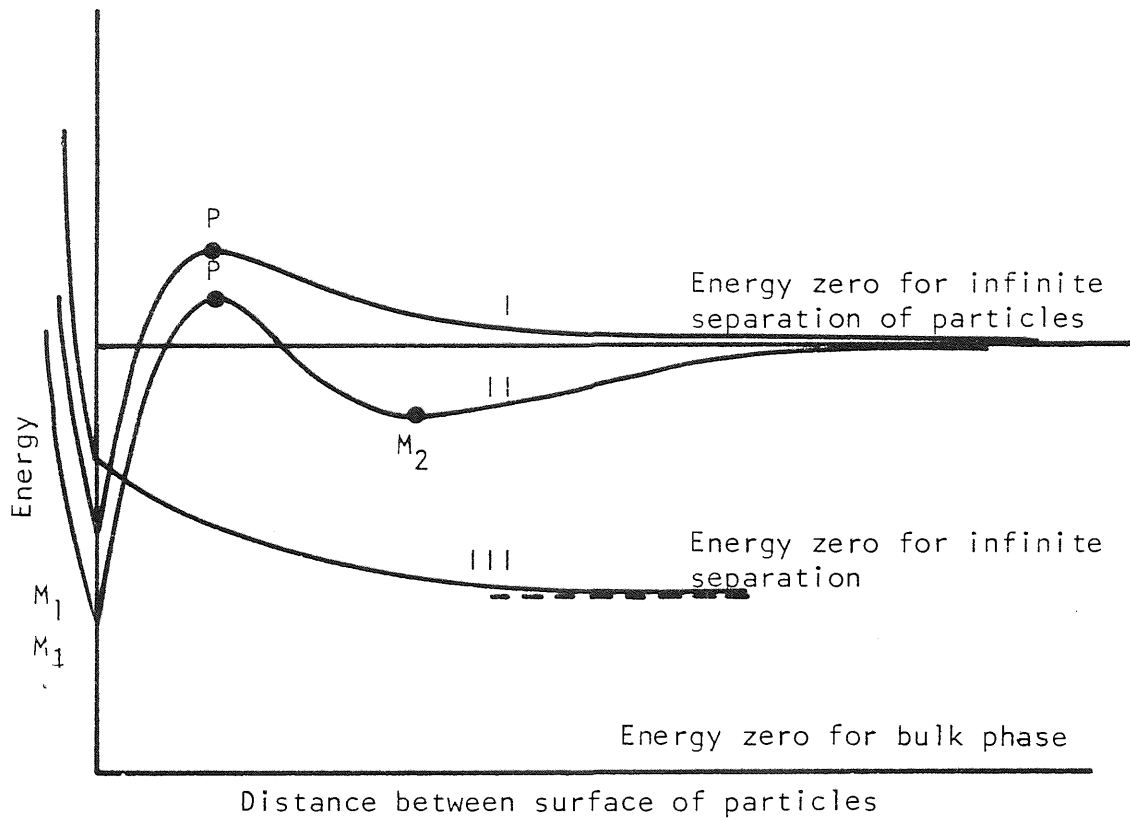


FIG. 2.2 Mutual potential energy of two colloidal particles as a function of the distance of separation between their surfaces:

- (i) Curve with primary maximum P and primary minimum M₁
- (ii) Curve with primary maximum P, primary minimum M₁ and secondary minimum M₂
- (iii) Curve for spontaneous (unactivated) dispersion

on attraction.

The implications of the potential energy curves shown in Fig. 2.2 can be qualitatively considered as follows:

In case I, if no barrier is present or the height of the barrier is negligible compared to the thermal kinetic energy associated with the collision, then the net force of attraction will pull the droplets together into the primary minimum, M_1 , after which the two behave as a single kinetic unit. Flocculation has occurred. If the height of the potential energy barrier is appreciable compared to the thermal kinetic energy, the particles are prevented from flocculating in the primary minimum. If the depth of the secondary minimum M_2 is small compared to thermal energy, then the particles will simply diffuse apart. This system is flocculation - stable.

There may be situations in which the two droplets may become associated as in case II; here, flocculation occurs in the secondary minimum, but the flocs in this case will clearly be much more easily disrupted than those which form by flocculation in the primary minimum and they may later either dissociate or pass over into the primary minimum. Two droplets associated in the primary minimum may remain in this state or may coalesce to form a larger droplet of a lower surface energy, as when an emulsion breaks.

If the interaction curve between two droplets has the form shown in case III, the dispersed state is stable, at constant particle size, so that dispersion of the

particles occurs spontaneously.

Curves of the form shown in Fig. 2.2 involve the separation between the drops or particles of the size being considered. Therefore to represent different monodisperse systems a three-dimensional surface such as that shown very schematically in Fig. 2.3 is used, although the shapes and characteristics of such surfaces depend on many other parameters besides size. Among the more important factors are the continuous phase properties, concentration of the dispersed phase, electrical state of the interface, structure and chemical state of the interface, structure and chemical state of the dispersed phase and the presence of adsorbed films at the interface. Therefore the surface illustrated in Fig. 2.3 is only one three-dimensional section of a multi-dimensional hyper-surface, but useful for a basic description of the phenomena of dispersion and coalescence. Secondary dispersions may be formed by subdivision of the bulk phase, by nucleation and growth or by spontaneous emulsification.

2.2.1 Sub-division of the Bulk Phase

A liquid phase may be broken down into droplets of colloidal size by mechanical means, i.e. emulsification. This process may be represented schematically in Fig. 2.3 by routes B - C if drops are already dispersed in the continuous phase, or route $BM_1P_1M_2C$ if the dispersed phase is introduced as a continuum into the continuous phase then if the activation energy for the passage of the system from M_1 over P_1 is low enough, thermal motions or mechanical disturbance (stirring) will take the system to the dispersed state C.

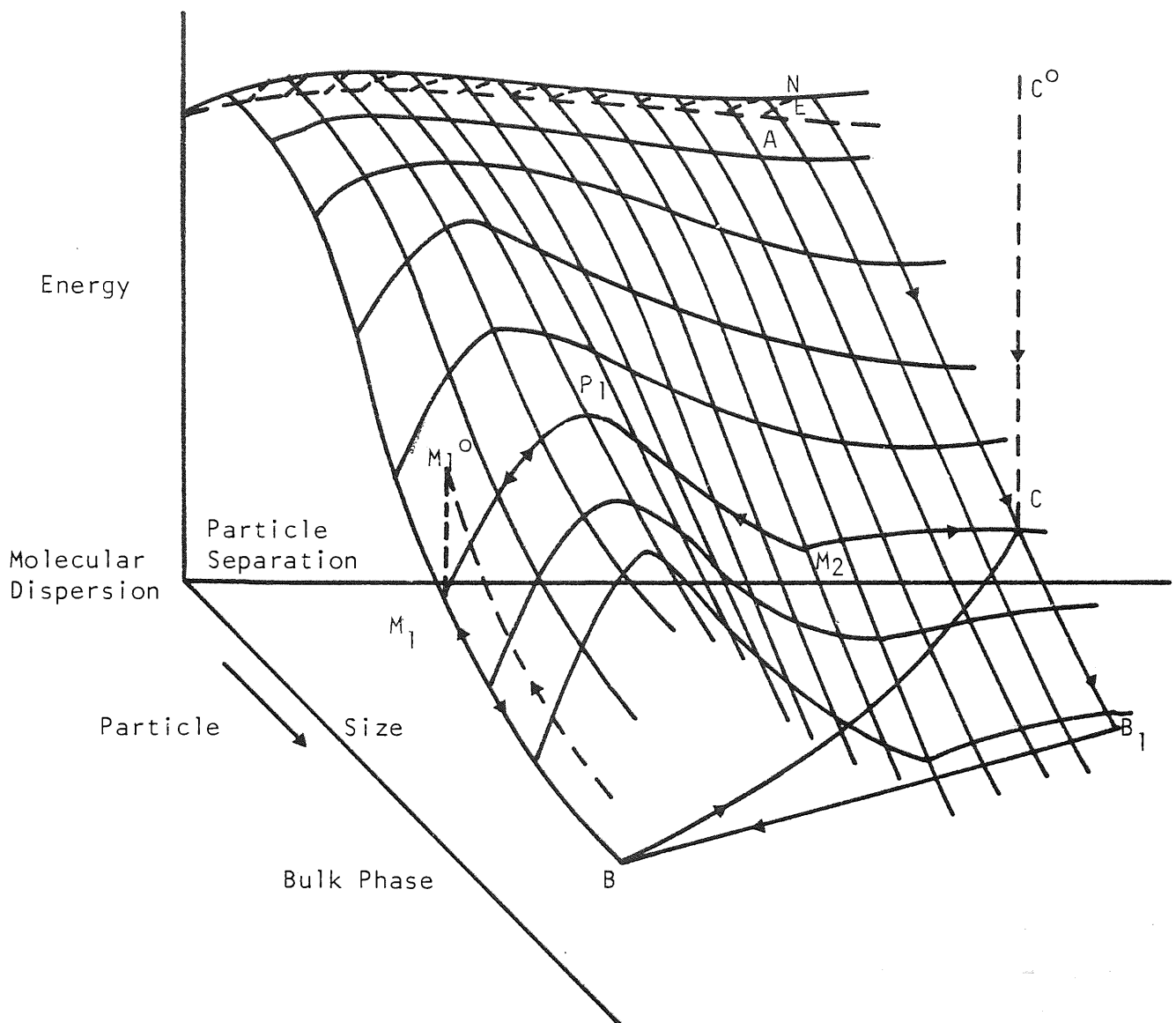


FIG. 2.3 Mutual potential energy surface of two colloid particles of a lyophobic colloid in a liquid medium as function of distance of separation and size of particles, showing routes by which colloid state C can be reached by (i) comminution, routes BC or $BM_1P_1M_2C$ or (ii) by nucleation and growth, ANC; and routes by which coagulation can occur (i) CB_1B and (ii) $CM_2P_1M_1B$. Note that the reverse route CNA in which a colloid would disperse to the molecular state does not in general occur spontaneously. (The short range repulsion "cliff" adjacent to the left hand face of the diagram is omitted for clarity). M_1^0 and C^0 are points representing energies in a vacuum environment.

2.2.2 Nucleation and Growth

The building-up of colloidal particles (C) from atomic or molecular units (A) involves following the path AENC on Fig. 2.3. The formation of an embryo (E) of a new phase in an existing bulk phase involves an increase in energy, which when the embryo reaches a critical size (at N, when is called a nucleus) passes through a maximum. Thereafter, the decrease in surface energy which accompanies growth acts as a driving force for spontaneous growth of the nucleus. However, if a large number of nuclei are present and the bulk phase is of limited extent, then growth involves the depletion of the bulk phase of the components of the growing particles, whose ultimate size (at C) is thus limited by the amount of material available. A high degree of dispersion is obtained when the rate of nucleation is high and the rate of growth is low. Since not all nuclei are formed simultaneously, they will have been growing for different times when growth ceases and consequently the final dispersion will contain a range of particle sizes (polydispersed).

2.2.3 Spontaneous Emulsification

In some systems the energy barrier to dispersion is absent, or so low that dispersion occurs in the absence of any mechanical agitation, and even downwards against the direction of gravity, when the components are placed in contact.

2.3 PREPARATION OF SECONDARY DISPERSIONS

The thermodynamically stable state of two immiscible liquids is their bulk form with a minimum of interface, the heavier liquid lying below the lighter one. To get a metastable dispersion with a large number of droplets of one liquid dispersed in the other liquid the mechanisms of formation based upon the energy changes as described in Section 2.2 are followed. In a general way, droplets of the required size may be obtained by either breaking up large drops of the bulk liquid into small droplets, which is the basis of the dispersion method, or starting from very tiny nuclei and then allowing them to grow to the required size, which is the basis of the condensation method. In addition to these two methods, Bikerman (2) also considers the critical emulsification method.

2.3.1 Emulsification by Dispersion Methods

Mechanical dispersion involves breaking up the liquid-liquid interface into fine shreds and globules. Under shear, a droplet undergoes distortion in a way characteristic of the system as a whole, and elongates into threadlike filaments. These cylindrical shapes, once formed becomes unstable as soon as its length exceeds its circumference and two spherical drops form. If the cylinder is extended far beyond its stability limit, it will have a tendency to break down into many droplets (3).

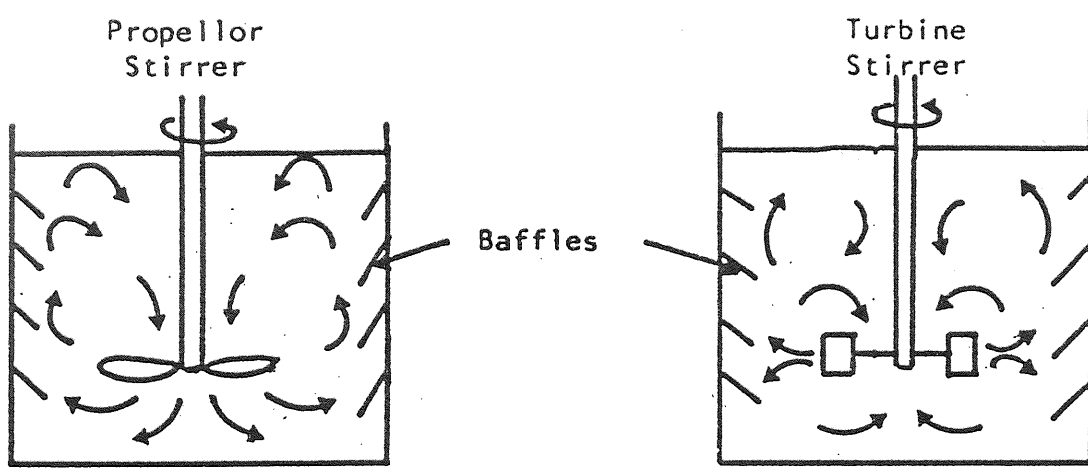
The above mentioned process can be achieved in practise by several methods and the effects of the system

parameters on the process have recently been reviewed (4). It is also noted (3,5,6) that when long filaments are formed, at the removal of the shear the thread remained stationary, and after a short time, spontaneously broke up into droplets. This advantage of interrupting agitation was used by Brigg (7) in the preparation of emulsions in which polydisperse systems of 50-100 μm were prepared by intermittent shaking the two bulk phases, with rest periods between shakes.

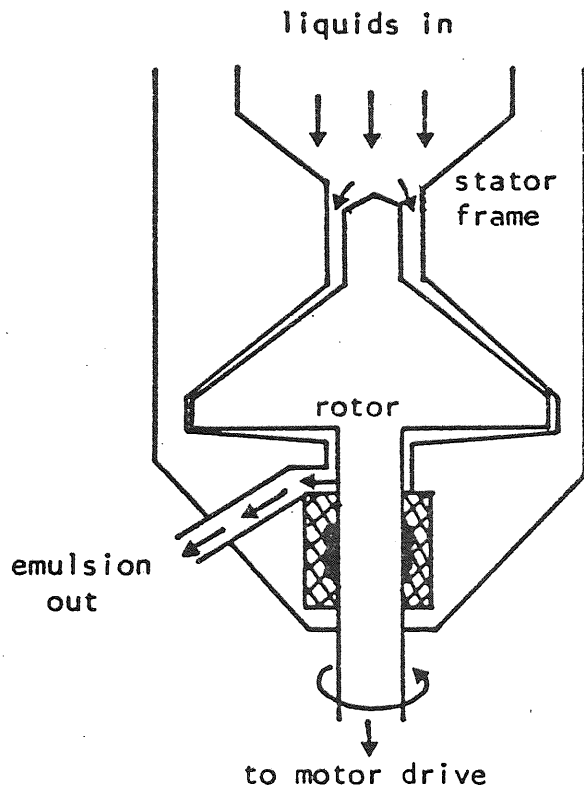
It is often required to produce smaller droplets in a shorter time which necessitates the application of large velocity gradients. To achieve this there are various types of emulsification equipment which can be considered such as simple mixers, homogenizers, colloid mills, and ultrasonic devices.

The simple mixers may be of various types, ranging from high-powered propeller shaft stirrers immersed in a small tank or drum to large self-contained units with propeller or paddle systems and jacketed tanks through which heating or cooling materials may be circulated (Fig. 2.4a). Careful design of the geometry and materials of the mixer produces a homogeneous turbulent flow field capable of reducing the drop diameter to as low as 5 μm . The properties of the prepared dispersion also depend upon the agitator speed and the physical properties of the bulk phases (8).

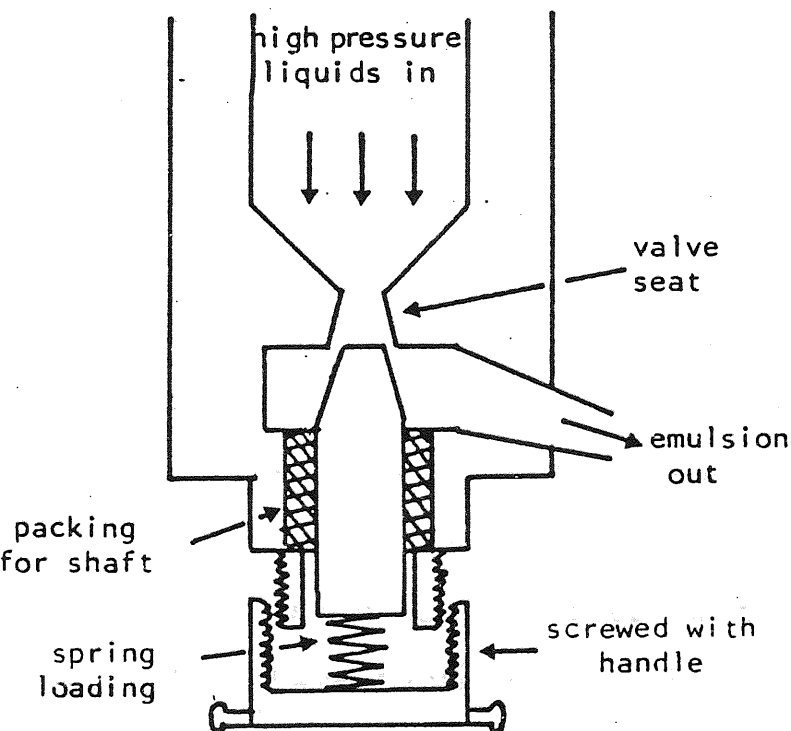
In a colloid mill or blender, Fig. 2.4b, emulsification is carried out by means of a shearing action imparted to the liquid by a rotor, revolving at speeds of from



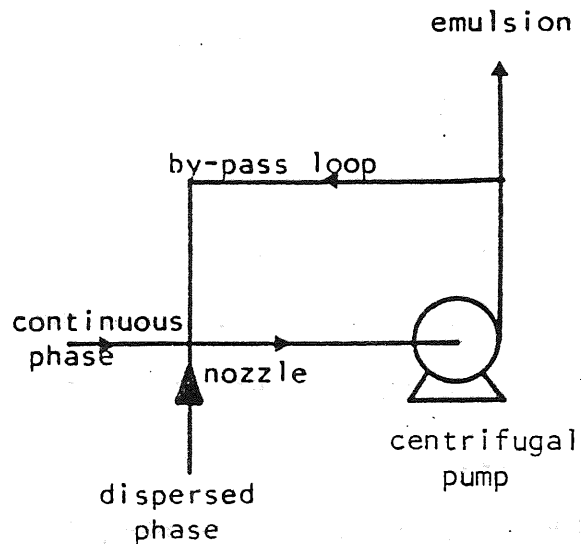
(a) Mixer



(b) Colloid Mill



(c) Homogeniser



(d) Centrifugal Phase Pump

FIG. 2.4 Mechanical Methods of Emulsification

1,000 to 20,000 r.p.m., and a stator surface. The emulsion passes between these two opposing faces through a clearance which may be as small as 0.025 mm. Commercial units of this type are readily available of varying materials of construction selected on the basis of the liquids to be emulsified (10) which can produce drops of 2 μm diameter (7).

A homogeneizer is a device in which dispersion is effected by forcing the mixture to be emulsified through a small orifice under very high pressure. A production homogeneizer will consist of a pump which provides the required pressure of between 70 and 350 bars, and a special spring-loaded valve which constitutes the orifice, may be about 10^{-8} m^2 in area, and which can produce droplets of 1 μm . Homogeneizers are produced either single - or double-stage units, the double-stage homogeneizer being so constructed that liquid passes through two orifice valves arranged in tandem. Sub-micron droplets can be produced by repeated passes of the dispersion through an orifice at lower pressures of about 2 bar (10) and larger drops formed by a single pass through larger diameter capillaries at low pressures (11) (Fig. 2.4c).

Many other emulsifying devices resemble the three types just described. Mention may be made here of a simple but effective method of producing secondary dispersions by passing the bulk phase through a centrifugal pump which is associated with a by-pass circuit (Fig. 2.4d) The characteristics of the dispersions formed in this

manner have been investigated (12,13,14,15) which typically produce a mean drop size of about 20 μ m. Also, recent research work (16) has investigated the possibility of producing secondary dispersions by pumping the dispersed phase through a micromesh distributor.

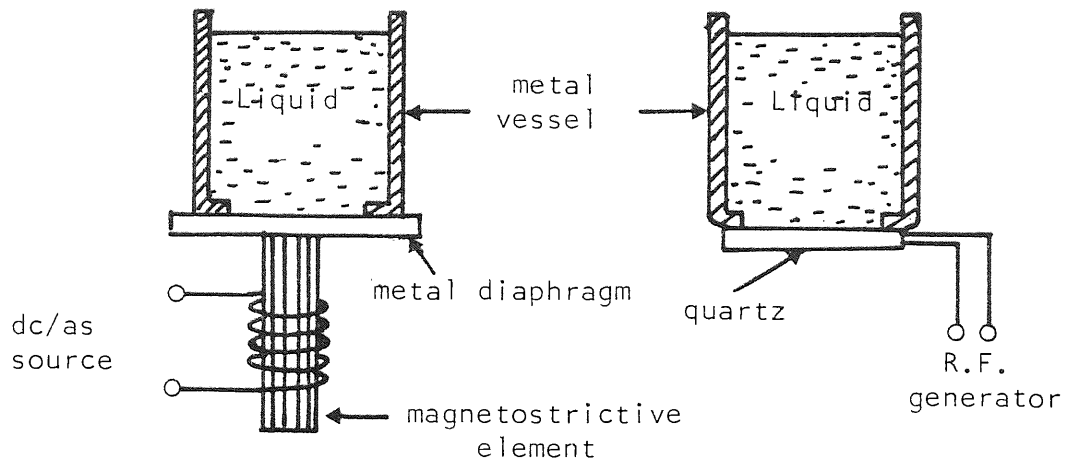
While the use of mixing and shearing devices obviously represents a simple way of introducing the energy required for the formation of an emulsion, such mechanical methods are not the only ones to be employed.

In sonic and ultrasonic techniques, electrical energy is converted into mechanical vibrations in the audio or radio frequency range, by the use of electro-mechanical transducers. There are four general methods whereby acoustic waves of the required energy can be generated (17).

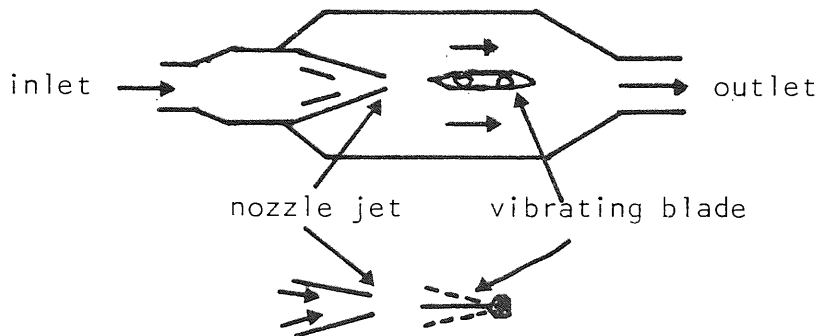
Piezoelectric effects, which depends on the fact that certain crystals contract in an electric field. If an alternating current of the same frequency as the natural mode of vibration of the crystal is applied across the crystal's faces, extremely powerful oscillations can be produced.

Magnetostriction effects by which certain ferromagnetic metals, particularly nickel, are found to change in length when put in a magnetic field. If an alternating field of the natural frequency of the metal rod is imposed, large amplitude oscillations can be obtained.

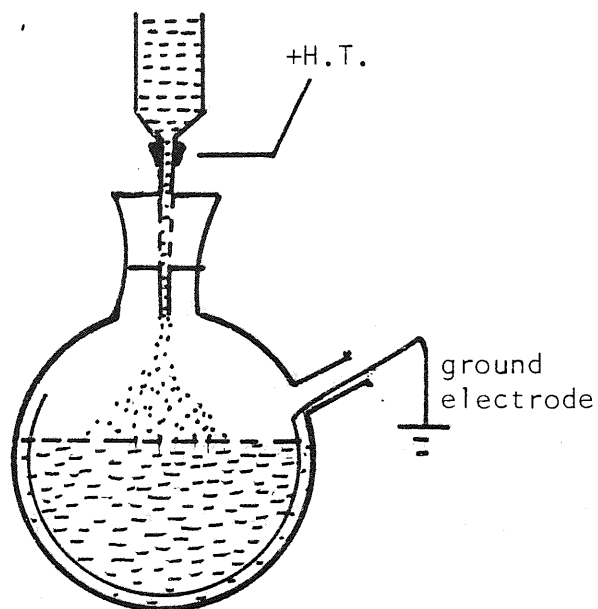
A diagrammatic representation of the emulsification vessel of a piezoelectric and of a magnetostrictive



(a) Magnetostrictive and Piezoelectric Emulsators



(b) Sonic Emulsification



(c) Electric Dispersion of Liquids

FIG. 2.5 Emulsification Using Electromagnetic Transducers

emulsator are given in Fig. 2.5a.

By using the electromagnetic effects the acoustic waves are, in fact, sound waves produced by means of the familiar moving-coil loudspeaker.

The "liquid whistle", shown diagrammatically in Fig. 2.5b is a way of setting up acoustic waves in a liquid by using its mechanical effects. When a stream of fluid impinges upon a sharp edge, inherent instabilities of the fluid excite the characteristic vibration of the system thereby increasing the acoustical energy of the jet. The system is adjusted to operate at the resonant frequency of the blade by optimizing the fluid pressure, fluid velocity, and the spacing between the orifice and the free edge of the blade.

The chief disadvantage of the sonic and ultrasonic techniques is that the methods are most efficient at the lower frequencies in the audio range and the use of high intensity sound waves is objectionable on physiological and sociological grounds.

Another method of emulsification is the use of strong electrical stresses, which produces high concentration, monodisperse emulsions on the laboratory scale. The basic equipment is illustrated in Fig. 2.5c in which application of an appropriate high voltage (about 8 KV) between the bulk dispersed and continuous phases produces an aerosol of the dispersed phase which passes into the bulk continuous phase.

The disadvantages of this method are that the emulsified droplets are charged and this may seriously interfere

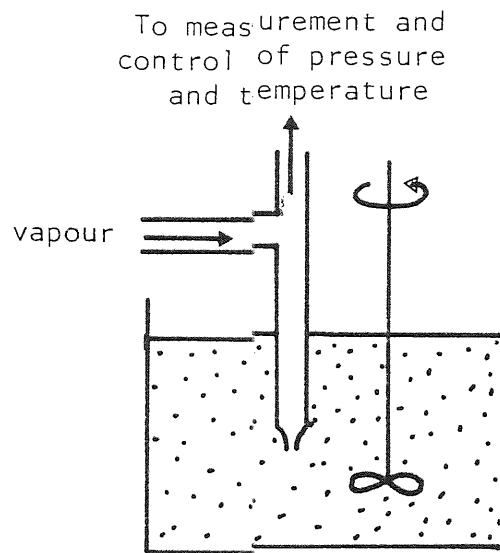
with many measurements and interpretation of the results. Also emulsification becomes difficult if the viscosity of either phase is high.

2.3.2 Emulsification by Condensation

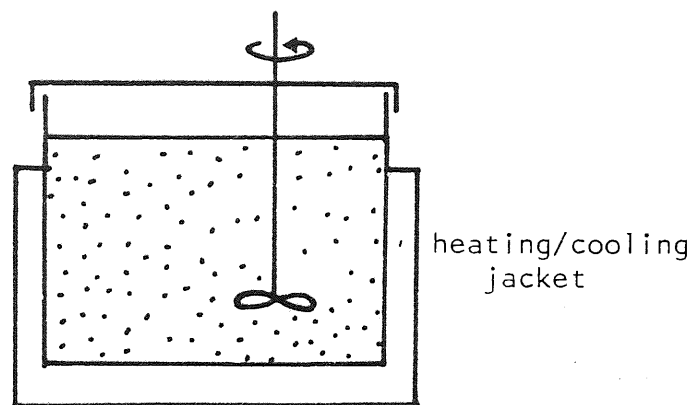
The essential principle of this method is that the materials from which the dispersion is prepared are originally present in true solution, as ions or molecules, and they tend to deposit on any nuclei that may be present in the system as described in Section 2.2. The nuclei may be spontaneously formed by the aggregation of molecules into droplets of submicron size, may be natural impurities of dust or smoke, or may be ions and other seeds that are artificially introduced.

Vapour injection is a condensation method of emulsification which involves the injection of a supersaturated vapour of the dispersed phase using a jet orifice which is submerged in the continuous phase containing a suitable emulsifying agent. The supersaturated vapour condenses as micron-sized drops whose size is dependent on the pressure of the injected vapour, the diameter of the jet orifice, and the emulsifier added to the continuous phase (7). This procedure is illustrated in Fig. 2.6a.

Another condensation method is the freeze-heat technique which involves varying the temperature of an agitated mixture of the organic and aqueous phases in a sealed system containing an emulsifier until condensation occurs. As it relies upon the temperature dependence



(a) Vapour Injection



(b) Freeze-Heat Technique

FIG. 2.6 Emulsification by Condensation

of the mutual solubility of the two liquid phases (18), it is extremely sensitive to temperature changes and may become heterodispersed once formed (19,20). Fig. 2.6b illustrates the arrangement.

Condensation methods have not grown beyond the stage of laboratory development and not many examples of this type of emulsions are known. This is due to the complexity of the equipment required to control the conditions of formation adequately.

2.3.3 Critical Emulsification

If two liquids are partially miscible at room temperature and completely miscible above an "upper critical dissolution temperature", then warming a mixture of the two liquids to the vicinity of the "upper critical dissolution temperature" often causes appearance of critical opalescence due to the formation of an emulsion. These emulsions are reversible in the sense that a further increase in temperature causes their destruction but a new lowering of the temperature to the vicinity of the "upper critical dissolution temperature" gives rise to an emulsion very similar to that observed initially. Also, a "lower critical dissolution temperature" exists for many systems; this means that the two liquids are miscible in all proportion below this temperature but form to mutually saturated phases at higher temperatures. As previously, critical emulsions exist near the "lower critical dissolution temperature".

2.4 INDUSTRIAL OCCURRENCE OF SECONDARY DISPERSIONS

In the previous sections the production of more-or-less stable secondary dispersions have been described. In many laboratory situations and/or industrial processes, unwanted dispersions are formed, very often with considerable stability, representing an economical and ecological problem of considerable magnitude, which has imposed tighter restrictions upon all types of effluent discharge and promoted research into the areas of pollution control and waste recovery for re-use. In this section, the principal offending sources of unwanted emulsion formation will be briefly described.

2.4.1 Effluent from the Oil Industry

Oil wastes can be classified into those originating from oil production and those originating from oil refining. Waste from oil fields include free and emulsified oil and salt water, the later presenting the most difficulty because although pumping rates are controlled to prevent this briny water from seeping into the oil this cannot completely be accomplished and they are often pumped out of the well with the oil and later separated to alleviate corrosion in the refinery and minimise the contamination of refinery products (21). Also if steam-injection is used to stimulate oil production in low-gravity oil fields, the waste water obtained by the dispersion removal must also be disposed of (22).

One of the largest sources of oil-contaminated water

is the operation discharges from oil tankers, which includes the loading, and unloading of the crude oil, the cleaning operations and the use of clean ballast water in the fuel tanks, in order to compensate for the weight of fuel used in the journey and in order to load the ship, among others.

There are also the inevitable spills and the tanker accidents which in most cases imply the problem of massive oil pollution.

Wastes from the oil refining include those resulting from desalting, distilling, fractionating alkylation and polymerization processes, among others.

2.4.2 Other Sources

Undesirable effluents result from several industrial practices, such as the wool industry producing a waste dispersion from the process of scouring wool.

A similar effluent arises in the operation of steam engines which produces a condensate from the cylinders of such engines which is often found to form stable oil/water emulsions with the lubricating oil. Waste effluents also emanate from most industrial operations which use oil as a lubricant or process fluid.

Solvent extraction processes in the chemical industry and some processes of the food industry also produce contaminated effluents.

In conclusion, this section illustrates the many and varied areas of undesirable occurrence of secondary dispersions and emphasises the obvious reasons for their

efficient removal. It can also be said that the various methods of dispersion separation rely upon similar conditions under which unwanted formation of dispersions occurs in industrial processes.

CHAPTER THREE
METHODS OF SEPARATION OF
SECONDARY DISPERSIONS

CHAPTER THREE

METHODS OF SEPARATION OF SECONDARY DISPERSIONS

3.1 STABILITY OF SECONDARY DISPERSIONS

The most fundamental characteristic of an emulsion is its overall thermodynamic instability. A dispersion of droplets of a liquid in another has a high free energy associated with its large interfacial area and will always tend to reduce this free energy via the interfacial area decrease that accompanies droplet coalescence. Thus, a secondary dispersion is unstable if, in a significant proportion of collisions between particles, association occurs, and the aggregates so formed continue to grow by further collisional processes until they are of such a size that Brownian motion is no longer sufficient to overcome the tendency, arising from density differences, for bulk separation to occur.

The phase which separates out may have various forms depending on the type of system considered. An aggregate is an ensemble of two or more droplets held together by forces of unspecified magnitude (23). Quantitizing the interdroplet forces, aggregates comprise flocculated droplets when the secondary minimum is sufficiently deep (Fig. 2.3), and the associated state has a loose open structure with interdroplet distances of the order of 0.1-1 μm (1). The height of the primary maximum controls the rate at which droplets transfer to the primary minimum corresponding to a separation of a few nanometers at the most. If the activation energy for

this process is not too high, the aggregated state may transform to a more compact structure of coagulated droplets. Whether flocculation is an intermediate stage in the overall coagulation process depends on the relative positions of the secondary minimum and primary maximum points. This is represented by the path $CM_2P_1M_1B$ on Fig. 2.3.

Emulsions can show instability in three ways: by creaming, by phase inversion and by complete demulsification. Each of these processes represent a somewhat different situation, though the borderline between them is not well defined.

Creaming occurs when the system separates into two emulsions, one having a higher concentration of the dispersed phase and one lower than that of the original dispersion. Gravity is the usual motive force, but creaming in electrostatic or magnetostatic fields is also possible.

The observed long-term stability of many emulsions towards creaming can be attributed to slowness of the settling speed of the droplets. It produces a high internal phase ratio emulsion in which they pack together as some transition form between spheres and polyhedra (24). However the drops remain separate during contact unlike primary drops which undergo coalescence as dispersion bands are formed (25).

A phase inversion occurs when the emulsion changes from O/W to W/O type or viceversa. It may develop when the concentration of the dispersed phase reaches about

75% which corresponds to the volume fraction occupied by a close packing of a number of rigid spheres of same size.

Demulsification is the complete break up of an emulsion into its component parts. The term break-up covers the two consecutive processes flocculation/coagulation and coalescence. In the first stage the droplets of the dispersed phase form aggregates in which the drops have not entirely lost their identity (such aggregation is often reversible). In the second stage, each aggregate combines to form a single drop. This is an irreversible process, leading to a decrease in the number of droplets of dispersed phase and finally to complete demulsification.

3.2 TREATMENT OF SECONDARY DISPERSIONS

An ideal solution to the coalescence problem, having obtained a reasonably concentrated dispersion, is to bring about

- (a) an increase in the attractive forces between droplets,
- (b) the reduction or annihilation of known or suspected stabilizing factors,
- (c) change in the mechanism of coalescence by introduction of a third body of large surface area: droplet coalescence then occurs via the third body and spreading.

Various methods are used to coalesce secondary dispersions into large drops so that the disperse phase

can ultimately be separated by gravity settling. Most of the following methods utilize one or more of these principles.

3.2.1 Addition of Chemicals

Chemical methods are probably the most widely used technique for breaking up emulsions. They operate on the principle of removing the barriers that hinder coalescence. The demulsifiers counteract the influence of the protective films that surround the dispersed drops or neutralizes the surface charges. Some break the film by trying to invert O/W emulsions into W/O emulsions and viceversa. Carbon disulphide and carbon tetrachloride, for example are good solvents for the materials forming the protective film, albeit of limited practical value. Agents such as polyvalent salts and acids neutralize the surface charges. It is thus obvious that for each given emulsion there is a specific demulsifier which will produce optimum results, and this choice must be made after careful study of the physical and chemical properties and drop size distribution of the emulsion.

3.2.2 Centrifugal Separation

The gravity-driven sedimentation of an emulsion can be accelerated if the emulsion is centrifuged. Centrifuges are particularly effective in separating two liquids of low density difference, high continuous phase viscosity or small drop size and which may contain

particulate matter as contaminant. They are used in ordinary chemical processes only when low residence time is essential or when phase separation is difficult; examples therefore arise in pharmaceutical and radiological processes.

3.2.3 Coalescence by Electrical Methods

Emulsion droplets are generally charged to some degree, so that the use of an electrical field to induce coalescence seems obvious. Electrical methods of inducing coalescence are based on one of two mechanisms; namely, due to forces exerted on drops having net charges (electrofining) and the forces between neutral drops resulting from either acquiring induced dipoles in a.c. or d.c. field. For dispersions containing uncharged drops, dipole coalescence is the operative method (26) for high concentration of the dispersed phase but the efficiency decreases rapidly at concentrations below 0.1% due to a decrease in the uncoalesced droplet population. The bulk of research on electrically induced coalescence, however, has focused on W/O systems, a reflection of the importance of these emulsions to the oil industry, where they occur during extraction of crude oil. High field strengths can be used in such systems because of the low conductivity of the continuous phase.

3.2.4 Air Flotation

This technique involves the use of jets of air, or other gas, in the form of a stream of fine bubbles of 10 to 100 μm diameter which capture the suspended

dispersion drops. This results in the formation of an extremely active froth, and highly efficient separations are possible (27). This method finds extensive application in the treatment of oily wastes from refineries, petrochemical plants and steel mills (28) where quantities of up to 80,000 m³ per day are purified to a dispersed phase concentration of about 20 p.p.m. (29).

Generation of the air bubbles may be achieved by chemical reactions, electrolytic methods or by injection of air through a distributor of very small pore size (30) but dissolved air flotation is the principal method of application due to its simplicity, capacity and versatility.

3.2.5 Heat Treatment

Beyond the fact that boiling (or freezing) an emulsion can induce breakdown, little has been established until recently about temperature effects on emulsion stability. Increasing the temperature brings about changes in most of the factors that could affect stability : the bulk phase viscosity, interfacial tension, and adsorption at the interface all decrease while the activation energy and the Brownian velocity both increase. This method is often used in conjunction with chemical coagulation (31) since it increases the rate of reaction caused by demulsifying agents.

3.2.6 Coalescence Induced by a Third Body

A solid introduced into an emulsion, if wetted to some degree by the disperse phase, can act as a site for

the coagulation and coalescence of the droplets and also as a channel for the removal of coalesced liquid. If provision for the removal of coalesced material is made, such a coalescing arrangement can be self-regenerating and suitable for continuous rather than batchwise operation. This factor, together with the relatively small amount of maintenance required and the low initial costs has made emulsion breaking by solids very attractive as early as 1911.

Because of the current emphasis on pollution control, there has been new interest in porous-bed coalescers. A wide variety of porous media has been investigated including pebble beds (32), ungraded gravel beds and stainless steel gauges (33), and polymeric materials (34).

Commercial designs of emulsion separating equipment nowadays incorporate coalescers in a three stage process (35,36). After gravity settling and straining, to remove particulate matter, the dispersion is passed through a cylindrical coalescing element. Entrainment of coalesced drops is prevented by installation of a surface coalescer which consists of a porous membrane preferentially wetted by the continuous phase (37).

The beds are sometime dependable and sometimes not, and the mechanism of their operation has been described in rather vague terminology (38,39,40,41). Recently, efforts have been made to incorporate these mechanisms into a workable theory which will predict the general behaviour of the porous beds (14,42,43,44,45,46,47).

3.2.7 Disadvantages of Separation Methods

All the existing methods available for separating emulsions suffer from certain disadvantages. With chemical additions the contamination of the liquid system may arise. Care is therefore needed in the choice of chemical(s) and level of addition. Also, as additives may be surface active, they reduce the interfacial tension between the phases of the dispersion leading to the formation of very small drops and also by forming coatings on coalescer elements, thus preventing them from functioning efficiently (48). Consequently, chemical coagulation is often employed in conjunction with flotation processes (31) when recovery of the dispersed phase is not mandatory. This method also suffers the disadvantage of high cost and technical and practical limitations in its application. Reproducibility of the rate of separation can only be obtained with a high degree of control. Results have been found to vary dependent upon traces of impurities, degree of aeration and variation in the type and intensity of agitation during the flocculation stage.

Centrifugation also suffers from high capital and operating costs. Consequently the use of centrifuges has been restricted to military applications such as the purification of aviation fuel.

Electrostatic coalescers are unsuitable for applications where high separation efficiency are required (less than 0.1%). They also possess the disadvantage of high capital costs but are simple and simply adaptable to

automatic operation and problems from scaling-up seldom arise.

Air flotation processes operate more efficiently when the dispersion is pretreated with flocculating agents providing that it is not necessary to recover the dispersed phase from the "float" which may be contaminated by addition of chemical coagulants.

The use of heat treatment as a method for coalescing dispersion results uneconomical when large quantities of dispersion are treated due to the high energy consumption of the process.

As most methods available for separating emulsions suffer from certain disadvantages, the trend is now to use porous bed coalescers as they are relatively inexpensive, small and simple to operate. These are discussed in more detail in Chapter 4.

CHAPTER FOUR
COALESCENCE IN PACKED BEDS

CHAPTER FOUR
COALESCENCE IN PACKED BEDS

There are numerous methods available for the separation of secondary dispersions. The largest collection of documentation concerning porous-bed coalescers is available in the form of patents, which first appeared about 1911. Previous studies of secondary dispersions will now be discussed to establish the preferred features of a coalescing bed.

4.1 EFFECT OF OPERATING CONDITIONS

Burtis and Kirkbride (49) were among the first to investigate the use of glass-wool packing for the removal of aqueous salt solutions from crude oil. They varied bed density, bed thickness, amount of fresh water added to the crude oil, flow rate and temperature, measuring effluent salt content and pressure drop. They found that improved separation efficiencies were obtained by:

- (i) Decreasing superficial velocity in the range 0.66×10^{-2} to 0.027×10^{-2} m/s.
- (ii) Decreasing the water to oil ratio in the range 0.3:1 to 0.2:1.
- (iii) Increasing the temperature; 408°K was found to be the optimum temperature since operation above 450°K was impractical due to the high pressure required to prevent vapourisation.
- (iv) Increasing fibre packing density from 140 to 240 kg/m^3 .

(v) Increasing bed depth; 12.7×10^{-2} m was capable of reducing the concentration of salt in oil to 30 p.p.m.

Hayes et al (50) did a full-scale study of desalting crude oil in a refinery using glass-fibre for a period of 58 weeks. They also concluded that desalting by glass-fibre beds was commercially attractive.

Voyutskii et al (51) studied water-in-oil emulsion filtration by fibrous materials. They found separation occurred only below a certain critical velocity; below this velocity coalescence was found to depend on total fibre contacting surface rather than on pore size.

Gudesen (52) investigated the coalescence of petroleum fractions dispersed in water by turbulent mixing, using mixed fibrous beds of cotton and glass wool. He also found a critical separation velocity below which complete coalescence was achieved. The critical separation velocity was found to pass through a maximum with bed depth and a minimum with bed composition. He attempted to explain this behaviour in terms of two separate limiting effect.

Farley and Valentin (33) investigated the coalescence of high-viscosity oils, with viscosities of 3.5 to 20.0 Ns/m^2 , dispersed in water by pumping with application to ballast water treatment. A number of beds were used including porous porcelain, activated alumina and fibre-glass as water wetted solids, and polypropylene, polystyrene and steel gauze as oil wetted solids. Effluent oil content was determined by light absorption following

extraction with chloroform. As would be expected it increased with increase in superficial velocity, decrease in bed thickness and decrease in oil viscosity. It was considered more efficient to split the total packing thickness into two beds in series, with an intermediate oil take off, the second bed having twice the thickness of the first.

Graham (53) and Sweeney (54) investigated coalescence by beds of glass fibres with subsequent gravity settling of water-in-Aroclor dispersions prepared by turbulent mixing. Fibre diameter and bed depth were varied and the total water content in the effluent was determined by titration. Effluent water content was found to increase with either increase in superficial velocity or decrease in total surface.

Sareen et al (39) observed visually the performance of single fibres (cotton, polypropylene, glass and p.t.f.e.) and mixed fibres (cotton-glass fibre bed and cotton-Dynel fibre bed) in coalescing several oil-in-water emulsions prepared by turbulent mixing. The superficial velocity was varied from 0.1×10^{-2} to 1.8×10^{-2} m/s and the dispersed phase viscosity from 1.4×10^{-3} to 137×10^{-3} Ns/m²; dispersed phase concentration was in the range 2% to 5% by volume. Coalescence performance improved with decrease in fibre diameter and increase in bed length but there was a practical limit to the maximum bed depth. While residence time in the bed increased, the coalescence was better but there was a corresponding increase in pressure drop. Furthermore,

redispersion of the coalesced drops occurred due to channels being formed within the bed. Coalescence performance decreased with increase in dispersed phase viscosity but then became constant at values above $90 \times 10^{-3} \text{ Ns/m}^2$. A critical separating velocity was also identified. Photomicrographs of exit drop indicated that a drop would break away from the fibre after attaining an equilibrium size; when the superficial velocity was higher than the critical velocity a retained drop was carried away before attaining the equilibrium size. These results were later confirmed by Davies and Jeffreys (55).

Essentially 100% oil separation efficiency was achieved by Langdon et al (56) at a superficial velocity of $1 \times 10^{-2} \text{ m/s}$ using a coalescer made from phenol-formaldehyde coated glass fibre $3.2 \times 10^{-6} \text{ m}$ in diameter. Both inlet and effluent oil content were determined by a light reflectance technique. The pressure drop during the run increased from 13.8×10^3 to $172.4 \times 10^3 \text{ N/m}^2$ due to oil accumulation in the bed and to a lesser extent, to mechanical degradation of the fibres. The possibility of solids contamination was ruled out. Because of the differential increase in pressure, efficiencies were in fact determined under unsteady-state conditions. If solid contaminants were present, they would be deposited in the bed causing gradual but permanent decrease in voidage. This cannot be avoided and replacement or intermittent back washing of the bed would eventually become necessary. Thus the bed ought

not to be used as a filter as suggested by Hazlett (57).

Vinson and Churchill (58) used photo-etched screens to separate a 0.05% oil-in-water emulsion with an average drop size of 3×10^{-6} m. The emulsion was prepared using a homogenizer and drop size estimated by a light scattering technique. Coalescence efficiency decreased with increase in superficial velocity from 0.025×10^{-2} to 2.08×10^{-2} m/s, increase in screen filament width, from 8.5×10^{-6} to 31.4×10^{-6} m, and increase in aqueous phase viscosity from 0.9×10^{-3} to 9.4×10^{13} Ns/m².

4.2 SYSTEM CHARACTERISTICS

Whether or not the packing should be preferentially wetted by the dispersed phase has been the subject of much discussion. Voyutskii et al (51) concluded that for best performance the fibre should be sufficiently 'water-wetted' to coalesce the water, but not so 'wetted' as to become clogged by the accumulation of water. The appearance of a secondary dispersion in the effluent was attributed to excess water wetting. In a second study, Voyutskii et al (59) found that mixtures of viscose and wool fibres resulted in improved coalescence performance compared with single fibre material.

Sareen et al (39) using a photomicrographic technique, concluded that preferential wetting was not the controlling factor since drops that adhered to the fibre did not wet it. The results were justified by the relative surface roughness of the fibres used. A similar conclusion was reached by Davies and Jeffreys (55). Since droplet

sizes were much smaller than the equilibrium drop size, droplets that adhered to the packing would be spherical regardless of material. However, surface roughness was considered extremely important.

For coalescence to take place, Burtis and Kirkbride (49) concluded that the packing must be preferentially wetted by the dispersed phase. Hazlett (57) accepted this principle to explain the attachment mechanism.

Farley and Valentin (33) concluded that water wetted packings were far superior to oil wetted ones for the separation of oil from water. The latter held the drops too tightly and did not allow coalesced drops to leave the packing; this resulted in their finally being broken up into clouds of small droplets by the water stream.

Langdon et al (56) considered the separation performance of a packing to be mainly determined by its wetting properties. An improved element with well defined and stable wetting characteristics could be achieved by using a packed bed composed of two materials, one essentially hydrophobic and the other essentially hydrophilic.

Recently Austin (14) studied the coalescence of emulsion through beds of stainless steel woven meshes and found that the critical velocity for beds initially free from dispersed phase was approximately 1.5×10^{-2} m/s but presoaking of the packing in dispersed phase increased this value to 3.5×10^{-2} m/s without increasing the two phase pressure drop. Also the time required to reach steady state operation was shortened with presoaking.

From this brief review of previous work on fibre

wetting phenomena it is clear that there is a lack of understanding as to the effect of the nature of the coalescing media on the coalescence process. The consensus is however that preferential 'wetting' of the packing by the dispersed phase is not critical, but surface roughness is extremely important. Suggestions that improved coalescer performance achieved by dipping the bed in the dispersed phase, i.e. 'priming', is due to prewetting effects are unproven. The phenomenon is more probably due to filling up the 'active sites' in the bed, i.e. increasing the hold up of the dispersed phase which is a major factor affecting the ultimate effectiveness of the coalescer.

As would be anticipated system interfacial tension is important in the operation of a coalescer element. Generally, the higher the interfacial tension, the easier the separation. Values as low as 20×10^{-3} N/m can be separated satisfactorily, but below this value separation becomes increasingly difficult (60). Rose (61) confirmed this from a study of nine different water-organic dispersions. Sareen et al (39) found that, during the separation of oil in water emulsions, for an interfacial tension value of 20×10^3 N/m incomplete coalescence was observed for water soluble surfactants while coalescence was complete with oil soluble surfactants for values as low as 3.52×10^{-3} N/m.

Some theories have been presented as to how surfactants poison coalescer elements. Bartle (60) suggested adsorption of the surfactants by the element. This would

cause re-emulsification of the dispersed phase present on the media. Osterman (48) suggested there was adherence of the surfactants to the media thus allowing the emulsion to pass through unaffected due to the change in fibre wettability. Lindenhofen (62) disproved the above theories experimentally and suggested that the surfactant film at the oil-water interface, water dispersed, may present a mechanical or electrical barrier to the coalescence of water droplets in the media. Flushing the element with Iso-propyl alcohol improved its coalescence performance and lowered its pressure drop. More recently (63) he suggested that commercial coalescers, which normally have a cotton outer wrapping or 'sock', malfunction due to the adsorption of surfactants from the continuous phase by the sock, i.e. water wetted, causing a high surfactant concentration at the release point. By coating the sock with a fluorocarbon resin a hydrophobic surface was produced and this operated normally even if poisoning was attempted. These results supported the theory first presented by Hazlett (57) that poisoning is caused by interference with the detachment process at the point of release of the coalesced drop from the sock.

From a study of the effect of the sodium sulphonate surfactant on fibrous bed coalescence, Hazlett (57) concluded that doubling the surfactant concentration from 0.5 ppm to 1.0 ppm influenced the coalescence phenomena to a greater extent than 30 fold change in velocity. The additive did not affect the approach or attachment

processes but only affected droplet release. Thus instead of the drops growing into balloon-shaped globules and detaching from the same site by rupture of the neck, they were extended by the force of the continuous phase film into thin fingers, which oscillated normal to the flow and released drops from the tip.

With continuous phase soluble surfactants, a reduction in interfacial tension from 40×10^{-3} to 10×10^{-3} N/m reduces the thermodynamic instability of dispersions and stable emulsions can readily be formed. At values of 0.1×10^{-3} N/m droplets break up spontaneously to form a stable emulsion (64); such an emulsion cannot be coalesced in a fibrous bed. Even in very low concentrations surfactants affect the interfacial tension. In larger concentrations, however, the drops are completely covered with a 'skin'. For dilute surfactants, the drop surface is not completely covered and size distributions change may occur due to drop interactions. For higher concentrations, the coverage becomes complete and the drops are isolated causing a distribution highly resistant to change. However for primary drops falling through a continuous phase at low Reynolds numbers the surfactant is swept to the rear of the drop by the tangential velocity on the surface forming a 'dust cap' (65). No comparable work has been published for secondary drops.

CHAPTER FIVE

MECHANISMS OF DROP DISPERSION
COALESCENCE IN PACKED BEDS

CHAPTER FIVE
MECHANISMS OF DROP DISPERSION COALESCENCE
IN PACKED BEDS

5.1 INTRODUCTION

An extensive literature survey indicates that there is no accepted theory to explain the mechanisms involved in the coalescence of drops during passage through a packed bed. Since both primary and secondary dispersions may coexist during the coalescence process and the distinctions between the two types are not well defined, discussion of the mechanisms, whereby their drop sizes are increased will be combined. Most previous workers have defined three basic stages, namely capture of dispersed drops, coalescence of the drops and flow of the bulk phase through the packing and finally, release of the coalesced drops.

5.2 DROP CAPTURE

Any coalescence device designed to treat flowing secondary dispersions must be able to capture the drops which then maintain close proximity to others. The drops should be retained for a sufficient time to permit drainage of the continuous phase between them thus allowing coalescence to take place. Capture of a drop suspended in a flowing continuous phase is theoretically possible by one or more of the following occurrences,

- (i) Collision with another drop suspended in the dispersion;

(ii) Collision with an obstruction in the packing structure;

(iii) Collision with another drop which has been captured attached to the packing structure.

The probability associated with the first occurrence is reported to be low by Sareen et al (39) who made photomicrographic studies and observed little or no coalescence between freely moving drops. Although collisions with the packing structure are important, especially during the initial transient operation of the coalescer, the drop collection rate is considerably enhanced by the presence of drops held within the interstices and attached to the packing media.

Bitten (66) made a photographic study of the coalescence rates of tap water droplets on single fibre positioned perpendicular to a moving emulsified jet-fuel stream. He observed growth of drops attached to the fibre by coalescence with drops captured from a flowing dispersion. The significant role of retained drops in contributing to capture is also confirmed by the experimental data of Ghosh and Brown (67) and Farley and Valentin (33) who both reported increased drop removal efficiencies in a coalescing bed after several hours operation.

Microscopic observations reveal that drops from the stream become attached to the fibres and grow. Coalescence occurs in one of two ways (68): drops flowing in the stream collide with those being held by the fibres and may coalesce, or drops attached to the fibres can

contact each other and coalesce. This second phenomenon accounts for only about 5% of the total number of coalescences which take place. A number of authors (39,61,69) have defined the mechanisms by which particles from the stream collide with those attached to the fibres.

The effect of the dispersed phase saturation in assisting drop capture has been incorporated into models describing drop capture mechanisms. Sherony and Kintner (44) considered the size distribution of retained drops which act as potential collectors and this approach was further modified by Rosenfeld and Wasan (70) by inclusion of an effective fibre diameter. The latter was intended to account for the effect of held drops, but this concept is not consistent with their model which applies only when the dispersed phase does not form a continuum within the bed. Spielman and Goren (71) assumed that the dispersed phase exists entirely as discrete, spherical globules and evaluated the capture rate from analysis of the trajectory of a drop approaching a spherical collector. This method permitted independent evaluation of drops captured by packing fibres and those captured by held drops.

Modelling of drop capture processes is difficult due to the complex interfaces which exist between dispersed and continuous phases and the solid phase of the packing structure. Definition of collector geometry and formulation of a mathematical model to describe the hydrodynamic behaviour of the liquids flowing in a coalescer, where the dispersed phase saturation may

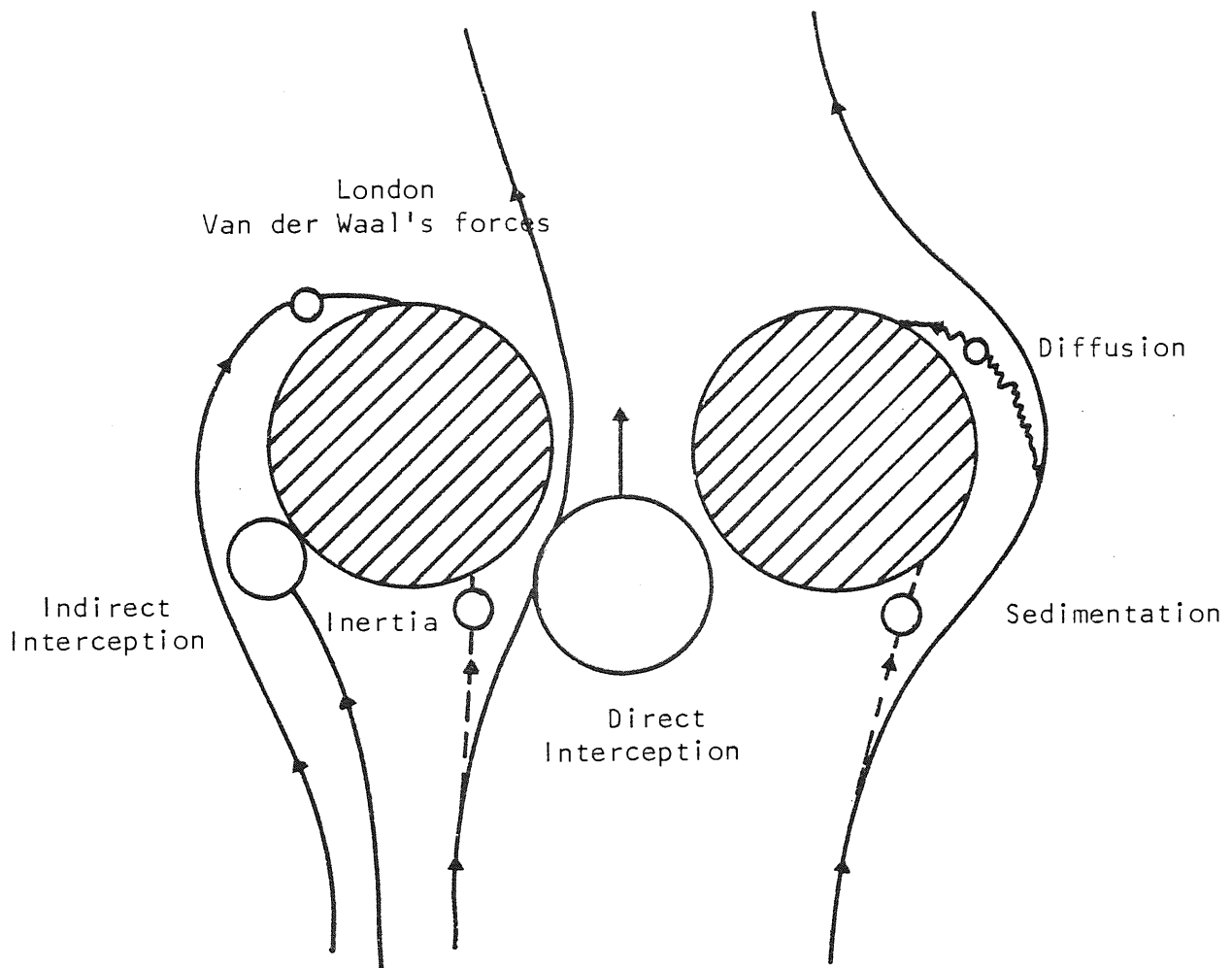


FIG. 5.1 Depiction of Drop Capture Mechanisms

exceed 50% (72), are the chief problems. The first attempts to hypothesise the mechanisms of removal of particles suspended in a flowing fluid were made in studies of aerosol filtration in fibrous beds having porosities greater than 95%. A convenient way of analysing the collection mechanisms is to consider the behaviour of a drop or particle as it approaches a collector. Cylindrical collectors describe the geometry of fibrous beds and spherical collectors characterise granular media.

To describe and compare the possible drop capture mechanisms, the geometrical model illustrated by Fig. 5.1 is proposed which represents drops approaching either a cylindrical or spherical collector. Also, initially the presence of held drops and the effects of interaction with neighbouring collectors will be ignored. The mechanisms which influence drop capture will now be independently examined to ascertain their relative contributions to the overall capture efficiency.

5.2.1.1 Indirect Interception

In aerosol filtration and coalescence processes, the diameter of the collector may be comparable to the drop diameter. Under these conditions, the finite size of the drops cannot be neglected and interception between the drop and collector becomes significant. This mechanism is characterised by the value of the Interception number, $R = \frac{d_p}{d_c}$. The capture efficiency, η_I is defined as the ratio of the number of drops captured to the number of drops approaching within

the projected area of the collector per unit time. Drops are assumed to follow the fluid flow streamlines around the collector and are captured if the distance between the centre of the drop and the periphery of the collector is less than the drop radius.

Happel's (73) model for arrays of cylinders with axes perpendicular to the filter face velocity, associates a coaxial cylindrical cell with each representative solid-cylinder element and assumes no slip at the solid-cylinder surface and that the outer cell boundary is a free surface, i.e. the shear stress tangential to the cell boundary vanishes there. Kuwabara's (74) model is very similar except the free-surface assumption is replaced by that of vanishing vorticity at the outer boundary. Both models are equally adaptable to assemblages of spherical collectors with spherical cells (75).

The cylinder efficiency for capture by interception is

$$\eta_I = \frac{\psi_f}{u a_c} \dots\dots\dots (5.1)$$

where ψ_f , the stream function in cylindrical coordinates takes the form

$$\psi_f = \frac{2A_F u}{a_c} (r-a_c)^2 \sin \theta \dots\dots\dots (5.2)$$

with the radial coordinate, r , equal the sum of the drop and fibre radius respectively at interception. The dimensionless coefficient, A_F , is an increasing function of the volume fraction of fibres in the array. Happel's model gives

$$A_F = 1/\{-\ln \alpha - 1 + \alpha^2/(1+\alpha^2)\} \dots\dots\dots (5.3)$$

and Kuwabara's model gives

$$A_F = 1/\{-\ln \alpha - 3/2 + 2\alpha - \alpha^2/2\} \dots\dots\dots (5.4)$$

for $\alpha = 1-e$

The stream-function equation 5.2, very near the collector, varies as $(r-a_c)^2$, which is a direct consequence of satisfying incompressible continuity with no slip at the collector surface. The effect of crowding by neighbouring fibres is to compress the streamlines and increase the fluid speed adjacent to the central fibre because A_F increases with α .

For beds of granular collectors the situation is somewhat similar and the analogous calculation for the efficiency by interception is:

$$\eta_I = \frac{2\psi_S}{a_c^2 u} \dots\dots\dots (5.5)$$

The stream function near a representative sphere, in spherical coordinates, takes the form

$$\psi_S = \frac{3}{4} A_S u (r-a_c)^2 \sin^2 \theta \dots\dots\dots (5.6)$$

A_S is a dimensionless function of the bed voids, which varies from one flow model to another, as it does for the case of cylinders. For Happel's model

$$A_S = 2(1-\gamma^5)/(2-3\gamma+3\gamma^5-2\gamma^6) \dots\dots\dots (5.7)$$

with $\gamma = \alpha^{\frac{1}{3}}$ and $\alpha = 1-e$

Because of the ambiguity associated with flow fields in collector assemblages, particle capture from flow past simple collectors have been studied. Low Reynolds number flow past an isolated cylinder has been used by Chang (77) to study capture of waterborne particles. This flow field can be represented using Lamb's (78) solution. To lowest order in the distance from the cylinder surface the Lamb stream function is conveniently given by equation 5.2 with $A_F = 1/\{2(2 - \ln N_{Re})\}$, where N_{Re} is the Reynolds number based on cylinder diameter. Creeping flow past an isolated sphere is given by Stokes' solution which, to lowest order, is given by Equation 5.6 with $A_S = 1$.

It is evident that any analysis of particle capture by cylinders or spheres, that depends on phenomena near enough to the collector surface that Equations 5.2 or 5.6 apply, can be used to describe either isolated collectors or collector assemblages provided the appropriate expression for A_F or A_S is used.

Hazlett (69) presented a model of a fibrous bed coalescer where interception was assumed to be the principal mechanism of approach. An equation developed by Langmuir (79) was used to describe the approach of the drops:

$$\eta_I = \frac{1}{2(2 - \ln N_{Re})} \left\{ 2(1+R) \ln(1+R) - (1+R) + \frac{1}{(1+R)} \right\} \quad (5.8)$$

where η_I is the capture efficiency of a single isolated cylindrical collector under viscous flow conditions, with $N_{Re} < 1$ for viscous flow over a cylinder.

The Reynolds' number, N_{Re} , based on the diameter of

the collector, is included since the streamlines are influenced by it. They are affected at a greater distance upstream and displaced further from the collector laterally as N_{Re} decreases. Equation 5.8 predicts that as the velocity increases, the capture efficiency increases which generally contradicts experimental evidence (33,58,80). Rosenfeld and Wasan (70) employed the equivalent of the above expression written for irrotational flow conditions,

$$\eta_I = (1+R) - \frac{1}{(1+R)}; N_{Re} > 1000 \dots\dots\dots (5.9)$$

This equation, however, is no better description since it does not predict a reduced capture efficiency with increasing N_{Re} . Rosenfeld and Wasan accounted for the effect by empirically fitting their data for velocities greater than an experimentally observed critical value. Further, Equation 5.9 is only valid for high Reynolds' numbers which are not encountered in practical coalescers (see Table 5.1).

The decrease in filter coefficient as the superficial velocity increases may not be due to a decrease in drop capture efficiency since Davies and Jeffreys (55) concluded that an optimum velocity exists for a given packing. When the local viscous shear forces exceed the forces of adhesion between the drops and collector, detachment of the drop, or part of the drop, occurs which is manifested as redispersion.

For a spherical collector, Rajagopalan and Tien (81) described the efficiency due to interception (when the drag correction is not considered) by the following equation:

INVESTIGATOR	Dimensionless Groups Characterising Mechanisms										Predominant Mechanisms Proposed for Drop Capture
	N_{Re}	R	R_d	N_{Stk}	N_G	N_{Ad}	N_{RePe}^a				
Ghosh (67)	10^7	10^{-3}	-	10	-10^{-5}	10^{-9}	10^6	Electrophoresis			
Hazlett (57)	1	0.1	-	10^{-4}	10^{-6}	10^{-6}	10^4	Interception/Inertial Impaction/Diffusion			
Rajagopalan (81)	10	10^{-4}	-	10^{-6}	0.1	10^{-9}	10^6	Interception/London/Diffusion/Sedimentation			
Sareen (39)	1	0.1	-	10^{-4}	-10^{-4}	10^{-6}	10^5	Interception/Inertial Impaction/Diffusion			
Shalhoub (13)	1	10	-	0.1	-10^{-6}	10^{-6}	10^5	Interception			
Sherony (44)	1	1	-	0.1	10^{-4}	10^{-5}	10^6	Interception/Inertial Impaction/Diffusion			
Spielman (71)	0.1	1	-	10^{-2}	10^{-7}	10^{-2}	10^3	London Forces			
Spielman (72)	10	10^{-2}	-	10^{-2}	0	10^{-6}	10^6	London Forces			
Vinson (58)	10^{-2}	0.1	0.1	10^{-3}	-10^{-3}	-	10^4	Interception/Inertia Impaction			
Austin (14)	10	0.1	0.1	0.1	-10^{-2}	10^{-5}	10^5	Interception/London/Sedimentation			
This Study	10	1	2	10^{-3}	-10^{-5}	10^{-2}	10^8	Interception/London/Diffusion ^b			

a. Minimum values of the Peclet number are stated since N_{Pe} decreases, the contribution by diffusion to drop capture increases;

b. See Section 10.2

TABLE 5.1 Maximum Values of Dimensionless Groups Encountered in Coalescence Studies

$$\eta_I = 1.5R^2 \dots\dots\dots (5.10)$$

This equation shows the increasing influence of interception for increasing values of R. On the other hand, when the drag corrections are included in the trajectory analysis, a drastic decrease in collection rate results for $R > 5 \times 10^{-3}$. This follows from the fact that the hydrodynamic retardation introduced by the presence of the collector is effectively negligible when the particle is beyond a distance of about $10 d_p$ from the collector surface (82).

5.2.1.2 Hydrodynamic Retardation

Inspection of Equations 5.8 and 5.9 indicate that η_I increases as the parameter, R is increased and although this trend is observed in aerosol filtration, it does not apply to coalescers. The theory of classical interception, which is based on a non-slip continuous model for flow around the collector, becomes invalid when the separation between drop and collector is of the order of the mean free path length of the fluid molecules. For gaseous molecules, this length is approximately $0.1 \mu\text{m}$ and when the drop/collector separation approaches this value, the hydrodynamic resistance is reduced, thus facilitating capture by interception. For liquids, however, the mean free path is of the order of molecular dimensions and viscous interactions between drop and collector increases as the separation decreases because the rate of drainage of the intervening continuous phase film is reduced.

Hydrodynamic retardation of the interception mechanism

has been incorporated into the model of Spielman and Goren (80) which describes the trajectory of a drop in the vicinity of a cylindrical collector. Correction for the increase in drag forces, due to both fluid velocity and motion of the drop, was made using the universal hydrodynamic functions. Unfortunately the only available means to include hydrodynamic retardation effects is to perform a rigorous trajectory analysis. Rajagopalan and Tien (81) theoretically investigated the effect of retardation on deep bed filtration. Their trajectory analyses, using a single spherical collector model, predicted a monotonic reduction in capture efficiency as R was increased. It was also shown that retardation is significant when the drop/collector separation is less than ten drop diameters.

Consequently, for large values of R , hydrodynamic retardation is an important factor, specially when coalescence is induced in low porosity beds. Rajagopalan suggested that, in packed beds, the decrease in capture efficiency is offset by capture of drops by pores whose diameters are less than those of the drops. Although these effects are likely to occur simultaneously, their relative contributions to the drop capture efficiency have not been quantified.

5.2.2 Direct Interception

Interception by pore catchment occurs when an approaching drop is arrested by a pore through which it cannot pass (see Fig. 5.1). Bartle (60) suggested that other

drops would be captured and coalesced with a retained drop. This mechanism predominates in the coalescence of primary dispersions since it is well known that when the drop diameter is less than the equivalent diameter of the packing interstice, the coalescence rate is very low, even when the dispersed phase wets the packing (83). Direct interception of drops, with subsequent mechanical retention by the packing may be characterised by a second interception number, $R_d = \frac{d_p}{d_a}$. Inspection of R_d shows that pore catchment will contribute significantly to the capture rate when either drop diameter increases by coalescence, or when the equivalent diameter of the interstices, d_a is decreased. The latter occurs when drops captured and retained by the collectors reduce the effective area of the aperture available for flow of the dispersion. The capture efficiency by direct interception may be mathematically expressed as follows:

$$\begin{aligned} \eta_{DI} &= 1; & R_d &\geq 1 & \dots\dots\dots (5.11) \\ \eta_{DI} &= 0; & R_d &< 1 \end{aligned}$$

5.2.3 Inertial Impaction

When the density of the drops exceeds that of the continuous phase, sufficiently massive particles are unable to follow curvilinear fluid motion and tend to continue along a straight path as the carrier fluid curves around the collector, owing to inertia. This gives rise to enhanced collection on the approach side. The importance of impaction for gas-borne particles was recognised

quite early by numerous workers (84,85,86,87,88,89,90,91) in aerosol filtration where the density difference is high and the viscosity of the continuous phase is low (92).

In analysing impaction it is usually assumed that the particle deviates from the fluid motion in accord with Stokes' law for a sphere in an unbounded fluid. Hazlett (69) and Sherony (44) suggested this mechanism to be relevant to coalescence in fibrous beds and characterised its contribution by the magnitude of the Stokes' number

$$N_{Stk} = \frac{d_p^2 \rho_c u}{9\mu_c d_c}$$

Impaction becomes significant when N_{Stk} exceeds a critical value which depends on the Reynolds number. For viscous flow, values of $N_{Stk_{crit}}$ of between 0.1 and 0.9 (90) have been proposed and for potential flow conditions, Langmuir (90) determined $N_{Stk_{crit}}$ to be 0.063. The latter value was used by Sherony (44) for viscous flow conditions which would have overestimated the significance of impaction. Referring to Table 5.1 it appears that the majority of studies in coalescence appear to have been conducted under conditions where N_{Stk} is less than the critical value. Notable exceptions are the investigations of Sherony (44), Shalhoub (13) and Austin (14), but of these, only the work of Sherony involved a situation where the density of the dispersed phase was greater than that of the continuous phase. The other studies were therefore completed under conditions which preclude any contribution to capture by impaction.

An empirical expression relating capture efficiency by inertial impaction to the Stokes' number has been proposed by Landahl (90).

$$\eta_{II} = \frac{N_{Stk}^3}{N_{Stk}^3 + 0.77 N_{Stk}^2 + 0.22} \dots\dots\dots (5.12)$$

for $N_{Re} \leq 10$; $N_{Stk} > N_{Stk_{crit}}$

Impaction efficiency predictably increases with increasing particle size and fluid velocity. Impaction is important only for gas-borne droplets. For liquid-borne droplets the Stokes' number is usually very small, primarily because the viscosity is much larger. An important consequence of drop capture by impaction is the occurrence of a minimum in capture efficiency for increasing particle size.

5.2.4 Sedimentation

The density difference between dispersed and continuous phases also causes the drop trajectories to deviate from the fluid streamlines due to buoyancy forces. Their magnitude is characterised by the Gravity Number, $N_G = \frac{d_p^2 (\rho_d - \rho_c) g}{18 \mu_c u_c A}$ which is the ratio of the drop terminal velocity, assuming viscous flow conditions, to the superficial velocity of the dispersion flowing through the bed. Stechkina et al (93) showed that the efficiency for settling codirectional and counterdirectional to the mean flow is:

$$\text{Codirectional } \eta_G = (1 + \frac{d_p}{d_c}) \frac{u_s}{u} \dots\dots\dots (5.13)$$

$$\text{Counterdirectional } \eta_G = -(1 + \frac{d_p}{d_c}) \frac{u_s}{u}$$

Where $u_s = \frac{(\rho_d - \rho_c) g d_p^2}{18 \mu_c}$, the Stokes' settling velocity.

For $(\frac{d_p}{d_c}) \ll 1$, the second term in parentheses can be ignored giving $\eta_G \approx \frac{u_s}{u} \approx N_G$. This last result also holds for settling of very small particles onto spherical collectors (76). Theory shows for settling counter-directional to the flow that the negative contribution given by equation 5.13 cannot exceed the positive contribution owing to interception; otherwise net collection is zero (94).

Rajagopalan and Tien (81) recently confirmed that the capture efficiency is equal to the value of the Gravity number,

$$\eta_G = N_G; N_G > 10^{-3} \dots\dots\dots (5.14)$$

The condition associated with this equation is not restrictive since the contribution due to sedimentation is negligible for $N_G < 10^{-3}$.

With reference to Fig. 5.1, it should be emphasised that gravity forces aid drop capture upstream of the collector but oppose collection on the downstream side. This effect may be taken into account in rigorous determination of efficiency by trajectory analyses.

5.2.5 London-Van der Waals' Forces

Spielman and Goren (80) recognised that the long range attractive forces between a drop and collector may contribute to drop capture. These London or dispersion

forces increase rapidly as the drop approaches the collector to overcome the hydrodynamic retardation effects discussed in Section 5.2.1.2 or to offset any double layer interaction described in the following section. Dispersion forces arise due to the polarization of one molecule caused by fluctuations in the charge distribution within an adjacent molecule and vice-versa. These forces are, however, retarded because a finite time is required for propagation of electromagnetic radiation between the particles.

Hamaker (95) derived an expression from which the London attractive forces between a sphere and a plane surface neglecting electromagnetic retardation may be evaluated,

$$F_{Ad} = - \frac{2}{3} \frac{Q}{a_p} \frac{1}{(H+2)^2 H^2} \dots\dots\dots (5.15)$$

where a_p is the sphere radius

H is the dimensionless separation between the sphere and plane surface, $H = \frac{h}{a_p}$

Q is the Hamaker constant

Since the London force depends on separation, knowledge of the motion of a drop in the vicinity of a collector is required to determine the capture efficiency. Spielman and Goren (80), by considering a force balance on a drop, derived an equation to describe the critical trajectory. The capture efficiency may then be deduced since approaching drops, whose paths lie within the flow area associated with the critical trajectory, will contact the collector. The London force term given by

Equation 5.15 was modified using a more rigorous expression developed by Rosenfeld (46) to describe the attraction between a sphere and cylinder. Correction for electro magnetic retardation is also included.

$$\text{The Adhesion number } N_{Ad} = \frac{4Q}{9\pi R^2 A} \left\{ \frac{1}{\mu_c u d_p^2} \right\}$$

measures the ratio of London attraction to hydrodynamic forces and Spielman solved the trajectory equation analytically for small Interception numbers and large Adhesion numbers to give the capture efficiency in terms of this dimensionless parameter,

$$\eta_L = 2A_F R^2 \left(\frac{3\pi}{4} N_{Ad} \right)^{\frac{1}{3}} \dots\dots\dots (5.16)$$

which corresponds to Natanson's (96) result obtained by ignoring the hydrodynamic interactions. This occurs because the limiting trajectory gets displaced farther from the collector as N_{Ad} gets too large, diminishing the hydrodynamic interactions.

For the case of a spherical collection, Spielman and Goren (80) gave

$$\eta_L = 2A_S R^2 \left(\frac{9}{5} N_{Ad} \right)^{\frac{1}{3}} \dots\dots\dots (5.17)$$

for $N_{Ad} \gg 1$

5.2.6 Electrical Double Layer Forces

When two conducting phases are in contact, a difference of the electric potential is generally established between them. This potential is associated with an electric double layer at the surface, an unsymmetric distribution of electrically charged particles near the

phase boundary. A negative charge may arise when one phase is a metal and both positive and negative charges occur due to preferential adsorption or dissolution of one ionic species. The ionic double layer then forms by retention of mobile ions adjacent to the phase boundary by electrostatic attraction to the boundary charge. The interaction between the double layers surrounding the drop and collector may be repulsive or attractive depending on whether their respective charges are like or opposite.

The expression used for the repulsive double layer force was that derived by Hogg et al (82)

$$F_{DL} = \epsilon \xi_p \xi_c N_{DL} \left\{ \frac{e^{-N_{DL}H}}{1+e^{-N_{DL}H}} \right\} \dots\dots\dots (5.18)$$

where ϵ is the dielectric constant of the continuous phase; ξ_p and ξ_c are the zeta potentials marking the onset of the particle and collector Debye lengths respectively.

The Double Layer group $N_{DL} = \frac{\kappa d_p}{2}$, where κ is the reciprocal Debye length indicates the relative thickness of the double layer.

When the Electrokinetic group $N_{E2} = \frac{2\xi_c \xi_p}{(\xi_c^2 + \xi_p^2)}$ is positive, the force given by Equation 5.18 is repulsive and when the converse is true, the force is attractive.

For low electrolyte concentration in the continuous phase, double layer forces only become significant when the distance between drop and collector is less than to an order of 20 nm (97). As London forces also become important for separation of this magnitude, the relative

numerical values of these forces determine whether the surface interactions are favourable to promote drop capture.

Spielman (98) developed a criterion to neglect double layer forces in trajectory analysis which was based on the requirement that,

$$F_{DL} \ll F_{Ad} \quad \text{at} \quad H = H^* \dots\dots\dots (5.19)$$

where H^* is the dimensionless separation at the rear stagnation point of the critical trajectory.

Rajagopalan and Tien (81) established that the resultant force, calculated as the sum of the double layer interaction and the retarded London attraction, indicated no barrier against drop-collector contact for parameters relevant to coalescence processes. They concluded that these surface interactions, when considered as transport mechanisms are unimportant providing that their net effect is attractive in the vicinity of the collector.

An expedient way considering the case of unfavourable surface interaction is to regard the collection efficiency under these conditions to be a fraction of that under favourable interaction. This fraction could be related to the parameter, β introduced by Sherony (44) to account for the ratio of the number of coalescence events to the collision frequency.

5.2.7 Diffusion

Submicron sized drops possess a random transverse motion, Brownian motion, which causes them to depart from

the flow streamlines and promotes their deposition during flow past a collector, and may contribute to the capture efficiency. Inclusion of the random force that induces Brownian motion into equations describing drop trajectories, considerably complicates their solution but Prieve and Ruckenstein (99) have demonstrated that separate treatment of this mechanism is adequate.

The Brownian-diffusion coefficient of a particle with radius d_p is given by the Stokes-Einstein equation (100):

$$D = \frac{k'T}{6\pi\mu_c d_p}$$

where k' is the Boltzmann's constant and T is the absolute temperature. Langmuir (79) first treated Brownian deposition on a cylinder by a very approximate method. Natason (96) and Friedlander (101) improved upon this independently by solving the boundary-layer form of the equation of steady-state convective diffusion.

Brownian particle diffusivities are generally much smaller than molecular diffusivities, assuring large Peclet numbers so the approximation of a thin boundary layer may be used. The Peclet number, $N_{Pe} = \frac{d_c u}{D}$, is often introduced to characterise diffusion and is a measure of the ratio of transport by convective forces to transport by molecular diffusion. Many workers investigating diffusion for low Reynolds' numbers and small particle sizes employ the Sherwood number, $N_{Sh} = \frac{I}{\pi d_c \delta c}$ as a measure of the mass transfer or deposition rate. This approach is useful for correlation of results for different collector geometries. For a cylindrical

INVESTIGATOR	Proposed Transport Equation	Diffusion Capture Efficiency, η_D (Modified Form)	Calculated Value $\times 10^{-5}$
Spielman (71)	$\eta_D = 2.3 A_S^{1/3} N_{Pe}^{-2/3}$	$2.3 A_S^{1/3} N_{Pe}^{-2/3}$	4.00
Langmuir (79)	$\eta_D = 2.16 A^{1/3} N_{Pe}^{-2/3}$	$2.16 A_S^{1/3} N_{Pe}^{-2/3}$	3.76
Rajagopalan (81)	$\eta_D = 4.04 N_{Pe}^{-2/3}$	$4.04 N_{Pe}^{-2/3}$	2.09
Natanson (96)	$N_{Sh} = 1.17\pi A_S^{1/3} N_{Pe}^{1/3}$	$3.64 A_S^{1/3} N_{Pe}^{-2/3}$	6.33
Prieve (99)	$N_{Sh} = 0.995 N_{Pe}^{1/3}$	$3.98 N_{Pe}^{-2/3}$	2.06
Ranz (90)	$\eta_D = \frac{\pi}{N_{Pe}} \left\{ \frac{1}{\pi} + 0.55 N_{Sc}^{1/3} N_{Pe}^{1/2} \right\}$	$N_{Pe}^{-1} + 1.727 N_{Re}^{1/6} N_{Pe}^{-2/3}$	0.95
Friedlander (215)	$N_{Sh} = 1.035\pi A_S^{1/3} N_{Pe}^{1/3}$	$3.25 A_S^{1/3} N_{Pe}^{-2/3}$	5.66
Levich (216)	$\eta_D = \frac{7.98}{\pi} A_S^{1/3} \left(\frac{D}{a_g} \right)^{2/3}$	$4.03 A_S^{1/3} N_{Pe}^{-2/3}$	7.01
Eml (214)	$\eta_D = 6 N_{Re}^{1/6} N_{Pe}^{-2/3}$	$6 N_{Re}^{1/6} N_{Pe}^{-2/3}$	3.31

a - Calculations performed for A_S 37.98 from Happel's Cell Model

$$N_{Re} = 1.458 \quad N_{Pe} = 8.49 \times 10^7$$

TABLE 5.2 Comparison of Equations Describing Drop Capture by Diffusion

collector, the Sherwood number is related to capture efficiency by the following,

$$N_{Sh} = \eta_D N_{Pe} \dots\dots\dots (5.20)$$

Rajagopalan and Tien (81) give the following relationship for a spherical collector:

$$\eta_D = 4.04 N_{Pe}^{-\frac{2}{3}} \dots\dots\dots (5.21)$$

The equations developed through several investigations of transport by diffusion have been arranged using Equation 5.20 and presented in Table 5.2. They show a common relationship between capture efficiency and Peclet number, with slightly differing dependancy on Reynolds' number, and any of the equations may be applied without incurring significant errors especially since the capture efficiency due to diffusion alone is relatively small.

In addition to capture of the drops by a stationary collector, coalescence between pairs of drops moving in the interstices of the packing is feasible by the mechanism of turbulent coagulation. There have been a number of attempts to analyse the coalescence and breakup of a dispersion in a turbulent field (102,103,104) and it is apparent that this mechanism is less important in the drop capture, as it is dependent upon the flow in the bed and the coalescence efficiency falls off at large values of N_{Re} .

However, Sherony (44) and Shalhoub (13) evaluated a theoretical collision frequency due to coagulation using the hydraulic diameter of the interstices as a first

estimate for the size of large scale turbulence. Their calculations indicate a negligible contribution by this mechanism which is supported by experimental observations as discussed in Section 5.2.

This section concludes the description of drop capture mechanisms known to feature in secondary dispersion coalescence; their relative contributions to the overall capture efficiency are further investigated quantitatively in Section 10.2.

5.3 COALESCENCE PROCESSES

5.3.1 Coalescence Sites

The suspended drops captured by the packing fibres will continue to grow by further capture and coalescence until they eventually become so large that hydrodynamic forces cause their detachment from the coalescence site. When the drops are small compared with the collector and aperture diameters, coalescence may take place between adjacent drops located on the collector surface (Fig. 5.2a). Bitten (66) reported that this is a slow process for the coalescence of drops on single fibres compared to growth by acquisition of the dispersed phase from the flowing dispersion (Fig. 5.2b).

Coalescence of a drop into a liquid film, which either adheres to the collector surface or occupies the packing void, has been proposed by Davies and Jeffreys (55) as the predominant mechanism for primary dispersions when the dispersed phase wets the packing (Figs. 5.2c and 5.2d). For the converse situation, coalescence may occur



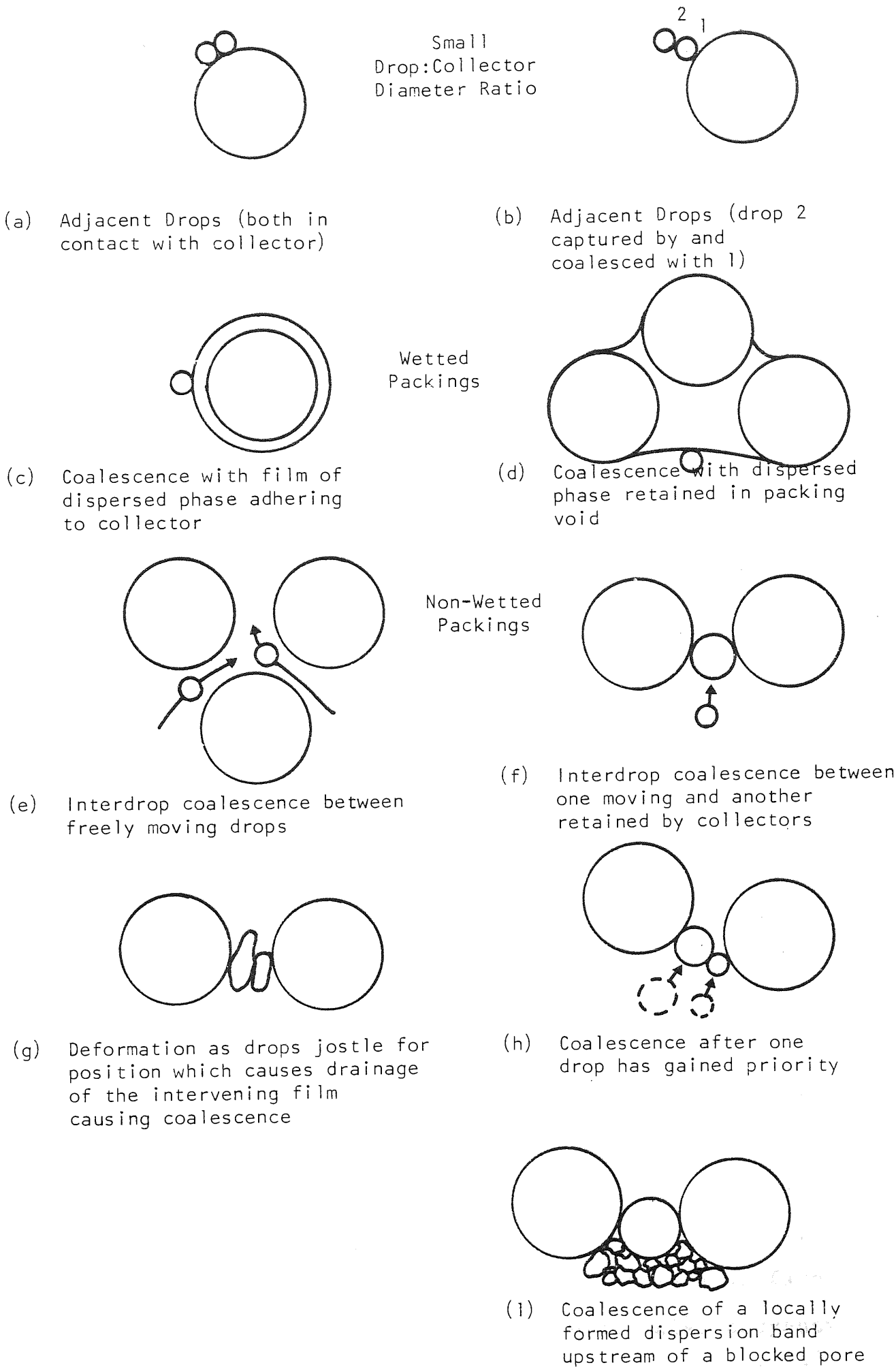


FIG. 5.2 Coalescence Mechanisms in a Packed Bed

between two freely moving drops (Fig. 5.2e) which may be important for primary dispersions but experimental observations refute this possibility for secondary dispersion coalescence (39,44). Alternatively, drops captured by direct interception and retained by the collectors, may then trap other approaching drops and subsequently coalesce with them (Fig. 5.2f). Wilkinson (105) investigated the behaviour of primary drops, that did not wet the packing, trapped in the interstices of a bed of random packed glass spheres. He showed that drops increase their volume by coalescing until the buoyancy forces exceed the restraining interfacial tension forces; deformation of the drop then occurs as it is squeezed through the aperture.

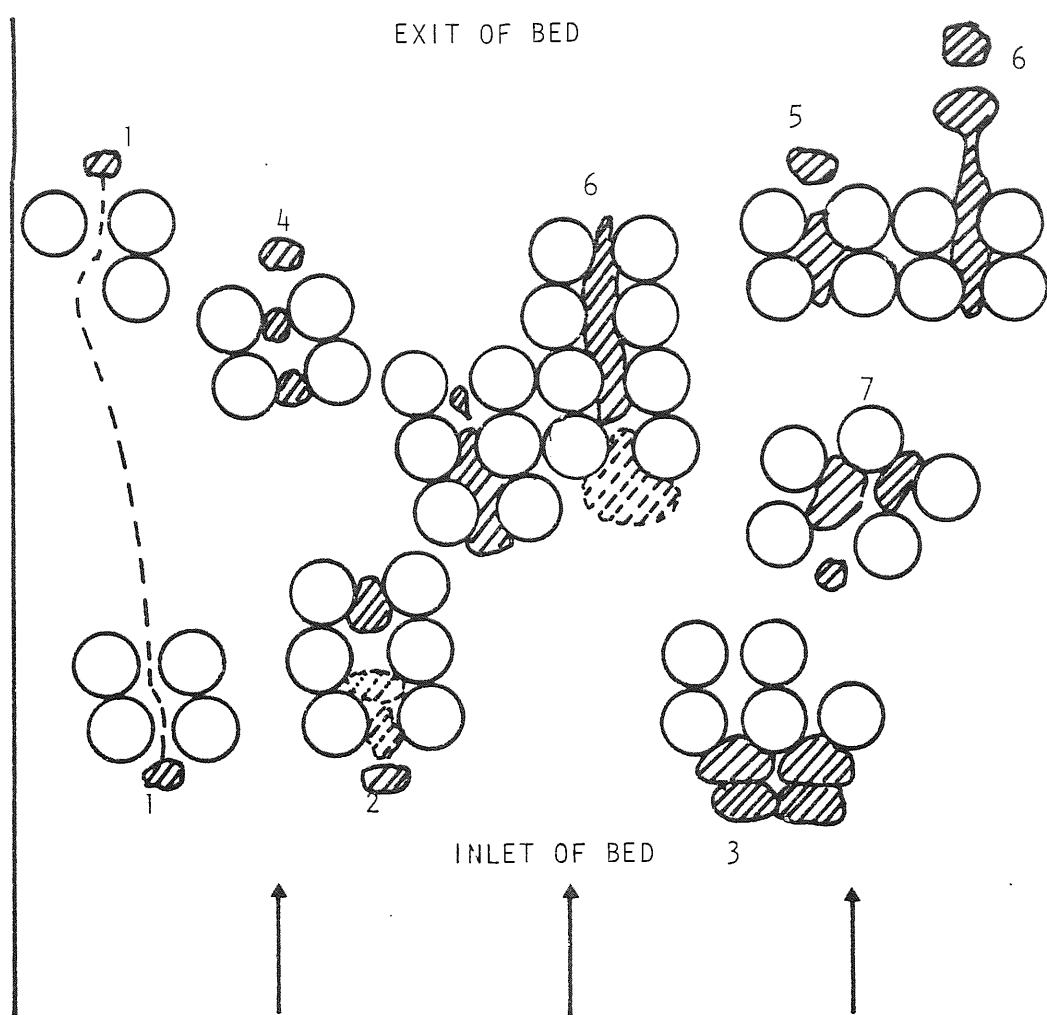
5.3.2 Drop Passage Through Interstices

Drops which simultaneously approach a pore are likely to jostle for priority before one of them passes through it (Figs. 5.2g and 5.2h). Various mechanisms for the passage of drops through the packing voids have been proposed by Wilkinson (105) as illustrated in Fig. 5.3. It is clear that the probability associated with each mechanism depends on the value of the direct interception number, R_d (See Section 5.2.2).

However, important differences exist between the conditions under which secondary and primary coalescers operate. Firstly, secondary drops possess more surface energy per unit mass due to their size and also buoyancy forces are usually negligible as shown by the magnitude

of the gravity number in Table 5.1. Therefore drop deformation and drainage of the intervening continuous phase film prior to coalescence is less easily accomplished. For this reason, the retention-impact-release mechanism, whereby small individual drops deform to pass through micron sizes pores is unlikely to be important for secondary dispersions.

Unrestricted drop passage, may also be insignificant since as will be demonstrated in the following section, drops attaining a critical diameter for release from a collector are likely to be immediately recaptured by direct interception. This provides evidence that pores may become blocked by large drops or by simultaneous approach of smaller ones. If it happens frequently fewer channels are available for flow of the dispersion and the pressure gradient per unit length of the bed will increase. Captured drops will then be induced to retreat to sites where the interstitial velocity is low so offering least resistance to the flow of the continuous phase. As a result, the drops will tend to concentrate in relatively few channels where they queue in a localised 'dispersion band' type formation until coalescence occurs with adjacent drops and the drop which blocks the pore. As more flow paths become blocked, eventually the increasing pressure gradient will be sufficient to force coalesced drops through the pores. This proposed mechanism, illustrated in Fig. 5.2i, is also consistent with observations of thread formation by restricted drop release (see Fig. 5.3) as coalesced pools of



1. Unrestricted drop passage
2. Restricted drop passage (penetration due to kinetic forces)
3. Inlet drop restriction
4. Retention - impact - release
5. Unrestricted drop release
6. Restricted drop release
7. Preferential flow-path

FIG. 5.3 Proposed Droplet Hydrodynamics in a Non-Wetted Packing of Equal-Sized Spheres

dispersed phase are squeezed through the apertures of the packing.

This discussion has been confined to cases where the dispersed phase is non-wetting but it is suggested that this mechanism could equally apply to wetting situations. An experimental study of collisions and coalescence of drops on single fibres (66) showed that capture efficiency is unlikely to be affected by whether or not the fibre is wetted. But the passage of drops through the pores will meet with less resistance, due to capillary action, as they coalesce directly with a flowing continuum of the dispersed phase. This behaviour would imply a relatively lower pressure drop for beds where the dispersed phase wets the packing. Lower pressure gradients, due to easier drop removal from the coalescence site, may, however, alleviate deformation of drops in the local 'dispersion bands' with a possible lowering of coalescence efficiency.

5.4 DISPERSED PHASE FLOW REGIME

Drops, which have been collected by the packing fibres and reside in the packing interstices until they are coalesced, act as potential collectors for other drops entering the bed. Therefore, both the number and distribution of drops within the packing are important factors governing capture rate and pressure drop under steady conditions.

5.4.1 Drop Redispersion

After coalescence by one of the mechanisms described in the previous section, movement of the coalesced dispersed phase may occur by release of the drop from the fibre when the drag forces exceed adhesive and London attractive forces as shown in Fig. 5.4.

Adhesive failure causes release of the whole drop but when adhesion is strong and interfacial tension low, Vinson (58) states that cohesive failure results when only part of the drop is detached. The cohesion mechanism involves formation of threads which subsequently break up into smaller drops which are then redispersed into the flowing continuous phase. The size of these drops depends on attenuation of the liquid threads which is suggested to be a function of the viscosity ratio μ_d/μ_c (58) although there is no experimental evidence to support this hypothesis. Internal drop release by cohesive failure is thought to be responsible for low filter coefficients when the dispersed phase exhibits a high wetting affinity for the packing material (33). Also the existence of a critical velocity, above which redispersion considerably reduces efficiency has been reported by many workers but the value of this velocity varies over two orders of magnitude (13). Therefore, these values are of little use in practical coalescer design because they are specific to the liquid systems and properties of the packing studied. Clearly, further work is required to discover the relationship between critical velocity and system characteristics to predict the conditions likely

to cause redispersion.

In addition to cohesive failure, redispersion may also be attributed to secondary drop formation during the coalescence process (106) and when coalesced drops are squeezed through pores at high velocities (105).

5.4.2 The Travelling Drop Hypothesis

Sherony and Kintner (44) and Rosenfeld and Wasan (70) among others proposed that drop release is by adhesive failure, after which the large drops travel through the pores of the medium, eventually being released at the downstream face. Their models, presented in Section 10.1 describe coalescence of secondary dispersions in high porosity beds and are based on this travelling drop hypothesis.

They assume that a pendular saturation (Fig. 5.5a) regime prevails within the bed which precludes the existence of a dispersed phase continuum. Rosenfeld (46) claims that the assumption is justified when the dispersed phase is dilute and because channels should not be present in beds with porosities greater than 0.9. However Brown (107) showed that the dispersed phase passed through the intermediate portion of a bed using the same channels repeatedly. The threads were observed to pulse and they varied in diameter and flowrate with time. In many cases, the threads were discontinuous, but when flow restarted, the same channels were utilised. Similar behaviour was reported by Hazlett (57) when threads of water were observed in a fibrous bed during the coalescence

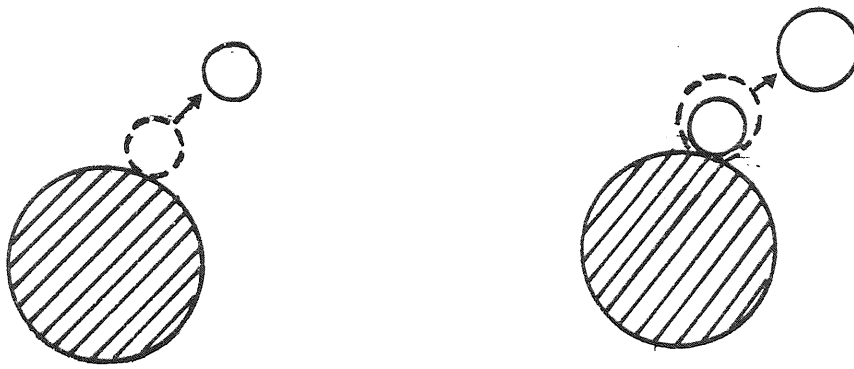
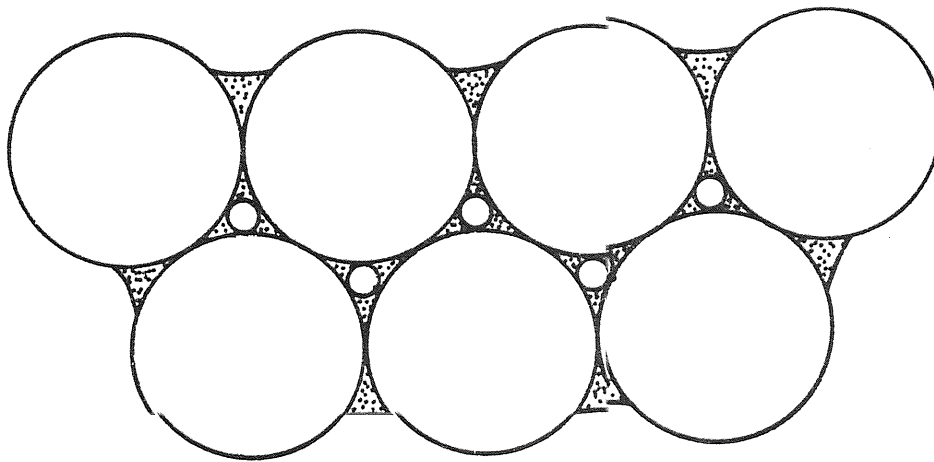
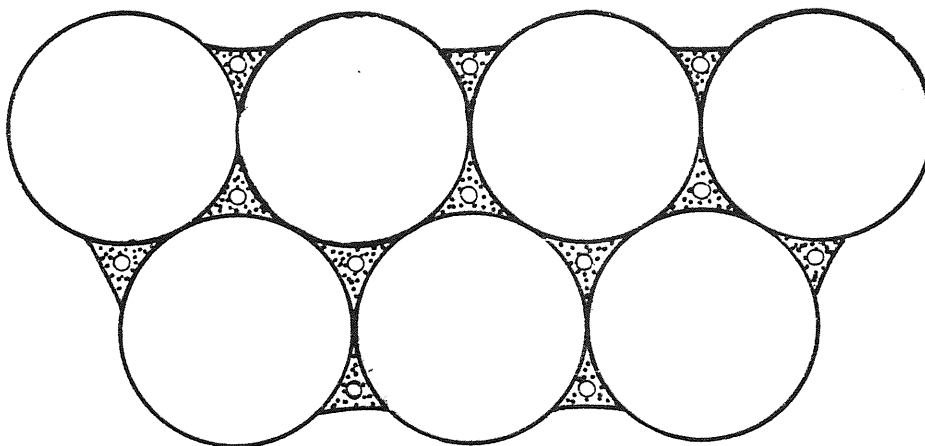


FIG. 5.4 Internal Drop Release Mechanisms



(a) Pendular



(b) Funicular

Fig. 5. 5 Pendular and Funicular Saturation Regimes for an Idealised Porous Medium of Packed Spheres

of a water in fuel dispersion. This experimental evidence suggests that a funicular saturation regime would better represent the dispersed phase distribution (Fig. 5.5b).

The saturation in a coalescer, defined as the fraction of pore space occupied by the dispersed phase, cannot be a unique function of the phase ratio of the inlet dispersion. It must also depend on interaction between the packing fibres and the two liquid phases and the superficial velocity. Shalhoub (13), using a conductivity technique, in high porosity beds showed that saturation was independent of phase ratio. Saturations in the region of 20% are typical for high porosity beds (45) but if the coalesced dispersed phase flows in a small number of preferential channels, then a low saturation does not necessarily imply the absence of a continuum.

5.4.3 Critical Drop Diameter

The travelling drop models also assume that when drops are detached from fibres, their passage through the bed to the exit face remains unimpeded. Their diameters should therefore be less than the pore diameters. Bitten (66) described visual observations of coalescence of water drops in jet fuel on individual fibres of treated and untreated glass, Teflon, Dacron and Nylon. With the exception of Teflon, individual fibres were reported to retain drops having diameters many times that of the fibres without re-entrainment by the flow at .

velocities up to 2×10^{-2} m/s. For glass fibres of diameter 5-6 μm , drops of diameters of 400-500 μm adhered to the fibre without being released. Even for the least retentive fibre tried - Teflon- with a fibre width of 16-17 μm , adhering drops reached diameters of 65 to 75 μm before release. It is therefore concluded that characteristic interfibre spacings of 2 or 3 fibre diameter for typical packed fibrous media will not permit progressive travel of drops whose diameters are 90 or even 5 fibre diameters. Such drops, if unattached, should become wedged in place where continued growth by coalescence with impinging drops occur which further ensure their immobility. Also, interfacial tension resists deformation of drops that might permit them to be squeezed through the pores by buoyancy forces. The travelling drop mechanism is thus improbable except possibly for media that are packed to very low density.

5.4.4 Dispersed Phase Continuum Model

Spielman and Goren (45) assumed that two readily distinguishable regimes of the coalescing oil phase exist within the packing. One regime consists of droplets that are suspended in the continuous phase; the other is the coalesced dispersed phase that is held up within the pores and assumed to form a network of channels which are sufficiently well connected to support viscous flow of the dispersed phase by capillary-conduction. This model implies that captured drops are immediately coalesced into the continuum which is

contrary to observations since coalescence time is large for drops of secondary dimensions.

Spielman and Su (72) recently proposed three distinct regimes of coalescing phase : dispersed microdrops suspended in capillary-conducted continuous phase; capillary-conducted dispersed phase forming well connected channels; held-up dispersed phase as discrete coalescing drops that act as an intermediary between the dispersed phase microdrops and the capillary-conducted dispersed phase. They assumed that the intermediary phase constituted the majority of the total dispersed phase saturation with only a negligible proportion being comprised of newly captured drops and the capillary-conducted phase. Although feasible, this assumption cannot be universally applied because, if the diameter of the captured drops are comparable to the mean pore diameter, then the proportion of the intermediary phase would be considerably less.

In conclusion, the dispersed phase flow regime proposed by Spielman and Su is probably the most accurate description and is, in most respects, consistent with experimental observations especially for low porosity packings.

5.5 SATURATION PROFILES

The distribution and quantity of dispersed phase held up in a packed bed depends on the capture, coalescence and internal drop release processes. Therefore, the nature of the saturation profile over the bed depth is closely related to the dispersed phase

flow regime.

Without exception, those workers who postulated the travelling drop hypothesis assumed that the saturation is low and independent of axial position in the bed. An increase in saturation decreases the effective void fraction of the packing and so decreases the continuous phase permeability. Sherony and Kintner (44), Shalhoub (13) and recently Austin (14) showed that the Blake-Kozeny equation accurately described single phase flow in packed beds (see Chapter 9). By substituting experimental values of two phase pressure drop into this equation, the effective voidage, e_2 may be calculated. The average saturation in the bed is then determined using:

$$\bar{S} = 1 - \frac{e_2}{e_1} \dots\dots\dots (5.22)$$

Rosenfeld (46) used this method to investigate the variation of bed saturation with velocity and produced the following empirical equation,

$$\bar{S} = 2.92 \frac{(1-e_1)u^{-0.2}}{e_1} \dots\dots\dots (5.23)$$

The use of an average saturation is however of limited value since experimental evidence has conclusively proved that saturation varies considerably through the length of the bed. Bitten and Fochtman (108) measured the distribution of water in a fibrous bed where a hydrocarbon jet fuel was the continuous phase. They determined the saturation profile by dismantling the bed after operation and analysing the quantity of water retained

in different sections of the bed after extraction using anhydrous methanol. The maximum saturation occurred at the influent face of the bed which rapidly decreased to a fairly constant value for the remaining two thirds of the bed length. Fluctuations about this constant saturation were observed in the end part of the bed which were attributed to local changes in interstitial velocity caused by perforated plates separating the bed sections.

These data are in sharp contrast with those of Richardson et al (109) who reported an increase in the saturation of the bed exit whilst remaining constant at the inlet and over a majority of the bed length. The discrepancy between Bitten's data and Richardson's results is the increase in saturation at the inlet of the bed. Collins (110) mentions that there are boundary effects at the inlet of the bed but these disappear after steady state is reached, but this is unlikely in Bitten's case in view of the consistency of his results.

An increase in superficial velocity always increased the saturation in the forepart of the bed and decreased the saturation in the middle. High velocities also produced a dampening of the internal fluctuations. Low porosity beds possessed much higher saturation values than high porosity packings and the phase ratio of the inlet dispersion did not significantly affect the saturation. These observations indicate that the majority of capture and coalescence predominates in a relatively narrow section in the forepart of the bed

and Bitten and Fochman (108) showed that increasing the length of a bed did not increase the coalescence efficiency or total holdup of dispersed phase.

Shalhoub (13) qualitatively investigated the holdup profile by measurement of electrical conductivity between copper meshes embedded in a fibreglass packing, whilst coalescing a toluene in water dispersion. His measurements confirmed the results of Bitten and Fochman (108) but the saturation was found to increase significantly near the exit face for which no explanation was given.

The inherent problem of determining saturation profiles, especially for thin, low porosity beds, is selection of a technique to measure the local holdup without disturbing the coalescence process. Spielman and Su (72) surmounted this difficulty by investigating saturation profiles in beds of glass ballotini having depths in excess of 200 mm. They were able to determine holdup using an x-ray absorption technique and also by calculation of permeability from pressure drop measurements taken over increments of the bed length. The results from these techniques exhibited close agreement and the shapes of the saturation profiles were very similar to those obtained by Bitten and Fochman. Also, samples of the dispersion were taken from corresponding positions in the bed and the rate of coalescence of the dispersion showed a first order dependence on the dispersed phase saturation.

Experimental data indicate, for both high and

low porosity beds, that saturation decreases from a high value near the inlet face to a constant value over the remainder of the bed. Drop capture and coalescence processes predominate where the saturation is high and flow of the coalesced phase, probably in discrete channels, is associated with a constant holdup.

The saturation profiles determined by previous experimental studies are examined in greater detail in Section 10.4 as they form the basis for a mathematical model which attempts to describe the variation of saturation with bed depth.

5.6 EXIT DROP RELEASE

Following repetitive capture and coalescence throughout the packing, enlarged droplets should ideally be released from the exit face with a minimum of redispersion or break up. Various observed drop release patterns are illustrated in Fig. 5.6.

(a) Ballooning

In an ideal situation, one thread feeds a drop at the downstream face of the bed. The balloon-shaped drop then grows until the hydrodynamic buoyancy forces exceed the interfacial tension. Hazlett (111) stated that adhesion forces may be significant when the dispersed phase wets the packing material. For the non-wetting situation, Hazlett (69) derived an expression to predict the size of released drops,

$$d_{pe} = \frac{0.55 d_a^{0.71} \gamma^{0.71}}{\Delta u \rho_c^{0.29} \mu_c^{0.43}} \dots\dots\dots (5.24)$$

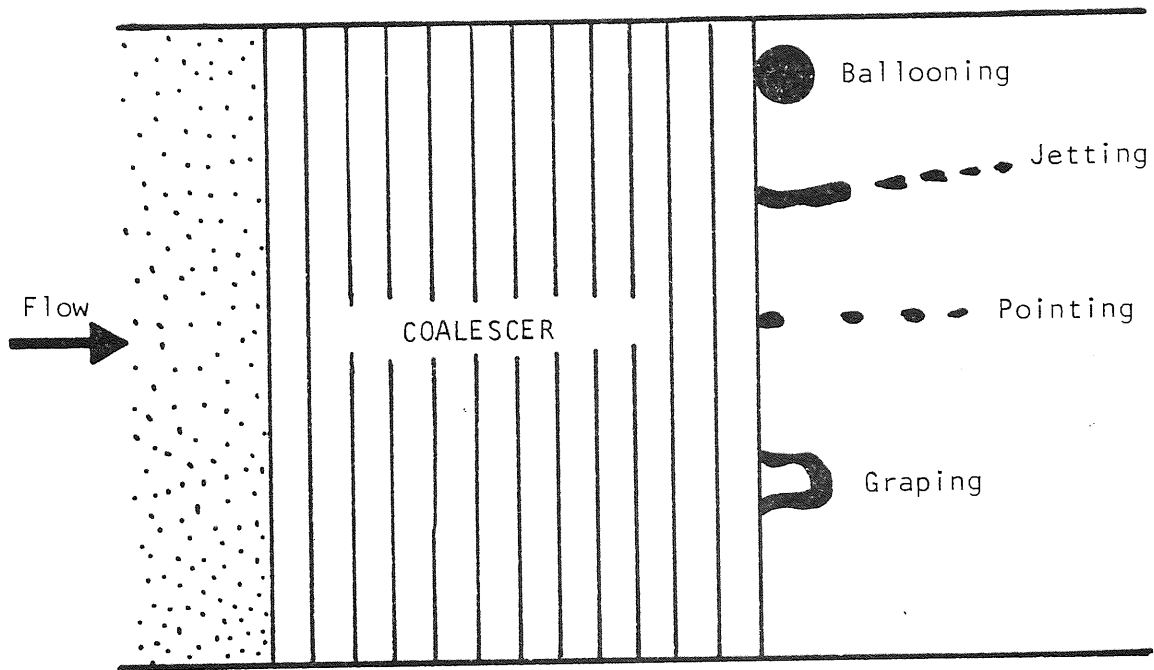


FIG. 5.6 Exit Drop Release Mechanisms

for $d_a < 0.1 d_{pe}$

and $0.3 < N'_{Re} < 100$ where

$$N'_{Re} = \frac{d_p \rho_c u}{\mu_c}$$

To apply this equation, it is necessary to experimentally determine the flowrate of dispersed phase in the supply channels so that the difference between drop and continuous phase velocities, Δu may be evaluated.

(b) Jetting

When surfactants are present in the liquid system, an extended thread or jet of the dispersed phase ruptures by Rayleigh instability to form a series of small drops of uniform diameter. Many correlations reviewed by Wilkinson (105) are available for prediction of drop sizes by jetting and other mechanisms but they only apply when the continuous phase is stationary. Inclusion of a term to account for hydrodynamic forces caused by the flowing continuous phase would considerably enhance the scope of such equations and this aspect is worthy of further study.

(c) Pointing

Another type of release mechanism is pointing, in which 'fingers' of collected drops project beyond the exit face. These 'fingers' taper to a point, vibrate and kick small drops from the tip.

(d) Graping

Langdon (40) and Lindenhofen (63) reported a graping release pattern which is encouraged when the phase ratio is high or when the dispersed phase wets

the packing. This mechanism produce bubbles of the continuous phase enclosed by a film of the dispersed phase. After release, the bubbles frequently agglomerate in clusters and may eventually burst to produce a large number of very small drops.

Attarzadeh (112) has recently observed that drop formation takes place by a combination of all the mechanisms described above when the bed consisted of random fibres. However formation by ballooning or the drip point mechanism is desirable since it produces large drops that require short residence times in a settler.

CHAPTER SIX
EXPERIMENTAL WORK

CHAPTER SIX
EXPERIMENTAL WORK

6.1 EQUIPMENT DESIGN

The function of the ancillary equipment used was to supply a secondary dispersion of known drop size and dispersed phase concentration at a specified flowrate to a coalescence section. Lines and apparatus were incorporated to facilitate recycling of the liquid during single phase pressure drop measurements, and for irrigation of the glass ballotini beds with the dispersed phase during coalescence operations.

The flow diagram of the apparatus is shown in Fig. 6.1 and the general arrangement presented in Fig. 6.2. The continuous phase was produced by distillation of tap water using an electrically heated still with a capacity of 8 dm³/h. Water leaving the still at 330°K was allowed to cool to ambient temperature in a 350 dm³ capacity tank of stainless steel construction. The baffles and turbine agitator were included in this design to permit investigation of coalescence when the continuous phase contains dissolved or dispersed solids. The maximum liquid level inside the tank was automatically controlled using a pressure sensor which is connected to the boiler power supply. It was essential to cover the storage tank because the partially de-aerated water would otherwise reabsorb air during cooling which would be evolved at many points throughout the equipment. The large number of potential nucleation sites and a relatively rapid fall

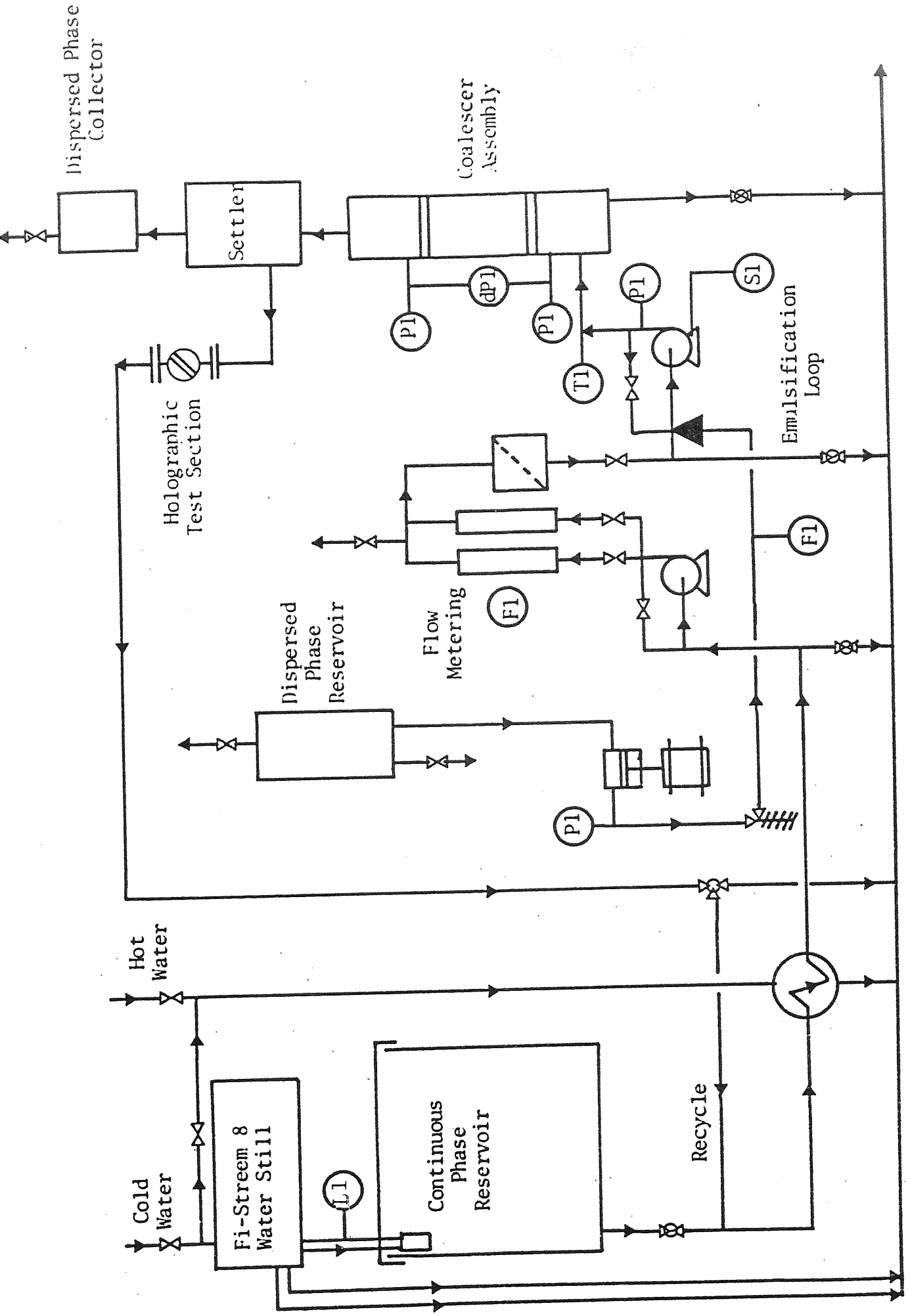


FIG. 6.1 Flow Diagram of Equipment

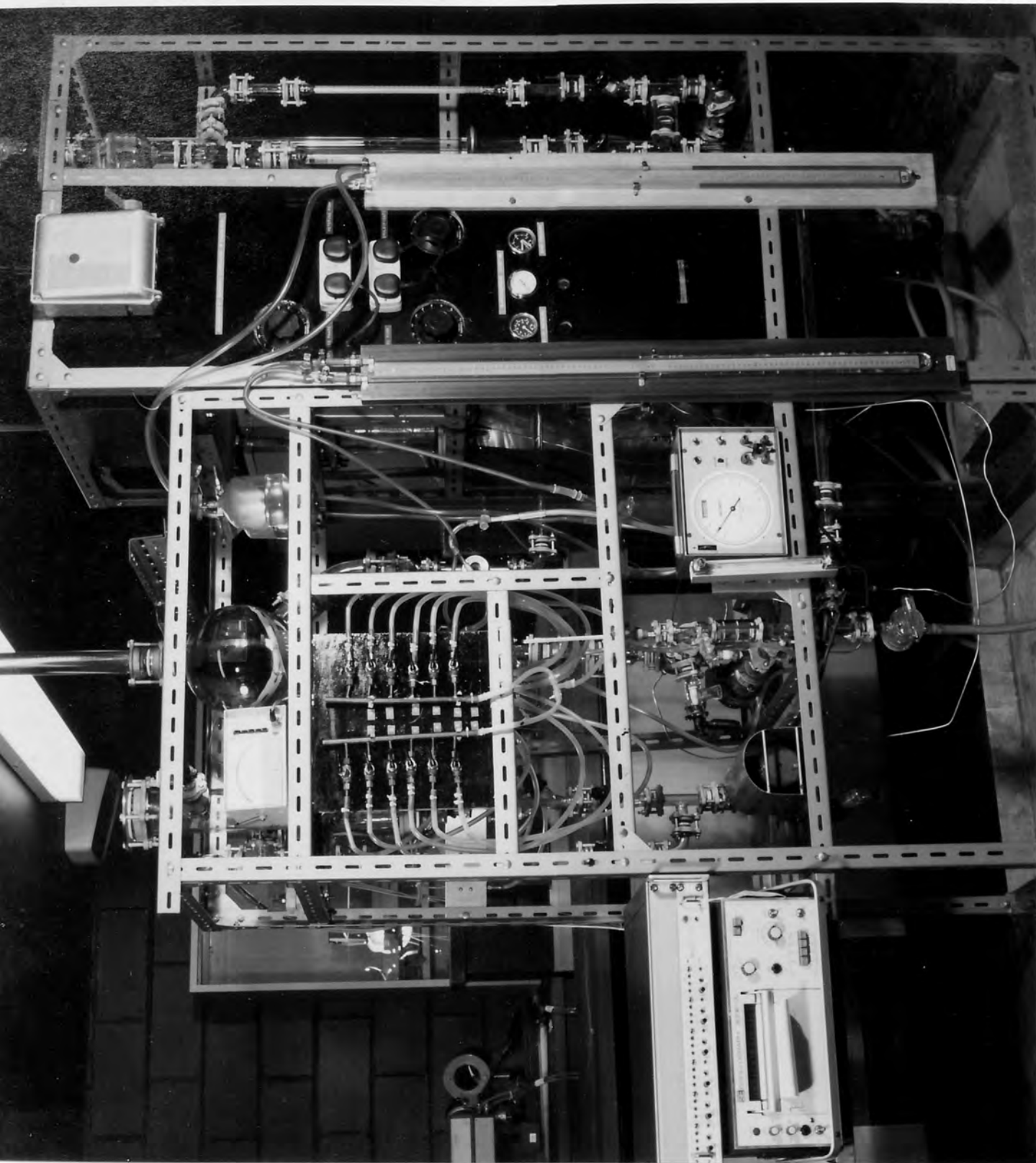


Figure 6.2
General Arrangement
of Equipment.

in pressure would cause considerable air evolution within the coalescer producing apparently high pressure drops and erratic drop release during operation.

Coarse adjustment of the continuous phase temperature was accomplished using a water cooled heat exchanger. A gravity-fed stainless steel centrifugal pump with Viton seals was used to transfer the water through the flow metering equipment, coalescence device, and via gravity settling vessel to drain. Accurate flow control was maintained using a combination of a rheostat installed on the pump power supply, control valve on the delivery line and a control valve on a loop line between the delivery and suction sides of the pump. Flowrates were monitored using two glass rotameters, one with a stainless steel float and one with a koranite float which provided a range of superficial velocity from 0 to 7×10^{-2} m/s within the coalescer. Preparation of the continuous phase was completed by filtration through a sintered glass disc of 110 μm pore size. Glass pipelines of 18.0 mm bore, connected using P.T.F.E. gasket rings were used throughout the construction to permit visual detection of possible air ingress, whilst facilitating easy cleaning and avoiding contamination of the liquid systems. Stainless steel was employed in the fabrication of non-standard components such as reducing flanges and vessel covers.

From a storage vessel, the dispersed phase was gravity fed through 3 mm bore stainless steel tubing to a metering pump operating at 100 strokes/minute and giving a maximum flowrate of $0.230 \text{ dm}^3/\text{hr}$ of the dispersed

phase. Using a pressure relief valve, the delivery pressure was maintained at approximately 3 bar which ensured efficient operation of the non return valves in the pump head during the suction stroke and prevented excess flow due to the head of the liquid in the storage vessel during delivery. A variable area flowmeter, containing a stainless steel ball float, placed downstream of the pressure relief valve confirmed that the pump delivered the desired flowrates consistently and accurately. However, due to the reciprocating action of the pump, fluctuations were observed in the delivery pressure and to a lesser extent in the measured flowrate.

The mixing and emulsification techniques available for production of a secondary dispersion are described in Chapter 2. A centrifugal pump with a recycle loop was selected for its inexpensive, simple construction and ease of operation and control. Previous work (12,13,14) showed that for a given throughput and pump design, the angular velocity of the impellor determined the mean drop size produced. This has been confirmed and the results are discussed in Chapter 8. The pump speed was monitored using an electronic tachometer and maintained at a constant value of 67 rev/s using a rheostat. The dispersed phase was injected through a 1 mm bore stainless steel tube into the suction line of the pump causing immediate break up of the organic phase forming a secondary dispersion. Separation of the dispersion within the recycle loop was not observed even after considerable operating periods and the oscillations caused by the

metering pump delivery were effectively damped for all throughputs.

Both transfer of the continuous phase and the emulsification process using centrifugal pumps caused variable and significant increases in the liquid temperature thus preventing isothermal operation over long periods. The liquid temperature was measured upstream of the coalescer using a thermometer inserted in the recycle loop.

After passing through the coalescer, the primary dispersion produced is recovered in a 685 mm diameter settler placed above the bed and the effluent flows through the holographic test section whose design has been discussed in earlier work (14).

6.2 COALESCER DESIGN

Difficulties in reproducing results in coalescence studies have often been attributed to system contamination via the materials of construction. In this study, surface active contamination was minimised by using only glass, stainless steel and P.T.F.E. The coalescer column was a 38.1 mm bore and 300 mm length glass pipe which allowed for different bed depth experiments to be carried out. Pressure taps made of 5 mm bore glass pipe were fitted at 10 mm intervals along the coalescer column. The glass ballotini packing was confined to the column by using Becosyn, stainless steel meshes supplied by Begg Cousland Ltd. with P.T.F.E. rings to be used as the gaskets when assembling the column to the rest of the

equipment. The mesh size used was the largest which would retain the granular material for each particular experiment. This minimised clogging effects at the inlet of the dispersion and less pressure effects at the pressure taps. The coalescer column and the mesh supports are shown in Fig. 6.3 and Fig. 6.4.

6.3 PACKING SELECTION AND PREPARATION

Many recent investigations into the coalescence of secondary dispersions in packed beds have employed randomly arranged matrices usually consisting of glass fibres (13,56,70,71). Glass as a raw material is favoured because it is relatively inexpensive, is resistant to the extreme thermal and chemical environment commonly used in cleaning procedures and its wetting properties may be modified by the attachment of silicone groups to the surface of the fibres (113).

Simple compression of a quantity of fibrous material to the required voidage fraction produces an acceptable structure, but frequently the glass fibres used have a distribution of diameters and the above packing technique produces a bed with a pore size distribution and where the fibre orientations are unknown. The lack of an accurate geometrical description of the bed has favoured investigations where the coalescer packing consists of layers of fine woven meshes, where the fibre diameter and mesh apertures are constant, the fibre orientation is known and different packing characteristics can be expressed mathematically in terms of these known factors.

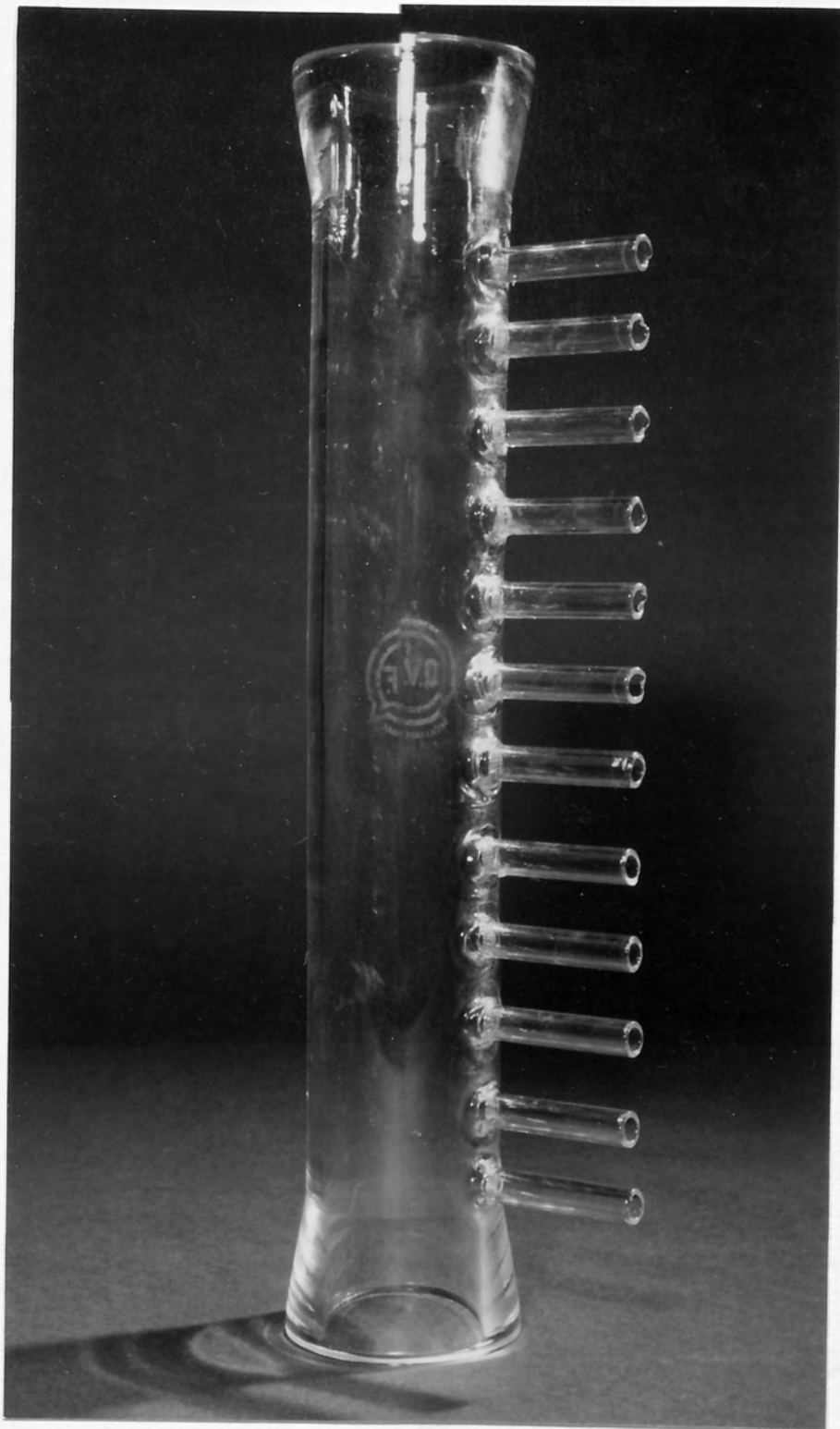


Figure 6.3 Coalescer Column for Pressure Drop Measurement

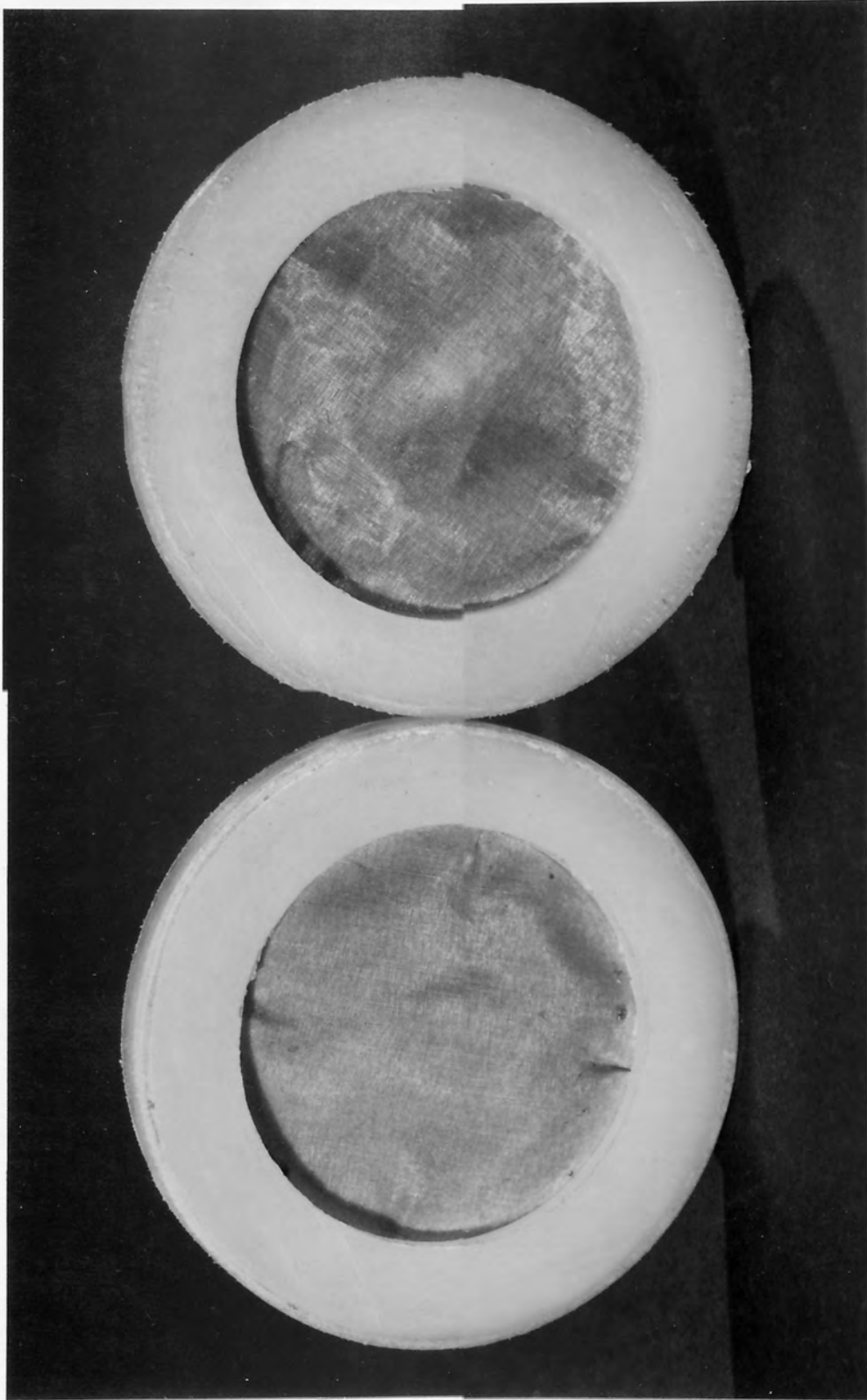


Figure 6.4 Stainless Steel Supporting Mesh with Polypropylene Moulding.

Fibrous media, which can be made to have both higher porosities and higher specific surface than granular media, are observed to give more complete phase separation than granular solids for the same bed depth and operating conditions. This makes fibrous media appear more attractive from the standpoint of space requirements. However, even small amounts of suspended solids, which are sometimes unavoidable present, can rapidly accumulate to clog fibrous media to such degree that their use over extended periods is prevented. Also, their permanent structure hinders periodic cleaning so frequent replacement would likely be necessary, although Shah (114) has made progress in regenerating fibrous media. Unconsolidated, coarse granular media have a much longer operating period and in the less frequent event of excessive solids build-up they can be periodically cleaned by fluidisation.

In many unit operations, packings of various geometries have been related to that of a sphere by a shape factor, where a sphere has a shape factor equal to 1.0. In this respect it is envisaged that the use of spheres as a packing may facilitate the use of a shape factor to equate the effect of surface area to volume ratios on the coalescence efficiency of different packings.

The theory and practice of packing arrangements of spheres has been widely reported in the literature (115, 116, 117, 118). Coordination numbers and voidage relationships have been evaluated from both regular and random packing spheres. Pore sizes and channel diameter variations have been evaluated from a theoretical (115) and

experimental (119) standpoint. Therefore, from these properties, it is possible to quantify the packing geometry and its effects on coalescence. Most of the previous work has not included an analysis of packing geometry and has restricted the geometrical description to that of a voidage value. Whereas voidage values are important with respect to limiting flow conditions, they do not provide any information with regard to coalescence mechanisms within the bed. Furthermore, examination of local voidage variations of either Rasching Rings or knitted mesh packing in small diameter columns show that very large wall effects exist. This is also true for spheres and indicates the importance not only of packing selection, but also using a column of adequate diameter. Ridgeway and Tarbuck (117) who investigated local voidage variation of spheres in cylindrical columns, concluded that the wall effects were virtually eliminated within two particle diameters from the wall. In this study, the ratio of column diameter to grain diameter was always greater than 35:1, thus eliminating wall effects.

The non-porous glass ballotini was obtained from Englass, English Glass Company Limited. Their properties are listed on Table 6.1. Glass ballotini diameters measured by volume displacement and by microscopy were within 5 to 10 per cent of the arithmetic mean of the manufacture's reported sieve range.

TABLE 6.1 PROPERTIES OF GRANULAR COALESCER MEDIA

Composition: Lead Glass

Physical Properties:

Specific gravity (approx.)	2.95
Refractive index	1.6
Thermal conductivity (at 20°C Kcal.m/m ² h deg C)	0.0018
Specific heat (between 20 and 100°C Cal/g. deg C)	0.156
Hardness (Moh's scale)	5.7
Linear coefficient of expansion (between 0° to 300°C x 10 ⁻⁶ /°C)	9 x 10 ⁻⁶
Maximum working temperature °C	350
Softening point °C	470

Diam. Range mm.	Test Sieves B.S. 410 : 1969		Approximate Weight per m ³ in kg.
	Pass	Retain	
0.045 - 0.070	63	53	1740
0.060 - 0.095	50	63	1720
0.210 - 0.325	300	250	1780
0.440 - 0.530	500	425	1840

Approximately 80% in "Diameter Range" specified. Less than 5% irregular shapes.

6.3.1 Surface Properties of Glass Ballotini

Coalescence mechanisms and droplet hydrodynamics within packed columns are, to a large extent, dependent on the surface energy of the packing. Considerable information is available on the surface properties of glass and its relationship to the contact angle, and wetting effects with many liquid-liquid systems.

This study was restricted to the coalescence process in a non-wetted packing. Glass, having a high surface energy value, was thus well suited when organic liquids were used as the dispersed phase.

To obtain a reproducible packing surface, the packing was subjected to the preferential wetting technique described by Thomas (120). The ballotini were first cleaned in chromic acid, then thoroughly washed with distilled water. After washing, the packing was placed in an oven at 150°C for 8 hours. The dried beads were stored in sealed polyethylene containers for subsequent use. The effect of surface renewal by acid etching and the thorough drying proved to be a suitable method of producing a highly active surface.

Thomas stated that this surface, if then immersed in either organic or aqueous phase, would be preferentially wet by the liquid which first came into contact with the surface; this effect was possible irrespective of the solid surface energy. Therefore, glass, which has a high surface energy and is preferentially wetted by water, would be made to be wet by the organic phase. However, in this study, surfaces wet by the continuous aqueous

phase were produced by immersion in distilled water. A technique for rendering the glass surface hydrophobic has been described by Wilkinson (105).

6.4 LIQUID SYSTEM DESCRIPTION

The equipment was designed for coalescence of an organic liquid dispersed in distilled water. Toluene was selected as a relatively non-toxic, non-corrosive and inexpensive solvent. G.P.R. grade toluene was distilled to within $\pm 1^{\circ}\text{K}$ of its boiling point and stored in clean, dark glass bottles to prevent exposure to sunlight which has been reported to cause degradation (121).

Any effects due to the mutual solubility of toluene and water were minimised by allowing the two phases to attain mutual saturation by contact for over 24 hours before use. Mass transfer effects could not be completely eliminated due to the temperature coefficients of solubility. Since accurate temperature was impractical due to heat generation by pumping and emulsification, the physical properties of the system were determined as a function of temperature and presented in Appendix A. The high sensitivity of both continuous and dispersed phase viscosities, and hence pressure drop to temperature changes emphasises the need for monitoring during single and two phase flow experiments. The continuous phase rotameters were calibrated experimentally at 20°C and the effect of temperature fluctuation was evaluated theoretically from the calibration handbook (122). An 8°C change in temperature was found to cause a 5% maximum error in flowrate.

Instruments of this type possess inherent errors, due to random flow disturbances, and accuracies of better than 3 or 4% would not be realised in practice. Temperature correction of the calibration curves was therefore unwarranted.

6.5 PRESSURE DROP MEASUREMENT

Initially, pressure drop was measured across the coalescer. This was done by using two differential 'U-tube' manometers. A mercury manometer was used to measure pressure drops greater than 100 mm Hg and one containing carbon tetrachloride used for the lower range of values. The manometers were connected in parallel to pressure tapings upstream and downstream of the coalescer by tubes containing distilled water. Location of the interface between the carbon tetrachloride and water was improved by colouring the organic phase using the dye, 'Oil Soluble Yellow'. Since the ambient temperature varied, the density of the carbon tetrachloride was determined gravimetrically and was found to be 1604 kg/m^3 ; it varied less than 0.4% over the temperature range $10\text{-}30^\circ\text{C}$.

During experiments for single phase flow through the coalescer, it was discovered that a different value of pressure drop was obtained for the same superficial velocity depending on whether the flowrate was progressively increased or decreased. Modification of the manometer system as described in Fig. 6.5 eliminated this hysteresis effect which was only detectable using carbon

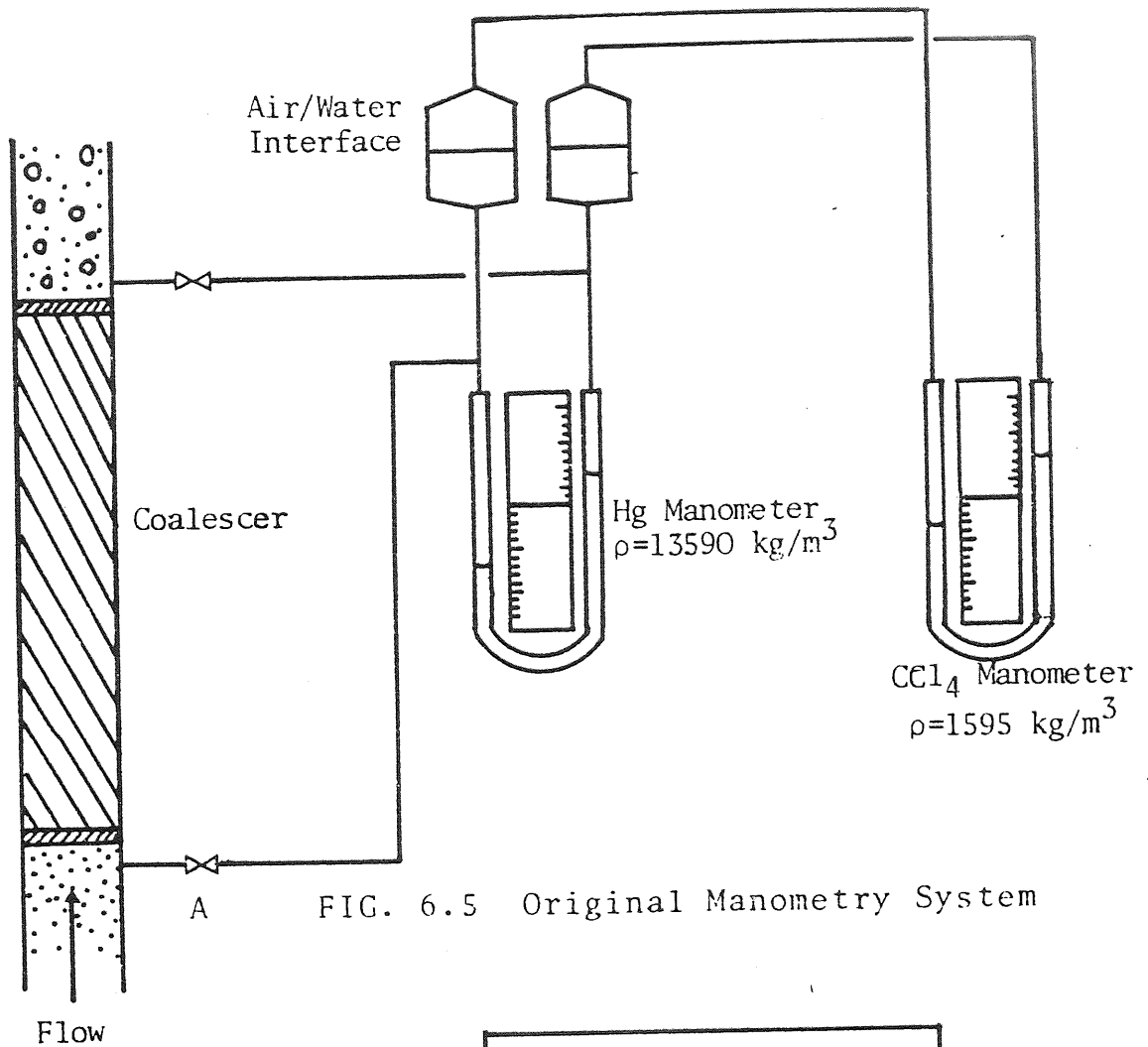


FIG. 6.5 Original Manometry System

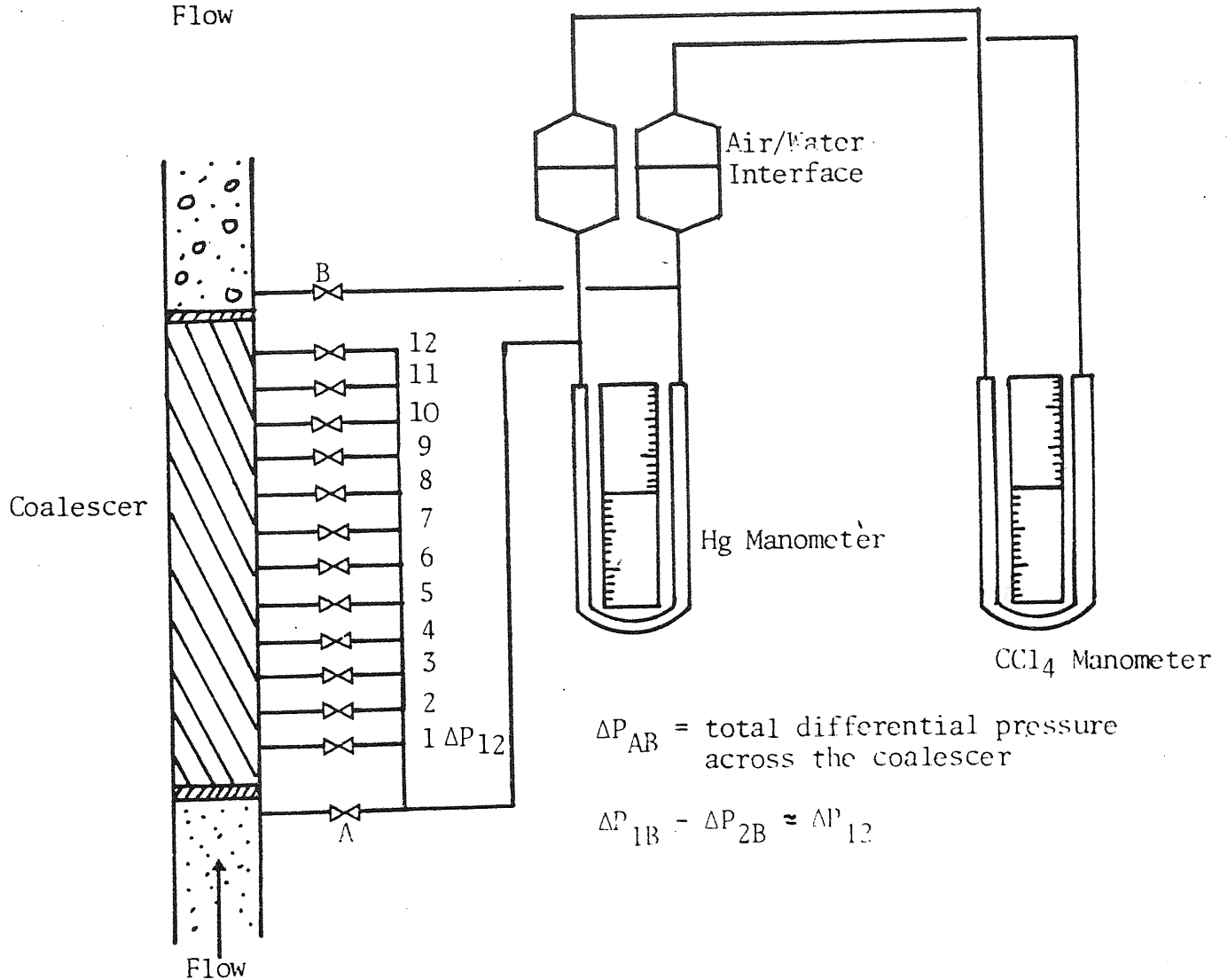


FIG. 6.6 Modified Manometric System with Pressure Taps

tetrachloride manometer. This phenomenon, which has been observed previously in low pressure drop measurements (123) may be attributed to an advancing and receding interfacial contact angle as the pressure drop rises and falls. The liquid levels in the water reservoirs were equalised before the measurements were taken from either manometer.

When the coalescer column was modified to measure pressure difference over its entire length, the manometer system already described was kept with the addition of pressure tapings which were isolated from one another by means of valves. Each pressure tapping on the coalescer column as well as the one upstream the coalescer, measured differential pressure with respect of the pressure tapping downstream the coalescer. The new system is illustrated in Fig. 6.6.

Since the measurement of pressure on each tap involved the opening and closing of valves it was thought that it may cause local pressure increase on the tap being assessed. Therefore, the first four pressure taps downstream on the column were changed to pressure transducers, measuring differential pressure and calibrated in the range $0-6230 \text{ Nm}^{-2}$. They were connected to a conditioning unit and a U.V. light recorder, calibrated accordingly, and recorded the transient pressure drop throughout the single phase and two phase experiments without manual intervention. This new arrangement is presented on Fig. 6.7.

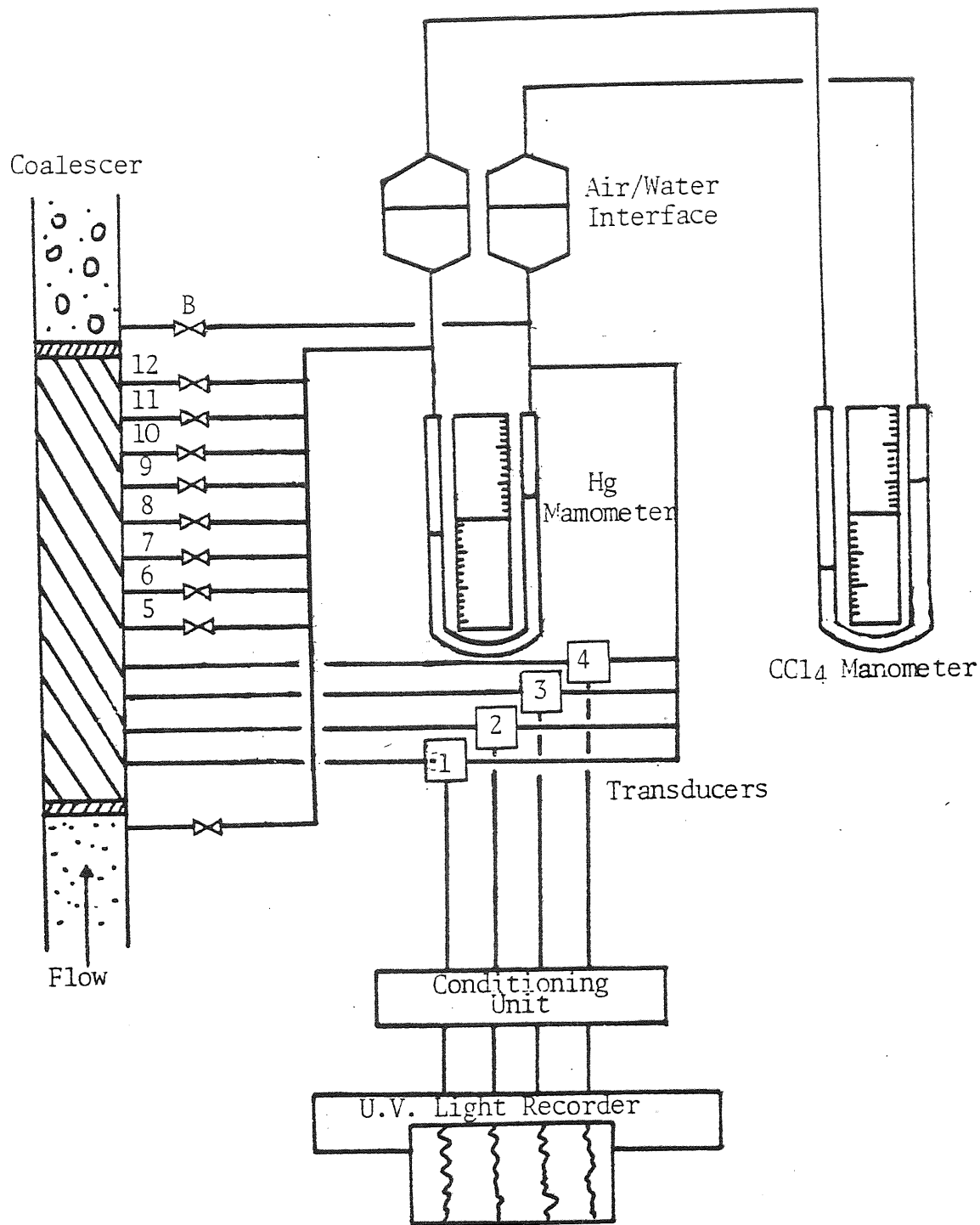


Fig. 6.7 Arrangement for Measurement of Pressure Drop with Taps and Pressure Transducers

6.6 OPERATING PROCEDURE

Following assembly, the equipment was filled with a 2% v/v solution of Decon 90 and allowed to stand for 24 hours with periodic recirculation of the cleaning solution. After soaking, the whole apparatus was rinsed thoroughly with tap water, followed by distilled water, the rig was filled with distilled water. Further contact with surface active agents was avoided to prevent contamination of the liquid system since minute quantities of surfactants which may be absorbed onto glass surfaces are extremely detrimental to the coalescence process.

To pack the coalescer, the column was half filled with the continuous phase, then a pre-weighed quantity of uniform glass beads was added through the top of the column by gently tapping the column wall to eliminate the possible accumulation of air bubbles and to ensure uniform porosity along the whole column.

After assembly, the equipment was operated in the recycle mode when only flow of the continuous phase was permitted. The temperature and pressure drop were recorded for a range of superficial velocities from $0.1 - 7 \times 10^{-2}$ m/s. This procedure provided sufficient data for single phase flow analysis and ensured correct assembly of the coalescer through pressure drop checks.

The isolation valves were then adjusted to alter the operating mode from recycle to a 'once through' condition and the flow regulated to the desired value. The emulsification pump was started, followed by the dispersed phase metering pump and after the appearance of a milky

haze in the pump recycle loop, characteristic of secondary dispersion, the temperature and pressure drop were recorded at regular intervals on each pressure tap. The performance of the bed was monitored throughout the transient period, typically of several hours duration, until steady state conditions were attained. At this stage, samples of the inlet dispersion and the effluent from the coalescer were taken for determination of mean drop size: the primary dispersion leaving the coalescer was photographed.

6.7 BED VOIDAGE DETERMINATION

The initial bed voidage was determined using a displacement method. Distilled water was pumped through the bed at high flowrates, 7×10^{-2} m/s, for fifteen to twenty minutes to displace all air bubbles. Some of the water was then drained down the bed to a predetermined level fifteen centimeters above the packing. A measured volume twenty millilitres, of water was removed from the column and the distance the water level dropped was measured. This procedure was repeated until the water level was about one centimeter above the packing. These initial measurements were used to obtain an average value for the water level drop per twenty millilitres since the column diameter could not be assumed uniform with the addition of the pressure taps. Following this, twenty millilitres were collected and the water level receded to beneath the packing. This reduction in the water level was measured, from this value together with the bed

depth, packing bulk volume and the initial average value recorded, the bed voidage was calculated, as shown in Appendix B.

6.8 EXPERIMENTAL DESIGN

The factors which affect the coalescence process may be categorised as those parameters relevant to the liquid system, those pertaining to the media employed and those determined by the operating conditions. Contamination of the liquid system by particulate matter, dissolved solids and surfactants also influence coalescence efficiency. In view of the complex interactions between the operating parameters summarised in Table 6.2, it is necessary to design experiments carefully. The scope of this research was restricted to investigation of coalescence of a single, pure liquid system so that the effects of bed properties and operating conditions could be determined in greater detail.

6.8.1 Operating Conditions

In this study, preliminary experiments were carried out to determine the optimum operating variables at which a high separation efficiency could be achieved. The aim was to obtain large exit drop diameters and thus, high separation efficiency, with low pressure drop and high superficial velocity. There is a wide range of ballotini sizes available and the selection of sizes was made based on the fibre diameters used in a previous coalescence study (14). Decreasing the ballotini size increases the

Bed Parameters	Ballotini diameter Bed thickness Bed Voidage Specific surface
System Parameters	O/W or W/O dispersion Interfacial tension Density - dispersed phase Density - continuous phase Viscosity - dispersed phase - continuous phase Contact angle Mutual solubility
Operating Parameters	Temperature Velocity Phase ratio Inlet drop size distribution
Measured Parameters	One phase and two phase pressure drop Inlet and outlet drop size distribution Effluent drop size Time to steady state Filtration Coefficient (separation efficiency)
Miscellaneous	Particle matter Dissolved Solids Surfactants

Table 6.2 List of Variables in Secondary Dispersion Coalescence Studies.

pressure drop, decreases the exit drop size and lowers the value of superficial velocity at which drop redispersion occurs. Increasing the ballotini size increases the exit drop size, decreases the pressure drop and permits higher throughput. A set of experiments was devised whereby the changes in ballotini size, bed depth, superficial velocity and dispersed phase concentration were measured as changes in the pressure drop, exit drop size, effluent drop size and separation efficiency. The operating temperature was only monitored since accurate control was impossible. In some cases the measurement of pressure drop had to be abandoned as it increased over the limits of the manometric system used. Changing the manometric system for one with a higher capacity, decreased the sensitivity and thus did not record small changes in pressure drop and therefore it was not developed any further. The experimental program is presented in Table 6.3.

Velocity $u \times 10^{-2}$ m/s	Bed Depth, $L \times 10^{-2}$ m		
	5	10	20
0.1	57.5	57.5	57.5
	267		267
	486*	486	486*
0.2	57.5	57.5	57.5
	267		
	486*		486*
0.3	57.5	57.5	57.5
	486	486	267
			486*
3.0	57.5	-	486*
	486*		
4.0	486*	-	486*
5.0	-	-	486*

Table 6.3 Experimental Design. The numbers in the grid are the ballotini sizes used. All experiments were carried out for 0.1% v/v Dispersed Phase Concentration.

* Dispersed Phase varied between 0.1-1% v/v.

CHAPTER SEVEN
DETERMINATION OF DROP SIZE DISTRIBUTIONS

CHAPTER SEVEN

DETERMINATION OF DROP SIZE DISTRIBUTIONS

7.1 INTRODUCTION

The method used to produce a secondary haze in this study gives a polydispersion which is a desirable feature of the technique since very few dispersions encountered industrially are monodisperse. In order to characterise a dispersion a knowledge of the drop size distribution, in addition to the mean drop size is necessary. Also, the capture efficiency of drops flowing through a packed bed depends on their diameters and the sole use of a mean diameter could be misleading when the mechanisms of coalescence are being investigated.

Various methods of measurement are available, including:

- (a) Optical methods such as microscopy, using manual or automatic scanning (124)
- (b) Light reflectance (125)
- (c) Light scattering (126)
- (d) Ultrasonics (112)
- (e) The Coulter-Counter (127)
- (f) Lasers (128) to produce holograms (14) or direct measurements (129)

7.2 MICROSCOPY

In microscopy, a sample of the dispersion is diluted, placed in a well of a glass slide and examined under the microscope. The various size ranges are then determined

by matching against a calibrated graticule situated in the eye piece of the microscope. The use of the microscope is applied most efficiently in the range 0.25 μm to 20 μm . The lower limit is imposed by the resolving power of the microscope; the upper limit is determined by the diameter of the drop in relation to the depth of field of the optical system. Further inaccuracies result from the long periods during which drops may settle and it is necessary to count more than 300 drops per sample; that is the number recommended to obtain statistically valid results for a polydispersion (130). Alternatively, photographs may be taken for sizing later. This method is clearly unsuitable for frequent sampling of the inlet dispersion.

7.3 LIGHT REFLECTANCE

This technique uses a linear relationship between the reflectance of coloured emulsions and droplet size data determined microscopically (125); the droplet size range is from 1 μm to 30 μm . This technique gives only an average particle size and special equipment is required (131,132,133).

7.4 LIGHT SCATTERING

This technique, first described by Tyndall in 1871, involves passing a coherent beam of light through the emulsion and measuring the intensity of the scattered light as a function of the scattering angle from the direction of the incident beam. If the emulsion is

sufficiently dilute, the total scattered light is simply the sum of light scattered from individual drops. The light scattered from a drop depends on the area intercepting the beam, and thus on the square of the effective radius of the drop.

Light scattering can be divided into three classes dependent upon the size of the droplet relative to the wavelength of the incident light and its refractive index relative to that of the continuum (126).

(a) Rayleigh Scattering: Droplets less than one tenth of the wavelength of the incident light in diameter, i.e. about 0.05×10^{-6} m.

(b) Debye Scattering: Droplet size is not small relative to the wavelength of the incident light and refractive index of the dispersed phase is within 10% of that of the continuum.

(c) Mie Scattering: For large droplets of high relative refractive index, where the interference between light waves scattered from different parts of the same drop is considered. Although this may be applicable to this study, the Mie theory of light scattering is very complex, and also is only valid for monodispersed systems or for determining an average drop size for a narrow distribution. The effects of polydispersed systems and multi-scattering are ill-defined.

7.5 ULTRASONICS

Measurement of drop size in liquid-liquid dispersions by means of acoustics depends upon the difference in elastic properties between the continuous and dispersed liquid phases and upon the consequent difference in the velocities of transmission of longitudinal acoustic waves (134). Based on the assumption that the dispersion behaves as a homogeneous fluid with the combined properties of both liquid phases, the composition of the mixture can be deduced by measuring the acoustic velocity of the mixture and if the acoustic velocity of the two components is known. Acoustic velocity can be measured by finding the wavelength at a fixed frequency. A variance in composition dependent upon the sizes of the droplets of the dispersed liquid is obtained when drops of dispersed liquid enter and leave the sample volume. Measurements of this composition variance allows the average drop volume to be calculated. Further details of this technique are to be found in Attarzadeh's dissertation (112).

7.6 THE COULTER COUNTER

The Coulter Counter is an analytical equipment used for measuring the size distribution of solid particles or immiscible droplets in a dispersion, the continuous phase of which is a liquid of low resistivity by measurement of a resistance change between two electrodes.

Shalhoub (13) concluded that the use of the Coulter

Counter is preferred for the analysis of secondary dispersions since it produces reliable results in a short time. A sample of the dispersion was taken, stabilized with a surfactant (Hyamine 2389) and diluted in an electrolyte (0.9% w/w sodium chloride). The sample was then withdrawn through an aperture whose diameter was accurately known and which was positioned between two electrodes. Since the conductivity of the dispersed phase droplets is considerably less than that of the continuous phase, the resistance between the electrodes changes instantaneously as a drop passes through the aperture. Voltage pulses, whose magnitude depends on the drop diameter, are produced and screened electronically by a series of threshold circuits. By selection of different threshold levels and recording the number of pulses, data was obtained for plotting cumulative frequency against drop size. A typical result is shown in Fig. 7.1 from which the mean diameter is obtained corresponding to 50% cumulative weight percent oversize.

The instrument must be calibrated for each orifice tube and electrolyte combination prior to use. Calibration is ideally performed using smooth particles of constant, known density or using 'monosized' particles supplied by Coulter Electronics Ltd. Most effective calibration results when the particle size is between 5% and 20% of the aperture diameter of the orifice tube selected.

For the 140 μm aperture tube, Red Mulberry pollen of 16.5 μm average diameter was used. From the

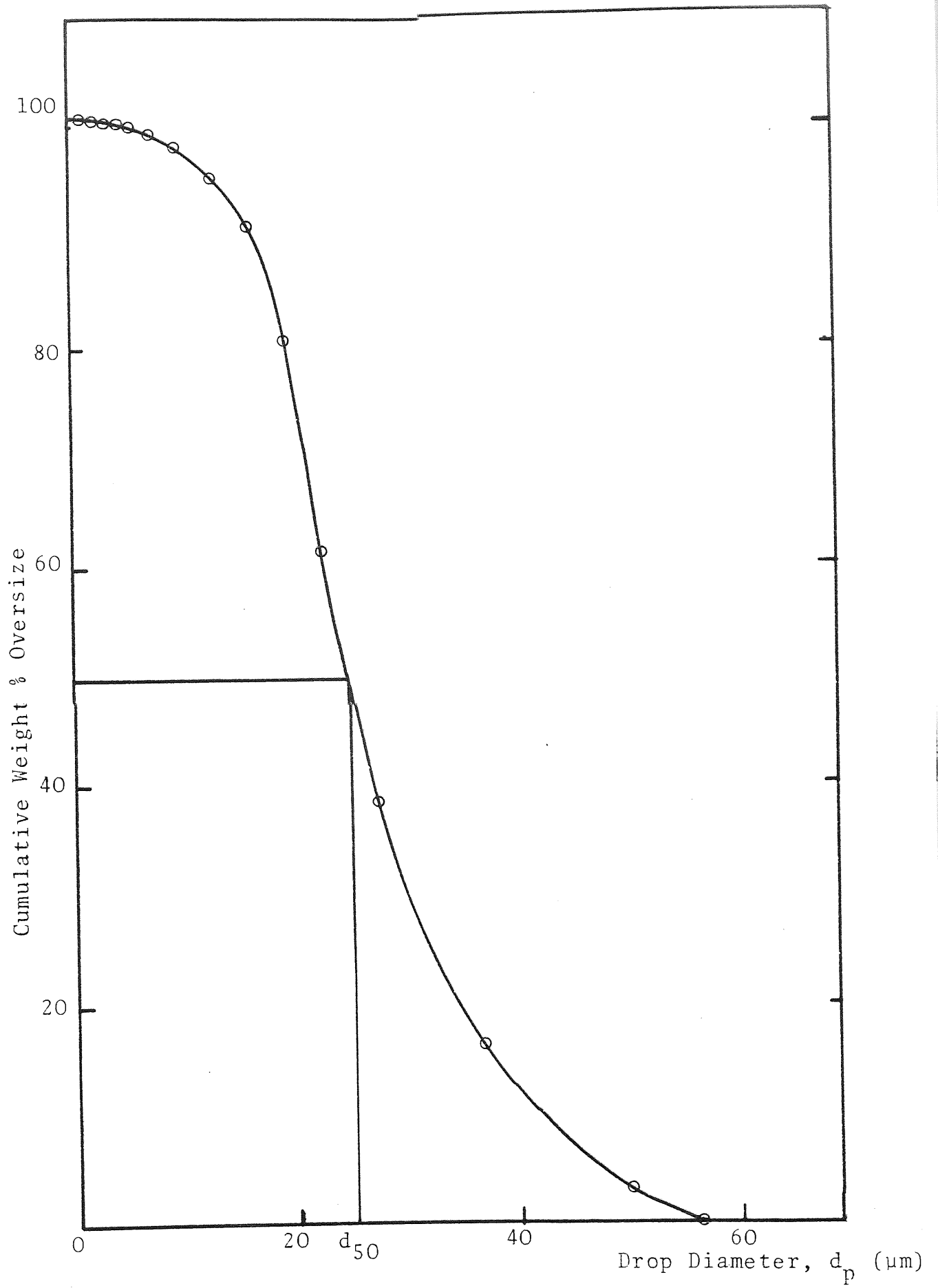


FIG. 7.1 Typical Size Distribution of Inlet Dispersion

instrument readings on a dispersion of the calibration material and the electrolyte that is to be used for the analysis, an equivalent particle volume is obtained and, using the mean diameter of the calibration particles, the calibration factor can be calculated.

As the pulse height and instrument response are essentially proportional to particle volume, this one factor can be used to calculate particle size from any other combinations of the instrument settings.

The size of the calibration material was measured by microscope and was found to be lower in its dried state and swelled when dispersed in the electrolyte to give a diameter range between 13.6 μm and 15.6 μm , still below the average of 16.5 μm . Sample photographs of this phenomena are shown on Fig. 7.2. Although this size difference does not affect the readings obtained from the instrument during the analysis of the sample, it affects the drop size calculated for different instrument settings and hence the mean drop diameter obtained from the cumulative frequency against drop size plot. The manufacturers now recommend the use of latex dispersions for calibration, as they will not change upon immersion or storage. This can reduce the error in calibration to $\pm 1\%$. One percent error in calibration leads to 3% error in volume of particles measured and therefore to 3% error in mass balance (135).

The size range over which the instrument may operate is from approximately 2% to 40% of the aperture diameter (136). For a 140 μm aperture tube, the working

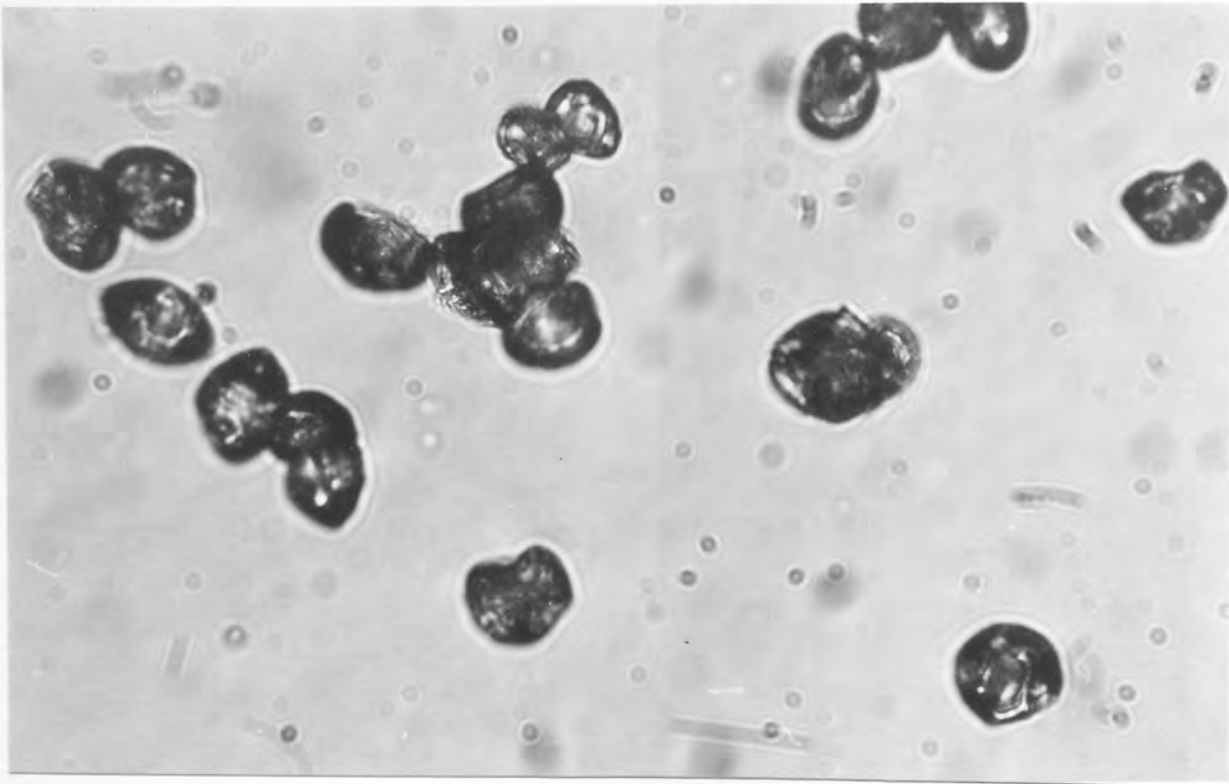
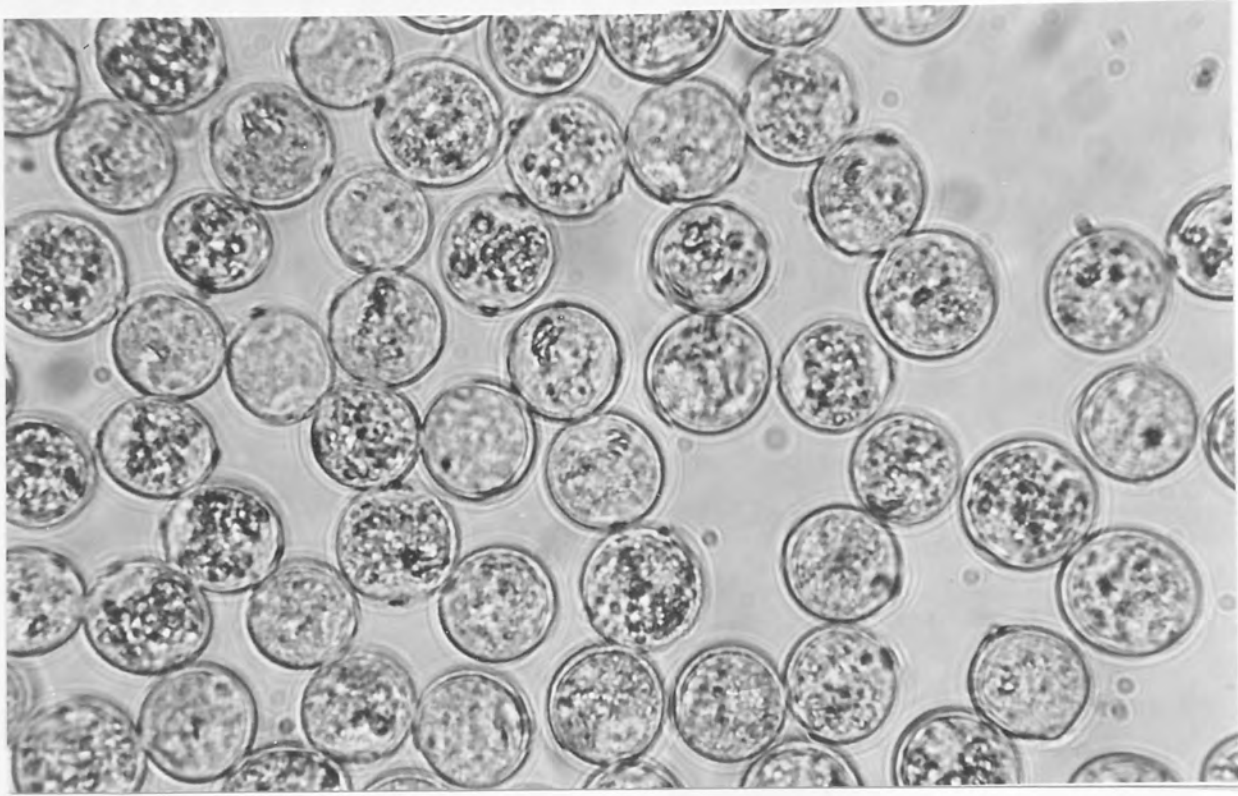


Figure 7.2 Microscope Photograph of Calibrating Red Mulberry Pollen in its Dry and Wet State.

range is between 2.8 μm and 56 μm . Experiments to determine sample mass were carried out and a lack of agreement between mass weighed in and mass calculated from Coulter data was found to exist. This was attributed partly to the error incurred in calibration and most probably to the failure of the equipment to capture the largest particles. Generally the Coulter Counter is considered linear between 2 and 40% of the aperture diameter, but there is a measurable non-linearity above say 20% since the equations that describe the aperture response do not actually predict a truly linear response (135). If sufficient particles lie in the range 20-40%, some measurable loss of balance will occur since the pulses from large particles would be undersized. Taking these factors into account, random checks of the dispersion were performed with the microscope.

7.7 LASER TECHNIQUES

An alternative method to size secondary dispersions involves the use of lasers. Holography is a method of recording an image of an object using the entire content of the light reflected or transmitted by that object. The light source used must be coherent, when the electromagnetic waves incident upon the object are in phase, and lasers are employed to provide a source of monochromatic, coherent light to satisfy this requirement.

Phase variations are caused by placing an object in the path of a coherent light beam (signal beam).

When combined with a similar undistorted beam (reference beam) on a photographic plate, the phase variation on the signal beam is transferred into an intensity variation by the formation of a complex interference pattern. The intensity variation acts as a diffraction grating which, on illumination with coherent light, superimposes the original phase distribution onto the illuminating beam causing an image of the object to appear in its original position and form. Not only does the photographic plate act as a diffraction grating but each part of the plate is, in itself, a grating so that the image consists of a large number of separate images each with a different perspective. This gives the image a three dimensional appearance and parallax may be observed.

Systems for recording holograms can be classified into Fraunhofer (Far Field) or Fresnel (Near Field) dependent upon the relative distance of the object from the film plane in which the hologram is recorded. Holograms used for particle size analysis are invariably far field (128).

Fraunhofer holograms consist of a series of concentric circular fringes, with a central maximum, associated with each drop. Unlike other holograms, far field patterns may be readily interpreted by direct analysis of the fringes.

A holographic technique developed by Austin (14) to size uncoalesced secondary drops reported a 30 μm average diameter. Further details of this technique are to be found in Austin's dissertation.

Another method of sizing dispersions by using lasers without recording, developing and reconstructing a hologram and interpreting the data obtained from it, involves the use of the Malvern 2200 Particle Sizer (129).

The instrument uses the principle of Fraunhofer Diffraction from the drops as means of measurements. A low power visible laser transmitter produces a parallel, monochromatic beam of light which is arranged to illuminate the particles by use of an appropriate sample cell. The incident light is diffracted by the droplets illuminated to give a stationary diffraction pattern regardless of droplet movement. As drops enter and leave the illuminated area the diffraction pattern "evolves" always reflecting the instantaneous size distribution in this area. Thus by integration over a suitable period and a continuous flux of droplets through the illuminated area, a representative bulk sample of the droplets may contribute to the final measured diffraction pattern.

A Fourier transform lens focusses the diffraction pattern onto a multi-element photo-electric detector which produces an analogue signal proportional to received light intensity. This detector is interfaced directly to a desk top computer allowing it to read the diffraction pattern and perform the necessary integration digitally. The basic arrangement is presented in Fig. 7.3.

Having measured a diffraction pattern the computer

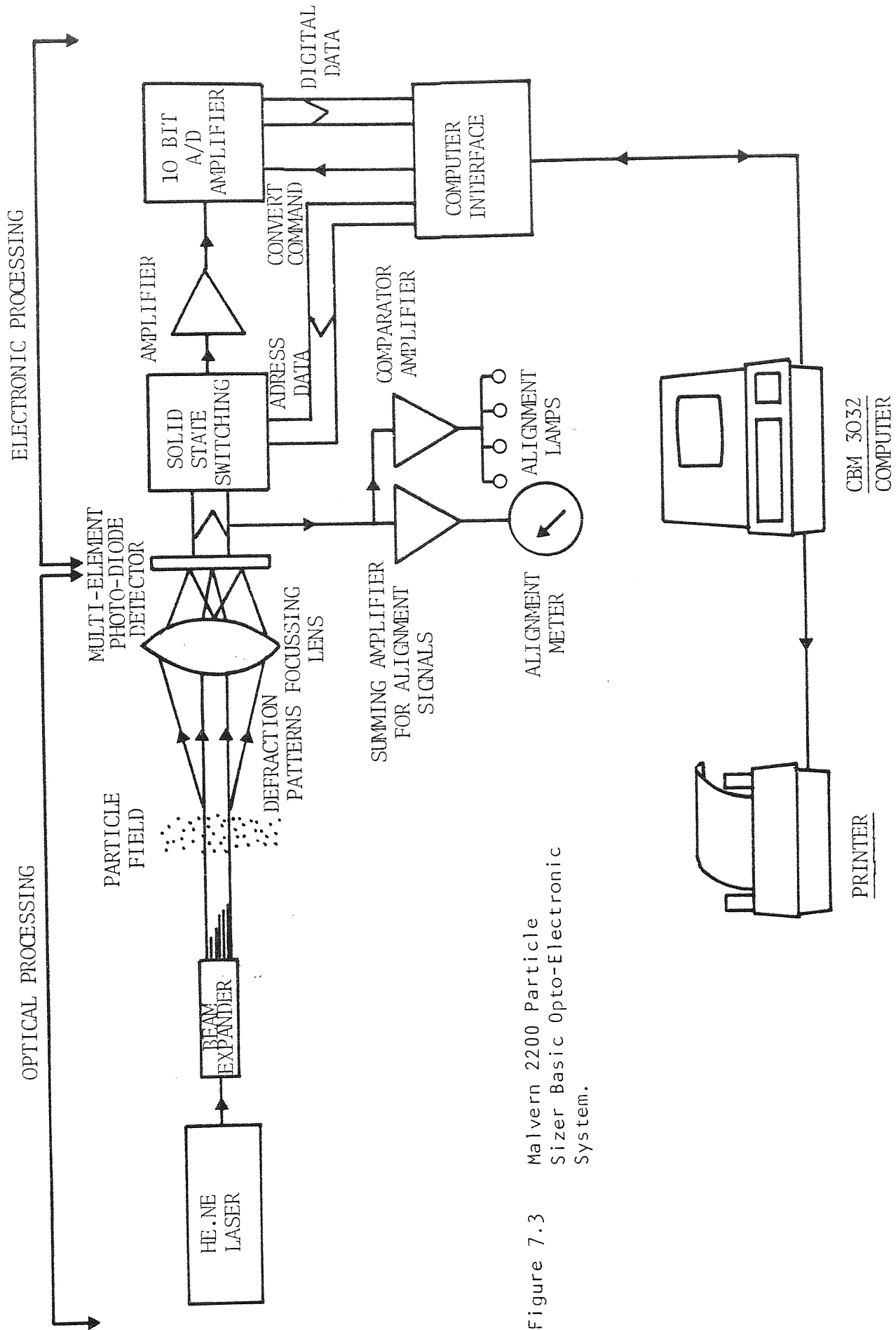


Figure 7.3 Malvern 2200 Particle Sizer Basic Opto-Electronic System.

uses the method of non-linear least squares analysis to find the size distribution that gives the closest fitting diffraction pattern. The size distribution can be analytically generated by either the well known two parameter models Rosen Ramler, Log Normal or Normal, or by using a model independent.

The result of the analysis, a size distribution of the sample by weight, may be displayed graphically on the V.D.U. screen of the computer or printed as a hard copy result on a line printer. The size distribution can be presented as the weight in size bands, the cumulative weight below a size or the cumulative weight above a size.

The experimental procedure involves firstly loading the computer with the analytical model processing, checking the optical alignment of the equipment, and taking a background reading with the continuous phase in the sample cell. A suitable background reading should be less than 30. If the level exceeds 30, realignment should give an improvement. An example background reading printout is shown in Fig. 7.4. Sources of high level of background reading are missalignment and dirty or scratched optical components.

The diffraction pattern of the sample dispersion has added to it a number of significant errors. They arise from diffraction from sources other than the sample, scattering, poor alignment, etc. The errors are minimised by deriving the estimate of the diffraction pattern from two practical measurements.

The first measurement is the diffraction pattern

PRINTING INPUT DATA

RUN NO.	TIME	OBSCURATION	
17	01-07-00	0.34	
INDEX	SIGNAL	BACKGROUND	DATA
1	15.09	8.72	3.50
2	15.21	9.37	3.50
3	14.73	11.84	1.81
4	11.82	7.82	2.66
5	13.23	8.99	2.97
6	13.08	7.01	3.97
7	14.74	8.06	4.56
8	12.24	5.35	4.91
9	13.51	6.14	5.47
10	14.12	5.24	6.84
11	15.45	5.83	7.59
12	16.80	5.87	8.81
13	18.73	6.31	10.25
14	21.18	6.69	12.09
15	23.50	6.91	14.06
16	26.10	7.11	16.31
17	28.86	7.51	18.41
18	32.78	8.52	20.97
19	36.52	9.83	23.28
20	40.40	10.05	26.81
21	44.01	9.90	30.41
22	47.29	10.77	32.84
23	50.87	10.94	36.25
24	53.81	12.67	37.72
25	57.05	11.97	41.78
26	60.78	12.93	44.81
27	63.95	13.54	45.97
28	65.35	15.54	47.89
29	68.55	13.47	53.34
30	74.65	12.73	61.66

Figure 7.4 Malvern 2200 Particle Sizer Background Reading Printout.

produced from the system without the dispersion sample being introduced. It is the 'background' data and measures directly all diffraction arising from sources other than the sample. Backgrounds are required each time the optical path is disturbed, including such operations as removal of sample cells for cleaning, lens changes, etc.

The second measurement is the diffraction pattern produced when the dispersion sample is introduced as it is referred to as the 'signal' data. This measurement gives the diffraction arising from the same stray source as were present for the background data and the dispersion diffraction.

The 'derived' data is the resultant estimate obtained from connection of the 'signal' data for the 'background'. It is the 'derived' data only that is used in analysis of the particle size distribution. The Particle Sizer obtains estimates of the distribution of drop sizes by least squares curve fitting to the diffraction energy measured and computed. The two parameter programme assumes that the sample size distribution can be modelled by an analytical function having two independent variables. The model independent programme assumes no analytical model for the weight distribution of the sample. Instead it sets up a set of 15 weight bands dictated by the receiver lens used in the measurement. By a heuristic technique it obtains a good guess to the proportion of weight in each of the size bands. In both cases, the initial distribution is then used to generate its representative diffraction pattern and compare it to that

measured in a least squares sense to obtain an error coefficient. The system then iteratively refines its initial distribution to minimise this error coefficient thereby improving the size distribution estimate. It is important to realise that the resultant size distribution is only accurate provided the least squares error is sufficiently low. For the two parameter programme the Log Error should be less than 5 to establish that the model is adequately fitting the sample data. For the model independent the Log Error should be less than 4.5 to assume a good fit to the sample data. It is normal for the model independent algorithm to obtain a better fitting to the data than the Two Parameter case. This is because it is better able to compensate for sample abnormalities such as the presence of fines or a bi-modal distribution. A printed output of sample analysis using both the Two Parameter and the independent models are shown in Fig. 7.5 and Fig. 7.6 respectively. Further details on the technique and mode of operation are to be found in the 2200 Particle Sizer Handbook (129).

In this study, the dispersion produced by the centrifugal pump was analysed at regular intervals during an experiment to ascertain the drop size distribution and to check that the feed to the coalescer was consistent. Outlet dispersions from the unit were also monitored to measure coalescence efficiency. These measurements were carried out by using the Coulter Counter and the Malvern Particle Sizer.

Preliminary experiments revealed that operation

MALVERN 2200 PARTICLE SIZER

MALVERN INSTRUMENTS LTD. SPRING LANE, MALVERN, ENGLAND.

PRINTING PARAMETERS

RUN NO.	TIME	MODEL	% BAR	N	LOG ERROR
44	02-09-40	ROS-RAM	12.14	0.96	4.08

PRINTING RESULTS FROM DATA BLOCK 1

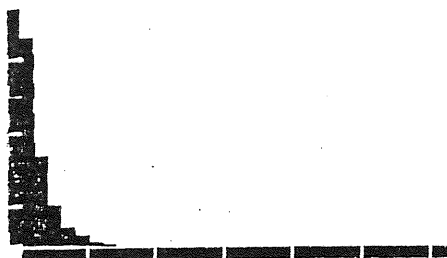
SAMPLE CONCENTRATION = 0.0383% BY VOLUME

OBSCURATION = 0.54

SIZE BAND UPPER	SIZE BAND LOWER	CUMULATIVE WT BELOW	WEIGHT IN BAND	CUMULATIVE % WT ABOVE
320	310	100.0	0.0	0.0
310	300	100.0	0.0	0.0
300	290	100.0	0.0	0.0
290	280	100.0	0.0	0.0
280	270	100.0	0.0	0.0
270	260	100.0	0.0	0.0
260	250	100.0	0.0	0.0
250	240	100.0	0.0	0.0
240	230	100.0	0.0	0.0
230	220	100.0	0.0	0.0
220	210	100.0	0.0	0.0
210	200	100.0	0.0	0.0
200	190	100.0	0.0	0.0
190	180	100.0	0.0	0.0
180	170	100.0	0.0	0.0
170	160	100.0	0.0	0.0
160	150	100.0	0.0	0.0
150	140	100.0	0.0	0.0
140	130	100.0	0.0	0.0
130	120	100.0	0.0	0.0
120	110	100.0	0.0	0.0
110	100	100.0	0.0	0.0
100	90	99.9	0.1	0.0
90	80	99.8	0.1	0.1
80	70	99.5	0.2	0.2
70	60	99.0	0.5	0.5
60	50	98.0	1.1	1.0
50	40	95.7	2.3	2.0
40	30	90.8	4.9	4.3
30	20	80.1	10.7	9.2
20	10	56.4	23.8	19.9
10	0	0.1	56.3	43.6

PAGE 1.

50%
WT/
SIZE



WEIGHT FROM 0 UM ON 10 UM FNT

Figure 7.5 Malvern 2200 Particle Sizer
Sample Analysis Printout using
Two Parameter Model.

MALVERN 2200 PARTICLE SIZER WS-1
 MALVERN INSTRUMENTS LTD. SPRING LANE, MALVERN, ENGLAND.

PRINTING RESULTS FROM DATA BLOCK 1

TIME 02-03-50 RUN NO. 12 LOG ERROR = 3.54

SAMPLE CONCENTRATION = 0.0253 % BY VOLUME
 OBTURATION = 0.70

SIZE BAND		CUMULATIVE WT BELOW	WEIGHT IN BAND	CUMULATIVE WT ABOVE	LIGHT ENERGY COMPUTED	LIGHT ENERGY MEASURED
UPPER	LOWER					
564.0	261.6	100.0	0.0	0.0	33	3
261.6	160.4	100.0	0.0	0.0	40	3
160.4	112.8	100.0	0.0	0.0	67	47
112.8	84.3	100.0	0.0	0.0	108	95
84.3	64.6	100.0	0.0	0.0	178	166
64.6	50.2	100.0	0.0	0.0	291	294
50.2	39.0	95.4	4.6	0.0	477	480
39.0	30.3	95.4	0.0	4.6	747	753
30.3	23.7	94.0	1.5	4.6	1106	1111
23.7	18.5	52.1	41.9	6.0	1529	1529
18.5	14.5	33.2	18.9	47.9	1893	1902
14.5	11.4	30.2	3.0	66.0	2047	2047
11.4	9.1	28.2	2.0	69.0	1838	1831
9.1	7.2	28.2	0.0	71.0	1579	1513
7.2	5.8	25.4	2.8	71.0	1767	1735

Figure 7.6 Malvern 2200 Particle Sizer Sample Analysis Printout using Independent Model.

at high velocities caused breakthrough of the secondary dispersion which flowed from the exit face of the bed cocurrently with the primary dispersion produced by coalescence. Simultaneous analysis of these drops was impossible due to their different sizes and not desirable since combination into a bi-modal distribution curve obscures information about capture and drop release mechanisms.

The effluent primary dispersion leaving the coalescer has been successfully analysed previously (13,14,104, 112,137) by means of photography. Photographs of the drops leaving the coalescer were obtained using an Asahi Pentax camera fitted with an Asahi Micro-lens on Kodak Trix-Pan 35 mm, 400 A.S.A. film. Shutter speeds of less than 4×10^{-3} s were employed to eliminate image distortions caused by drop movement. Illumination of the dispersion from the rear was provided by a 250 W Photoflood bulb through a diffuser.

The circular pipe section, which retained the flowing dispersion, did not cause detectable distortion or magnification of the drops thus eliminating the need for special optical arrangements. Enlargements of the prints to approximately 5 x magnification was found to be satisfactory with respect to size and contrast for the counting procedure. A metric scale placed on the outer tube wall for calibration purposes is shown by Fig. 7.7, a typical photograph of the coalesced dispersion.

Manual counting of the drops recorded on the photographs was accomplished by a Zeiss T63 Particle

Counter to identify and record linear drop dimensions.
The data acquired was then processed in a computer program
to output mean diameter and standard deviation of the
distribution. Typical results are shown in Fig. 7.8.

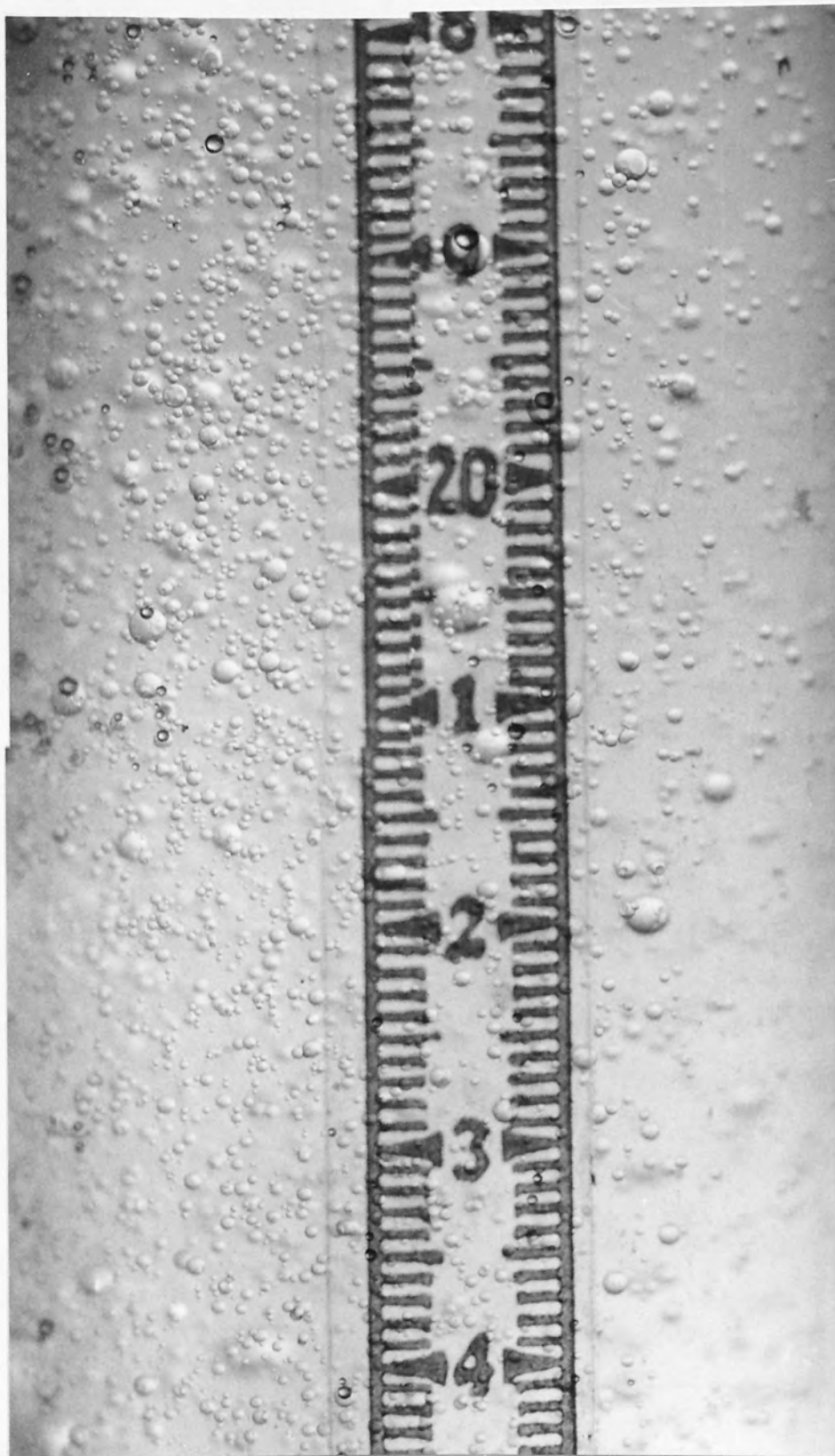


Figure 7.7 Typical Photograph of the Coalesced Dispersion.

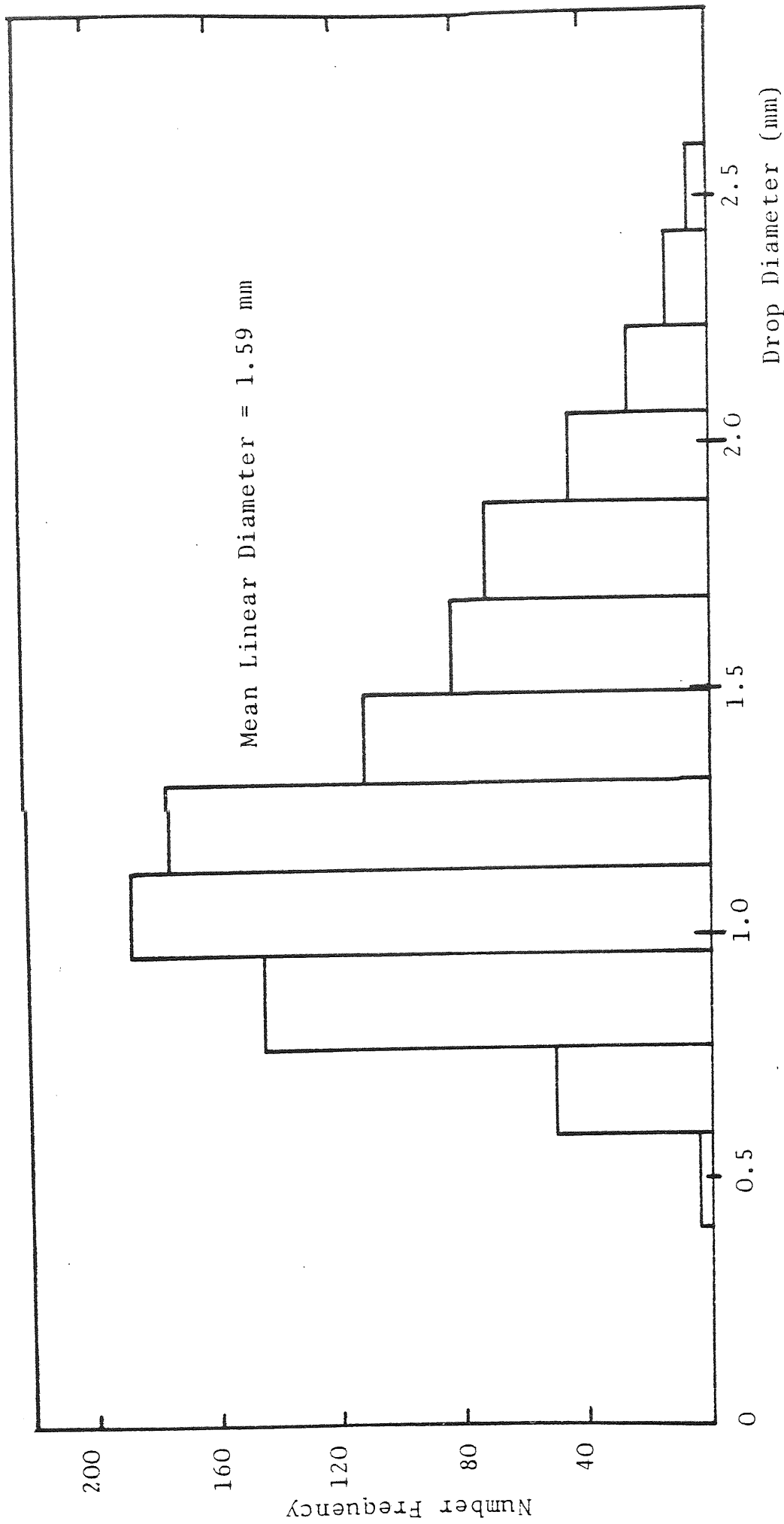


FIG. 7.8 Typical Size Distribution of Coalesced Drops Leaving Exit Face

CHAPTER EIGHT
EXPERIMENTAL RESULTS

CHAPTER EIGHT
EXPERIMENTAL RESULTS

8.1 INLET DROP SIZE

For a given liquid system, the mean drop size of a secondary dispersion produced by a centrifugal pump in a bi-pass loop depends on the pump speed (12,13,14,138). A recent study (139) showed that the level of turbulence in the vicinity of the pump impeller far exceeds that inside the loop so that drop break-up by viscous shear is the most likely mechanism. As the emulsification pump was operated at constant speed, the dispersion was analysed for each velocity since when the later increases, the residence time of the dispersion in the loop is reduced. The results, presented in Fig. 8.1, indicate that mean drop size is independent of superficial velocity above 2.5×10^{-2} m/s but decreases significantly at lower flow-rates for a constant phase ratio. For a constant velocity however, the mean drop size increases with increasing phase ratio for low velocities, as presented in Fig. 8.2, and again at high velocities not covered in this study. The reproducibility of the technique was estimated to be approximately $\pm 5 \mu\text{m}$.

8.2 COALESCED DROP SIZE

The mean size of coalesced drops, determined as the mean linear diameter, was found to decrease with an increase in superficial velocity as shown in Fig. 8.3. This is in agreement with other workers (14,39,43,138,

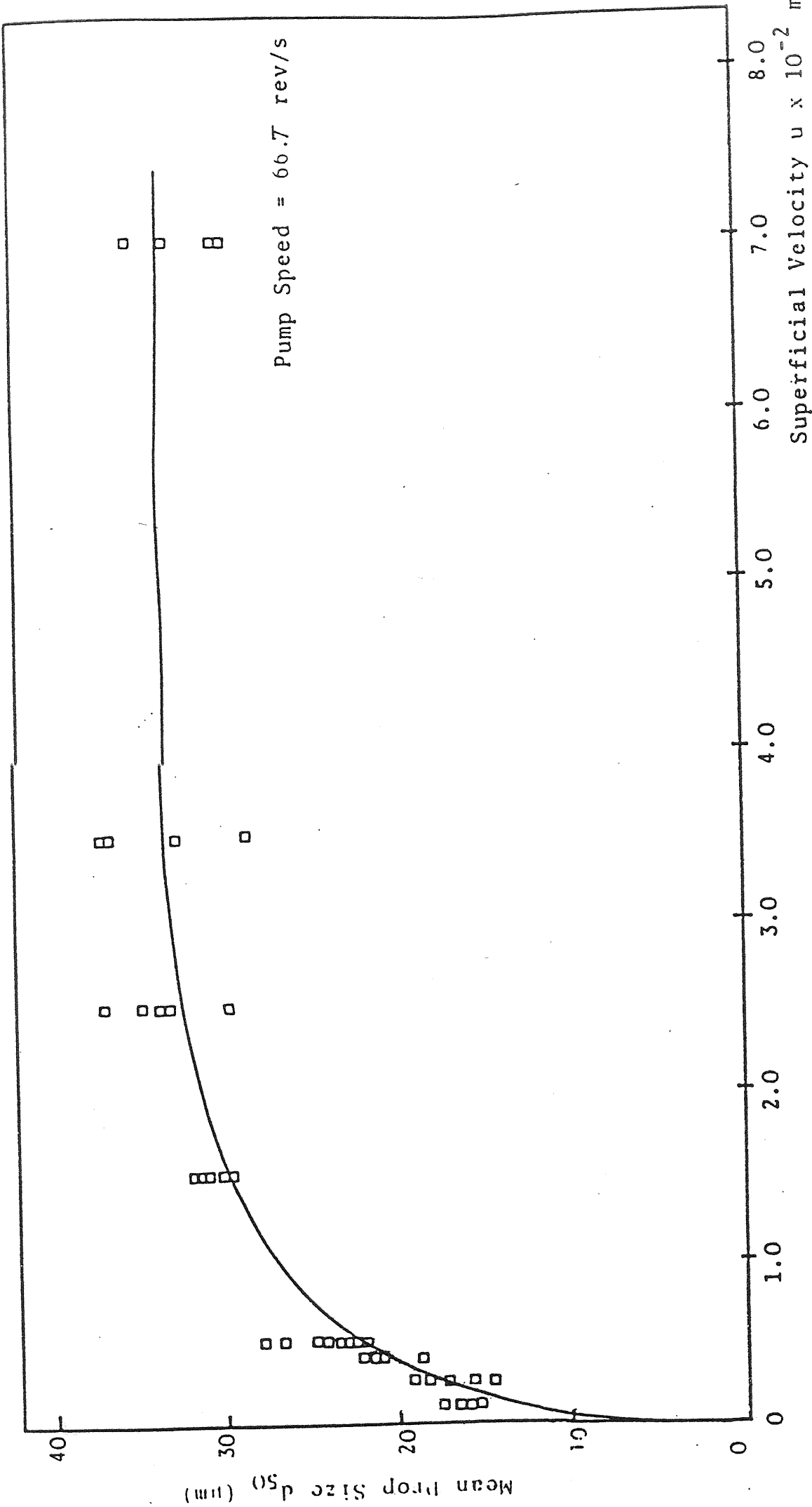


FIG. 8.1 VARIATION OF INLET DROP SIZE WITH VELOCITY FOR TOLUENE/WATER SYSTEM
 (0.1% v/v Dispersed Phase Concentration)

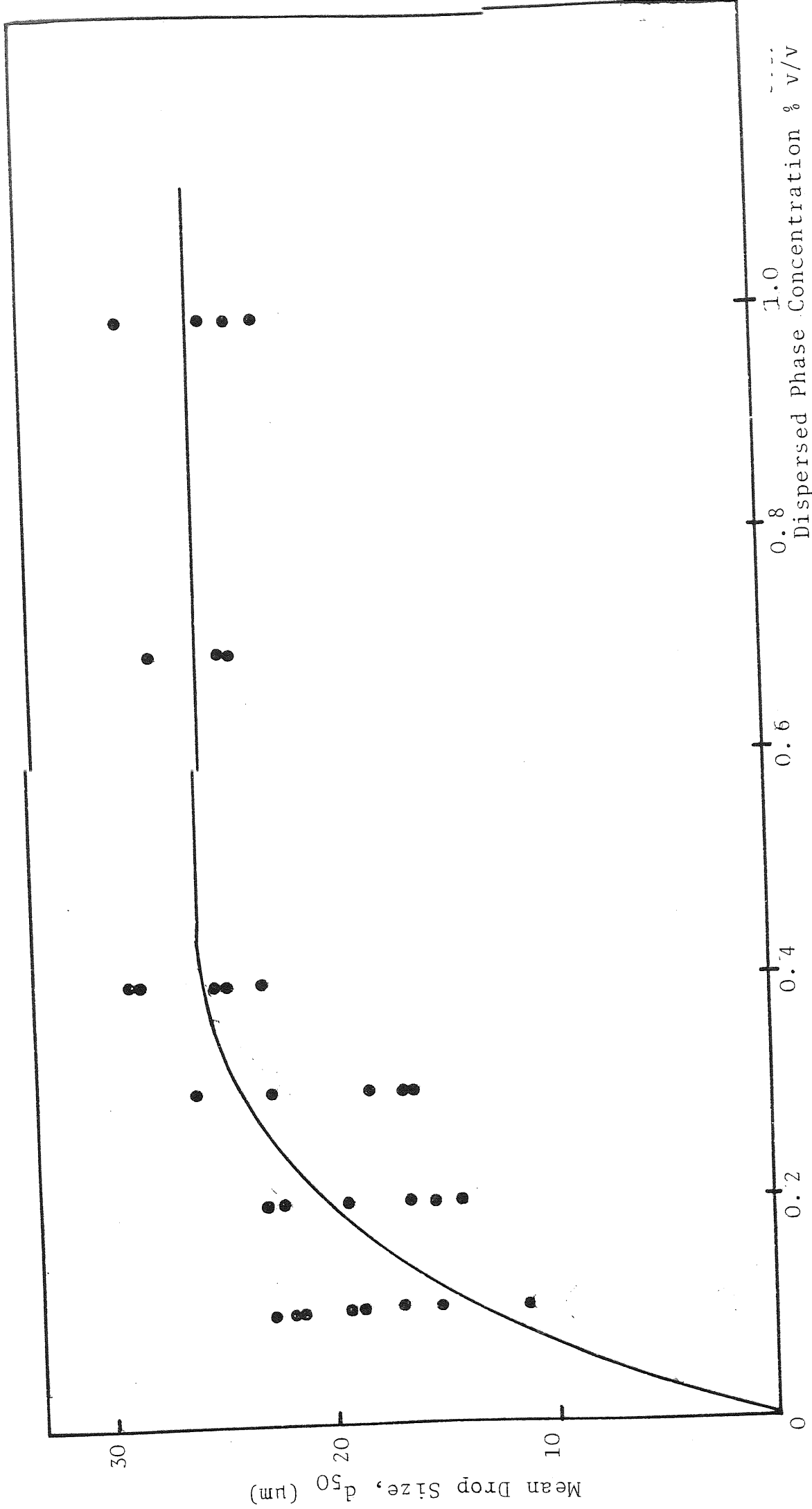


FIG. 8.2 CHANGE IN MEAN DROP SIZE WITH CONCENTRATION OF DISPERSED PHASE AT 3.0×10^{-3} m/s CONSTANT SUPERFICIAL VELOCITY

140), who found that the degree of coalescence decreased with increasing velocity. However, for a constant superficial velocity, the mean linear diameter was also found to be dependent upon bed depth and ballotini diameter as will be shown in the following sections.

8.2.1 Effect of Bed Depth on Exit Drop Size

An increase in bed depth led to an increase in exit drop size as presented in Fig. 8.4 but there appeared to be an optimum bed thickness after which any increase in thickness did not result in a corresponding increase in exit drop size. This was in complete agreement with the observations of previous workers (13,39). Sareen et al (39) suggested that the degree of coalescence increased with bed depth but within a practical limit to the maximum bed thickness. The bed depth was increased from 5×10^{-2} m to 20×10^{-2} m in this study.

8.2.2 Effect of Ballotini Diameter on Coalesced Drop Size

As shown in Fig. 8.5 changing the ballotini size and the bed depth did significantly change the coalesced drop size. This increase in the exit drop size with ballotini diameter arises because, for any random packing of spheres, the mean void diameter must increase as the particle size is increased. Previous work (105) investigating the effect of packing size in the exit layer showed that a relationship does exist between the packing size and exit drop size, and that the latter can be altered by simply altering the exit layer of packing. This is of importance in the design of a coalescing aid since, assuming that

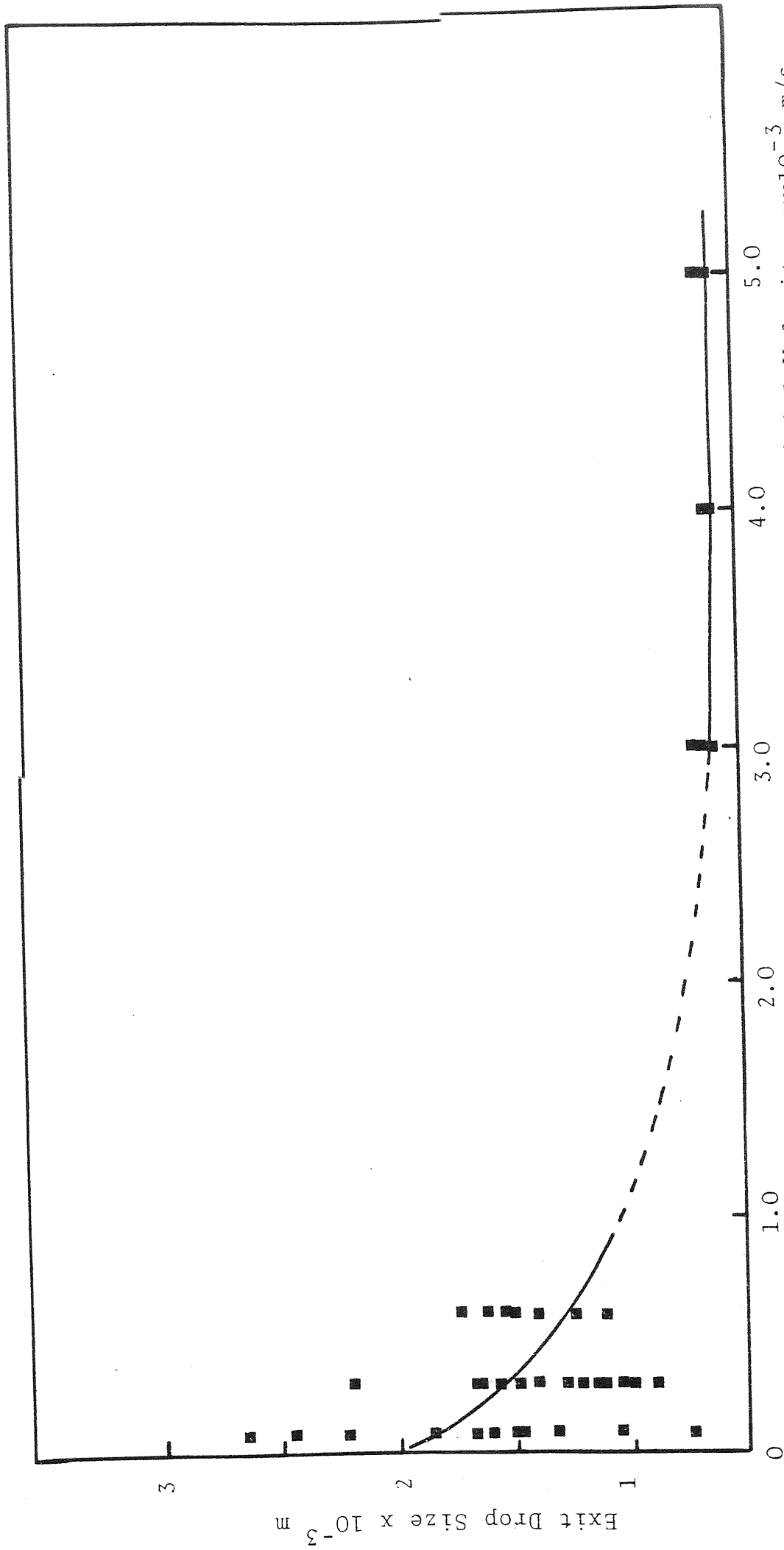


FIG. 8.3 VARIATION OF EXIT DROP SIZE WITH VELOCITY FOR BALLOTINI SIZE 486 μm AND BED DEPTH 20×10^{-3} m

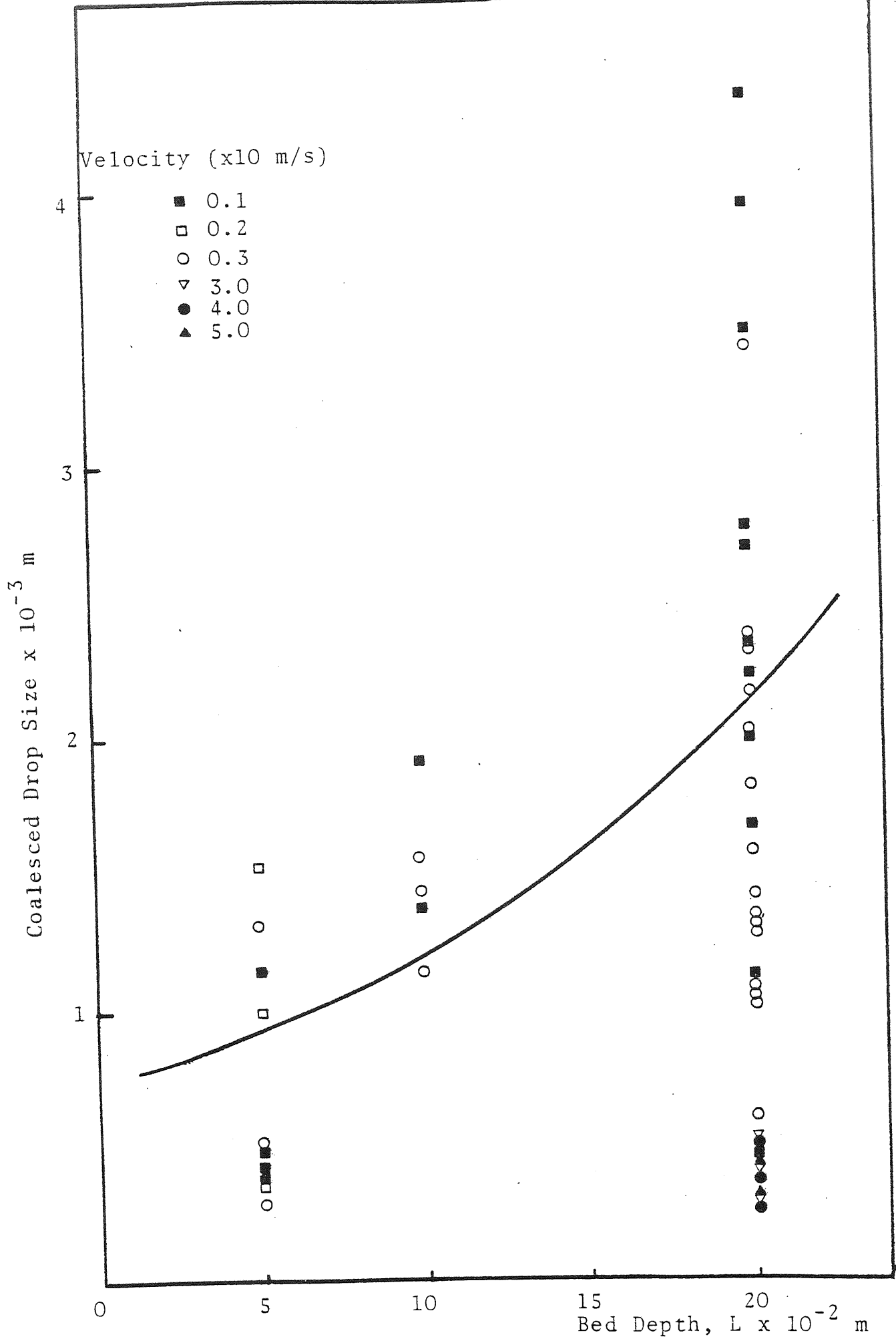


FIG. 8.4 VARIATION OF COALESCED DROP SIZE WITH BED DEPTH FOR BALLOTINI SIZE 486 μm

coalescence takes place within the packing, an increase in exit packing size will result in an increase in separation efficiency.

However, if the overall coalescence efficiency depends on drop capture efficiency, the smallest size ballotini with smaller mean void diameter, will be more effective in capturing the small drops than the larger size ballotini. On the other hand, coalesced drop release is more difficult for the smaller size ballotini than for the larger size, and for deep beds it may induce drop redispersion and hence hinder the separation efficiency.

For a 5×10^{-2} m bed depth, the average coalesced drop size is slightly higher for the smallest size ballotini used, but remains almost constant for the other sizes. For the 20×10^{-2} m, however, the largest exit drop size belongs to the largest ballotini diameter used, and the wide drop size distribution obtained may suggest that there is some drop redispersion for deep beds.

8.2.3 Effect of Phase Ratio on Coalesced Drop Size

Under steady state conditions, the average exit drop size was independent of phase ratio within the range 0.1% v/v to 1.0% v/v as shown in Fig. 8.6. This indicated that the degree of coalescence was independent of the ratio of dispersed phase entering the bed and is in total agreement with the results obtained in parallel studies for the dispersed phase ratio range 0.1% v/v to 7.0% v/v (13,112,138,141).

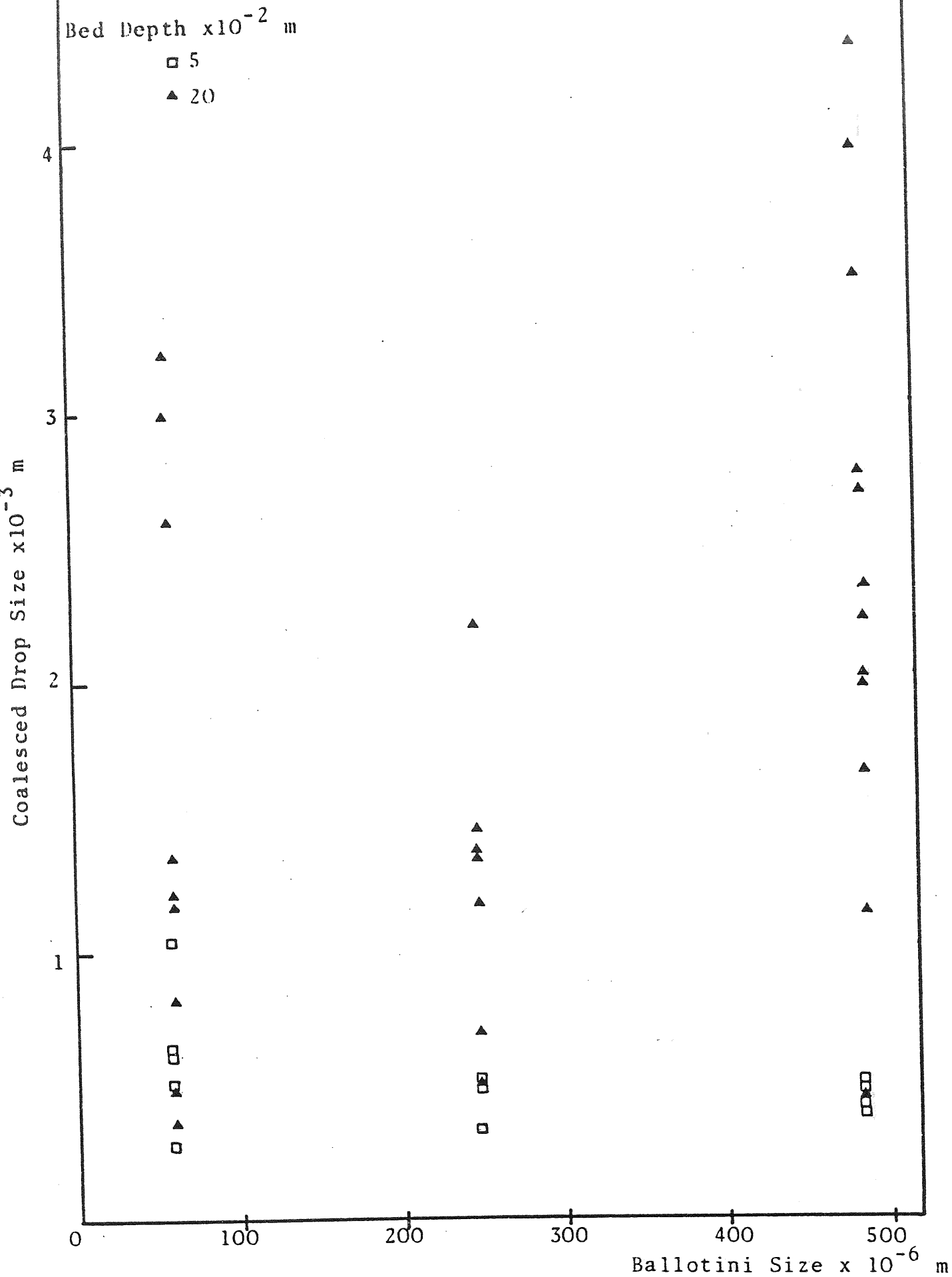


FIG. 8.5 VARIATION OF COALESCED DROP SIZE WITH BALLOTINI SIZE FOR BED DEPTH 5×10^{-2} m and 20×10^{-2} m AT CONSTANT VELOCITY 10×10^{-3} m/s

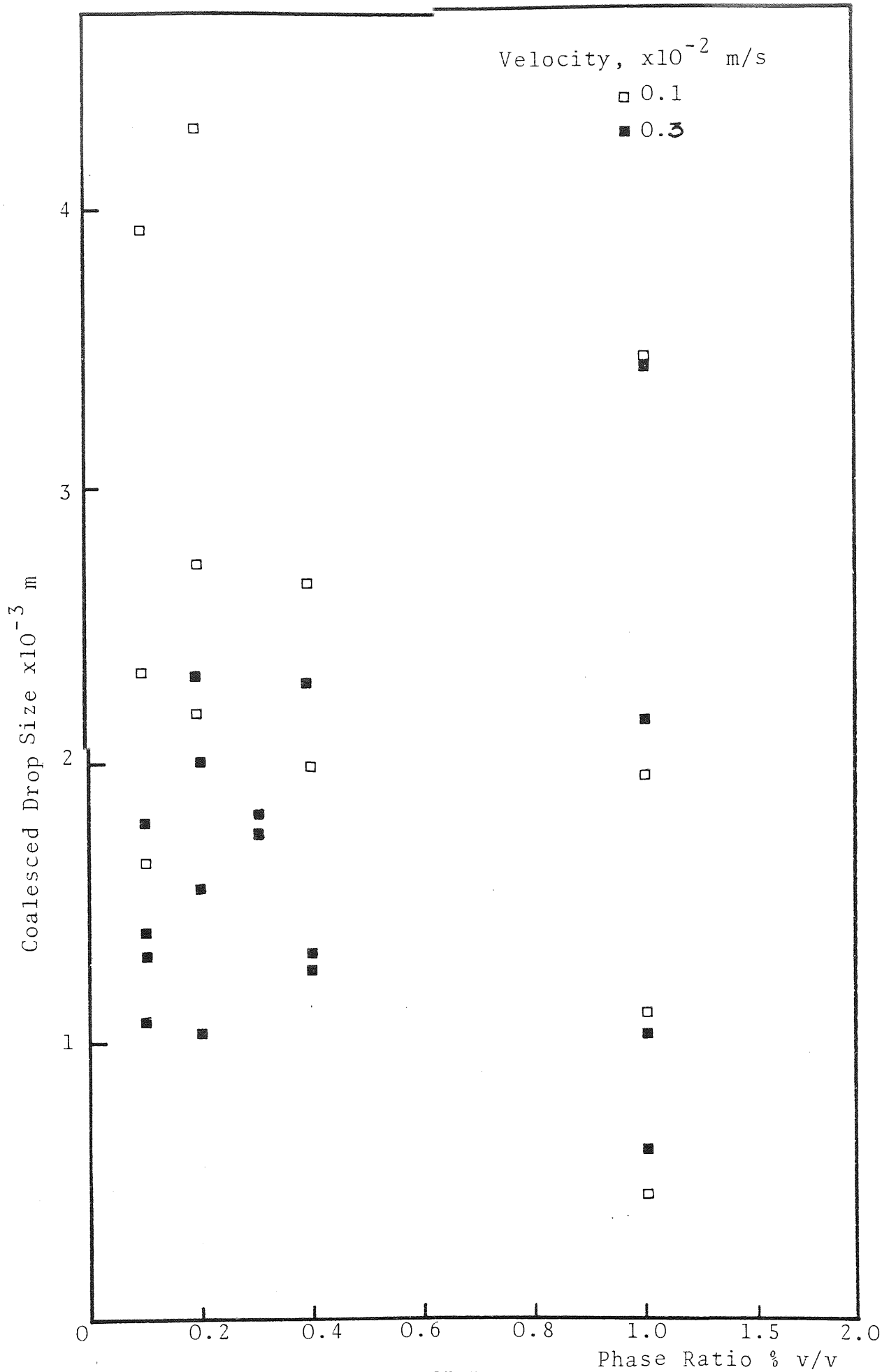


FIG. 8.6 VARIATION OF EXIT DROP SIZE WITH PHASE RATIO FOR BED DEPTH 20×10^{-2} m, 486 μ m BALLOTINI SIZE, CONSTANT VELOCITY

8.3 DROP RELEASE

Observation of the release of coalesced drops at the exit phase of the coalescer was performed in order to determine whether any of the previous reported release mechanisms took place (13,14,40,63,69,105,111,112,138).

There was no drip-point or ballooning type mechanisms of drop formation at the exit of the packing. The drops broke out, in clusters having a wide range of sizes at intermittent intervals, from fixed points at the exit of the bed which suggests the presence of fixed channels supplying the dispersed phase within the coalescer. This phenomenon is shown in Fig. 8.7. Also, there were single droplets leaving the coalescer rising slowly, but when observed more closely, it was noticed that glass ballotini was attached to them, being carried downstream similar to "froth-flotation" type operations, as shown in Fig. 8.8.

If the ballotini used for packing contained any foreign or irregularly shaped particles, these will collect at the bed exit after long operation, and some coalesced drops will become attached to them, and unable to overcome the impeding adhesion and interfacial tension forces attaching them to these particles, will remain at the bed exit throughout the experiments. This is shown in Fig. 8.9.

The intermittent break-out of group of drops at fixed points on the bed, suggested the existence of preferential channels for the release of the dispersed phase. The different exit drop sizes encountered within a cluster of drops however suggested that the dispersed

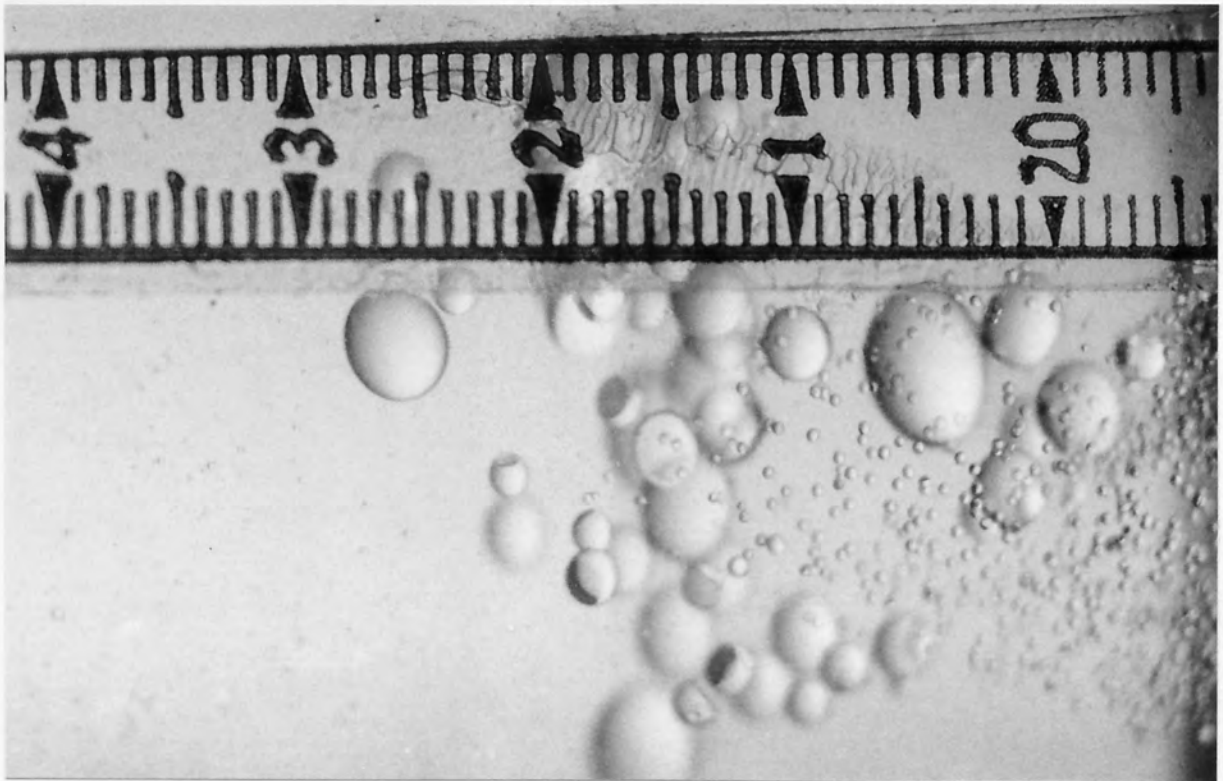
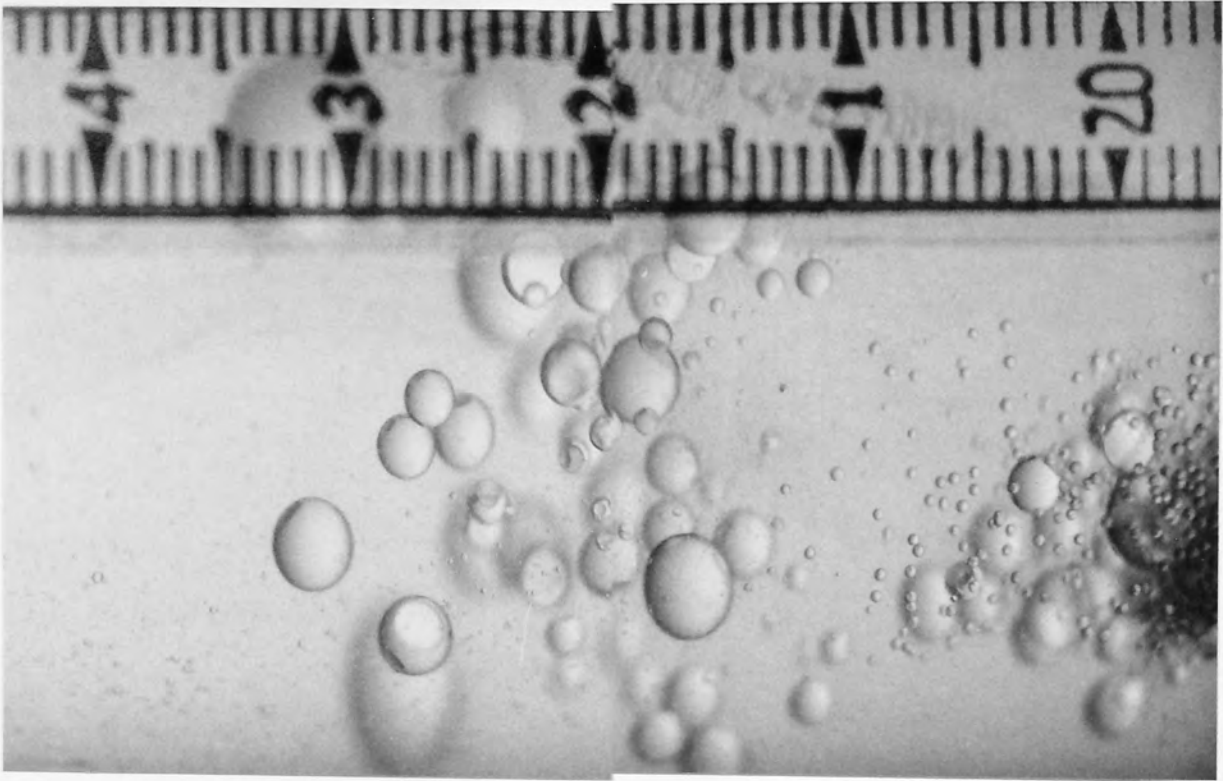


Figure 8.7 Drop Release of Coalesced Drops at Exit Face.

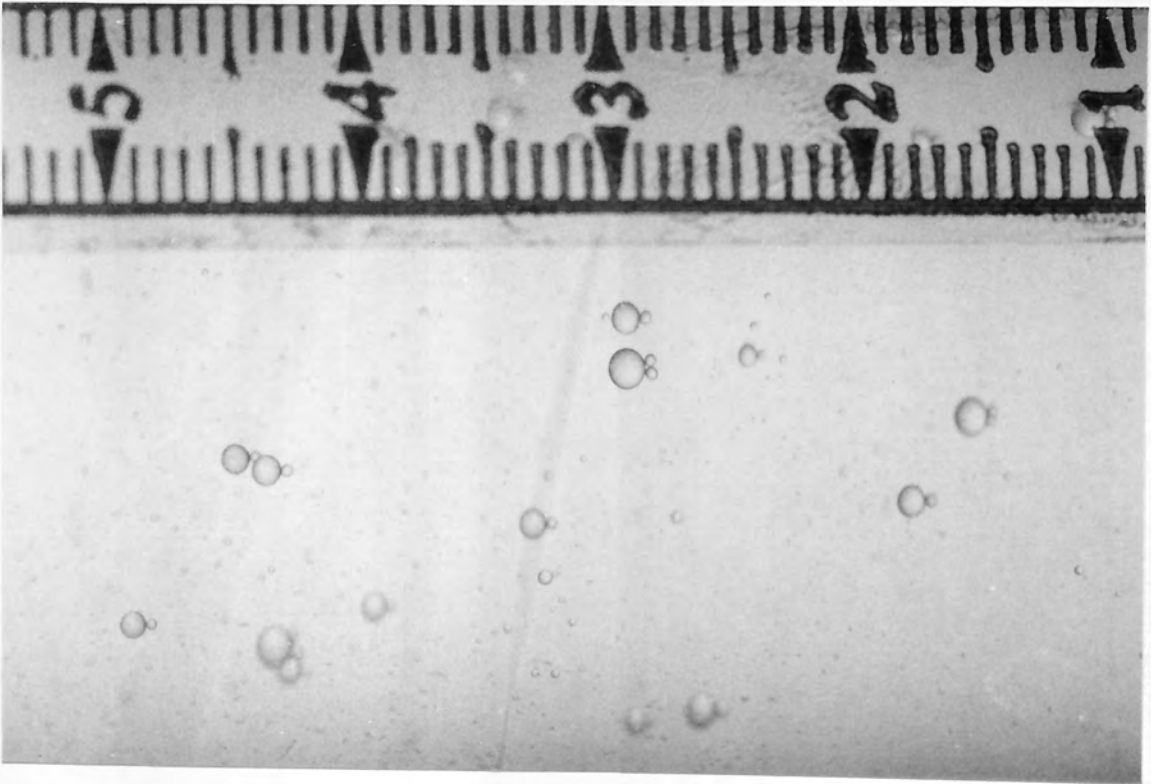
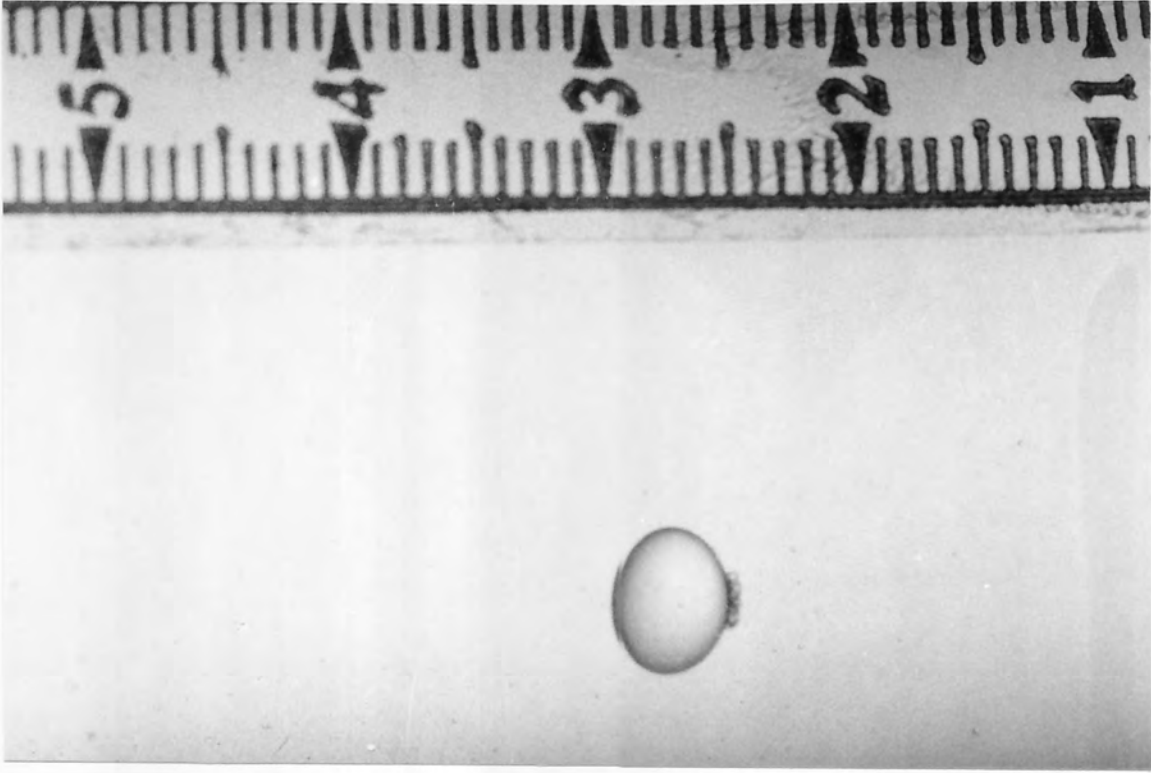


Figure 8.8 "Froth-Flotation" Type Mechanism Observed at Low Superficial Velocities.

phase channels did not exist as a continuum, but as single coalesced drops travelling together through the coalescer, possibly collecting more coalesced drops on their way towards the exit of the bed, and with inter-drop coalescence expected to occur at this stage.

Further experiments to prove this were carried out with the dispersed phase dyed with 'oil green' dye, which was immiscible with the continuous phase. This dye was preferred to the continuous phase soluble ones because with the packing being preferentially wetted by the continuous phase, after few experiments the packing was stained and it made difficult the observation of the coalesced drops within the packing.

Cine-films and photographs of the coalescer bed were taken and several previously unreported phenomena were observed.

The first 'coalescence sites' were formed nearer to the inlet face of the coalescer bed. As the drops became larger by coalescence or by flocculation with nearby 'coalescence sites', they move slowly upward, as threads, in a zig-zag motion adding smaller stationary coalesced drops as they advanced towards the exit of the coalescer bed. If the group of coalesced drops moving together was large enough to overcome the hindering forces within the coalescer, they would advance rather fast, deforming where necessary, and as the packing and continuous phase rearranged themselves, they trapped the smaller coalesced drops that trailed along the bigger droplets. These smaller droplets, may act as 'coalescer sites' or may be

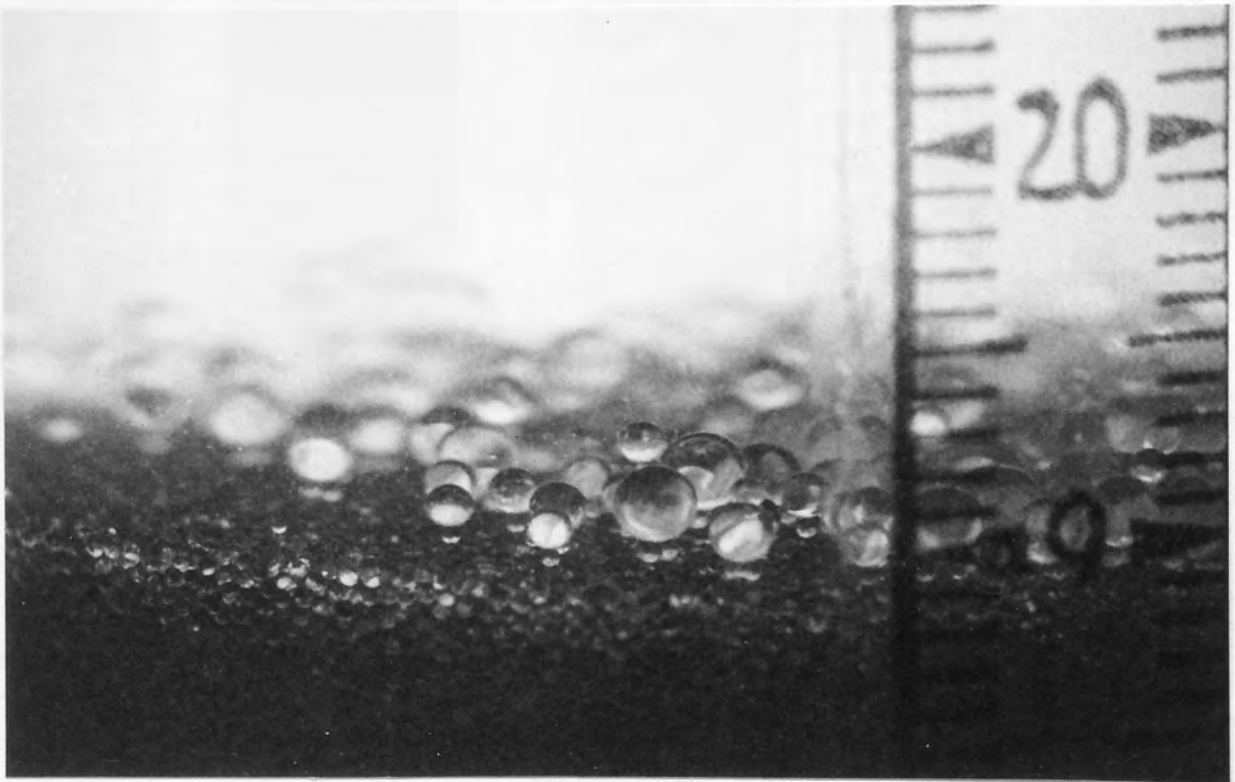
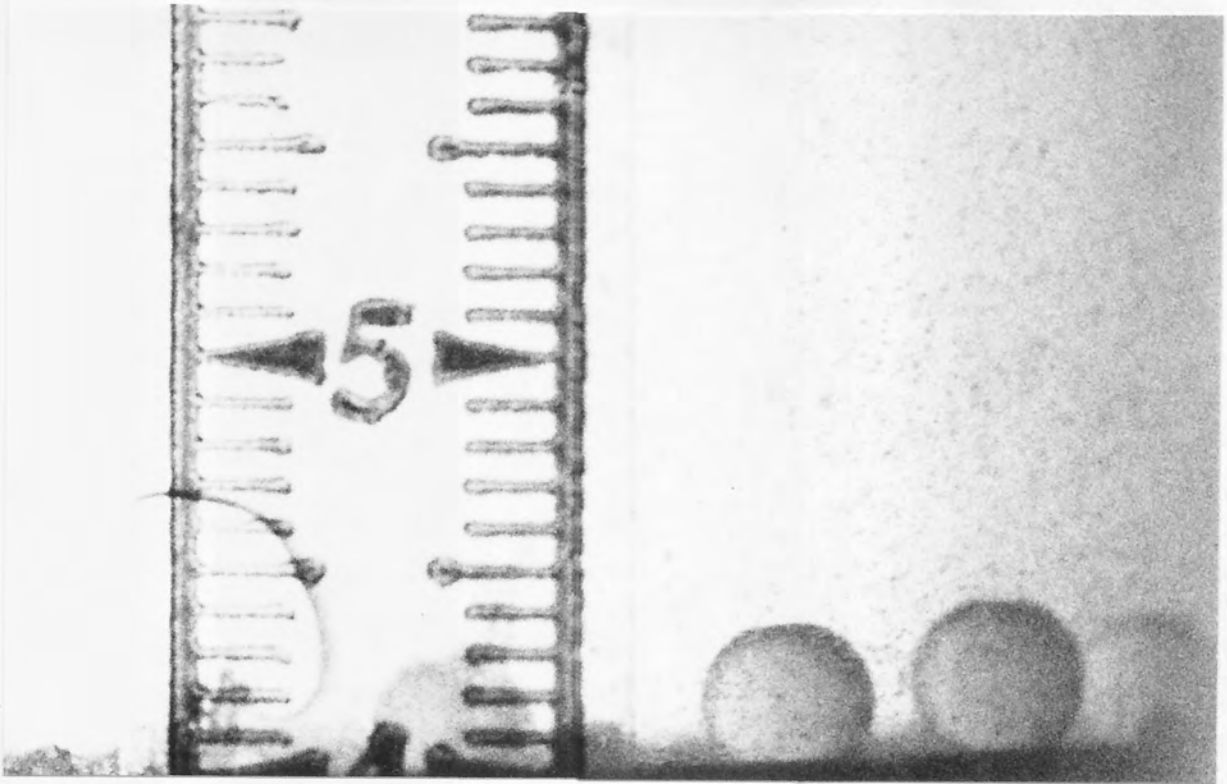


Figure 8.9 Coalesced Drops Residing at Exit Face at Low Superficial Velocities.

slowly carried downstream by the flow of continuous phase. If any of these newly formed 'coalescence sites' were disturbed by the motion of thread-like dispersed phase being released, it caused premature detachment of the droplets and hence, the different size range of the exit drop size.

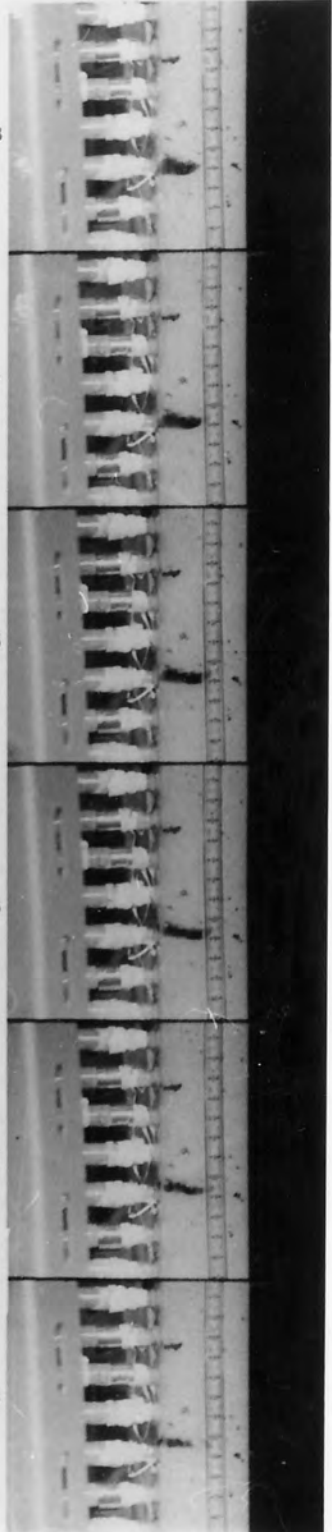
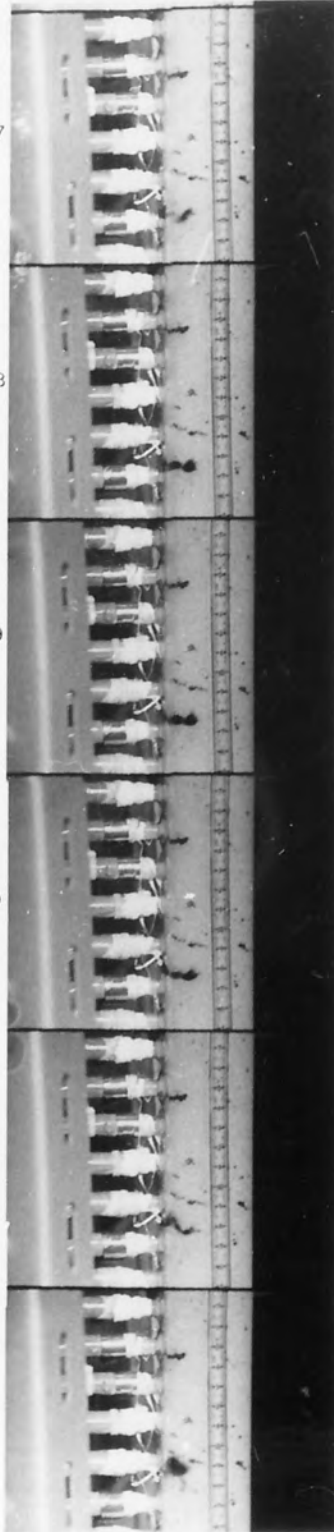
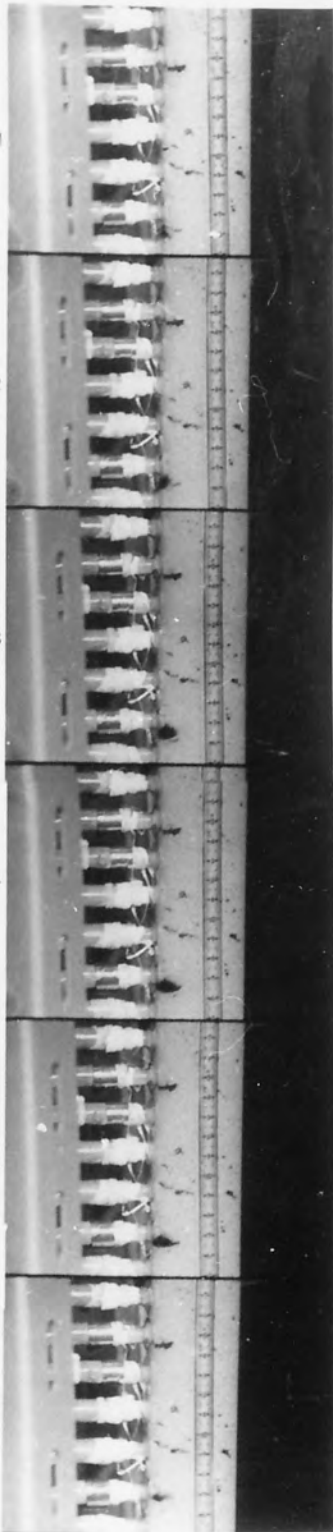
The zig-zag motion is shown in Figs. 8.10, 8.11 and 8.12.

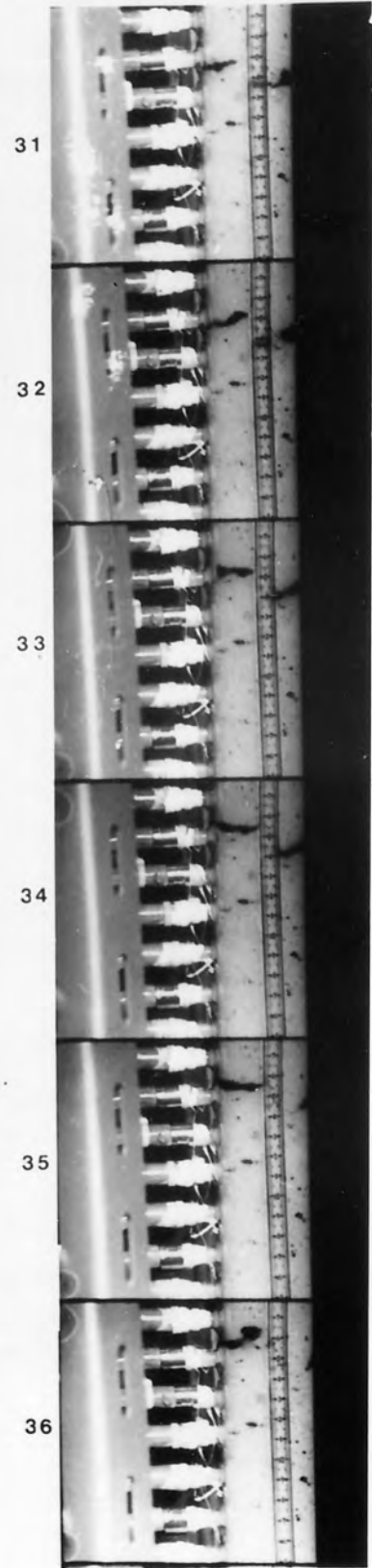
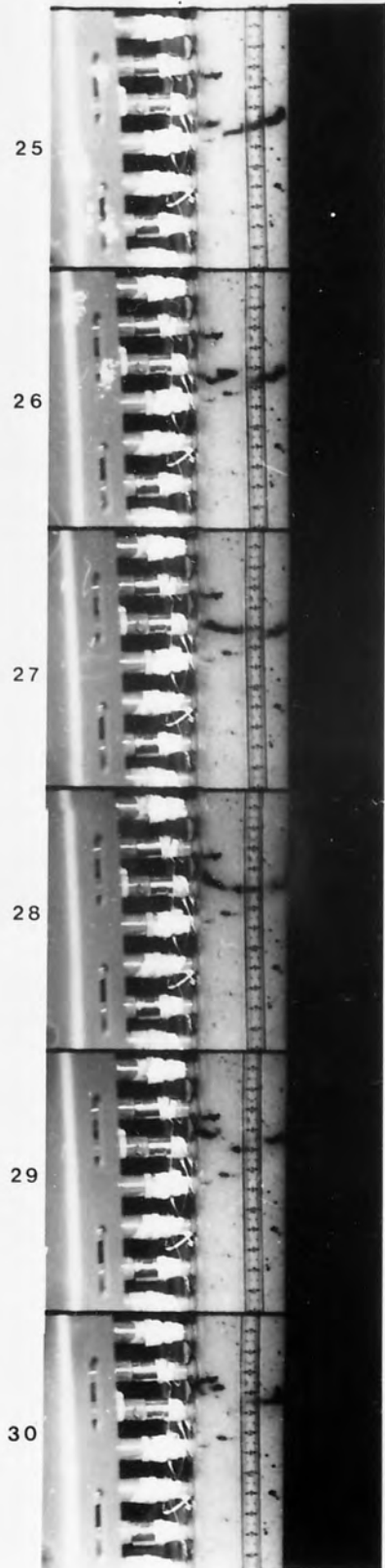
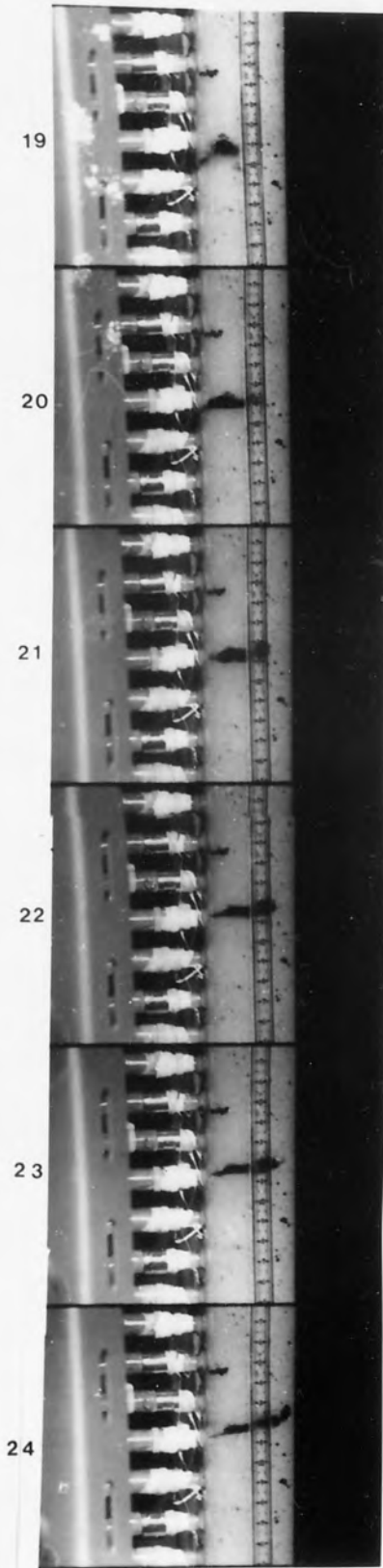
8.4 EFFLUENT SECONDARY DROPS

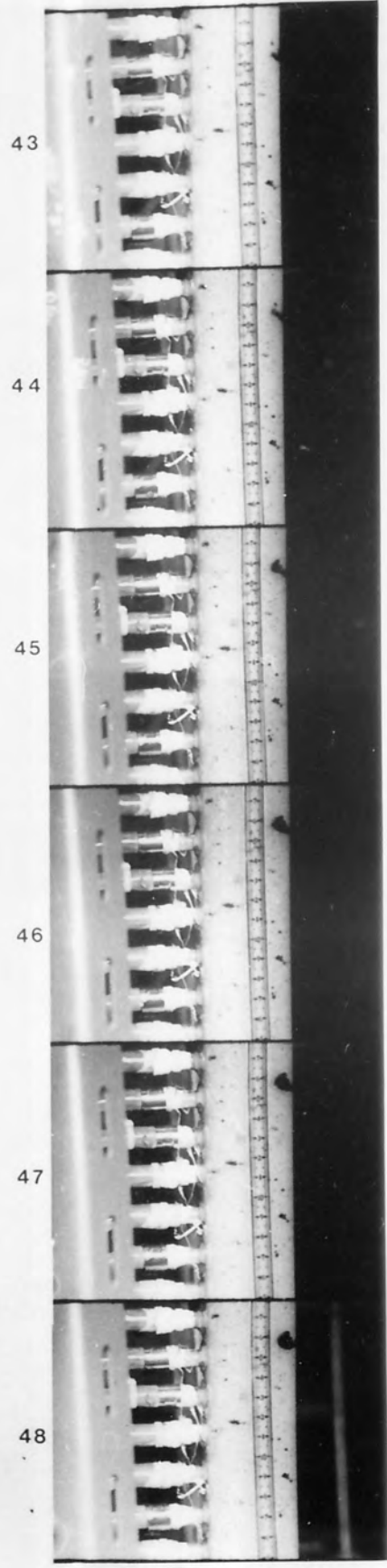
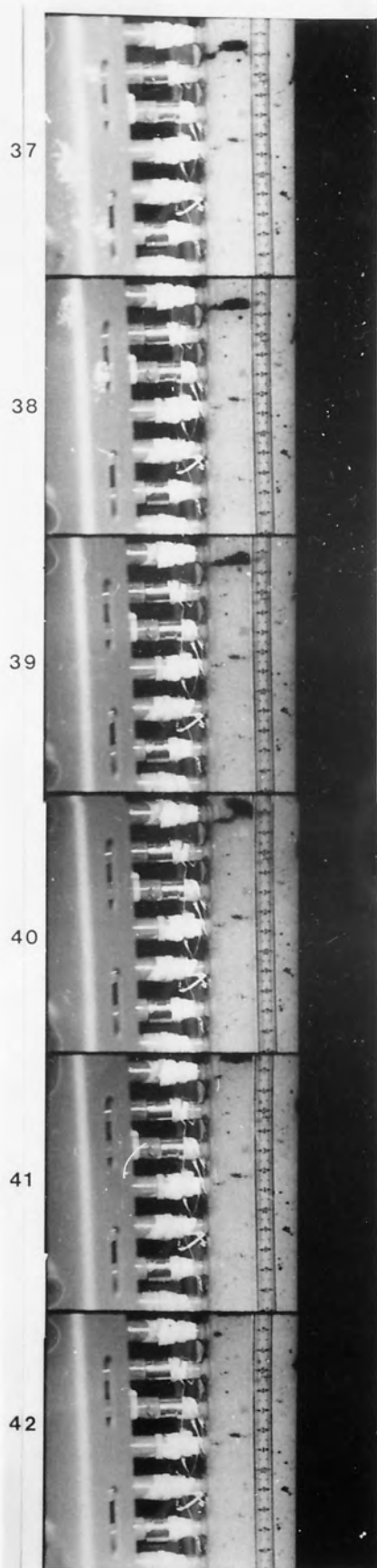
The mean diameter of the uncoalesced secondary drops determined by microscopy and by using the Malvern 2200 Particle Sizer as described in Chapter 7, are presented in Figs. 8.13, 8.14, 8.15 and 8.16. These show that the diameter of the secondary drops is not sensitive to change in bed depth, phase ratio or superficial velocity but it decreased with decreasing ballotini size. This suggests that the mean effluent drop size is related to the mean void diameter of the packing and the mean inlet drop size.

From calculations of mean void diameter for cubic and triangular packing arrangements the minimum inlet drop size required for capture by the pore can be calculated. For the 57.5 μm ballotini size the values of 47.6 μm and 17.8 μm are the predicted values of the mean void diameter for the cubic and triangular packing arrangement respectively. This means that, for the cubic packing, all the drops with sizes less than 47.6 μm will pass through the interstices. Assuming that the mean inlet drop size is 25 μm (Chapter 7), it means that no coalescence

Figures 8.10, 8.11 and 8.12:
Cine-Film Photographs of Coalesced Dispersed Phase Moving
Through the Coalescer. Starting at bottom left of frame
No.1, through to 41, the zig-zag motion of coalesced
dispersed phase through the coalescer can be observed.
Frames No. 43-48, a similar coalescence band from back
of coalescer is viewed.







will occur. For the triangular arrangement however, only droplets of less than $17.8 \mu\text{m}$ will pass through uncaptured. From the results in Fig. 8.14 it can be seen that the effluent drop sizes are less than $20 \mu\text{m}$ for different superficial velocities which suggests a triangular arrangement.

For the $486 \mu\text{m}$ size ballotini, the mean void diameters calculated are $402 \mu\text{m}$ and $150 \mu\text{m}$ for the cubic and triangular packing arrangements respectively, and given the mean inlet drop size considered, predicts no capture of drop by the interstices. From Fig 8.13 it can be seen that the effluent drop size is less than $40 \mu\text{m}$. The possible explanation for this is that the effluent samples were taken downstream the coalescer after the effluent has pass through a "settler" to ensure the separation of the primary dispersion.

For high dispersed phase ratio, the effluent drop size found was larger than for the lower ones, but as explained in Section 8.1, for high phase ratios the mean inlet drop size increases, and therefore aids capture (Figs. 8.15 and 8.16).

8.5 SEPARATION EFFICIENCY

The separation efficiency of the bed, determined by a material balance over the coalescer, is presented in Figs. 8.17 and 8.18. In Fig. 8.17 the separation efficiency decreases with increased superficial velocity to almost a constant value. This behaviour is similar to that exhibited by the coalesced drop size with increased

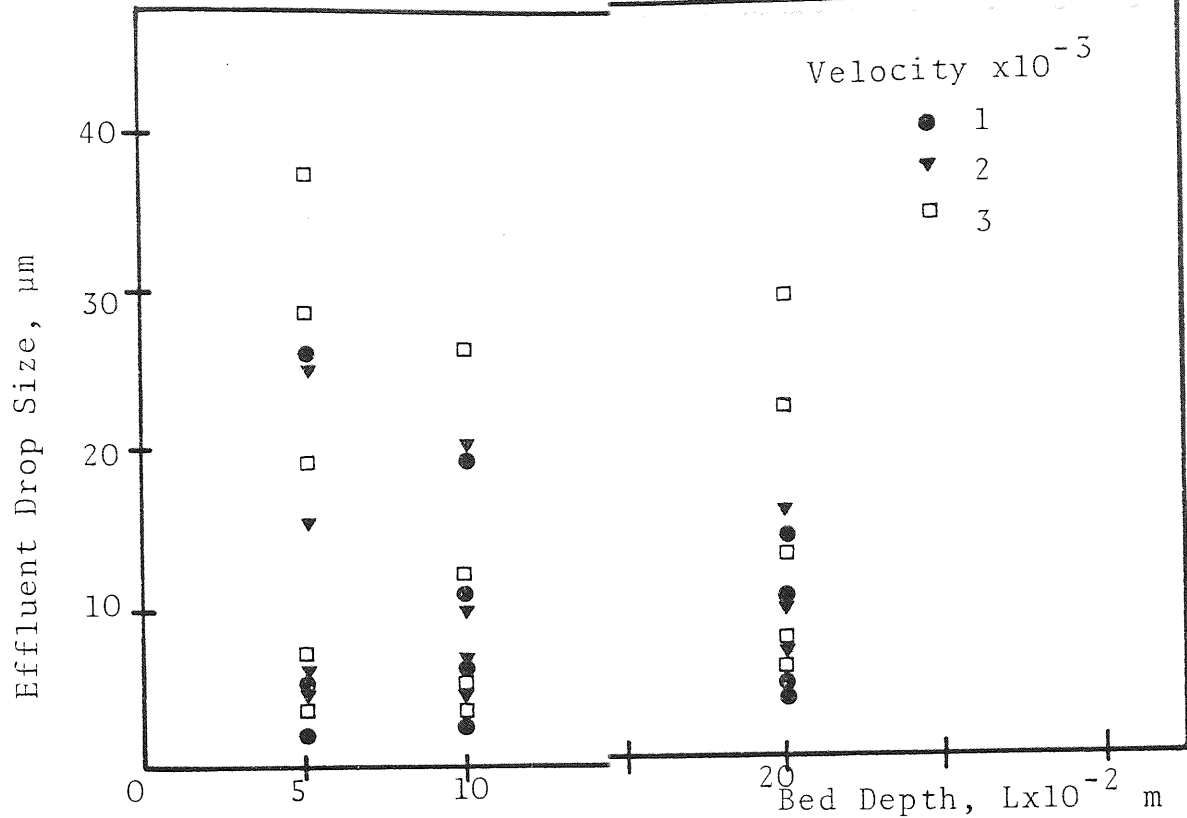


FIG. 8.13 VARIATION OF EFFLUENT DROP SIZE WITH BED DEPTH FOR BALLOTINI SIZE $486 \mu\text{m}$

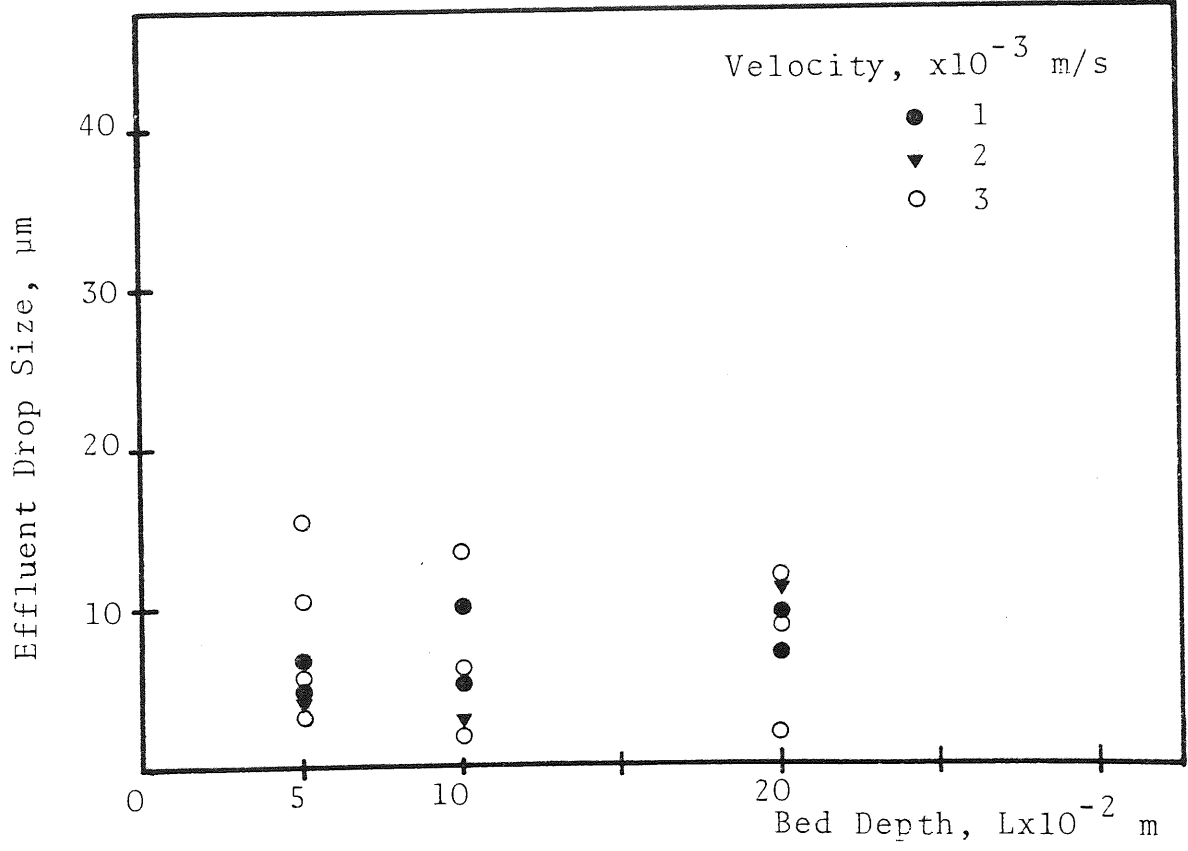


FIG. 8.14 VARIATION OF EFFLUENT DROP SIZE WITH BED DEPTH FOR BALLOTINI SIZE $57.5 \mu\text{m}$

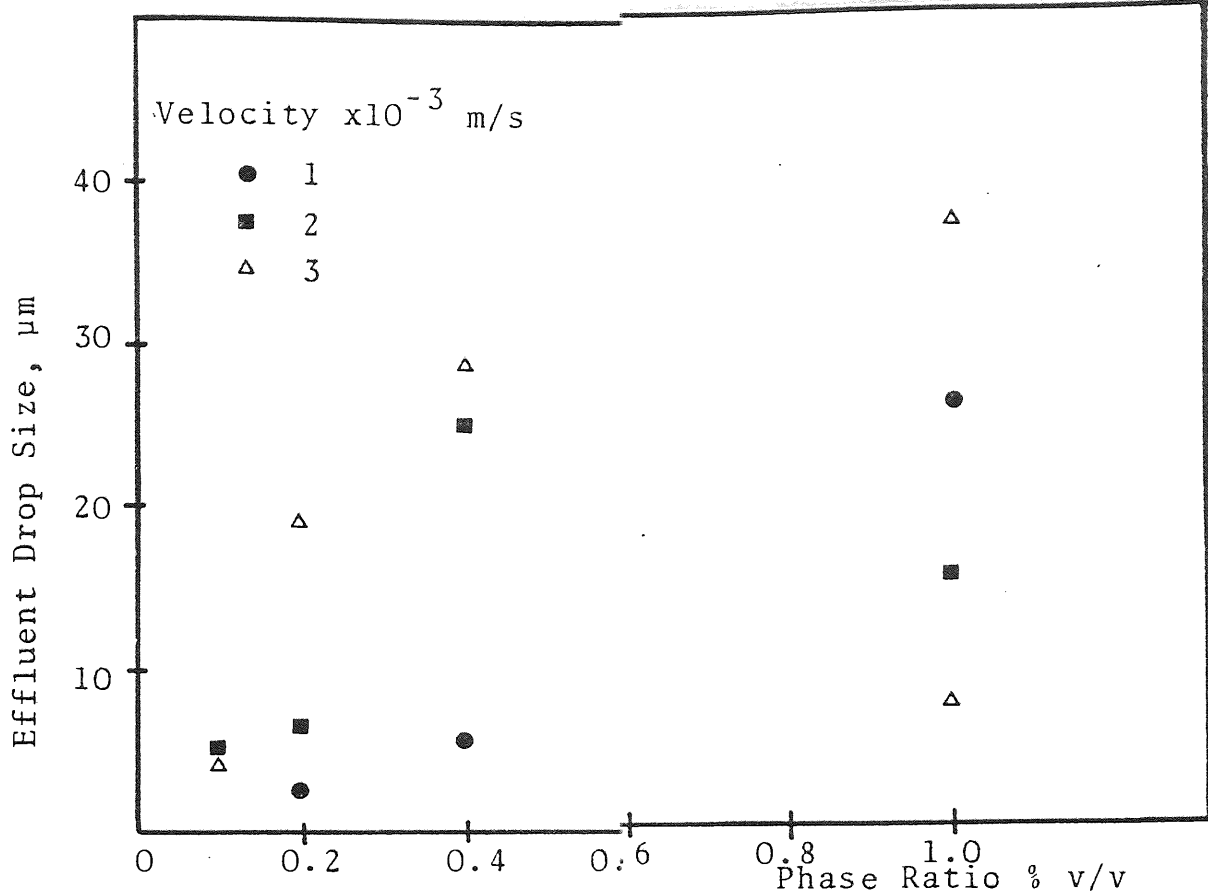


FIG. 8.15 VARIATION OF EFFLUENT DROP SIZE WITH PHASE RATIO FOR BALLOTINI 486 μm AND 5×10^{-2} m BED DEPTH

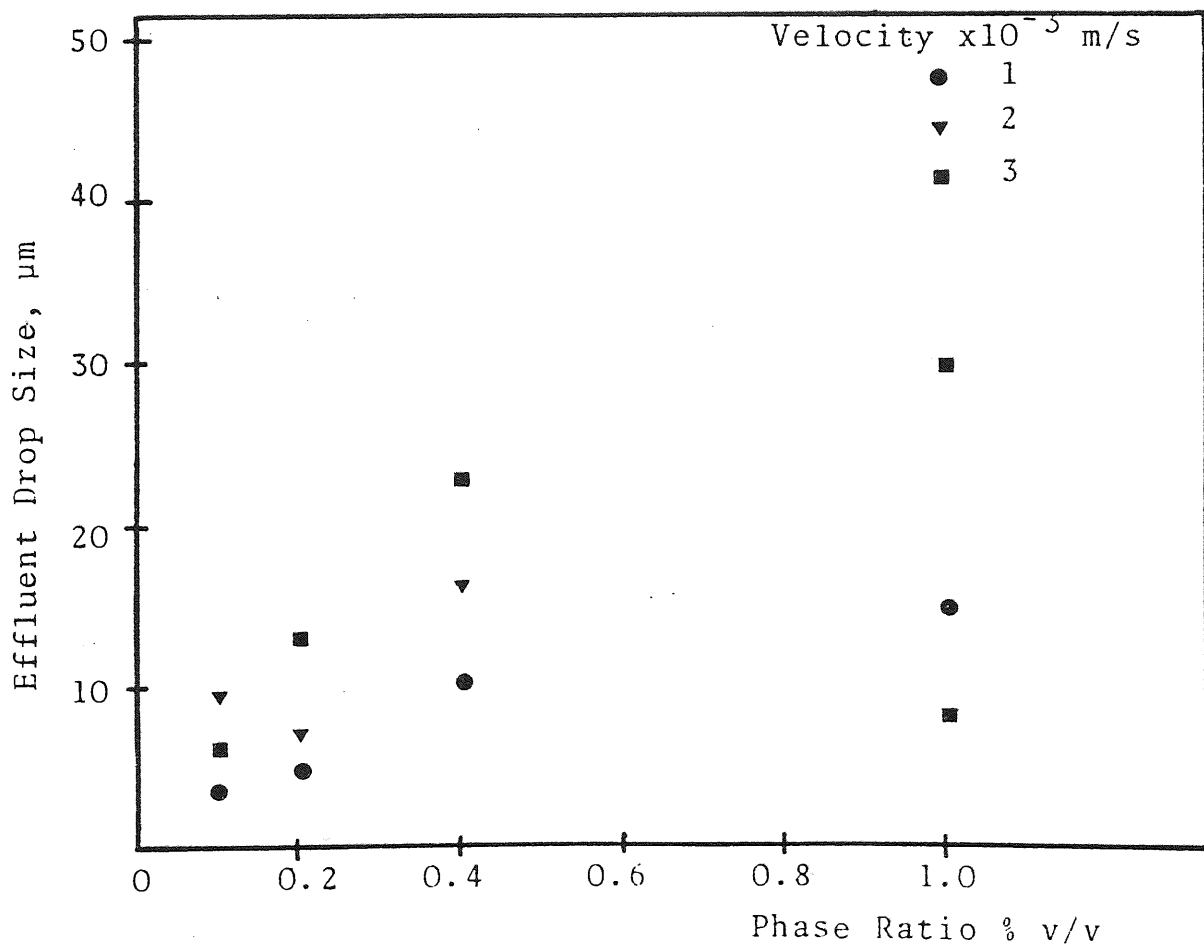


FIG. 8.16 VARIATION OF EFFLUENT DROP SIZE WITH PHASE RATIO FOR BALLOTINI 486 μm AND 20×10^{-2} m BED DEPTH

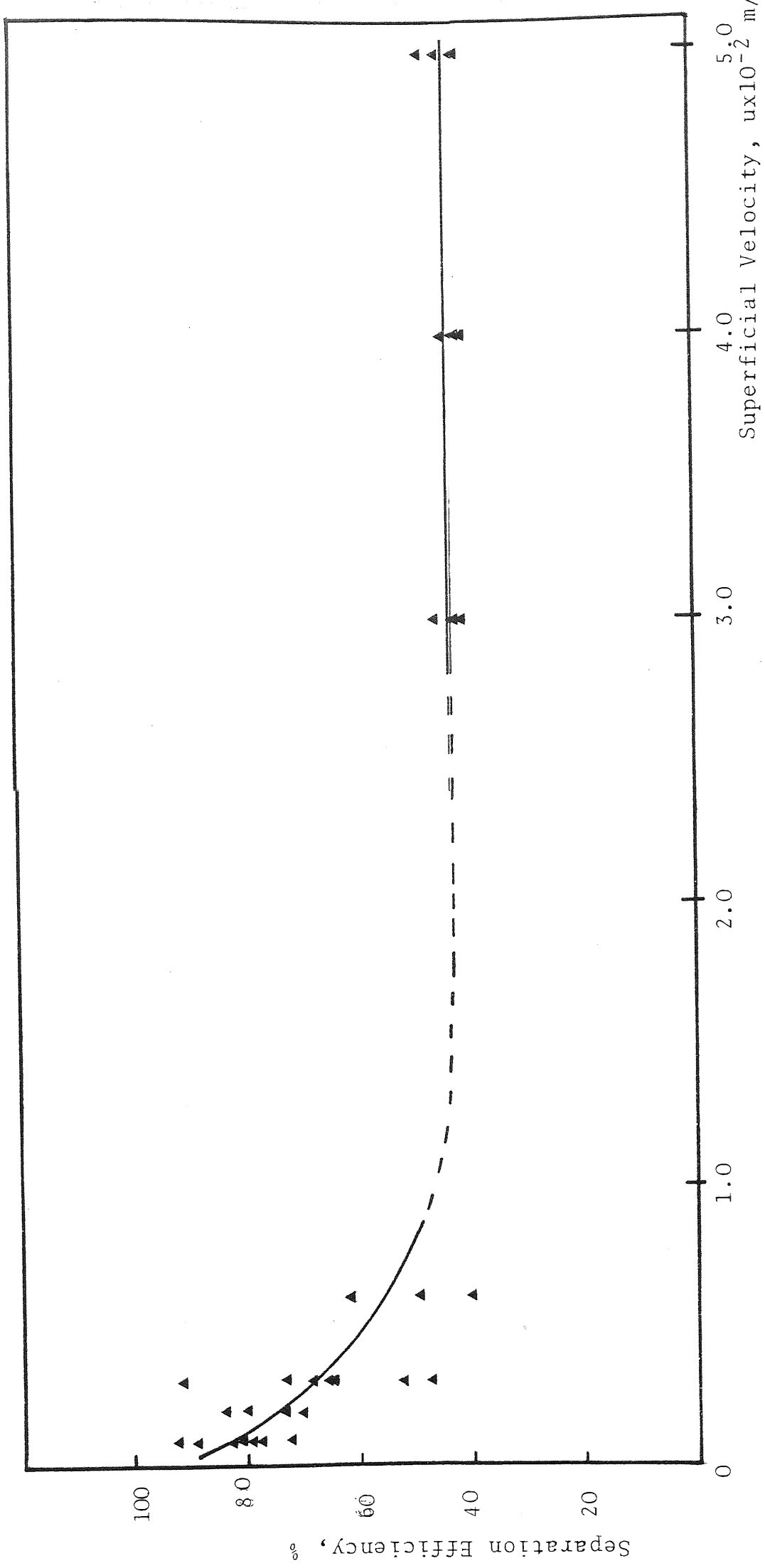


FIG. 8.17 VARIATION OF SEPARATION EFFICIENCY WITH VELOCITY

superficial velocity (Fig. 8.3). As the drop size decreases, greater hydrodynamic forces entrain the smaller drops downstream out of the coalescer with the effluent, thus lowering the separation efficiency.

For experiments at the same operating conditions, the longer the operating time the higher the separation efficiency. This suggests that as time increases more coalescing sites are filled, thus decreasing the effective porosity of the bed and impeding the passage of incoming drops, and therefore increasing interdrop coalescence with a previously capture drop and improving the coalescence efficiency of the bed.

An increase in dispersed phase ratio increased the separation efficiency and decreased the time required to achieve steady-state operation. This suggests that as the number of inlet drops increases they will fill the interstices of the bed faster than that at a lower rate of inlet drops thus reaching steady-state faster, and also that, perhaps a finite amount of hold-up of dispersed phase is required before steady state is reached. This is presented on Fig. 8.18.

Ultimately, for any given experimental conditions, there is a maximum limit to the separation efficiency for the system that remains constant regardless of the operating time.

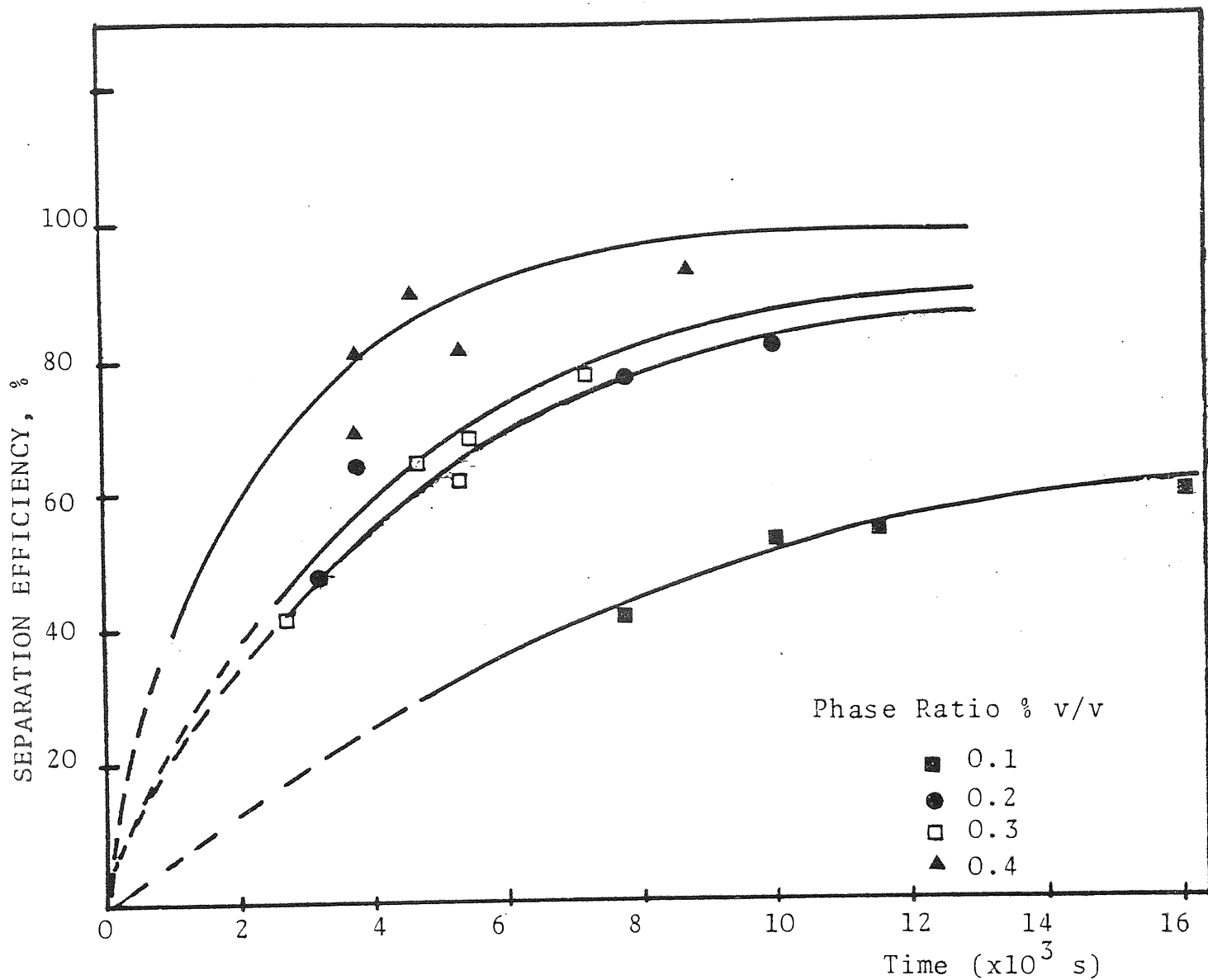


FIG. 8.18 VARIATION IN SEPARATION EFFICIENCY WITH PHASE RATIO FOR BALLOTINI SIZE $486 \mu\text{m}$ 20×10^{-2} m BED DEPTH AND 0.3×10^{-2} m/s SUPERFICIAL VELOCITY

CHAPTER NINE
ANALYSIS OF PRESSURE DROP DATA

CHAPTER NINE

ANALYSIS OF PRESSURE DROP DATA

9.1 FLUID FLOW EQUATIONS

As discussed in Chapter 6, monosized glass spheres were selected as the packing media since their internal geometry would be known. For the case of beds of particles or fibres there are different model approaches for the treatment of single phase flow. Two fundamentally different approaches can be distinguished: in one, the flow inside conduits is analysed; in the other, the flow around solid objects immersed in the fluid is considered. For low and intermediate porosities the conduit flow approach is more appropriate, whereas for very high porosities the second approach is more suitable.

The empirical correlations obtained, often aided by dimensional analysis and theoretical considerations, have been called "phenomenological models" (143). This approach is independent of considerations pertaining to conduit flow or flow around submerged objects.

Phenomenological models have proved to be particularly useful in the case of packs of fairly uniform and isometric particles or of fibres. They relate the transport coefficients of the porous media to grain properties and packing structures.

Within the conduit flow approach, the "geometrical" and "statistical" models are distinguished, both of which are, in part, based on available knowledge of pore structure. The simplest kind of geometrical model

consists of a bundle of straight cylindrical capillaries of uniform cross section. Other, more sophisticated, geometrical models have been suggested by several authors. In the statistical models the random nature of the interconnectedness and/or orientation has been emphasised.

Channel flow has been treated mostly in the approximation which neglects all but one velocity component, resulting in Hagen-Poiseuille type flow equations. Recently there have been reported a few contributions in which the complete Navier-Stokes equation have been solved for special channel geometries.

The continuum approach to modelling porous media does not distinguish between conduit flow or flow around submerged objects. This is essentially a deterministic approach because certain basic physical laws (the continuity equation for mass and the momentum equation) are assumed and these equations are averaged over the volume under consideration.

The approaches considering flow around solid objects, sometimes also called "drag theories", are variants, extensions, or generalisations of Stoke's Law.

Most of these models have been expressed in terms of the specific permeability k of the medium. The first relation of its kind was proposed by Darcy (144)

$$u = \frac{k}{\mu c} \cdot \frac{\Delta P}{L} \dots\dots\dots (9.1)$$

often termed as Darcy's Law, has subsequently been confirmed by a number of workers.

A different way of expressing the resistance of the porous medium to flow is with the help of the friction factor f_p , defined by the equation

$$f_p = \frac{d_c}{\rho_c u^2} \cdot \frac{\Delta P}{L} \dots\dots\dots (9.2)$$

as a function of the superficial or particle Reynolds number, N_{Re} .

$$N_{Re} = \frac{d_c u \rho_c}{\mu_c} \dots\dots\dots (9.3)$$

The different models are presented in the following sections in terms of either the permeability or the friction factor.

9.1.1 Phenomenological Models

Phenomenological permeability models have appeared at the end of the nineteenth century (145), but only relatively recently has there been published a more-or-less general dimensional analysis of the problem (146). According to the analysis of Rumpf and Gupte (146), there is the following relationship among the dimensionless parameters:

$$\frac{\Delta P}{\rho_c u^2} = f(\bar{u} d_c / \nu, L / \bar{d}_c, e_1, q_i, \phi_i, \text{structure}) \quad (9.4)$$

The various parameters that characterise particle shape and packing structure may be very difficult to evaluate in the general case. The complications may become unsurmountable if there are several very different particles present in the pack. Neglected in the dimensional analysis were the compressibility or expandability δ of the pack, the effects of interfacial energy,

suspended matter, dissolved gases, and in the case of gaseous flow, the mean-free path of the molecules.

For random packs consisting of various distributions of spherical particles over a wide range of voidages they gave an expression for the permeability as:

$$k = \frac{\bar{d}_{c2}^2 e_1^{5.5}}{5.6 k_1} \dots \dots \dots (9.5)$$

where \bar{d}_{c2} is the "surface average" sphere diameter and the value of the constant k_1 depends on the particle size distribution parameters, particle shape and packing structure.

Empirical permeability correlations with voidage and grain size distribution have been given for reservoir sands and sandstones by Morrow et al (147), Berg (148) and Pryor (149).

Various empirical correlations for the permeability of fibrous beds have been proposed by Davies (150), Chen (87), and more recently Kyan et al (151) among others.

The transition from the linear portion of f_p versus N_{Re} relation (range of validity of Darcy's law) to the non-linear one is gradual. It was pointed out by Scheidegger (152) that for various porous media the value of the Reynolds number above which Darcy's law is no longer valid has been found to range between 0.1 and 75. For most data analysed by Macdonald et al (153), the deviation from linearity starts to become noticeable in the range $N_{Re}/(1-e_1) \approx 1-10$

Chilton and Colburn (154) suggested that for low rates of flow ($N_{Re} < 40$)

$$2f_p = 850/N_{Re} \dots\dots\dots (9.6)$$

and for high rates of flow,

$$2f_p = 38/(N_{Re})^{0.15} \dots\dots\dots (9.7)$$

Morcom (155) carried out work where the flow is intermediate between streamline and turbulent. For spheres and irregular broken materials he proposed

$$f_p = \frac{800}{N_{Re}} + 14 \dots\dots\dots (9.8)$$

and for flat ended cylinders

$$f_p = \frac{1750}{N_{Re}} + 28 \dots\dots\dots (9.9)$$

At flow rates outside the range of validity of Darcy's law, the two best known relationships are, for intermediate values of N_{Re} up to about 10^3 , the Ergun (156) equation

$$f_p \{e_1^3/(1-e_1)\} = (150/N_{Re})(1-e_1) + 1.75 \dots\dots (9.10)$$

and, for higher values of N_{Re} , the Burke-Plummer equation

$$f_p \{e_1^3/(1-e_1)\} = 1.75 \dots\dots\dots (9.11)$$

Recently Macdonald et al (153) have tested the Ergun equation, using much more data than was ever used before by others. He found the following relations to give the best fit to all the data:

$$\text{smooth particles: } f_p \{e_1^3 / (1 - e_1)\} = (180 / N_{Re}) (1 - e_1) + 1.8$$

..... (9.12)

$$\text{roughest particles: } f_p \{e_1^3 / (1 - e_1)\} = (180 / N_{Re}) (1 - e_1) + 4.0$$

..... (9.13)

For intermediate surface roughness, the value of the second, so called "inertia" parameter lies between 1.8 and 4.0.

The data used by Macdonald et al in the preceding test was the one used in the work of Gupte (157) with mixtures of glass spheres; cylindrical fibre beds of Kyan et al (151); spherical marble mixtures, sand and gravel mixtures of Dudgeon (158); consolidated media of Fancher and Lewis (159); a variety of cylindrical packings of Pahl (160); and a wide variety of different materials (161,162,163).

Equations 9.12 and 9.13 can be expected to predict experimental data for a wide variety of unconsolidated porous media with a maximum error of $\pm 50\%$.

9.1.2 Models Based on Conduit Flow

The flow of a fluid in many porous media can be imagined to occur either in a network of closed conduits or around solid particles forming a spatial array.

The simplest approaches based on the idea of conduit flow do not take into account any irregular way in which different capillary sizes are interconnected with each other. These are considered "geometrical permeability models" in this study. Whenever a probability law is used

in the permeability model, the term "statistical model" seems appropriate, regardless of the other assumptions that may also be used in the model.

9.1.2.1 Geometric Permeability Models

The Carman-Kozeny model (164,165) often called the "hydraulic radius theory", is sometimes regarded as a phenomenological approach. In their approach the porous medium was assumed to be equivalent to a conduit, the cross section of which has an extremely complicated shape but, on the average, a constant area. A Hagen-Poiseuille type equation is assumed to give the average pore, interstitial, or seepage velocity and when related to Darcy's Law equation the value of the permeability is

$$k = e_1 d_H^2 / 16 K_o (L_e/L)^2 \dots\dots\dots (9.14)$$

The "hydraulic diameter" can be expressed as follows:

$$d_H = 4e_1/a(1-e_1) \dots\dots\dots (9.15)$$

where a is the specific surface area based on the solid's volume. By combining equations 9.14 and 9.15, the usual form of the Carman-Kozeny equation for the permeability is obtained:

$$k = e_1^3 / K_o (L_e/L)^2 (1-e_1)^2 a^2 \dots\dots\dots (9.16)$$

where $(L_e/L)^2$ is usually called "tortuosity" (T). According to Carman, the best value of the combined factor $K = K_o (L_e/L)^2$ to fit most experimental data on

packed beds is equal to 5, where K is the "Kozeny constant". Defining the mean particle diameter d_c as the diameter of the hypothetical sphere with the same specific surface, a , as the particle,

$$d_c = \frac{6}{a} \dots\dots\dots (9.17)$$

the final equation for permeability becomes

$$k = \frac{d_c^2}{180} \cdot \frac{e_1^3}{(1-e_1)^2} \dots\dots\dots (9.18)$$

Geometric Models based on the pore entry diameters were reviewed by Scheidegger (152), who distinguished straight-, parallel-, and serial-type capillarc models.

The first of these consist of a bundle of parallel capillaries of equal length and the same diameter d . For this model, the following expression was obtained for the permeability:

$$k = e_1 d^2 / 32 \dots\dots\dots (9.19)$$

In the "parallel-type" model the above expression is divided by three on the right hand side on the grounds that 1/3 of the capillaries should be pointing in each of three spatial directions. Second, a mean square diameter, $\overline{d^2}$, is evaluated according to some pore size distribution function. Each capillary is assumed to have a uniform cross section and there is flow only in 1/3 of the capillaries lying in the direction of the macroscopic flow in this model.

The permeability of Scheidegger's parallel-type capillary model is:

$$k = (e_1/96) \int_0^{\infty} d^2 \alpha(d) dd \dots\dots\dots (9.20)$$

where $\alpha(d)$ is a "pore size distribution" function.

In the "serial-type" capillarc model, the pore network is approximated by three identical sets of tortuous channels. Each channel is assumed to consist of segments of different diameters distributed according to some pore size distribution function. The expression for the permeability for this model is:

$$k = \frac{e_1}{96T} \frac{\{\int \alpha(d) dd / d^2\}^2}{\int \alpha(d) dd / d^6} \dots\dots\dots (9.21)$$

The factor 96 was again introduced on the grounds that 1/3 of the capillaries are pointing in each spatial direction.

9.1.2.2 Statistical Permeability Models

The cut-and-random-rejoin type model was introduced by the work of Childs and Collis-George (166) and was subsequently modified by Marshall (167) and Millington and Quirk (168). More recently, Brutsaert (169,170) has written reviews on this subject.

It is imagined that the sample is sectioned in two by a plane perpendicular to the direction of flow, and the two parts are joined together again in a random fashion. If the pores in the solid matrix are assumed to be distributed at random their chance of overlapping is governed by random probability.

Millington and Quirk (168) obtained the following expression for the permeability:

$$k = \frac{2e_1^{4/3}}{32} \int_0^\infty \alpha(d_e) dd_e \int_0^{d_e} (d_e^1)^2 \alpha(d_e^1) dd_e^1 \dots\dots\dots (9.22)$$

This differs in the expression obtained by Childs and Collis-George (166) and Marshall (167) in the voidage function, as they both used e_1^2 .

An improved version of a random network of capillary tubes was proposed recently by Haring and Greenkorn (171). They modelled the pore structure by a large number of randomly oriented, straight, cylindrical pores.

9.1.3 Models Based on the Navier-Stokes Equation

Published work making use of the complete Navier-Stokes equations can be divided into two different categories. In one, the complete Navier-Stokes equations have been solved numerically for flow channels of various, different geometries, whereas in the other the equations have been averaged over a representative portion of the porous medium. In the latter case, a special form of the equation of motion for porous media have been developed, whereas in the former the pressure and velocity fields have been numerically evaluated in representative flow channels.

In the models previously considered, only the z-velocity component was taken into account resulting in Hagen-Poiseuille type flow equations. It is evident that in convergent-divergent type of flow the radial velocity component may not always be negligible.

Payatakes et al (172) solved the Navier-Stokes

equations for periodically constricted tubes. The pressure drop and the velocity components have been obtained in dimensionless form for various values of Reynolds number.

Azzam (173) calculated the friction factors for the periodically constricted tubes considered by Payatakes et al using the Hagen-Poiseuille equation. He found that the ratio of the friction factor calculated by solving the complete Navier-Stokes equation is greater, in the worst case, only by a factor of about 1.3 than the value obtained by the Hagen-Poiseuille equation.

Other authors that have solved the Navier-Stokes equations for periodically constricted tubes are Runchal et al (174); Christiansen et al (175) and Azzam and Dullien (176).

Slattery (177) derived a theorem by which the Navier-Stokes equations could be averaged.

Using Slattery's averaging theorem and considering one-dimensional macroscopic flow, equations of the form of the Forchheimer equation could be obtained:

$$= -\frac{\Delta P}{L} = k_1 \mu_c u + k_2 \rho_c u^n \dots \dots \dots (9.23)$$

In the range of validity of the Forchheimer equation (178), k_1 and k_2 are constants by definition. At low velocities such as u^n is very much less than u , the Forchheimer equation reduces to Darcy's law. Ahmed and Sunada (179) and Heller (180) have obtained derivations of the Forchheimer equations by the averaging method suggested by Slattery.

The assumption of the Forchheimer equation to be the correct flow equation over the entire practical range of flowrates have been reviewed by Scheidegger (181).

9.1.4 Flow Models Based on Flow Around Submerged Objects

The subject of flow around submerged objects at low Reynolds numbers has been discussed in great detail in the work of Happel and Brenner (75). Using the concentric spheres cell model, they calculated the velocity through the bed compared with the Stoke's law velocity, as a function of voidage. Their treatment is limited to creeping flow where the inertial term in the Navier-Stokes equation may be neglected. Their result provides theoretical support for the validity of Darcy's law but does not attempt to answer the question of how the voidage of the bed affects deviations from Darcy's law at increasing Reynolds numbers.

Different models have been proposed by Brinkman (182), Kyan et al (151), Phillip (183), Lundgren (184) and Brenner (185) to predict the permeability but some of them lose their validity increasingly with decreasing porosities.

9.2 SINGLE PHASE FLOW PRESSURE DROP

A study of the single phase pressure drop was made to determine the flow characteristics of the packing media used. Measurement of pressure drop during flow of the continuous phase alone serves to check the reproducibility of the coalescer assembly and to detect

ingress of air or particulate matter into the bed. Single phase pressure drop data also provides a basis for comparison with two phase flow during coalescence.

Of the many equations used to describe single phase flow in packed beds, the Ergun equation (156) is the most frequently applied. Rearranging equation 9.10 and substituting for f_p and N_{Re} ,

$$\frac{\Delta P_1}{L} = \frac{150\mu_c u (1-e_1)^2}{d_c^2 e_1^3} + \frac{1.75\rho_c u^2 (1-e_1)}{d_c e_1^3} \dots (9.24)$$

for low values of Reynolds number, i.e.

$$\text{when } N_{Re} < 1$$

the second term on the right hand side is negligible and equation 9.24 reduces to the Blake-Kozeny equation.

Using the modified Ergun equation suggested by Macdonald et al (153), equation 9.12, and rearranging and substituting for f_p and N_{Re} :

$$\frac{\Delta P_1}{L} = \frac{180\mu_c u (1-e_1)^2}{d_c^2 e_1^3} + \frac{1.8\rho_c u^2 (1-e_1)}{d_c e_1^3} \dots (9.25)$$

which reduces to the Carman-Kozeny equation for low Reynolds number.

In both cases the value of the constant, 150 or 180, is equal to the product of the Kozeny constant, K and another constant relating the characteristic particle diameter to the specific surface. The commonly accepted value for the Kozeny constant is 5. However, as will be shown in the following sections K is dependent on the structure of the bed, voidage fraction and particle shape among other factors.

9.3 FACTORS AFFECTING THE VALUE OF THE KOZENY CONSTANT

9.3.1 Shape Factor and Tortuosity

According to Carman (164) the constant, K , can be written in the form:

$$K = K_0 \left(\frac{L_e}{L}\right)^2 \dots\dots\dots (9.26)$$

where K_0 is a shape factor believed by Carman to lie within the range 2.0 to 3.0 with a probable average value of 2.5. The quantity $(L_e/L)^2$, has been given the convenient appellation "tortuosity" by Rose and Bruce (186). It is the square of the ratio of the actual average effective length of fluid flow in a porous medium, L_e , to the geometrical length of the medium in the direction of macroscopic flow, L .

The value to be assigned to K is still controversial. Carman suggested that $(L_e/L)^2$ has the value of about 2.0 in all unconsolidated porous media. Then from equation 9.26, if K_0 is about 2.5, the magnitude of the Kozeny constant, K , would always be about 5.0. Much evidence that is now available certainly suggests that for unoriented particle aggregates in the void fraction range of 35 to 70%, K is $5.0 \pm 10\%$. The work of Coulson (187), however, strongly indicates that even in the restricted void fraction range of 30 to 45%, K is significantly dependent upon bed voidage and particle shape.

If Carman is correct and K_0 is substantially constant at a value of 2.0 to 3.0, it is apparent that K may be determined with an acceptable degree of precision if independent means of measuring tortuosity can be

found. It was first suggested by Thornton (188) that for multiphase fluid flow appropriate tortuosities were calculable from electrical resistivity measurements. Wyllie and Rose (189) extended this suggestion to all applications of the Carman-Kozeny equation. Cornell and Katz (190) modified the method of calculating tortuosity suggested by Wyllie and Rose while utilising the same basic electrical measurements. The method used by Cornell and Katz to compute tortuosity essentially is similar to that proposed by Winsauer et al (191).

In the derivation of the Carman-Kozeny equation it appears that a porous medium is envisaged as a pipe of complex but nevertheless statistically constant cross-sectional area (192). Wyllie and Rose have assumed that the equivalent Blake-Kozeny pipe is endowed with a cross-sectional area, $e_1 X$, and the effective length, L_e . Cornell and Katz, on the other hand, appear to have visualised a pipe with a constant cross-sectional area, $e_1 XL/L_e$, and an effective length, L_e . Wyllie and Gregory (193) tried to determine experimentally the ultimate justification to the use of either model. They found that for a packed bed of monosized spheres the constants computed using the Wyllie-Rose tortuosities agree with those originally suggested by Carman (164).

From available literature (164,171,176,193,194, 195,196) it was concluded: (a) Using different models of pore structure, widely different values may be obtained for the tortuosity, T , some of which completely lack any physical meaning. (b) Provided that the model

incorporates the most important features of the pore structure of the sample, the value of tortuosity factor should normally lie in the range $1 < T < 3$.

Bartell and Osterhof (197) arrived at the Carman-Kozeny equation by regarding the equivalent capillaries as circular, that is, $K_0 = 2.0$, and with the aid of Hitchcock's (198) assumptions that $\frac{L_e}{L} = \frac{\pi}{2}$. This gives $K = 2\left(\frac{\pi}{2}\right)^2 = 4.9$, in good agreement with their experimental value. The value of $K_0 = 2.0$ is reasonable, although it does not necessarily denote a circular channel, nor even a shape resembling a circle. On the other hand, it is doubtful whether L_e/L can be as large as $\frac{\pi}{2}$, and Carman (1964) assumption that $L_e/L = \sqrt{2}$ was a much more probable value. It can be seen from equation 9.26 that $K_0 = \frac{K}{2} = 2.5$, the value for a narrow, rectangular channel; these values are adopted for subsequent sections. Some values of the shape factor, K_0 , are presented in Table 9.1 for various channel cross-sections (199,200,201).

Also it can be seen from equation 9.26 that if, say K_0 were constant, then K would increase with increase in tortuosity. The reason for K being near to 5.0 for many different beds is probably that changes in tortuosity from one bed to another have been compensated by changes in K_0 in the opposite direction.

9.3.2 Wall Effect

In a packed bed the particles will not pack as closely in the region near the wall as in the centre of the bed, so that the actual resistance to flow in a

Shape	K_o
1. Circle	2.0
2. Ellipses -	
a) Major Axis = twice minor axis	2.13
b) Major axis = 10 by minor axis	2.15
3. Rectangles -	
a) length = breadth	1.78
b) length = 2 by breadth	1.94
c) length = 10 by breadth	2.65
d) length is infinite	3.0
4. Equilateral Triangle	1.67
5. Pipes and Cores	
a) Core set concentrically	2.0 - 3.0
b) Core set eccentrically eccentricity < 0.7.	1.7 - 3.0
c) Core set eccentrically eccentricity < 0.7	1.2 - 2.0

Table 9.1 Variable of K_o for streamline Flow
in Various Cross Sections (199, 200, 201).

bed of small diameter is less than it would be in an infinite container for the same flowrate per unit area of bed cross-section. If the only effect of the wall is to increase the average voidage of the bed, provided that e represents the average voidage of the whole bed, including the region at the wall, it may be concluded that no elaborate correction for wall effect is necessary. One factor, however for which correction might be made is the friction of the walls of the container. A correction factor f_w for this effect has been determined experimentally by Coulson (187) as

$$f_w = \left(1 + \frac{1}{2} \frac{A_c}{a}\right)^2 \dots\dots\dots (9.27)$$

where A_c is the surface area of the container per unit volume of bed.

The effect of the ratio of the diameter of the container, D , to that of the particle, d_c , has been studied in many different systems. It was concluded by Carman (164) that the wall effect is locally negligible if $D/d_c > 10$. In view of the work summarised by Rose and Rizk (202) concerning the magnitude of the wall effect when the ratio exceeds about 40, no effect was made to correct the experimental data for wall effects in this study, as the ratio of D/d_c for the largest size ballotini used is over 78.

9.3.3 Effect of Voidage

The Carman-Kozeny equation has been tested with spherical particles over a wide range of sizes and under

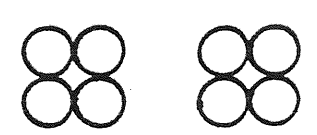
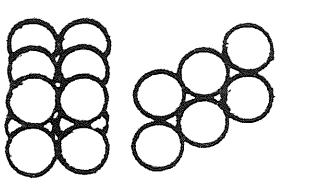
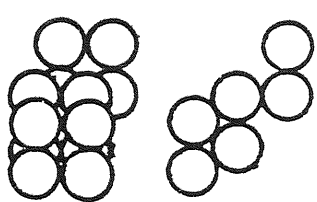
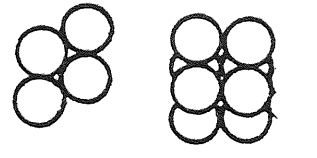
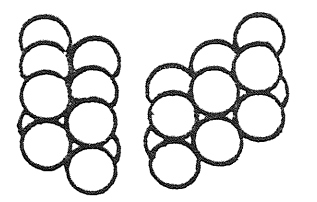
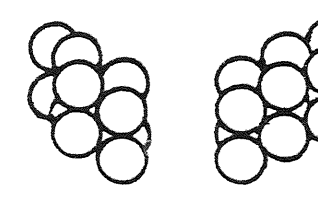
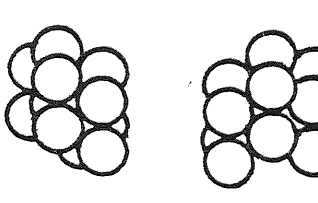
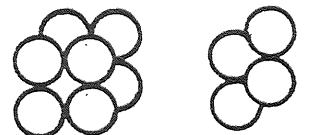
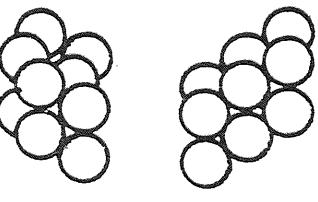
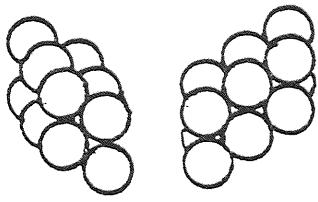
<p>1 Cubic Porosity 0.476</p>  <p>Top View Front View</p>	<p>2 Orthorhombic (clear passage) Porosity 0.3954</p>  <p>Top View Front View</p>	<p>3 Orthorhombic (blocked passage) Porosity 0.3954</p>  <p>Top View Front View</p>	<p>4. Orthorhombic Porosity 0.3954</p>  <p>Top View Front View</p>	<p>5 Tetragonal Sphenoidal (clear passage) Porosity 0.3019</p>  <p>Top View Front View</p>
<p>6 Tetragonal Sphenoidal (blocked passage 1) Porosity 0.3019</p>  <p>Top View Front View</p>	<p>7 Tetragonal Sphenoidal (blocked passage 2) Porosity 0.3019</p>  <p>Top View Front View</p>	<p>8 Rhombohedral Porosity 0.2595</p>  <p>Top View Front View</p>	<p>9 Rhombohedral (clear passage) Porosity 0.2595</p>  <p>Top View Front View</p>	<p>10 Rhombohedral (blocked passage) Porosity 0.2595</p>  <p>Top View Front View</p>

Figure 9.1 Systematic arrangement of spheres and their porosities.

many different experimental conditions (155,181,203,204) and the Kozeny constant, K , has been found to be about 4.8 ± 0.3 in the streamline region.

Spheres and particles which are approximately isometric do not pack to give beds with voidages in excess of about 0.6. Different arrangements of spheres and their voidages are given on Fig. 9.1.

With fibres and some ring packings, however, values of e_1 near unity can be obtained and rapidly increasing values of K are required to obtain agreement with experiments. This may be connected with a change in the shape of the channel with large changes in e_1 , or with a change in the actual length of path L_e for a given depth of bed L . The variation of the Kozeny constant with voidage for high voidage packings have been widely reported and should be considered when working with high porosity packings.

From equations 9.10 and 9.12 for low Reynolds number, the term $e_1^3/(1-e_1)^2$ could be considered the voidage function $f(e_1)$, for the Blake-Kozeny or Carman-Kozeny equations.

Various authors have suggested different forms of the voidage function so as to be able to represent all data points by the same numerical constant. These are presented on Table 9.2.

The value of the constant in the various equations naturally depends on the form of $f(e_1)$ used, but there are differences in the literature even for the same form of $f(e_1)$. For example the Blake-Kozeny equation

Author	1/f(e ₁)
Blake (1922), Kozeny (1927) Carman (1937) Zunker (1920)	$(1-e_1)^2/e_1^3$
Terzaghi (1925)	$(1-e_1)^2/e_1$
Rapier (1949)	$\{(1-e_1)^{1.3}/(e_1-0.13)\}^2$
Hulbert and Feben (1933)	$\{1.115(1-e_1)/e_1^{1.5}\}\{(1-e_1)^2+0.018\}$
Slichter (1898)	$69.43-e_1$
Kruger (1918)	$e_1^{-3.3}$
Hatch (1934), Mavis and Wilsey (1936)	$e_1^{-1.0}$
Fehling (1939)	$e_1^{-6.0}$
Rose (1945)	$e_1^{-4.0}$
Rumpf and Gupte (1971)	$e_1^{-4.1}$
	$e_1^{-5.5}$

TABLE 9.2 Different Porosity Functions for Low Reynolds Number Flow (146)

gives the value of 150 and the Carman-Kozeny equation gives 180. The two "best values" of the constant differ by as much as 20%.

9.3.4 Other Factors

Other factors that should be considered when making use of the Carman-Kozeny equation to describe single phase flow in packed beds are sphericity of the particles, their surface roughness, their orientation, the average diameter value used when working with mixed particles and the bed support, among others.

In this study, smooth monosized glass spheres were used as packing media, with the sphericity value for spheres equals unity. Although different arrangements of stacked spheres are possible (Fig. 9.1), such variations in orientation do not occur with random packings as encountered in ordinary industrial practice. The importance of the packing support should not be overlooked in considering the drop in pressure through the column since the support may itself form an important resistance, and by orientating the particles may also affect the total pressure drop.

Much effort has been expended in order to find a general expression that would best describe the single phase flow through packed beds. It is important to note that the different expressions available are not to be considered mutually exclusive approaches to the problem on hand, but merely represent the main view points emphasised by various workers. Each approach has

a certain validity, and the better the various models will be reconciled with each other, the more adequate will become our understanding of flow through porous media.

9.4 ANALYSIS OF SINGLE PHASE PRESSURE DROP DATA

The modified Ergun equation proposed by Macdonald et al (153) was initially used to correlate the experimental results. The maximum value of the Reynolds number N_{Re} , defined in Section 9.1, was calculated to be always <1 for the range of variables investigated. The term involving u^2 may therefore be neglected so that equation 9.25 reduces to the Carman-Kozeny form. The first order dependence on velocity was confirmed by the high correlation coefficient obtained for linear regression analysis on the pressure drop data.

∴ from equation 9.25

$$\frac{\Delta P_1}{L} = \frac{36K\mu_c u (1-e_1)^2}{d_c^2 e_1^3} \dots\dots\dots (9.28)$$

Rearrangement of equation 9.28 gives,

$$\left\{ \frac{\Delta P_1}{\mu_c} \right\} \left\{ \frac{e_1^3 d_c^2}{(1-e_1)^2 36L} \right\} = Ku \dots\dots\dots (9.29)$$

The first term, $\left\{ \frac{\Delta P_1}{\mu_c} \right\}$ describing the pressure drop, contains the only property pertaining to the continuous phase, and therefore is independent of temperature fluctuations, which often occurred during acquisition of data. The viscosity of water was determined as a function of temperature using the correlation given in Appendix A.

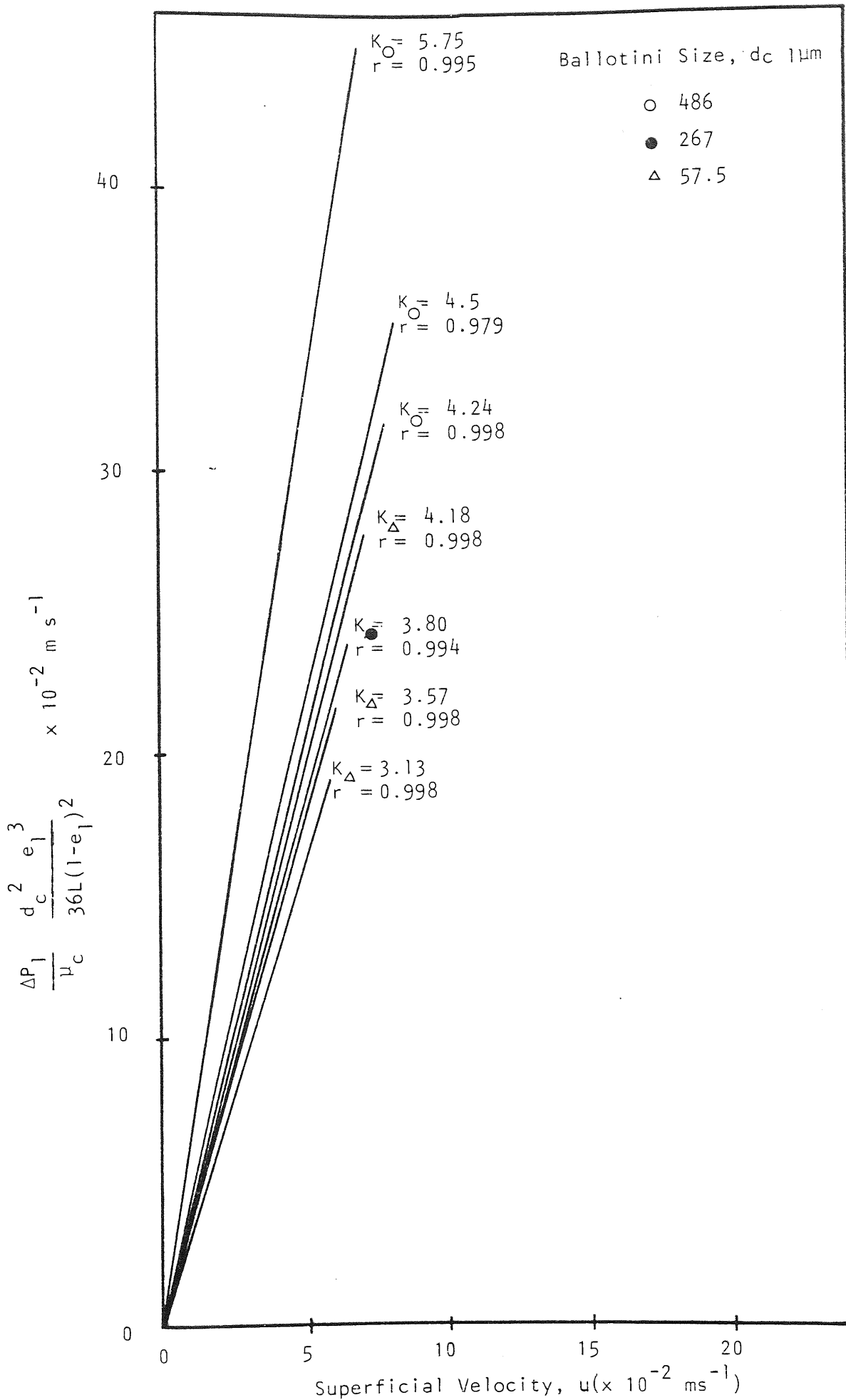


Figure 9.2 Correlation of Single Phase Pressure Drop for Different Ballotini Sizes.

The second term embodies all the properties of the packing which were evaluated experimentally.

The single phase pressure drop data was correlated against superficial velocity by linear regression analysis using equation 9.29. The correlations obtained for different ballotini sizes are illustrated in Fig. 9.2, where the slope of the best fit line is equal to the Kozeny constant. The results are shown in Table 9.3.

This study has emphasised the need for measurement of single phase pressure drop when investigating coalescence in packed beds. Despite great care taken to ensure reproducibility during data acquisition, the Kozeny constant exhibits some variation. It can be seen from Table 9.3 that the value of the Kozeny constant increases with ballotini diameter. Coulson (187) suggested that the variations in K were brought about by the influence of the container wall on the arrangement of the particles. As explained in Section 9.3.2, no correction for wall effect was made on the experimental data as its effect was considered negligible. However, although the average voidage of the bed measured experimentally, includes the region at the wall, at high superficial velocities the bed is packed under pressure and the voidage of the bed is reduced. It can be seen from equation 9.29 that an increase in superficial velocity, incurring a higher pressure drop, and a lower voidage function will produce a lower Kozeny constant value in order to fit the data. It is therefore suggested that two phase pressure drops be expressed as the ratio, $\frac{\Delta P_2}{\Delta P_1}$ to take account of

Ballotini Size d_c (m)	Bed Depth L (m)	Voidage e_1	Kozeny Constant K	Correlation Coefficient r	No. of Points
486×10^{-4}	0.2	0.384	4.24	0.998	38
	0.1	0.395	4.5	0.979	22
	0.05	0.397	5.75	0.995	30
2.67×10^{-4}	0.2	0.416	3.80	0.994	10
	0.05	0.41	3.75	0.991	10
5.75×10^{-5}	0.2	0.41	3.13	0.998	10
	0.075	0.395	3.57	0.998	10
	0.05	0.409	4.18	0.998	10

Table 9.3 Single Phase Pressure Drop Correlations.

this variation.

9.5 TRANSIENT PRESSURE DROP DATA

The overall pressure drop across the coalescer and at different bed depths was recorded at regular intervals after the dispersion was introduced to the inlet face. Typical examples of observed transient behaviour, prior to attainment of steady state conditions are illustrated in Figs. 9.3, 9.4 and 9.5.

In Section 9.4 it was proposed that division of the single phase pressure drop by the prevailing fluid viscosity provides adequate compensation for temperature changes. For two phase flow, however, correction of the pressure drop using continuous phase viscosity considerably overestimates the effect of fluctuating temperatures. As the operating temperature varied by up to 8°K, this produced a 10% change in pressure drop even after long periods when steady state conditions prevailed. To facilitate determination of steady state pressure drop and to compare the result with other data, Austin (14) suggested that it was essential to negate this temperature effect. He proposed that the two phase pressure drop should be expressed as $\frac{\Delta P_2}{\mu_d}$, which varied less than 1% for an 8°K temperature fluctuation.

However, if the dispersed phase in the system exists as discrete drops, not forming a continuum within the packed bed, most of the hydrodynamic forces contributing to the pressure drop should come from the continuous phase. Also, if the single pressure drop is presented as

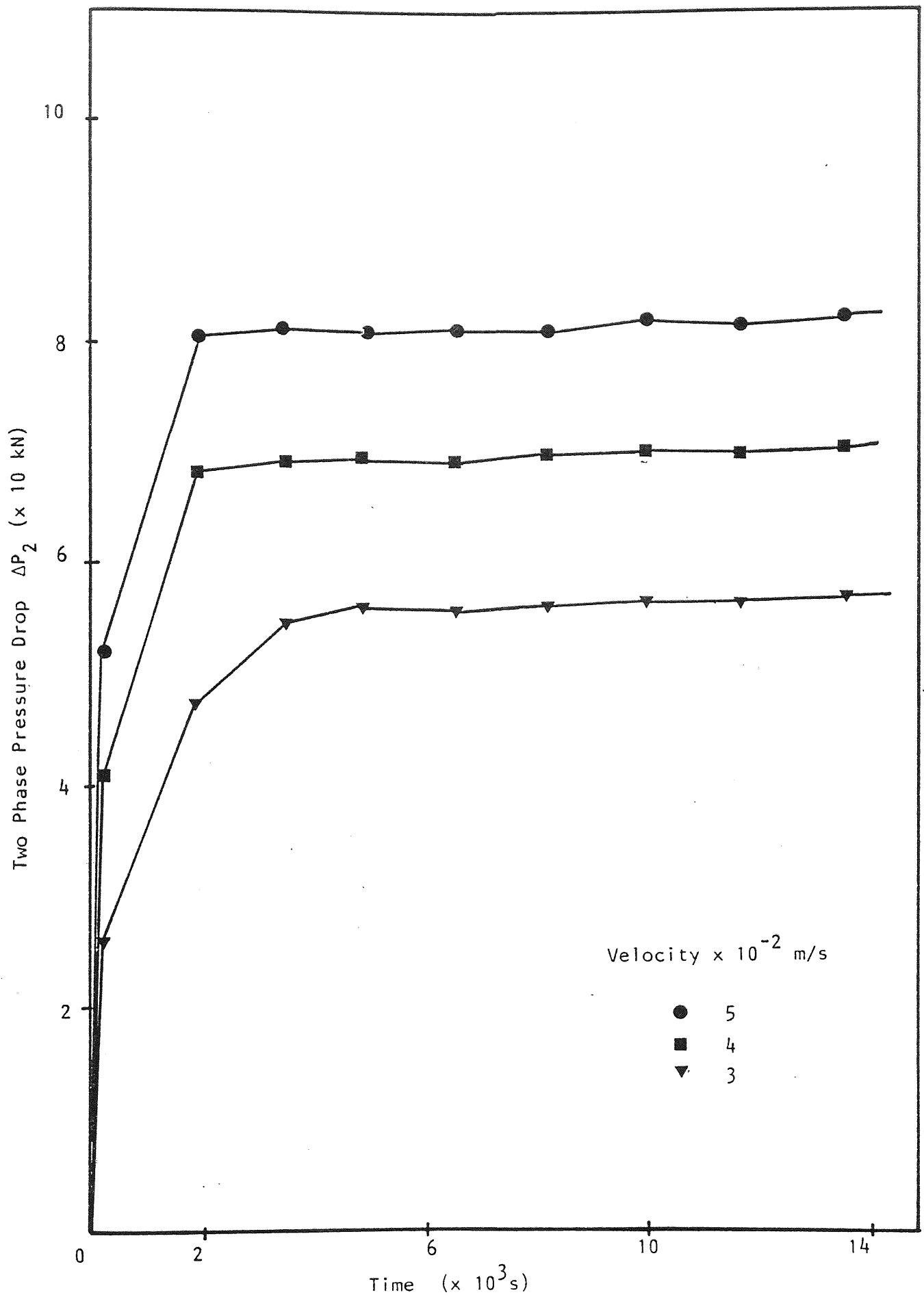


Figure 9.3 Overall Two Phase Pressure Drop for 20×10^{-2} m Bed Depth, $486 \mu\text{m}$ Ballotini Size and 0.1% v/v Dispersed Phase Concentration. Transient Behaviour.

$\frac{\Delta P_1}{\mu_c}$, the two phase pressure drop data should be handled the same way in order to calculate the contribution of the dispersed phase present within the packing. Since the dispersed phase viscosity is lower than the continuous phase viscosity the effect of the dispersed phase can be easily overestimated and as will be shown in Section 9.7.2, when calculating the dispersed phase saturation from relative permeability calculations, the difference between the saturation values obtained by using the dispersed phase viscosity instead of the continuous phase viscosity can be in excess of 10% in some cases. Therefore both the single phase and two phase pressure drop will be presented as $\frac{\Delta P}{\mu_c}$ in this study.

Figs. 9.3 and 9.4 show the effect of superficial velocity on pressure drop data. As expected, pressure drop increased with increasing superficial velocity. In all cases, it increases rapidly at first and remaining almost constant throughout the length of the experiment or with an increase detectable only over long periods of time.

The pressure drop measured over the length of the bed at fixed intervals is shown on Fig. 9.5, with the overall two phase pressure drop measured across the bed being the sum of all the pressure drop measured at different bed depths. This permits the calculation of the pressure drop within two points on the bed and can be used to predict saturation profiles across the bed as will be shown in Section 9.7.

To determine the steady state pressure drop it was

necessary to analyse the factors responsible for short term fluctuations; these are:

- (i) Temperature changes.
- (ii) Experimental errors in measurement of velocity and pressure drop.
- (iii) Flow disturbances, caused by pump speed fluctuation. Recovery of coalescers from such disturbance is very slow, especially at low velocities.
- (iv) Pseudo-steady state processes occurring within the bed, i.e. accumulation and release of dispersed phase.

The first factor can be eliminated by incorporating the dispersed phase viscosity into the pressure drop term, but as explained previously, this approach is somewhat empirical. Flow disturbances were minimised by careful operation and pseudo-steady state processes only appear to be manifested as pressure drop changes at low velocities when they are readily recognisable.

An analysis of the experimental accuracy was completed taking into account the following sources of error,

- (i) Density of manometer fluid and the associated temperature coefficient of density.
- (ii) Manometer reading error.
- (iii) Rotameter calibration error and the effect of temperature on the calibration curve.
- (iv) Error in value of continuous phase viscosity.

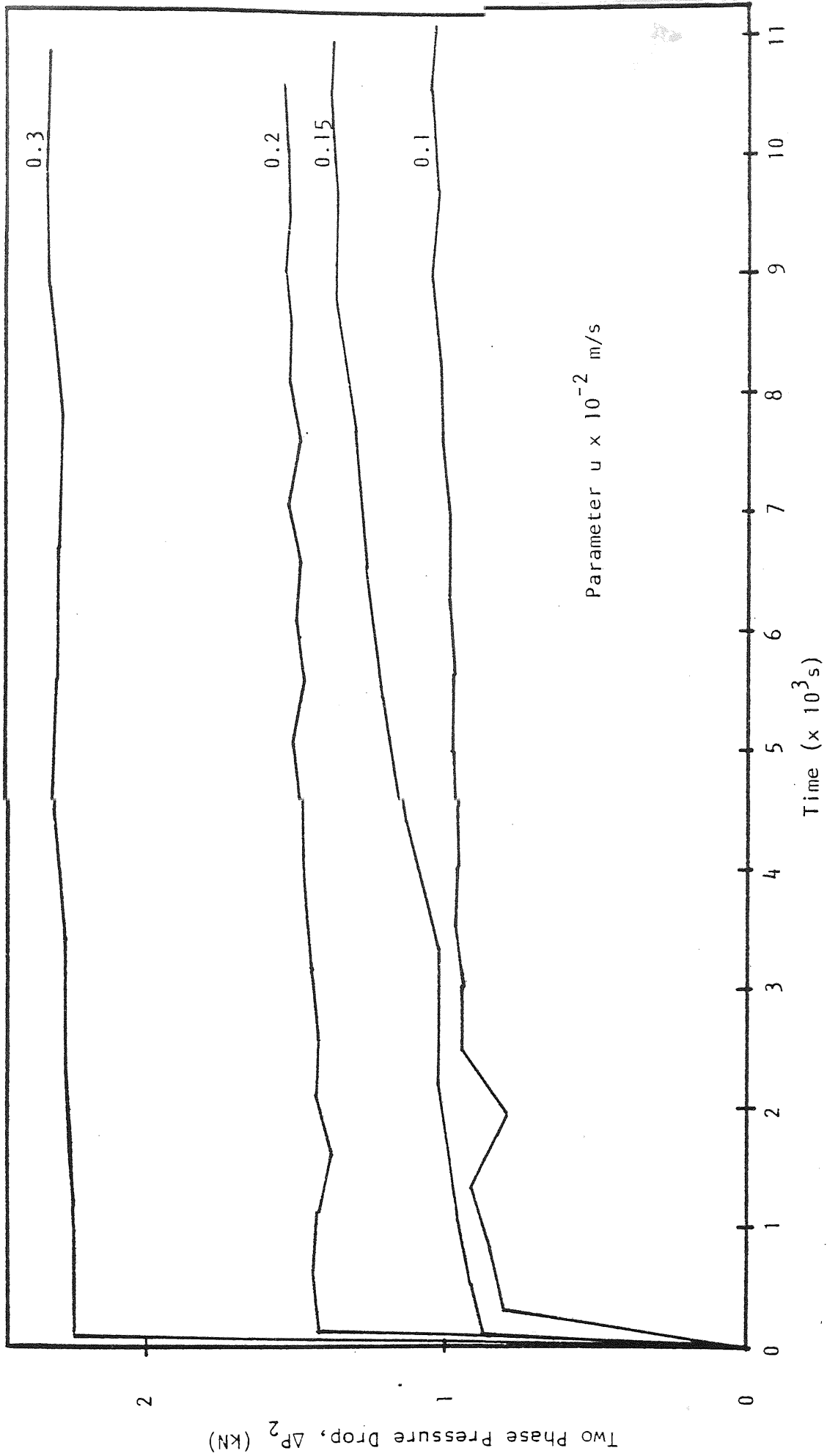


Figure 9.4 Two Phase Pressure Drop for 20×10^{-2} Bed Depth, $486 \mu\text{m}$, Ballotini Size and 0.1% v/v Dispersed Phase Concentration. Transient Behaviour

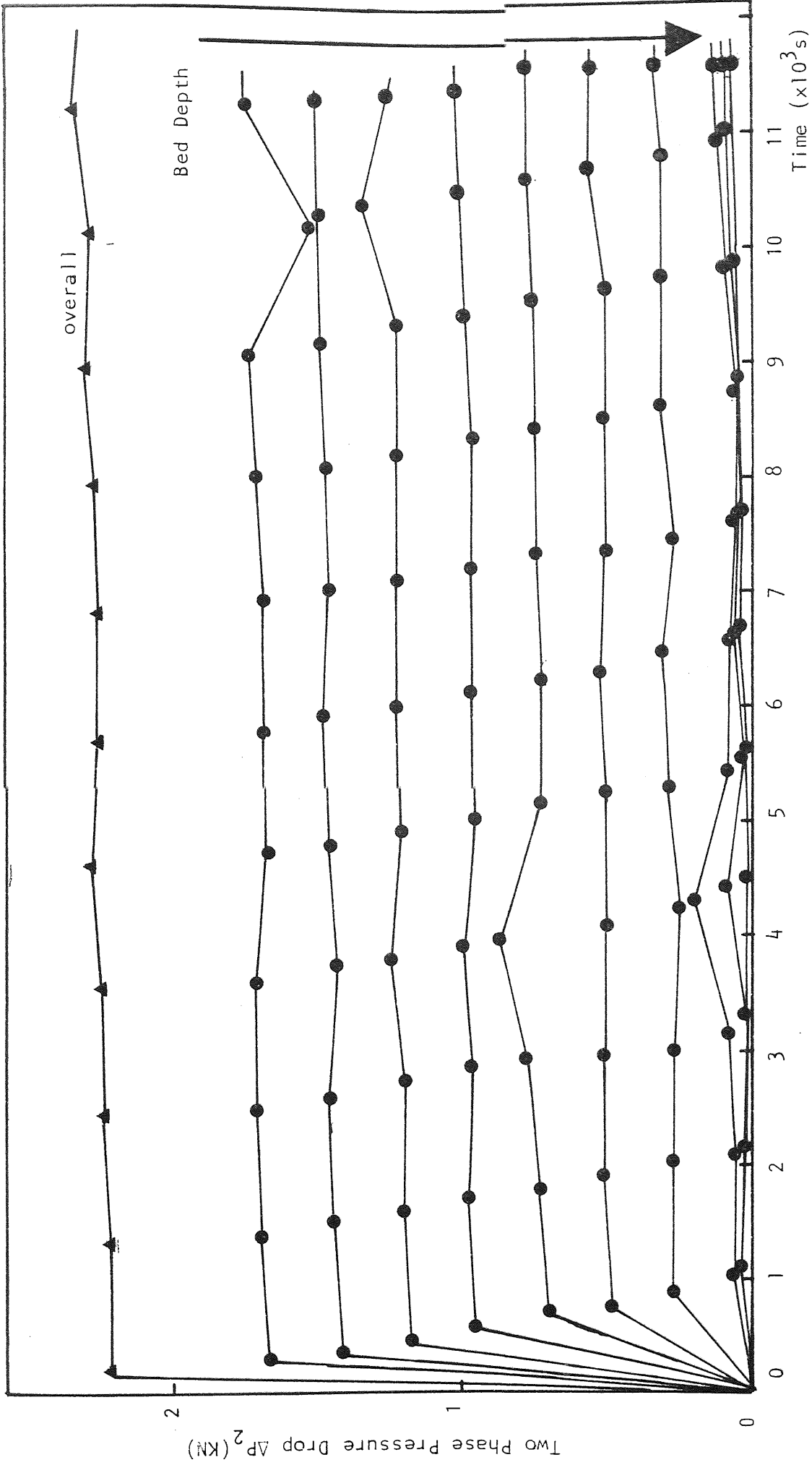


Figure 9.5 Pressure Drop Vs. Bed Depth, for 20×10^{-2} m Bed Depth, 486 μ m Ballotini Size and 0.3×10^{-2} m Velocity-Transient Behaviour

Of these sources, rotameter calibration error and the error in viscosity of continuous phase constitute over 75% of the total error which was calculated to be $\pm 3\%$ (Appendix F).

The transient pressure drop data was analysed as suggested by Austin (14) to find the time to steady state. Considerable variation, shown in Fig. 9.6, for the time to steady state results discouraged detailed analysis of this data.

9.6 TWO PHASE PRESSURE DROP

To account for variations in packing technique and operating temperature, the two phase pressure drop is presented as the ratio, $\frac{\Delta P_2}{\Delta P_1} \left\{ \frac{\mu_{C1}}{\mu_{C2}} \right\}$. As shown by Fig. 9.7, this ratio decreases as both superficial velocity and bed depth increase. This implies that the dispersed phase saturation increases as both velocity and bed depth decrease. This ratio also increases rapidly with increasing dispersed phase concentration for the same operating time, as shown in Fig. 9.8, since the level of dispersed phase saturation in the packing rises faster as more dispersed phase is input into the system for the same period of time. As it is well known that a high dispersed phase saturation aids both coalescence and separation efficiency, packing of the bed in a dispersed phase filled column rather than continuous phase and/or priming of the bed with dispersed phase only, prior input of the secondary dispersion, may improve coalescence and should be tested.

For different ballotini sizes, although the individual pressure drops increase with decreasing ballotini

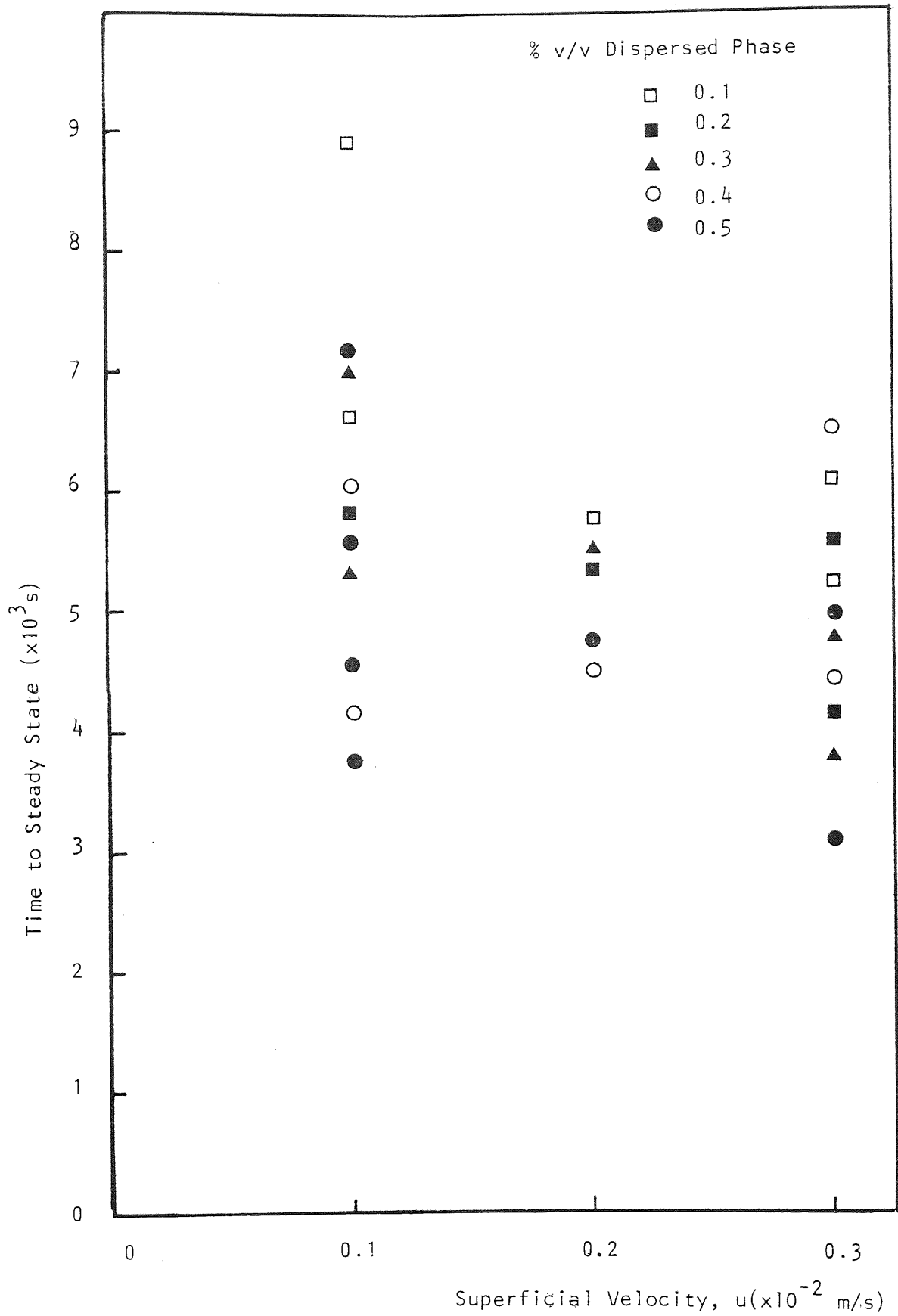


Figure 9.6 Effect of Concentration on Time to Steady State Vs. Superficial Velocity

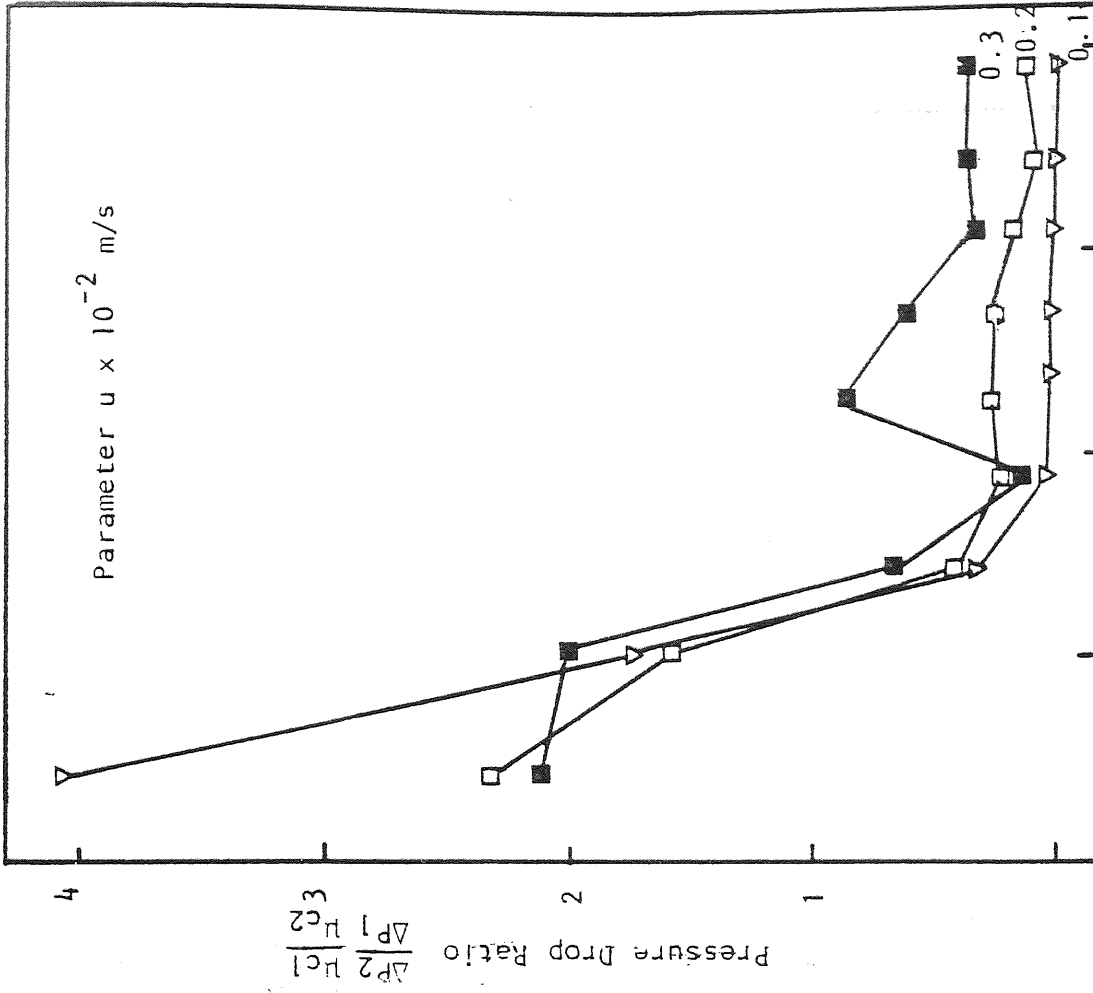
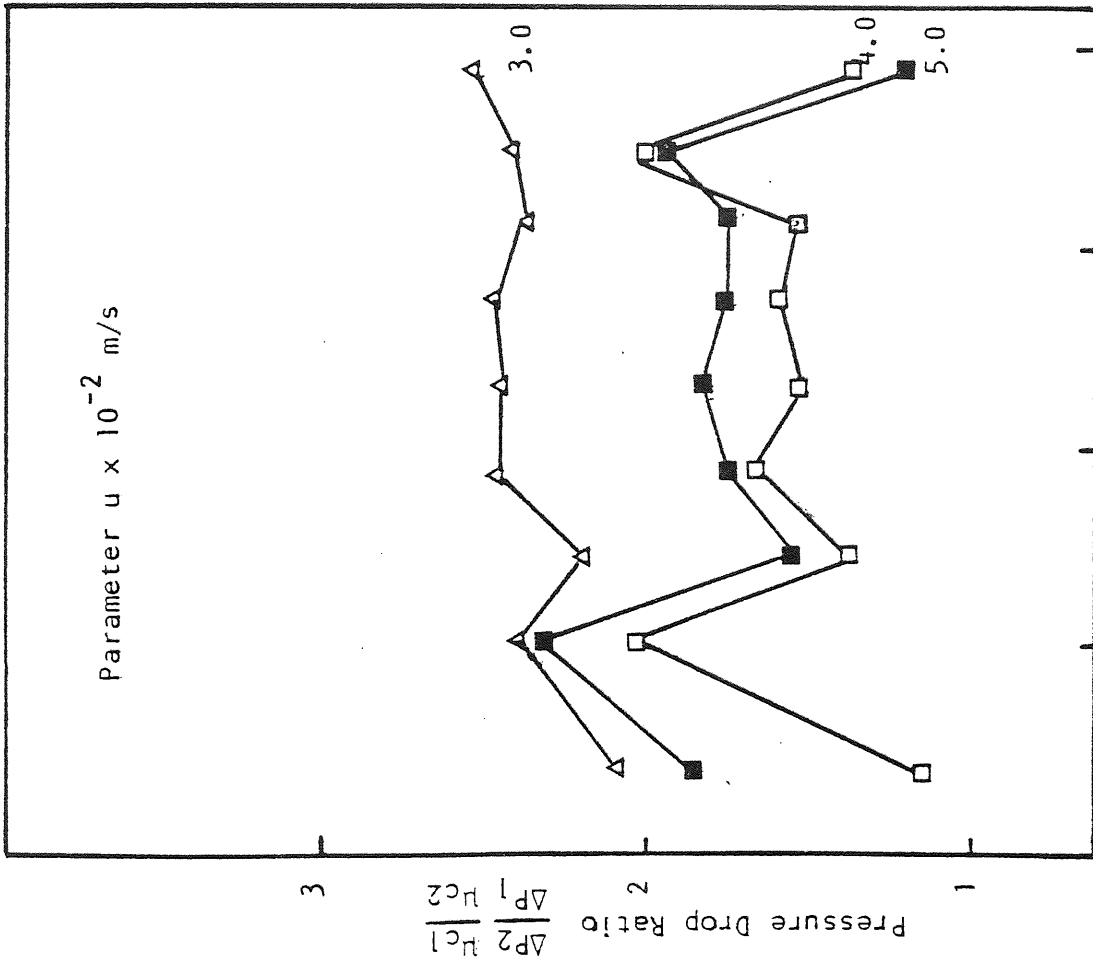


Figure 9.7 Variation of Pressure Drop with Velocity for 20 cm. Bed Depth, 486 μ m Ballotini Size and 0.1% v/v Dispersed Phase Concentration

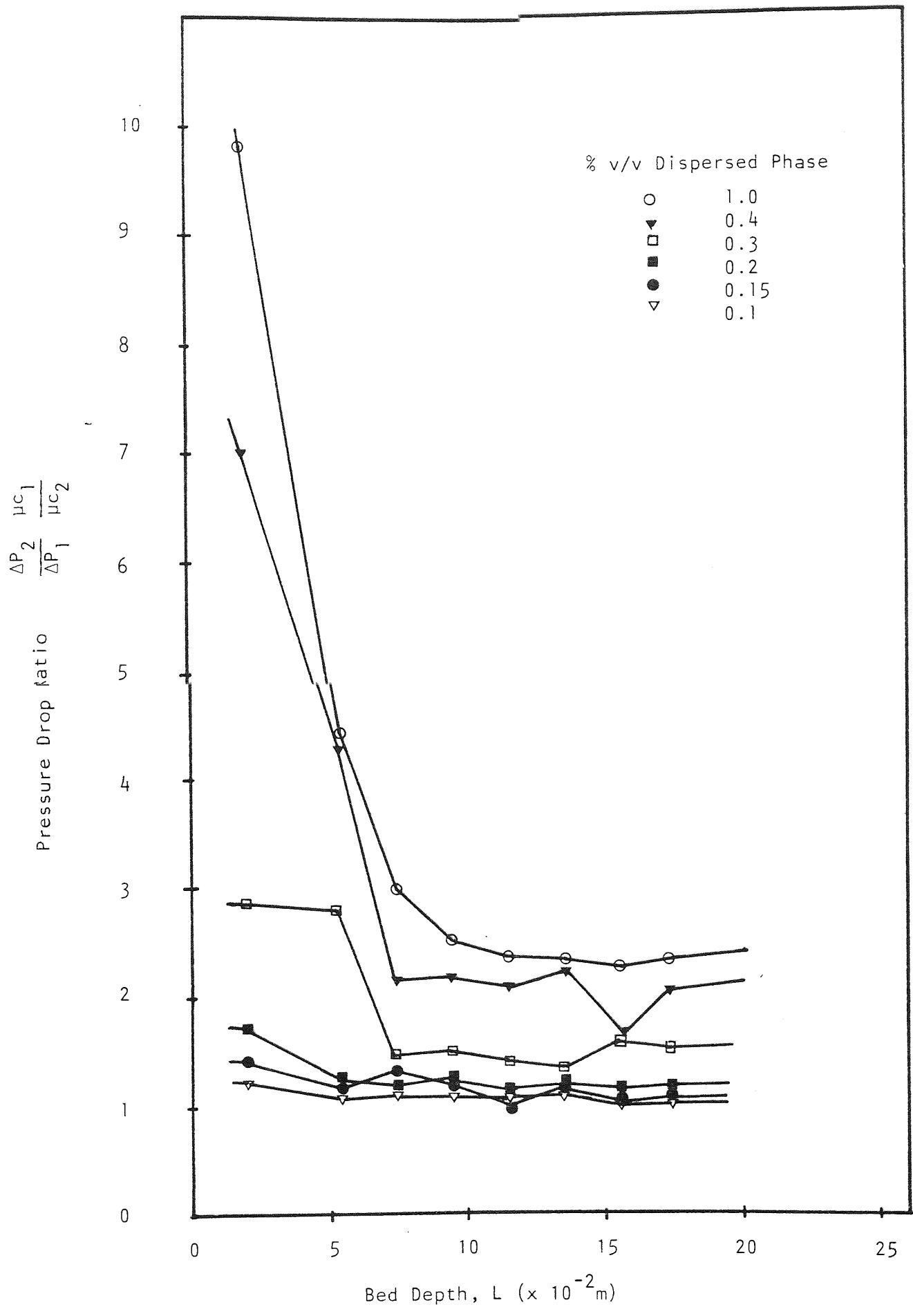


Figure 9.8 Variation of Pressure Drop Ratio with Concentration of Dispersed Phase. Ballotini $486 \mu m$, Bed Depth, $20 \times 10^{-2} m$, $0.3 \times 10^{-2} ms^{-1}$.

size, the actual ratio $\frac{\Delta P_2}{\Delta P_1} \left\{ \frac{\mu_{c1}}{\mu_{c2}} \right\}$ is almost equal for the different sizes suggesting that the dispersed phase saturation is about the same and therefore a function of the bed voidage as they all have similar voidages, i.e. $e_1 = 0.39-0.41$ (Fig. 9.9).

On Fig. 9.10 the change of the pressure drop ratio with time is presented. As time increases, the ratio increases rapidly at the bed inlet, but slowly further down the bed, until it reaches a maximum and remains almost constant throughout the experiment. The behaviour is also presented for different depth beds on Fig. 9.11.

9.7 SATURATION PROFILES

The importance of accounting for the presence of coalesced oil held-up within the void spaces at steady state is well established, since both pressure drop and coalescence efficiency have been observed to increase significantly as deposited oil accumulates in approaching steady-state from an initial oil-free condition (14, 140). Moreover the oil saturation explicitly appears in recent attempts to model the process (14,44,45,72). Thus it is important to determine the oil saturation (volume fraction of voids occupied by oil) inside the filter bed without disturbing it.

Various means to measure the oil saturation (or water saturation) have been developed and described in the literature, especially by petroleum reservoir engineers for measuring two-phase and three-phase permeabilities in porous media. Methods which received consideration

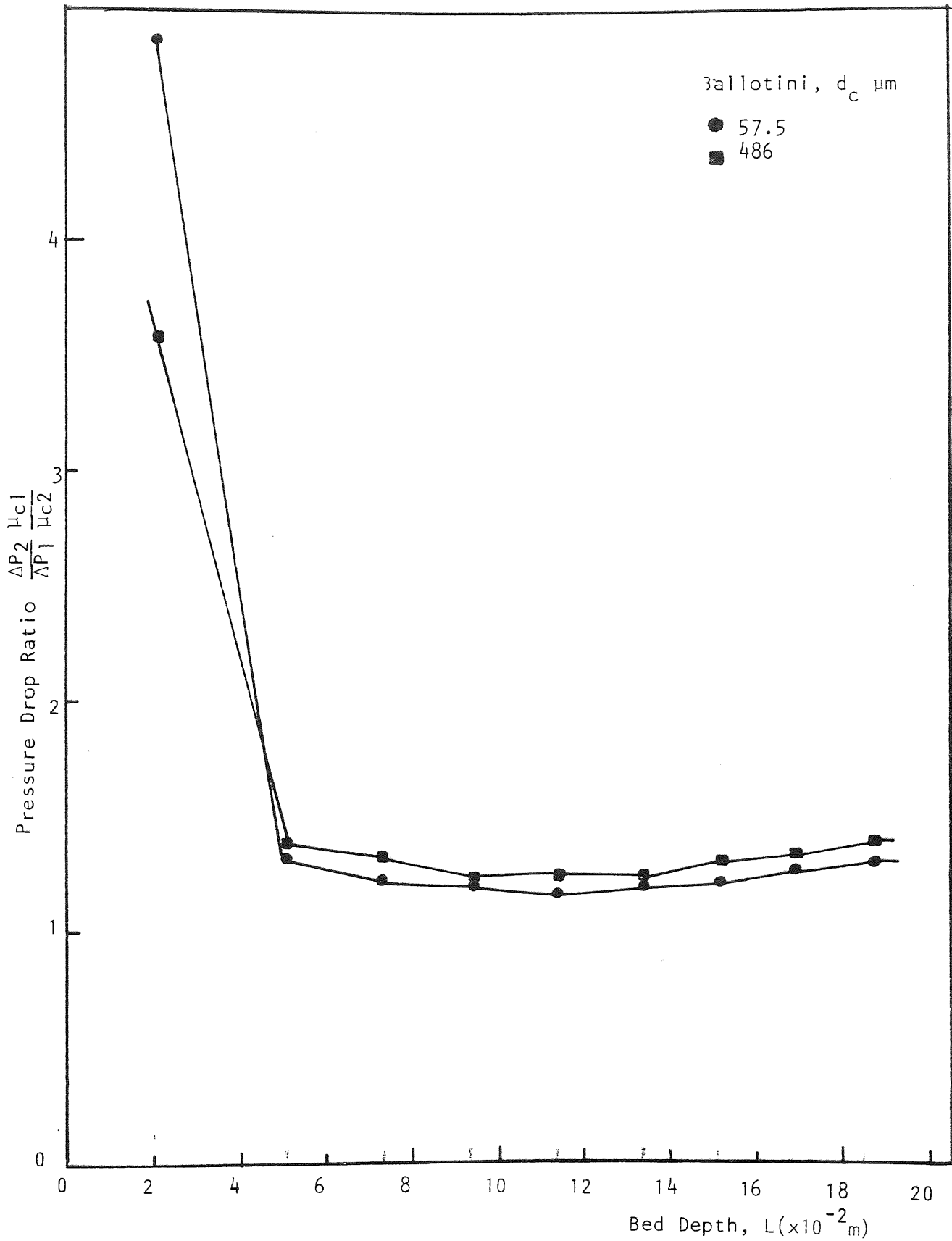


Figure 9.9 Effect of Ballotini Size on Pressure Drop Ratio Vs. Bed Depth

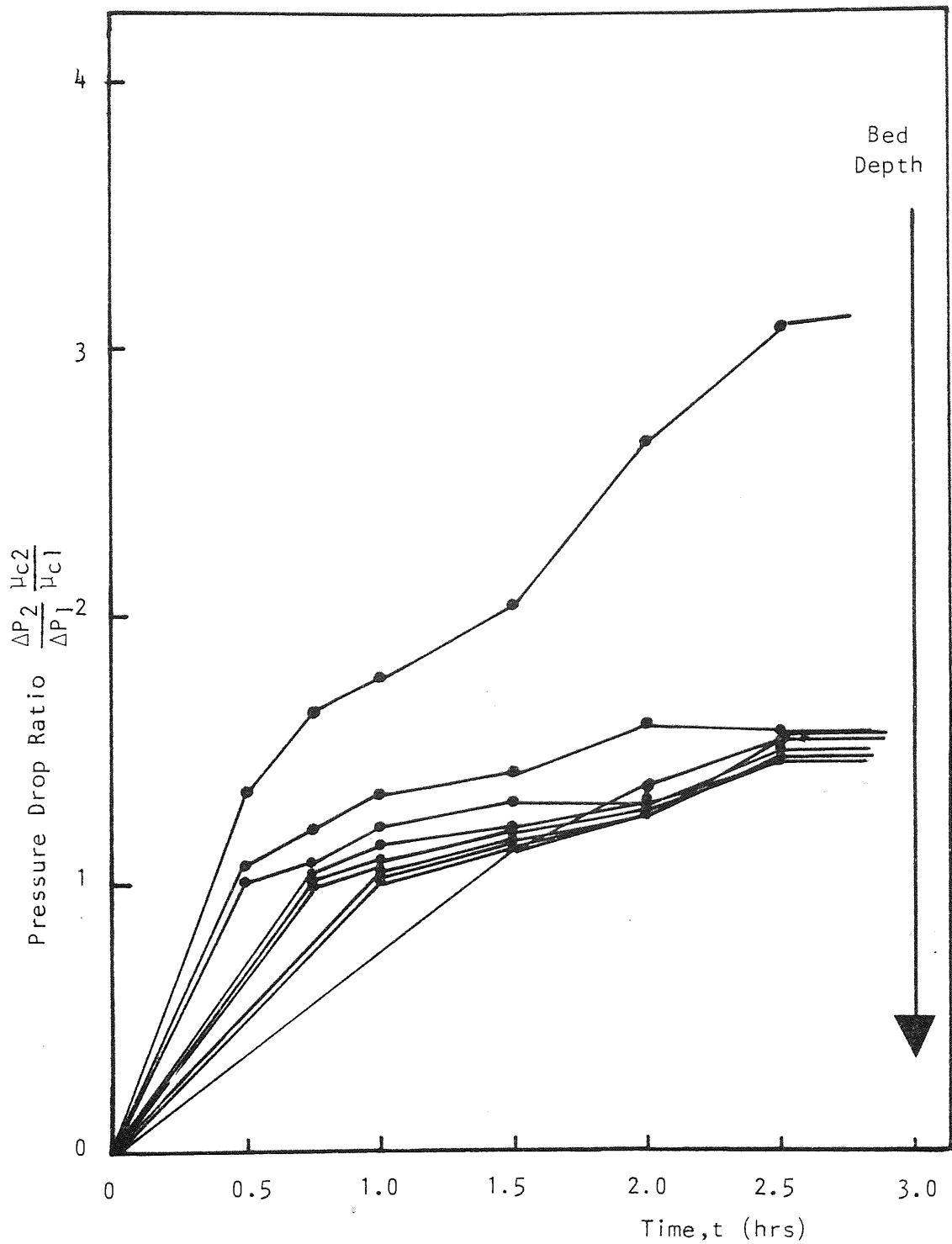


Figure 9.10 Pressure Drop Ratio Vs. Time for Different Bed Depths

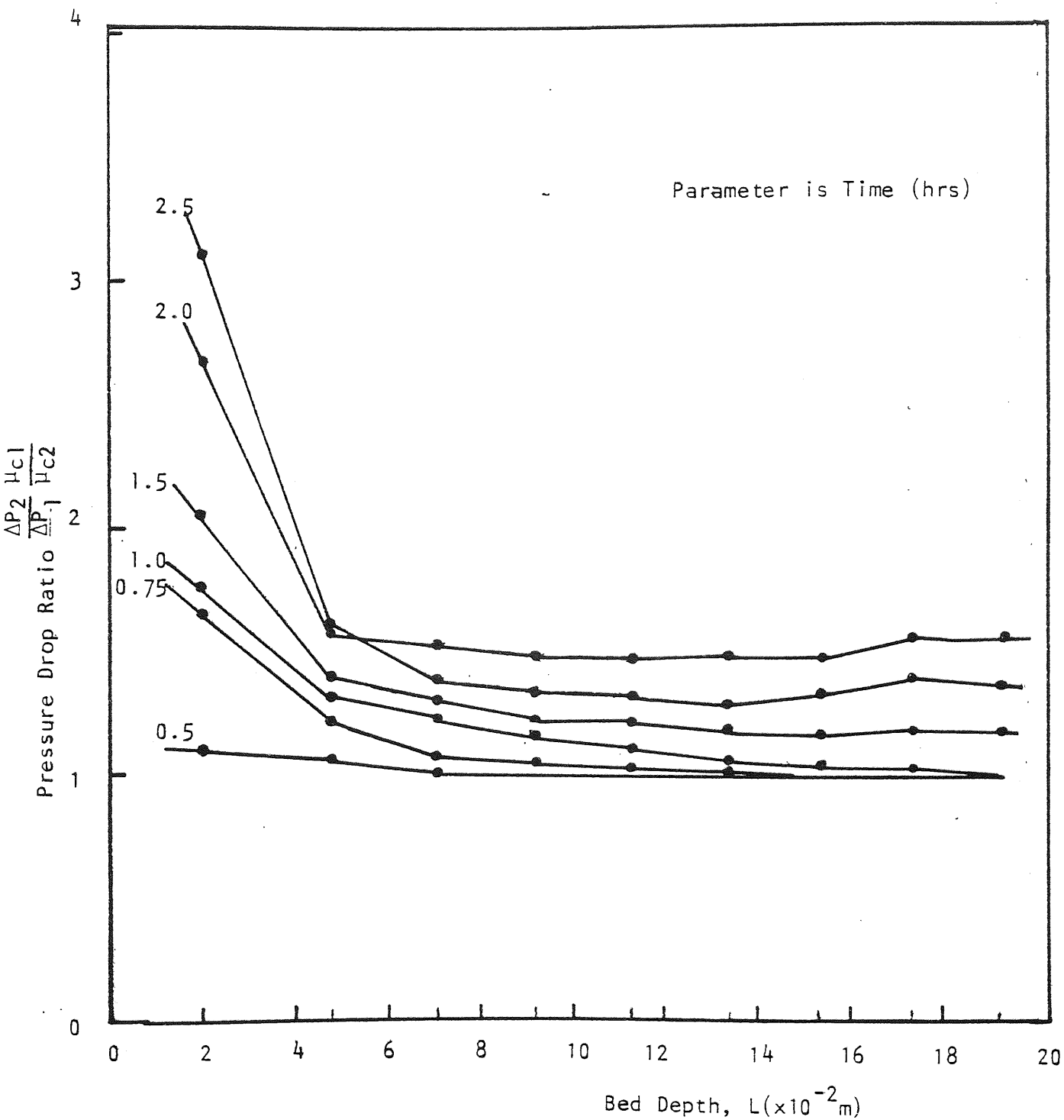


Figure 9.11 Pressure Drop Ratio Vs. Bed Depth for Increasing Operating Time

included electrical resistivity, gamma ray absorption, neutron bombardment, radioactive tracers, x-ray absorption and nuclear magnetic resonance. The relative merits of these techniques are discussed by Saraf and Fatt (205) and Josendal et al (206).

9.7.1 Relative Permeability Method of Oil Saturation

The measurement of relative permeability consists, essentially, of the determination of two flow rates under a given pressure drop and the determination of saturation. General discussions and reviews of measurement methods have been given by Osoba et al (207) and Richardson et al (109). Many relative permeability curves have been published for oil-water, air-water and oil-air-water systems, but only those relative permeability curves of oil-water systems flowing through unconsolidated porous media are concerned here.

Leverett (208) investigated the relative permeabilities of unconsolidated sands to different pairs of oil-water mixtures. The oils used were hydrocarbon products including a close-cut hexane fraction, kerosene and a commercial lubricating oil, with viscosities ranging from $76.5 \times 10^{-3} \text{ Ns/m}^2$ to $0.31 \times 10^{-3} \text{ Ns/m}^2$. In one run the viscosity of water was increased to $32 \times 10^{-3} \text{ Ns/m}^2$ by the addition of glycerol. The relative permeabilities were found to be substantially independent of the viscosity of either phase. Relative small variations in interfacial tension, porosity, permeability and liquid density differences were found to exert insignificant influences

on the relative permeability at a particular value of oil saturation.

Jones (209) was able to correlate relative permeability data to the continuous or dispersed phase saturations using the expressions

$$\frac{k_d}{k_o} = (1 - 1.11 S_c)^2 = (1.11 S_d - 0.11)^2 \dots\dots (9.30)$$

$$\frac{k_c}{k_o} = S_c^3 = (1 - S_d)^3 \dots\dots\dots (9.31)$$

from experiments using oil as the non wetting phase, and water as the wetting phase flowing through granular media. Carpenter et al (210) published the relative permeability data of the glass beads using halocarbon oils or refined white oils and the aqueous phase consisted of various mixtures of water, lithium, bromide and alcohol. The results of Leverett, Jones and Carpenter, showing typical relative permeability curves are plotted on Fig. 9.12 for comparison.

Both wetting and non-wetting curves are shown to exhibit limiting saturations of the respective fluids, below which permeability vanishes, because the phase under consideration cannot form sufficiently continuous channels to sustain flow. The limiting saturations for flow through these unconsolidated granular media are about 13% for the non-wetting phase and about 20% for the wetting phase. The value of the limiting saturation of the wetting phase is in agreement with their observed value of the irreducible wetting phase saturation in the capillary pressure tests.

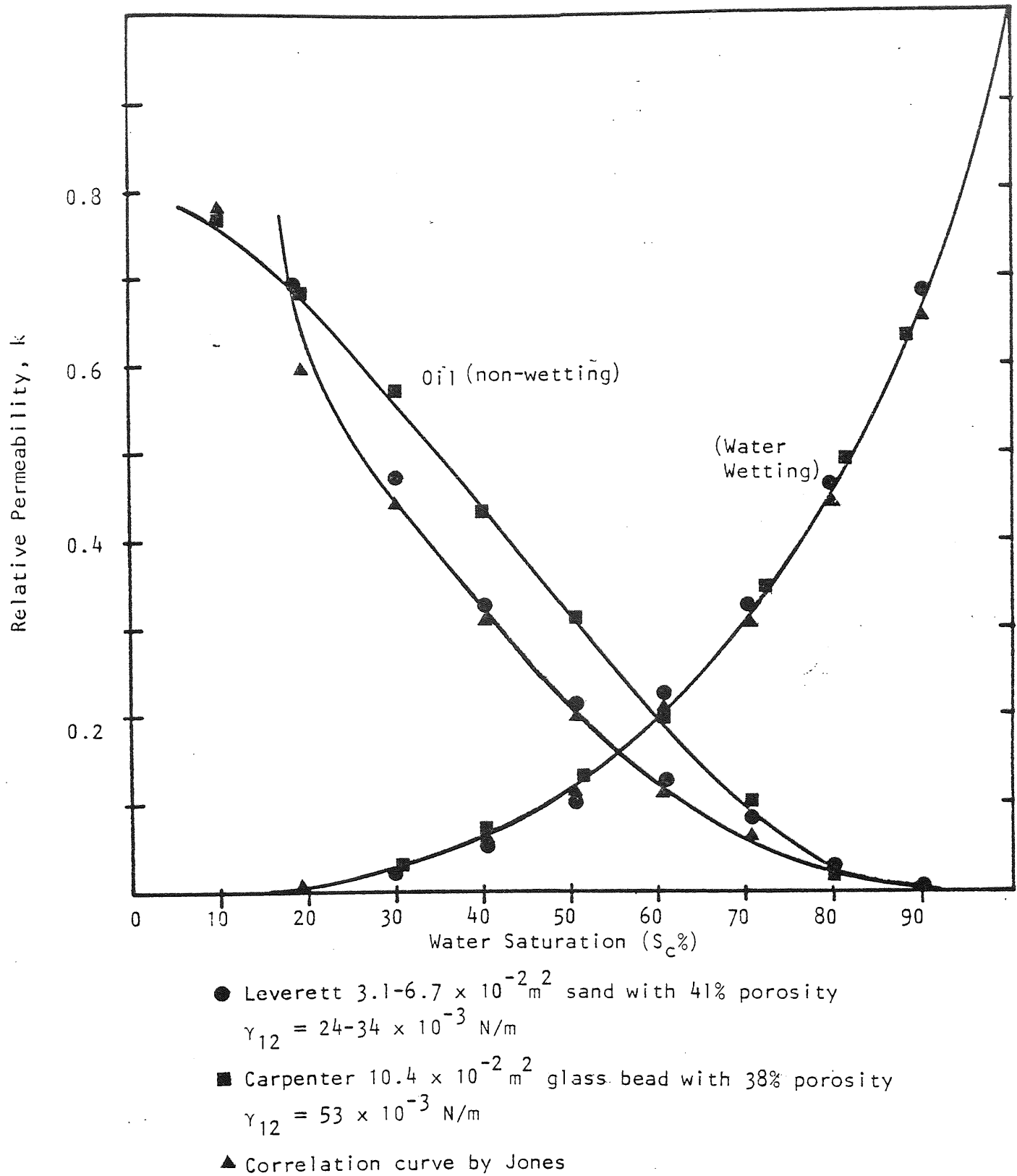


Figure 9.12 Relative Permeabilities Vs Saturation Curves.

All the data show relative permeability to the wetting aqueous phase is reproducible under different experimental conditions. This water relative permeability curve could therefore be used as calibration curve to obtain the oil saturation from the measured relative permeability to the water phase during a coalescence experiment. The discrepancy between Jone's data and Carpenter's data in predicting the oil saturation is less than 15% for any predicted value.

9.7.2 Relative Permeability Calculation from Pressure

Drop Data

For two phases flowing through a short column of porous medium with uniform cross section, the effective permeability to the water phase may be defined as

$$k_c = \frac{u_2 \mu_c \Delta L}{\Delta P_2} \dots \dots \dots (9.32)$$

where ΔL is the depth of the porous medium and ΔP_2 is the total pressure drop within the water phase and u_2 is the superficial velocity of the water phase. The permeability of the medium to a single (water) phase is defined by Darcy's law as

$$k_o = \frac{u_1 \mu_c \Delta L}{\Delta P_1} \dots \dots \dots (9.33)$$

where ΔP_1 is the total pressure drop. If the superficial velocity u_1 for one phase flow is adjusted to equal the value u_2 , the superficial velocity of the water phase in two-phase flow at the same temperature conditions, the ratio $\frac{\Delta P_1}{\Delta P_2}$ is equal to $\frac{k_c}{k_o}$, the relative permeability to water phase. Therefore, the relative permeability can be

calculated from the ratio of $\frac{\Delta P_1}{\Delta P_2}$, for each pressure tap along the length of the packed bed, to find the oil saturation from Fig. 9.12 (or equations 9.30 and 9.31) for the respective section of medium measured by that pressure tap. As explained in previous sections the ratio pressure drop/continuous phase viscosity will be used to account for any changes in temperature, so

$$\frac{k_c}{k_o} = \frac{\Delta P_1}{\Delta P_2} \frac{\mu_{c2}}{\mu_{c1}} \dots\dots\dots (9.34)$$

The Carman-Kozeny equation 9.18 gives

$$k_o = \frac{d_c^2 e_1^3}{180(1-e_1)^3}$$

from which a theoretical value for the permeability of the medium to water can be calculated, and compared with the experimental value obtained by using equation 9.33. The values of the theoretical and average experimental permeability to the continuous phase are presented in Table 9.4 for different ballotini diameters. Both values are very close and supports the assumption that the Carman-Kozeny equation can be used to predict the single phase flow of the system.

On Figs. 9.13 through 9.24 examples of the saturation profiles obtained by the relative permeability method of calculation are presented. In all cases, the oil saturation is higher at the inlet of the bed and then decreases rapidly to remain almost constant throughout the bed. This sudden drop in oil saturation is more steep as the dispersed phase concentration increases, which suggests that drop capture by interception is the predominant

TABLE 9.4 COMPARISON OF THEORETICAL VS. EXPERIMENTAL
SINGLE PHASE PERMEABILITY

	Ballotini Size ($\times 10^{-6}$ m)		
	57.5	267	486
MEASURED PERMEABILITY (average)			
$k_o = \frac{\mu_c u L}{\Delta P_1}$ (m^2)	2.87×10^{-12}	6.58×10^{-12}	2.26×10^{-10}
THEORETICAL PERMEABILITY			
$k_o = \frac{e_1^3 d_c^2}{180(1-e_1)^2}$ (m^2)	3.26×10^{-12}	6.60×10^{-12}	2.09×10^{-10}
<u>MEASURED PERMEABILITY</u> <u>THEORETICAL PERMEABILITY</u>	0.88	0.99	1.08

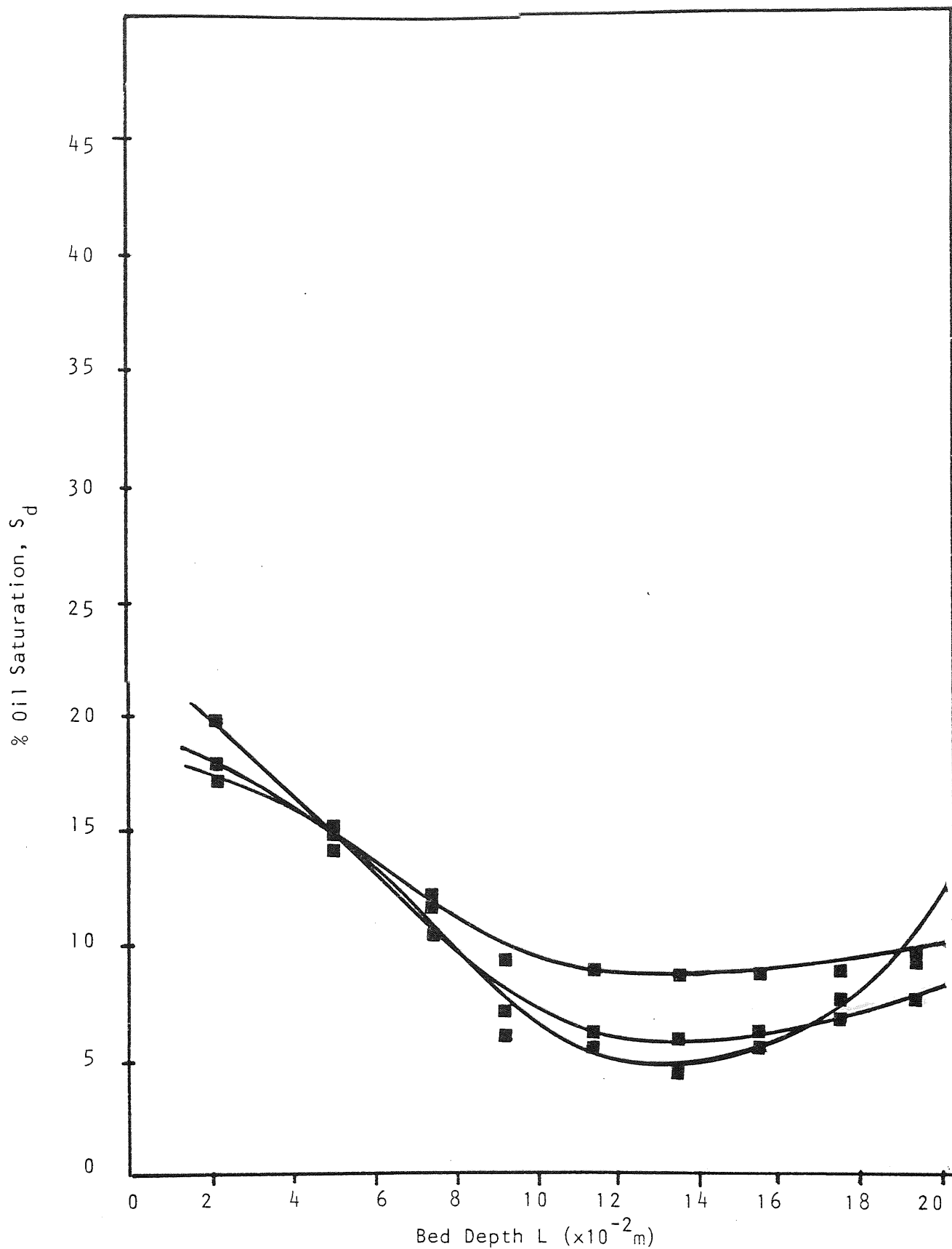


Figure 9.13 Saturation vs Bed Depth
 Ballotini $486 \mu\text{m}$, 20×10^{-2} m Bed Depth
 0.3×10^{-2} m/s Velocity and 0.15% Dispersed
 Phase Concentration.

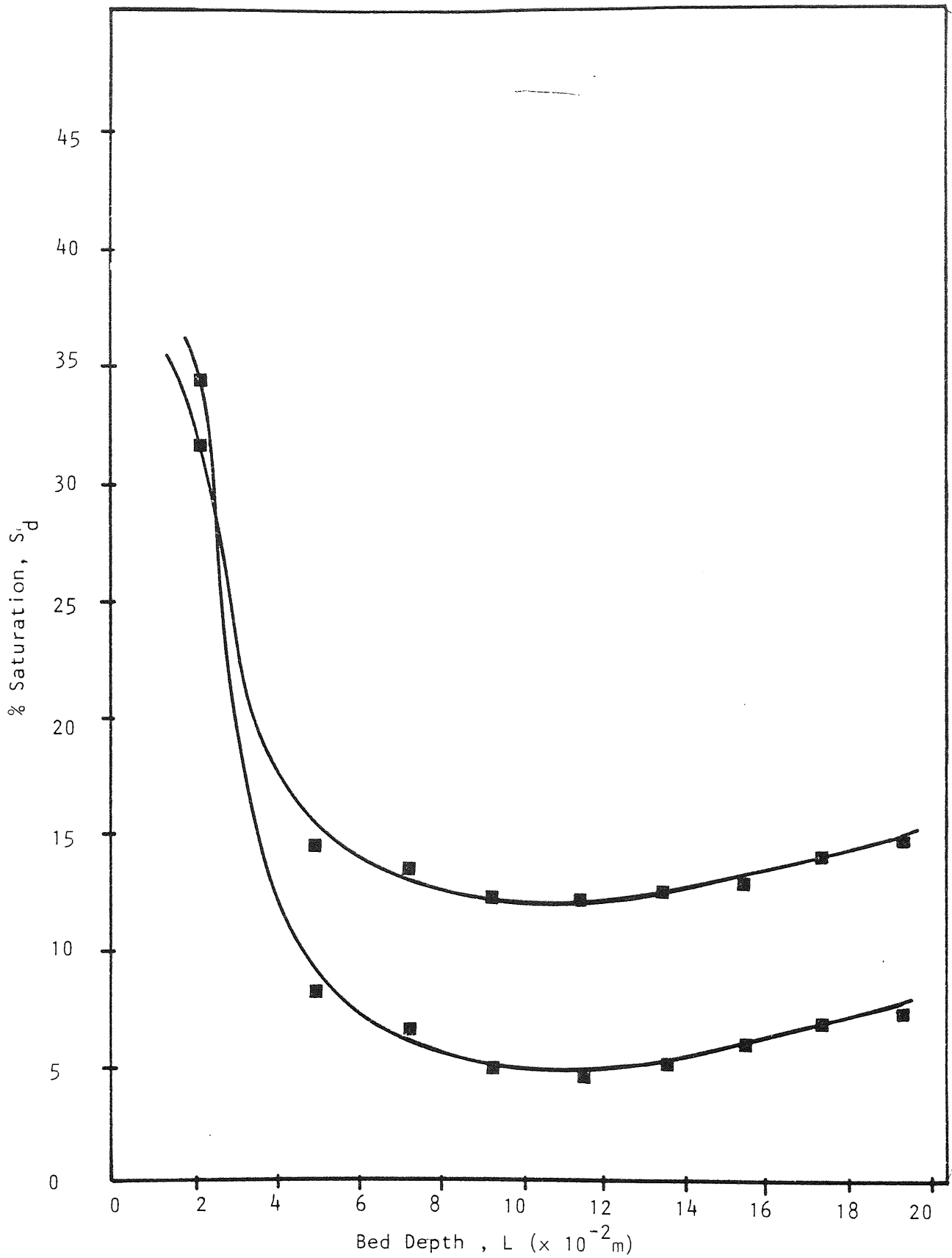


Figure 9.14 Saturation vs Bed Depth
 Ballotini 486 μm , $20 \times 10^{-2}\text{m}$ Bed Depth,
 $0.3 \times 10^{-2}\text{m/s}$ Velocity and 0.2% v/v
 Dispersed Phase Concentration.

mechanism at the inlet of the bed. The saturation for the remainder of the bed, however, increases only slightly with increased dispersed phase saturation.

For the lower velocity range, $0.1-0.3 \times 10^{-2}$ m/s, and keeping all the other operating parameters constant, the inlet oil saturation is higher for the lowest superficial velocity, which suggests a higher contribution of sedimentation to the drop capture efficiency with lower superficial velocity. For the remainder of the bed, however, the saturation is higher for the higher superficial velocity, which suggests that drops are being carried downstream of the coalescer by hydrodynamic forces due to the flow of continuous phase (Fig. 9.19).

For the high superficial velocity experiments, 3.0 to 5.0×10^{-2} m/s, shown in Fig. 9.20, the inlet oil saturation obtained is lower than those obtained for lower velocities with all the other parameters constant. Also the highest saturation is obtained further down the bed and therefore the term 'inlet saturation' is not accurate. This is likely due to the high superficial velocity pushing through the dispersed phase droplets from the forepart of the bed, but as their passage gets more tortuous, they may block an interstice or collide with other drops, making it more difficult for incoming droplets to pass through and thus increasing the held-up oil. For the purpose of comparison, this 'delayed' inlet dispersed phase saturation will be used as the inlet saturation. Further experimentation with higher dispersed phase saturation did not alter significantly the oil

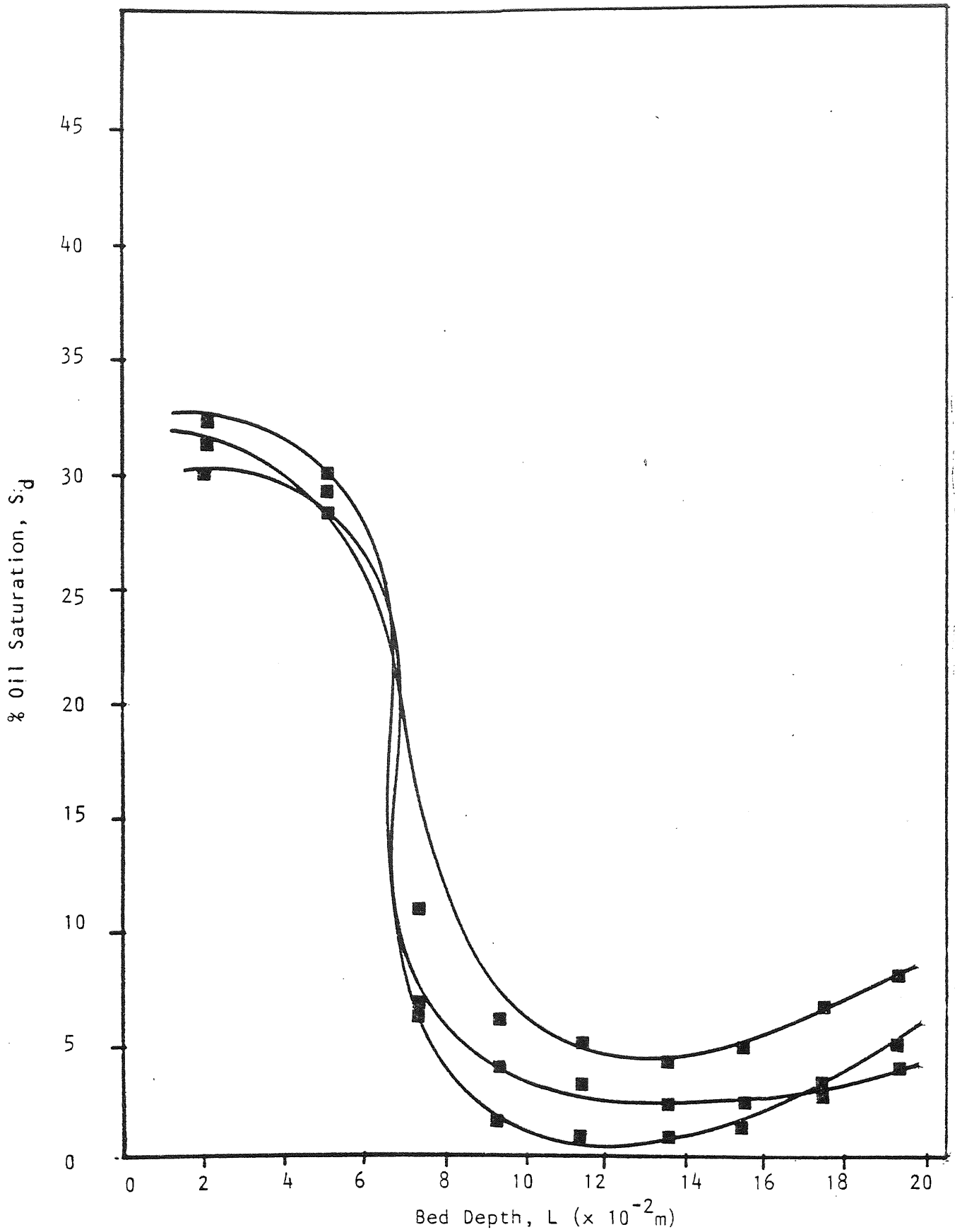


Figure 9.15 Saturation vs Bed Depth
 Ballotini 486 μ m, 20×10^{-2} m Bed Depth
 0.3×10^{-2} m/s velocity and 0.3% v/v
 Dispersed Phase Concentration.

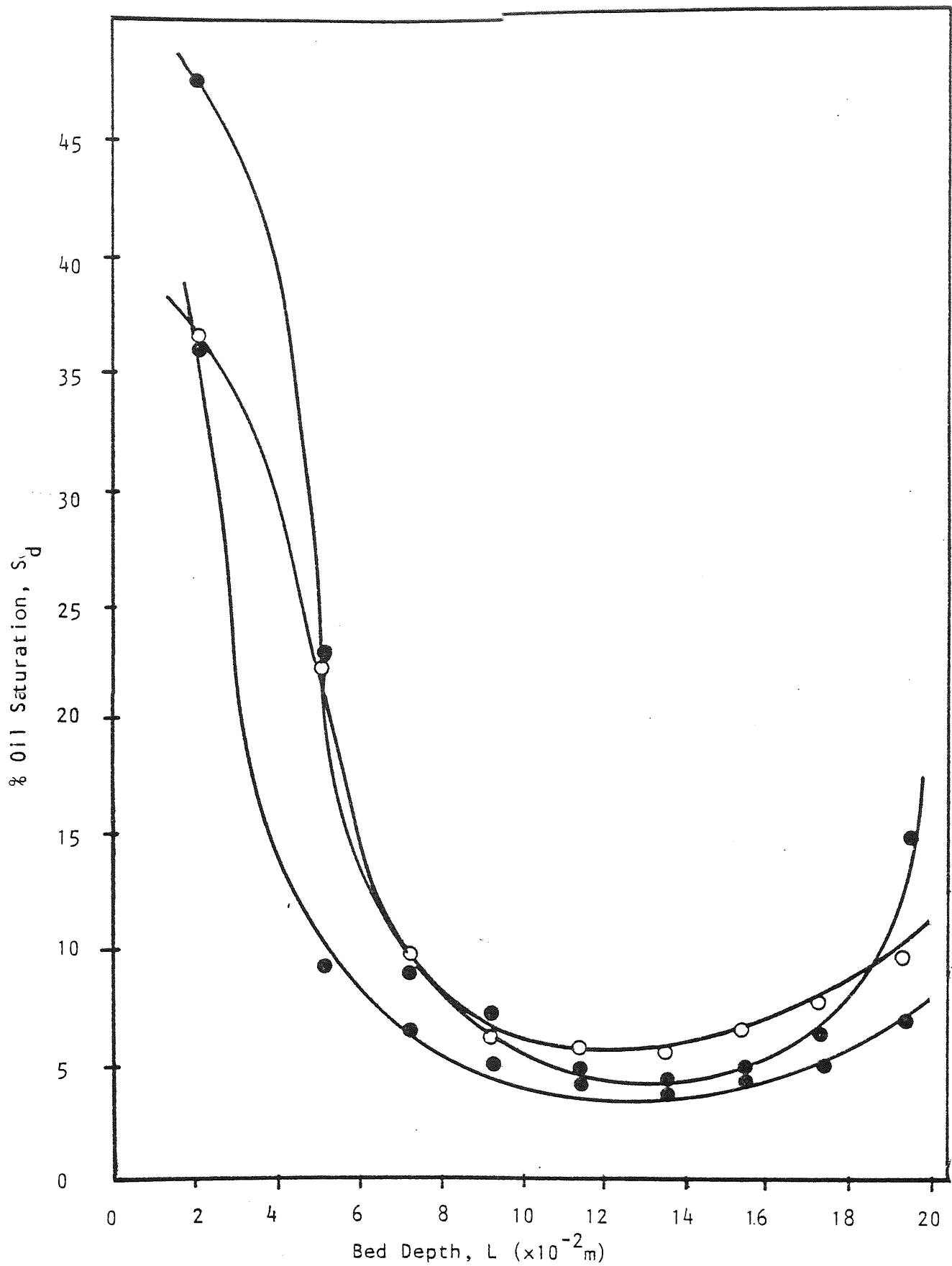


Figure 9.16 Saturation vs Bed Depth
 Ballotini 486 μm , 20×10^{-2} Bed Depth,
 0.3×10^{-2} m/s Velocity and 0.4% v/v
 Dispersed Phase Concentration

saturation pattern throughout the bed, which suggests that at high velocities the dispersed phase saturation is independent of dispersed phase concentration. This is further confirmed when compared with the results of Bitten and Fochtman (108) as shown in Fig.10.8.

The effect of ballotini size is presented on Fig. 9.21 and 9.22. The inlet saturation is higher for the smaller size ballotini, suggesting that drop capture by interception is aided as the size of the interstice is decreased. For the remainder of the bed, however, the saturation is higher for the larger size ballotini which may suggest that as the drop coalesce at the bed inlet they may move along the bed aiding further coalescence, whilst for the smaller size ballotini, it is more difficult for the coalesced drops to get dislodged and thus aid drop capture at the inlet of the bed.

Figs. 9.23 and 9.24 show the variation of saturation with bed depth and time. The oil saturation is seen to increase more rapidly with time near the inlet than near the outlet. The oil saturation corresponding to the shortest distance from the inlet face first rises sharply, and reaches steady state. The oil saturation of the second shortest distance rises secondly and reaches steady state secondly, and so on. A vertical cut at any fixed time on Fig. 9.24 will give the corresponding oil saturation vs. bed depth curve as shown in Fig. 9.23. This behaviour is typical of the system studied.

As explained in Section 9.5 the ratio $\frac{\Delta P_2}{\mu_{c2}} \cdot \frac{\mu_{c1}}{\Delta P_1}$ was used instead of $\frac{\Delta P_2}{\mu_d} \cdot \frac{\mu_c}{\Delta P_1}$ proposed by Austin (14).

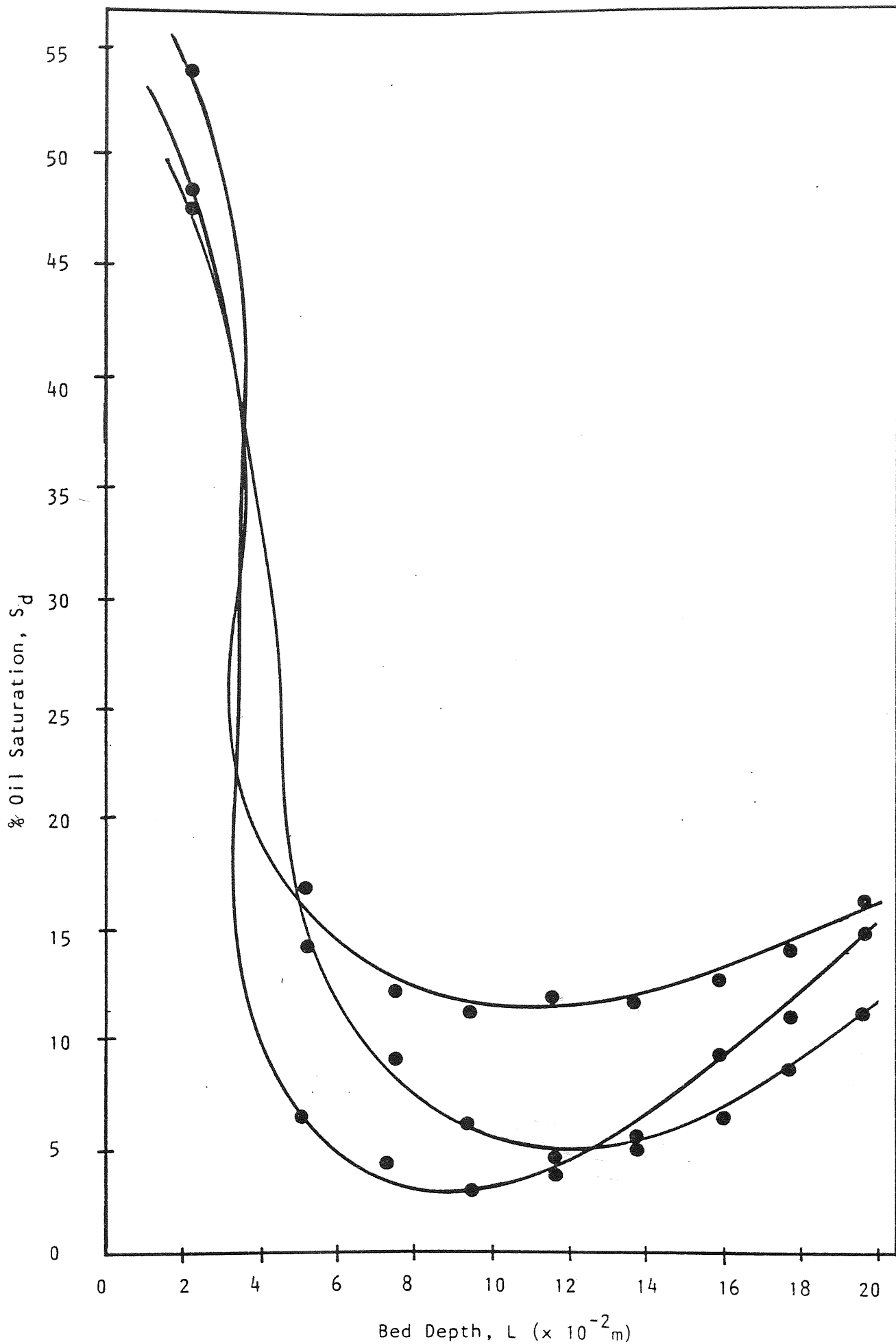


Figure 9.17 Saturation vs Bed Depth
 Ballotini 486 μm , 20×10^{-2} m Bed Depth,
 0.3×10^{-2} m/s Velocity and 1% v/v
 Dispersed Phase Concentration.

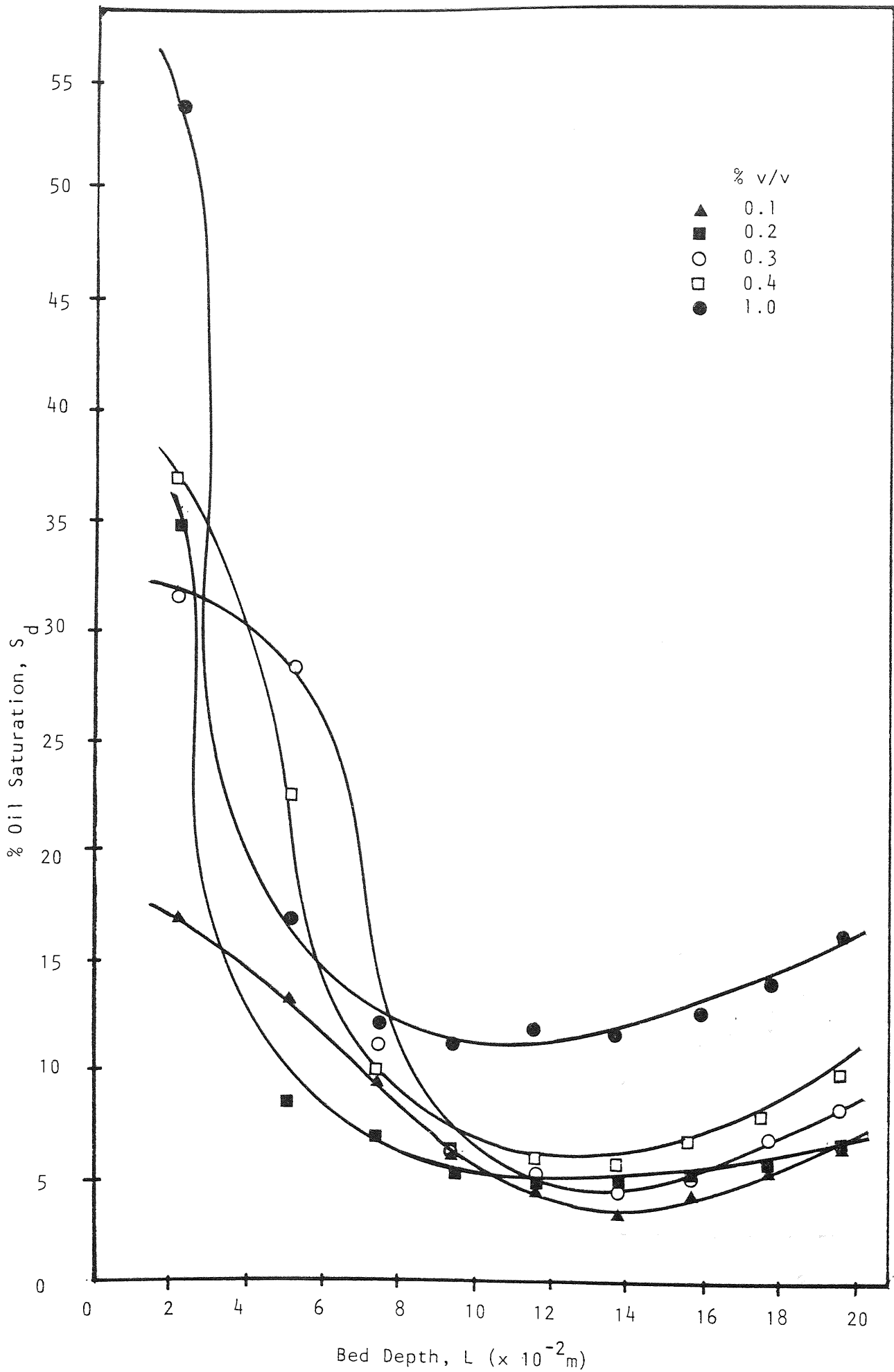


Figure 9.18 Effect of Concentration of Dispersed Phase on Saturation vs Bed Depth. Ballotini 486 μ m, 20×10^{-2} m Bed Depth $.3 \times 10^{-2}$ Velocity.

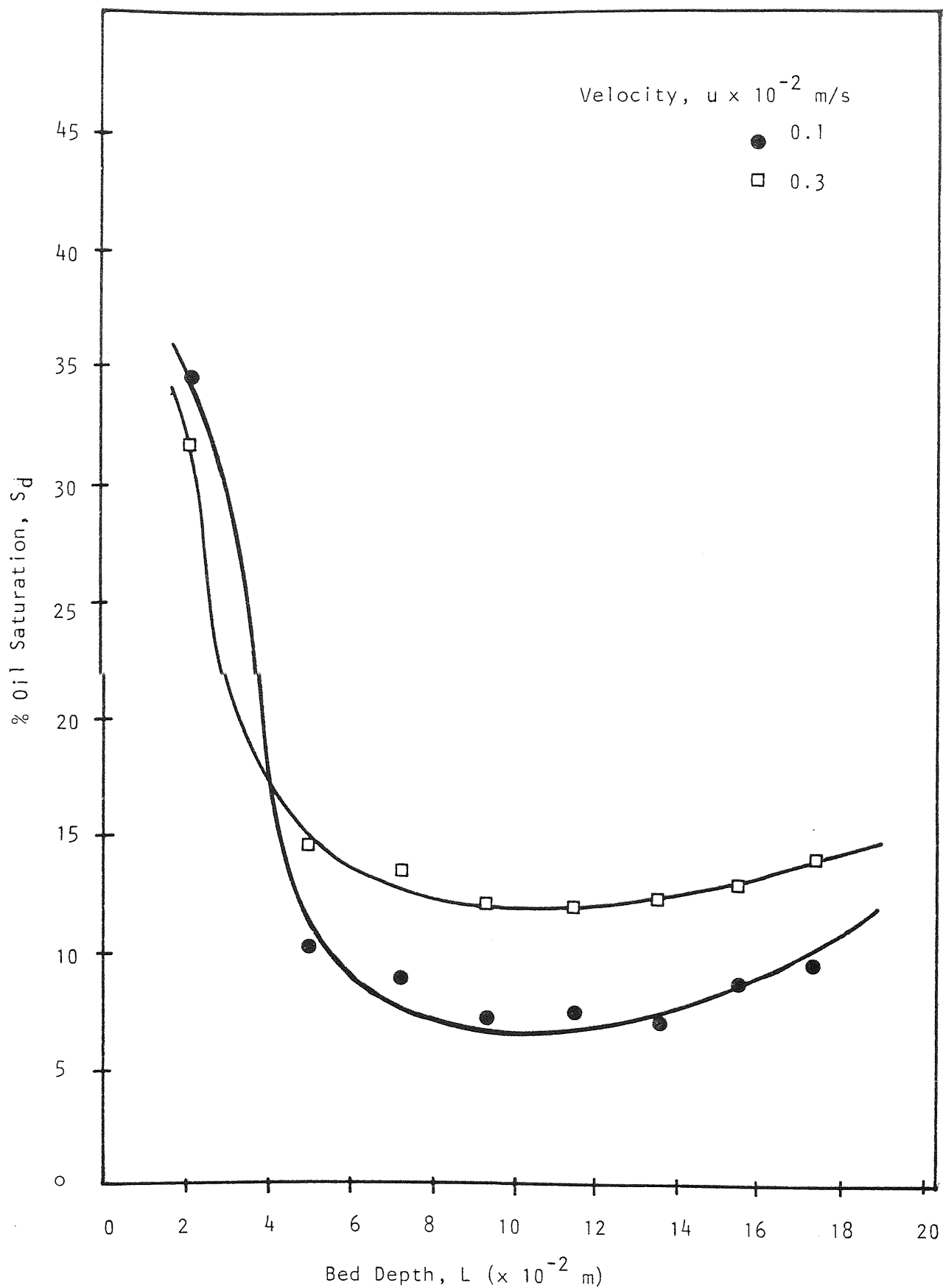


Figure 9.19 Effect of Velocity of Saturation vs Bed Depth
 Ballotini Size $486 \mu\text{m}$ and $20 \times 10^{-2}\text{m}$ Bed Depth.

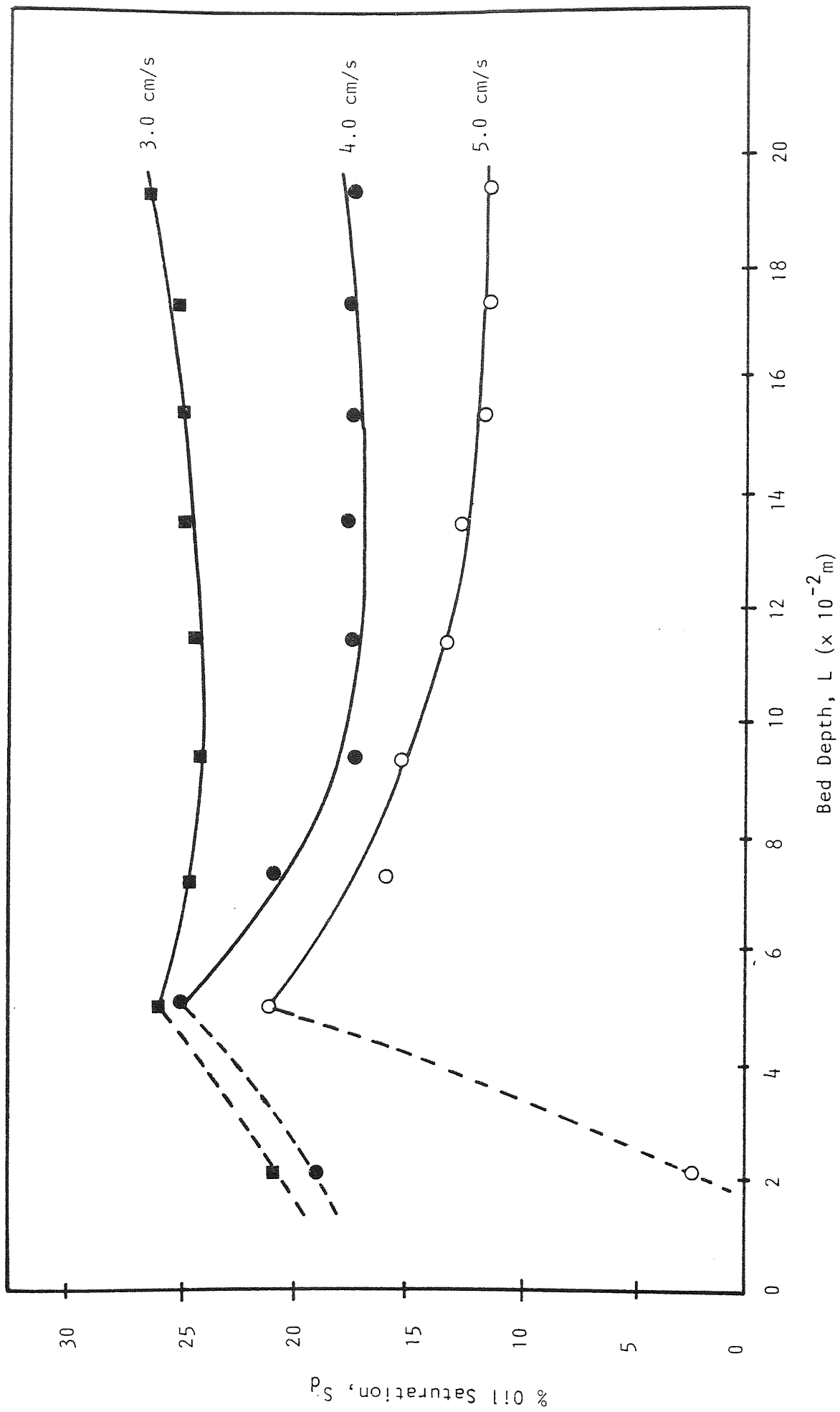


Figure 9.20 Effect of Velocity on Saturation vs Bed Depth

On Fig. 9.25 it can be seen that the oil saturation can be easily overestimated if the dispersed phase viscosity is used to correlate two-phase pressure drop, as its value is nearly half that of the continuous phase viscosity.

From a study of equations 9.30 and 9.31, it can be obtained that

$$\frac{k_d}{k_c} = \frac{(1.11 S_d - 0.11)^2}{(1 - S_d)^3} \dots\dots\dots (9.35)$$

and the relation between k_d/k_c and S_d is established. This is plotted on Fig. 9.26 along with the data of Leverett and Carpenter for unconsolidated sands and glass beads respectively. From this graph it can be seen that the minimum dispersed phase saturation required for the oil-water system to be capillary equilibrium is about 12% and the maximum dispersed phase saturation that can be obtained is 80% due to the irreducible continuous phase saturation.

This minimum dispersed phase saturation is required to form a nearly continuous network of capillary conducted oil within the packed bed. As can be seen from the saturation profiles shown previously, not all of them reached this minimum saturation value and therefore it can be assumed that, the flow of the dispersed phase occurs not only by capillary conduction, and/or steady-state operation was not reached. It can be concluded that during the initial stages of the coalescence process, the unsteady state oil saturation profile is roughly an exponentially decreasing curve which suggests that oil saturation is predominantly caused by deposition

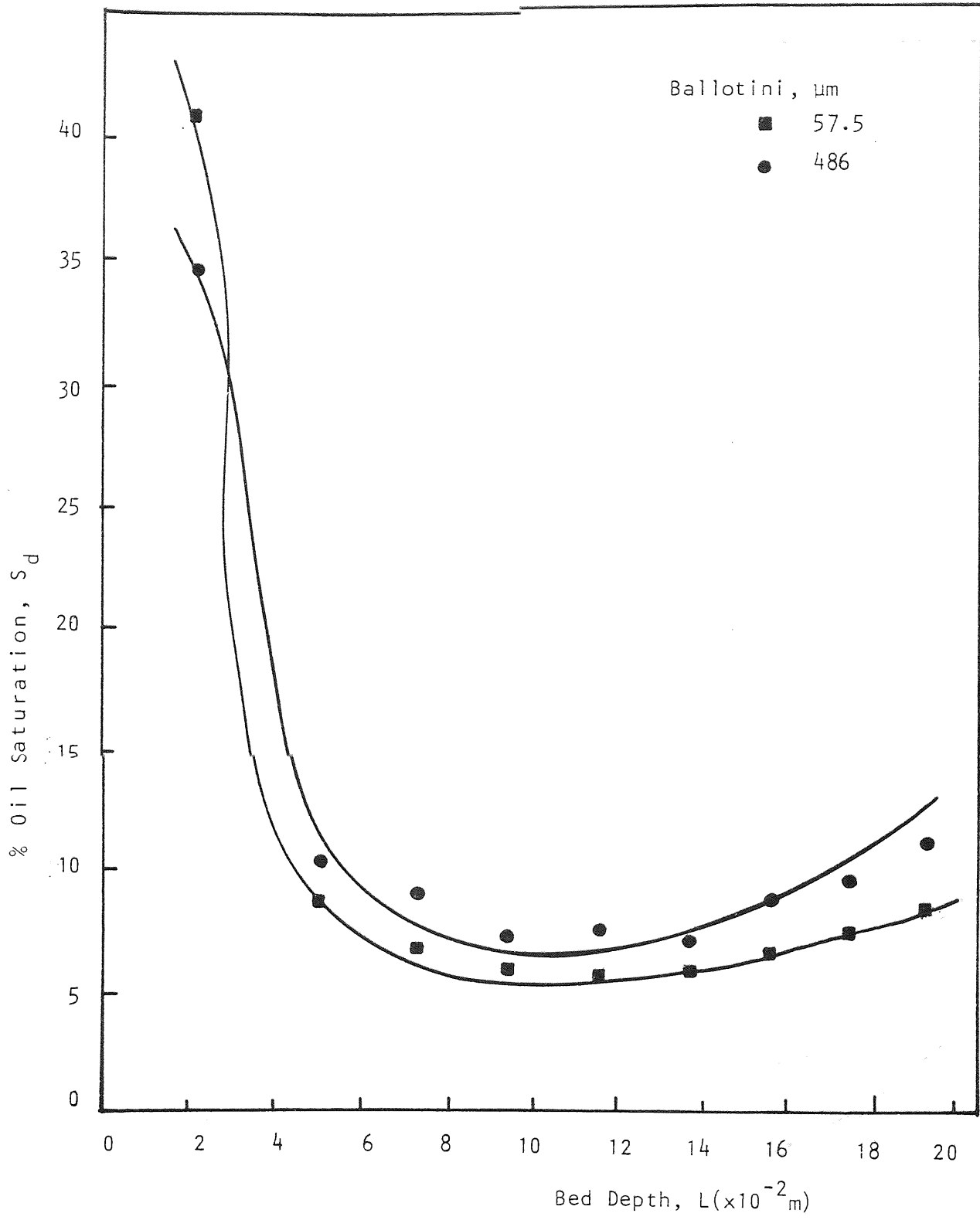


Figure 9.21 Effect of Ballotini on Saturation Vs. Bed Depth.
 $20 \times 10^{-2} \text{ m}$ Bed Depth, $0.1 \times 10^{-2} \text{ m/s}$ Velocity

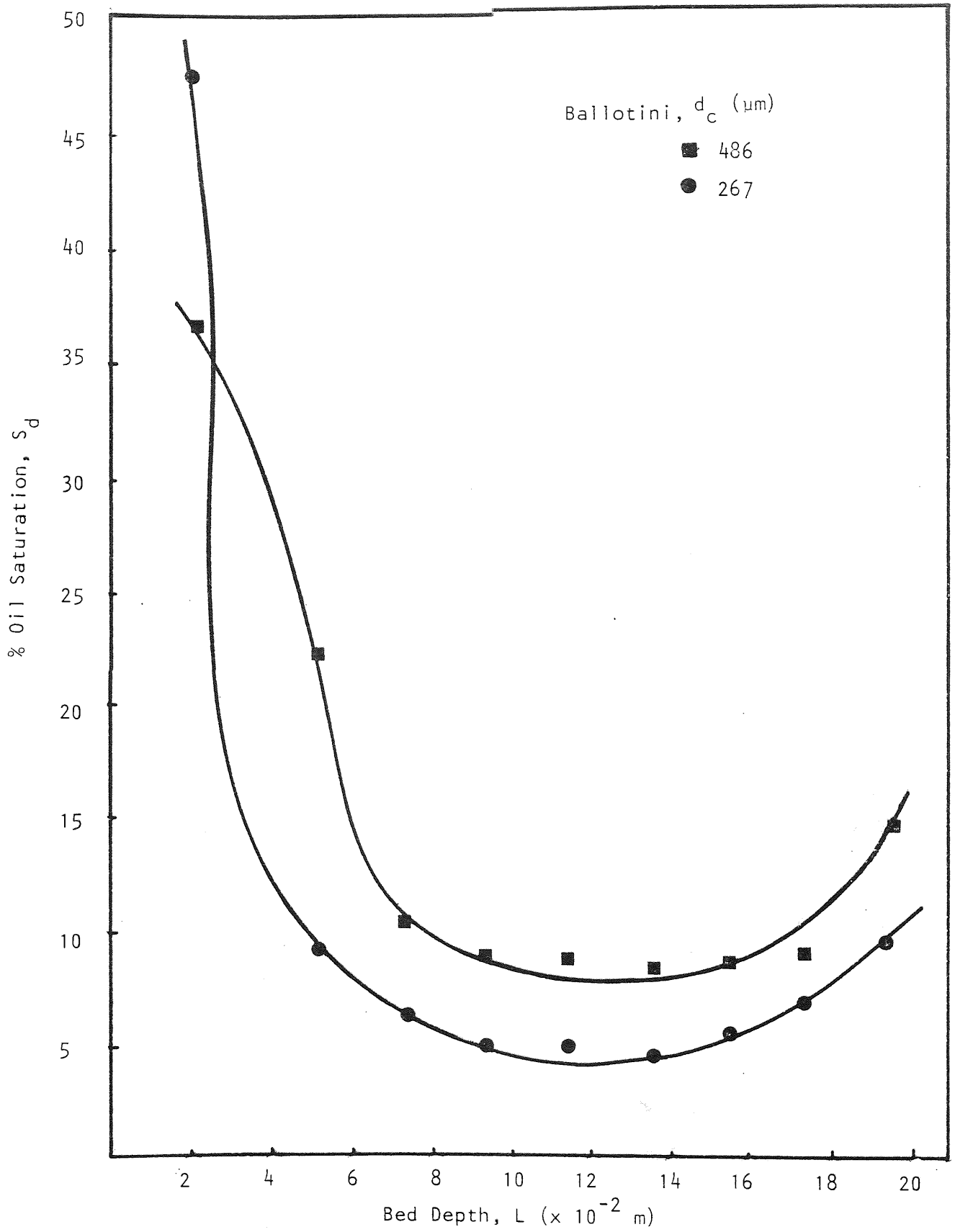


Figure 9.22 Effect of Ballotini Size on Dispersed Phase Saturation Vs Bed Depth, 0.1 % v/v Dispersed Phase Concentration, 0.3×10^{-2} m/s Velocity.

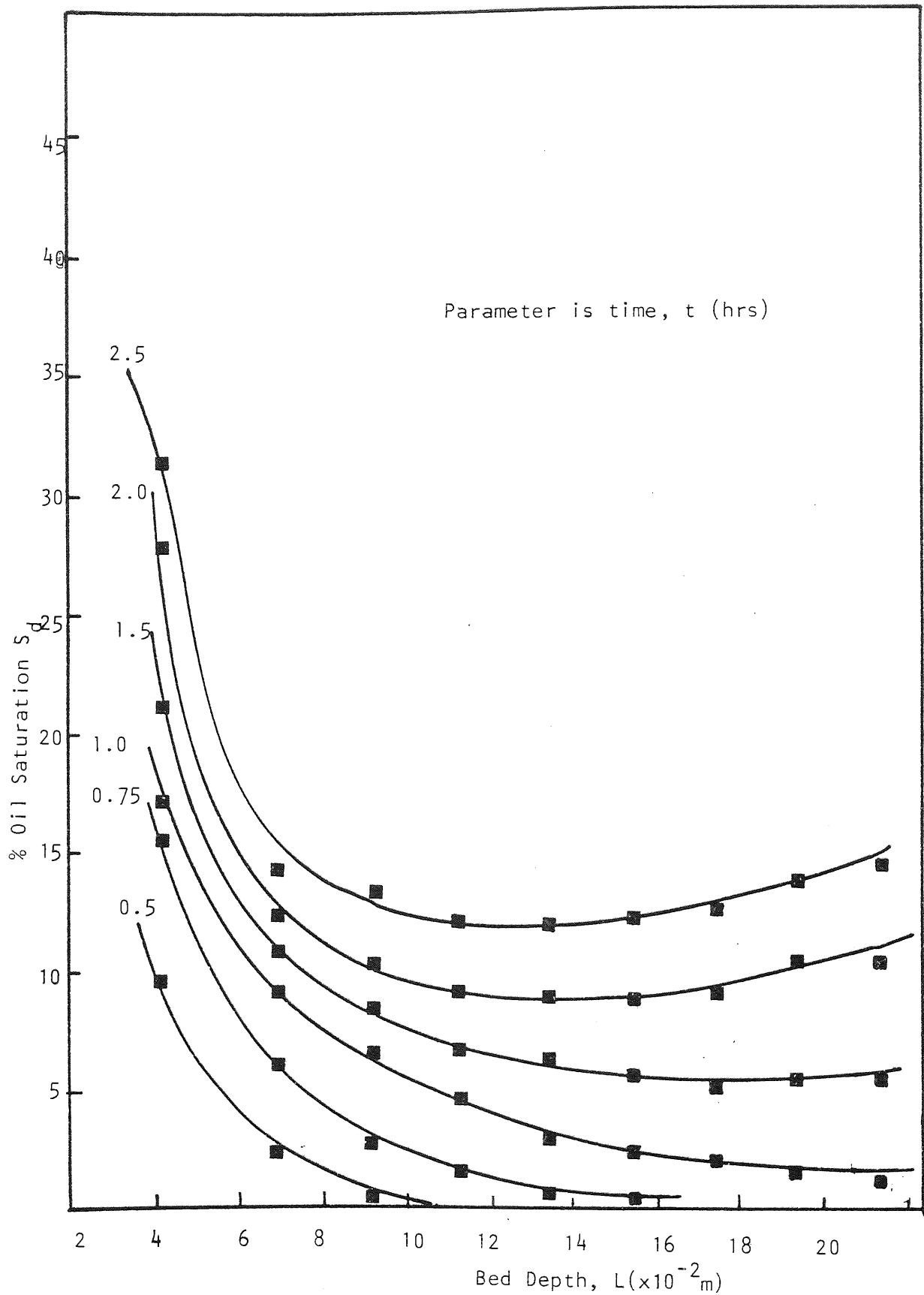


Figure 9.23 Saturation Vs. Bed Depth for Increasing Operating Time. Ballotini 486 μm , 0.3×10^{-2} m/s Velocity, 0.2% v/v Dispersed Phase Concentration

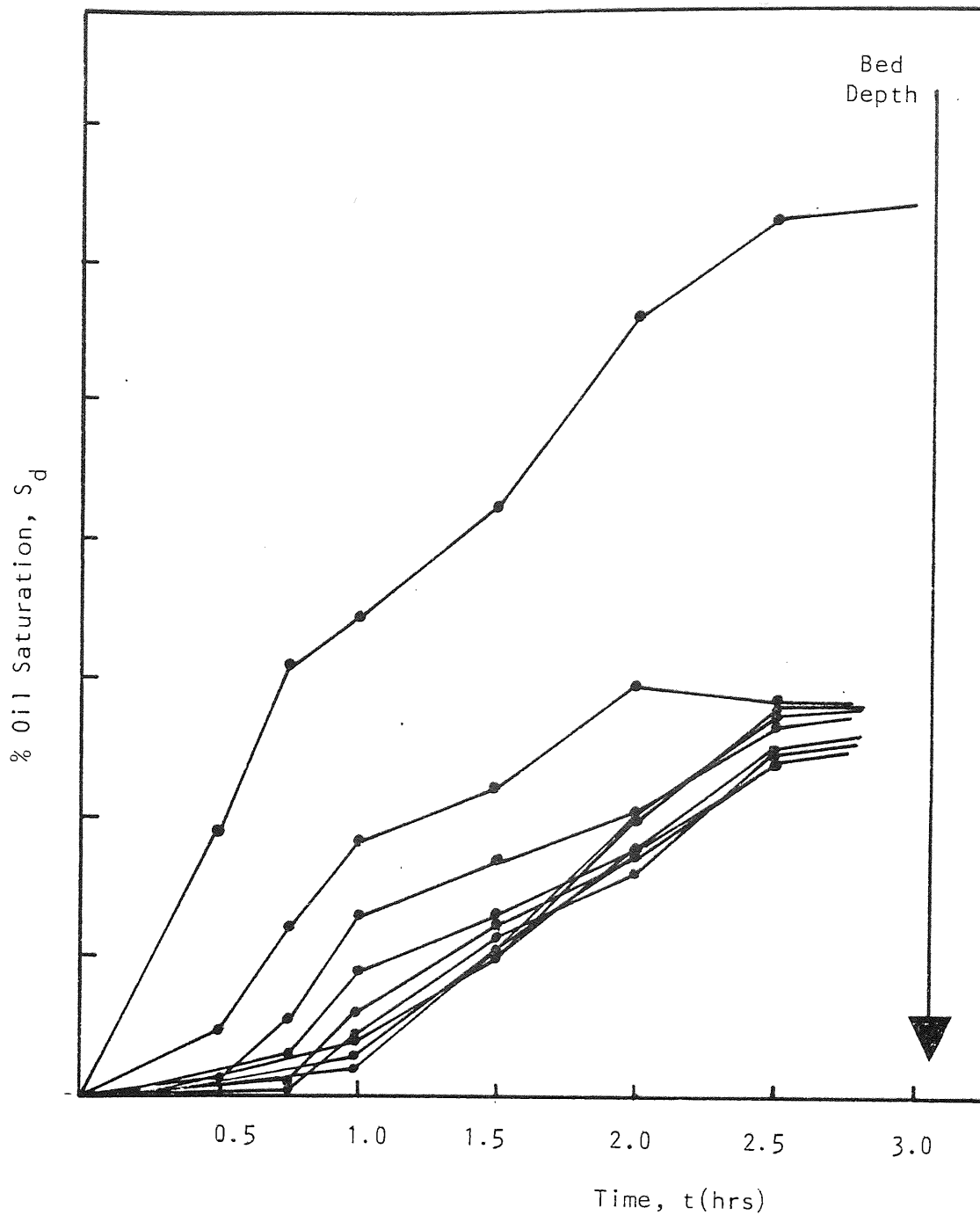


Figure 9.24 Saturation Vs. Time for Different Bed Depths.
 Ballotini $486 \mu\text{m}$, $0.3 \times 10^{-2} \text{ m/s}$ Velocity,
 0.2% v/v Dispersed Phase Concentration

of captured oil droplets. Some of the captured oil droplets coalesce into the bulk oil phase, some do not. During these early stages even the coalesced oil droplets cannot flow and tend to remain where they are captured and coalesce only with neighbouring or incoming drops to form continuous channels for flow. As time continues the oil saturation at or near the inlet face of the coalescer reaches a critical value (say, $S_d = 0.5$), and capillary pressure begins resisting further increase of local oil saturation and forces the coalesced oil to flow towards the exit face of the bed. Hence, an oil front is seen to propagate from inlet to outlet, with maximal local oil saturation fixed at a critical value which depends on the flow rate and capillary pressure.

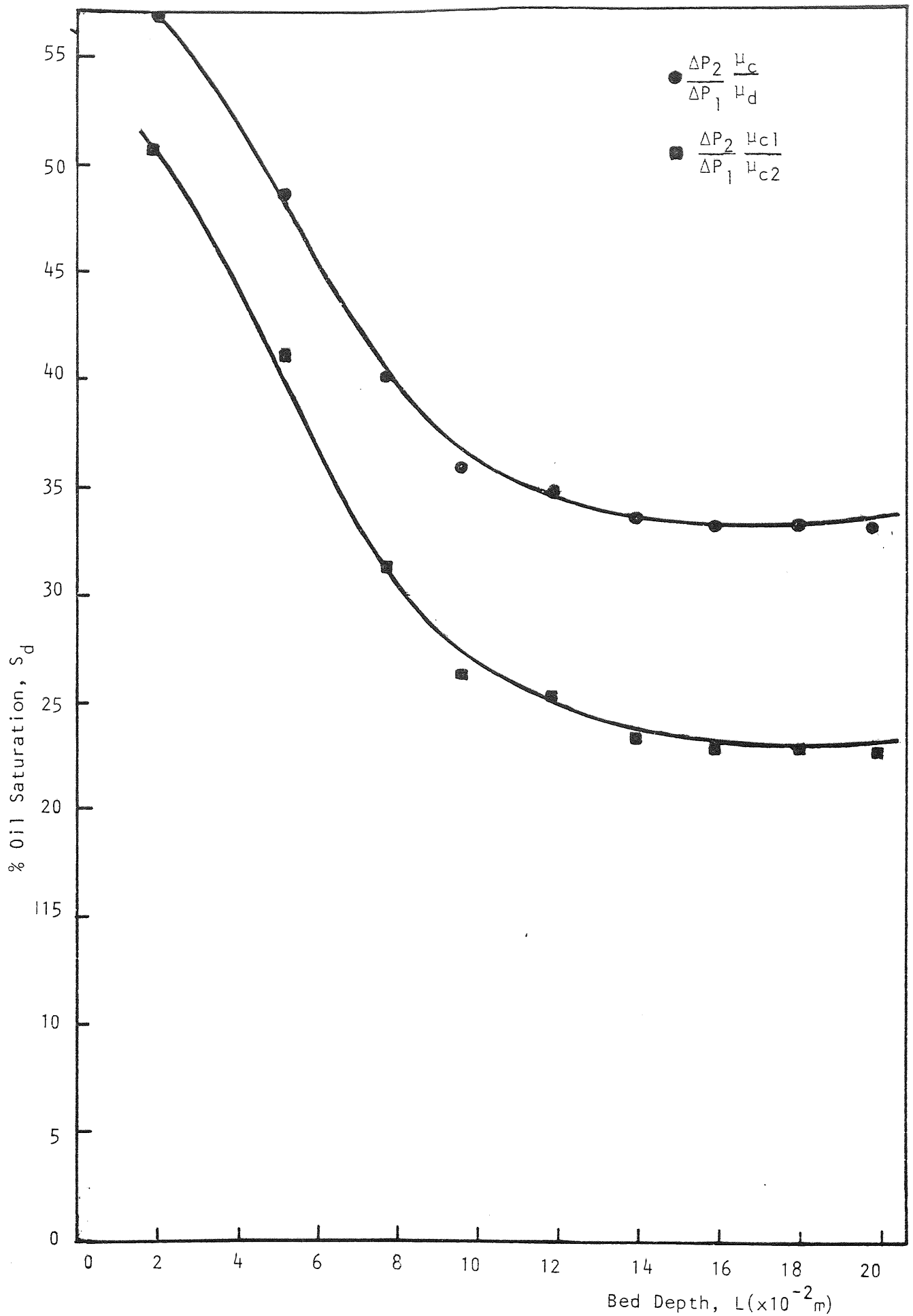


Figure 9.25 Comparison of Saturation Vs. Bed Depth Profiles
 Obtained Using $\frac{\Delta P_2 \mu_{c1}}{\Delta P_1 \mu_{c2}}$ and $\frac{\Delta P_2 \mu_c}{\Delta P_1 \mu_d}$

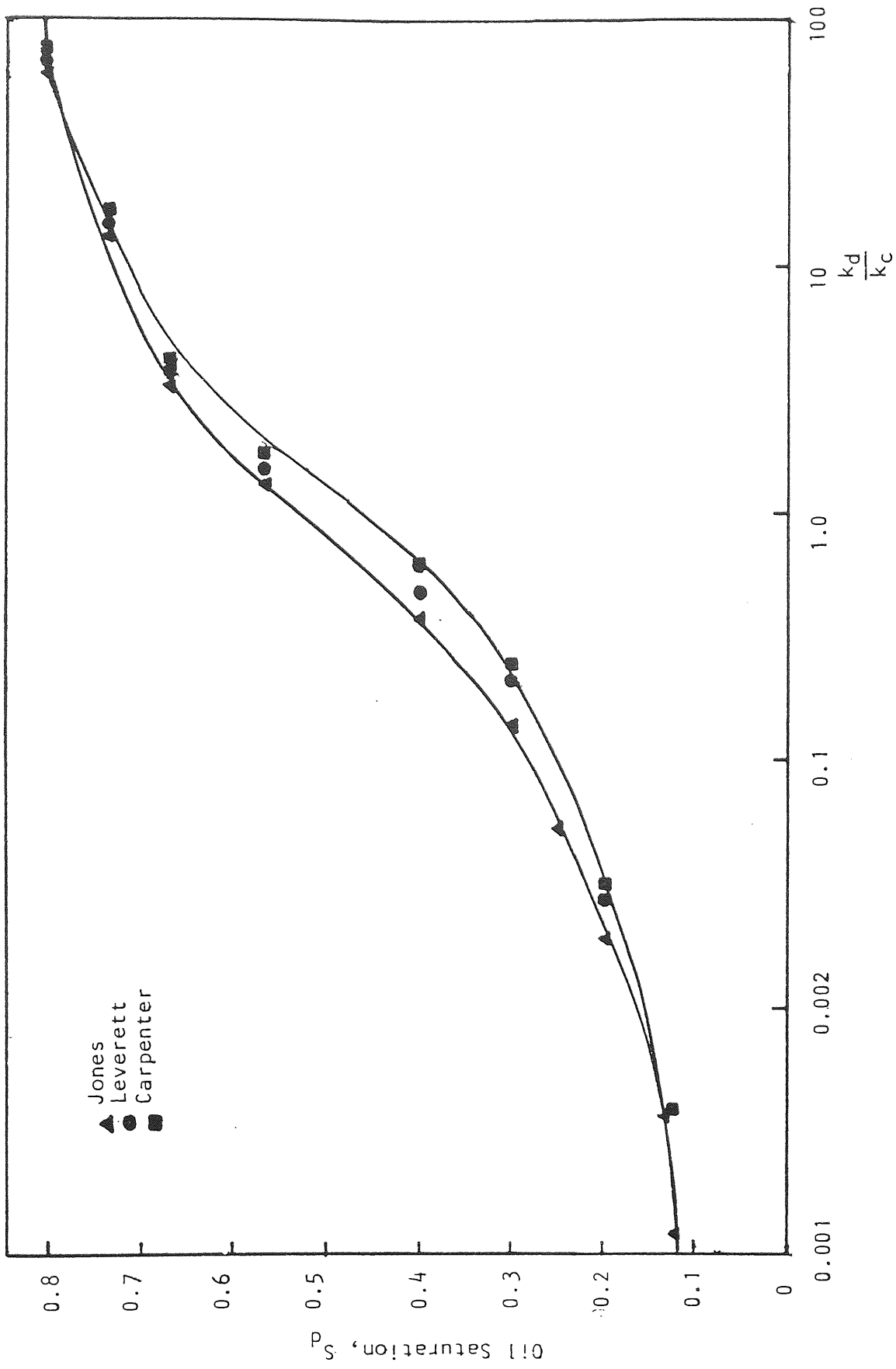


Figure 9.26 Saturation Vs. k_d/k_c

CHAPTER TEN
MODEL OF DISPERSION COALESCENCE

CHAPTER TEN

MODEL OF DISPERSION COALESCENCE

10.1 PREDICTION OF FILTER COEFFICIENT

The filter coefficient provides a measure of the overall drop coalescence efficiency of a bed and is defined as:

$$\lambda = \frac{-\log_e \left\{ \frac{\text{Outlet drop number density}}{\text{Inlet drop number density}} \right\}}{L} \dots\dots\dots (10.1)$$

The majority of existing models are for fibrous beds coalescers and attempt to predict the filter coefficient. The proposed equations and their shortcomings are reviewed below. Also, the different values of λ are obtained using the data on Table 10.1 as means of comparison.

10.1.1 Vinson and Churchill Equation

This model assumes that drops collide with fibres and have a probability of being retained. They then move along the fibre onto other fibres, and coalesce with other retained drops. The model further assumes that the drops are captured by interception and the thinning of the continuous phase film results from the normal stresses due to the flow and the Van der Waals attraction. The drop filament adhesion along with the wettability determines whether a drop remains on the fibre long enough to coalesce with other drops. In the case of strong adhesion, cohesive failure may occur. In this case, only

Parameter	Symbol	Value
Collector Diameter	d_c	486.0 μm
Aperture Diameter	d_a	99.6 μm
Dispersed Phase Density	ρ_d	866.9 Kg/m^3
Continuous Phase Density	ρ_c	100 kg/m^3
Dispersed Phase Viscosity	μ_d	$0.58 \times 10^{-3} \text{Ns/m}^2$
Continuous Phase Viscosity	μ_c	$1.00 \times 10^{-3} \text{Ns/m}^2$
Boltzman's Constant	k'	$1.38048 \times 10^{-23} \text{J/ K}$
Absolute Temperature	T	293 ^o K
Hamaker Constant	Q	$0.401 \times 10^{-20} \text{J}$
Hydrodynamic Function	A_s	37.98

Table 10.1 Basic Set of Parameters used in comparison of Capture Mechanisms and Filter Coefficients.

a part of the drop disengages leading to a drop phase which will be attenuated to sheets or threads downstream of the fibres by fluid forces. The size of the drops at disengagement depends upon the thickness of the sheets or threads.

Their equation represents the best fit of the data taken for a system where photoetched screens were used to simulate a fibrous bed (58).

$$\lambda = \frac{-\log_e\{0.128(u d_c \mu_c)^{-0.4} - 0.089\}}{L} \dots\dots\dots (10.2)$$

where the units of the independent variable are (gm)(micron)/s².

The obvious shortcoming of this model is that it is qualitative. No equations are presented which can be used to correlate the data. The authors merely studied the data to see which terms were important and then derived an empirical expression to fit the data, which is completely independent of their model.

Also the qualitative model itself has some shortcomings. Film studies (68,212) indicate that while drops strike the fibres they also strike drops which are attached to the fibres. It is this means of coalescence between drops which is more pronounced. The movement of a drop along a fibre after it has been captured by the fibre has been found to be of negligible importance (66). Also, while the authors consider the Van der Waals attraction in the film thinning process, they fail to consider this force as a factor in holding a drop on a fibre.

For a 486 μm ballotini, $20 \times 10^{-2} \text{m}$ bed depth and $0.3 \times 10^{-2} \text{m/s}$ superficial velocity, equation 10.1 predicts a filter coefficient of $\lambda = 19.29 \text{m}^{-1}$.

10.1.2 Spielman and Goren Equation

This model (45,71) assumes that when a dispersion flows through a fibrous bed, the suspended drops are transported to the fibres and entrapped liquid interfaces where they are captured and coalesced into the bulk of previously captured liquid. This coalesced liquid drains through the bed and leaves the bed at the same rate as the rate at which suspended drops are coalesced within the bed. Each immiscible fluid is considered to flow within a fixed channel, with the non-wetting fluid flowing on the inside. Each channel is described by Darcy's Law.

They suggested that London-Van der Waal's forces are of sufficient magnitude to overcome any hydrodynamic retardation effects and were included in the evaluation of capture efficiency. Their equation, for continuous phase wetted beds, was obtained by correlation of experimental data with a modified Adhesion number:

$$\gamma = 0.29 \frac{d_p^2}{d_c^3} \left\{ \frac{Q d_c^2}{\mu_c u d_p^4} \right\}^{0.25} \dots\dots\dots (10.3)$$

The main shortcoming of this model is that the model is not general. It is unique only for geometrically similar solids, having the same dispersed phase saturation. Thus the final expression is independent of the porosity of the bed. Also, a considerable amount of data is

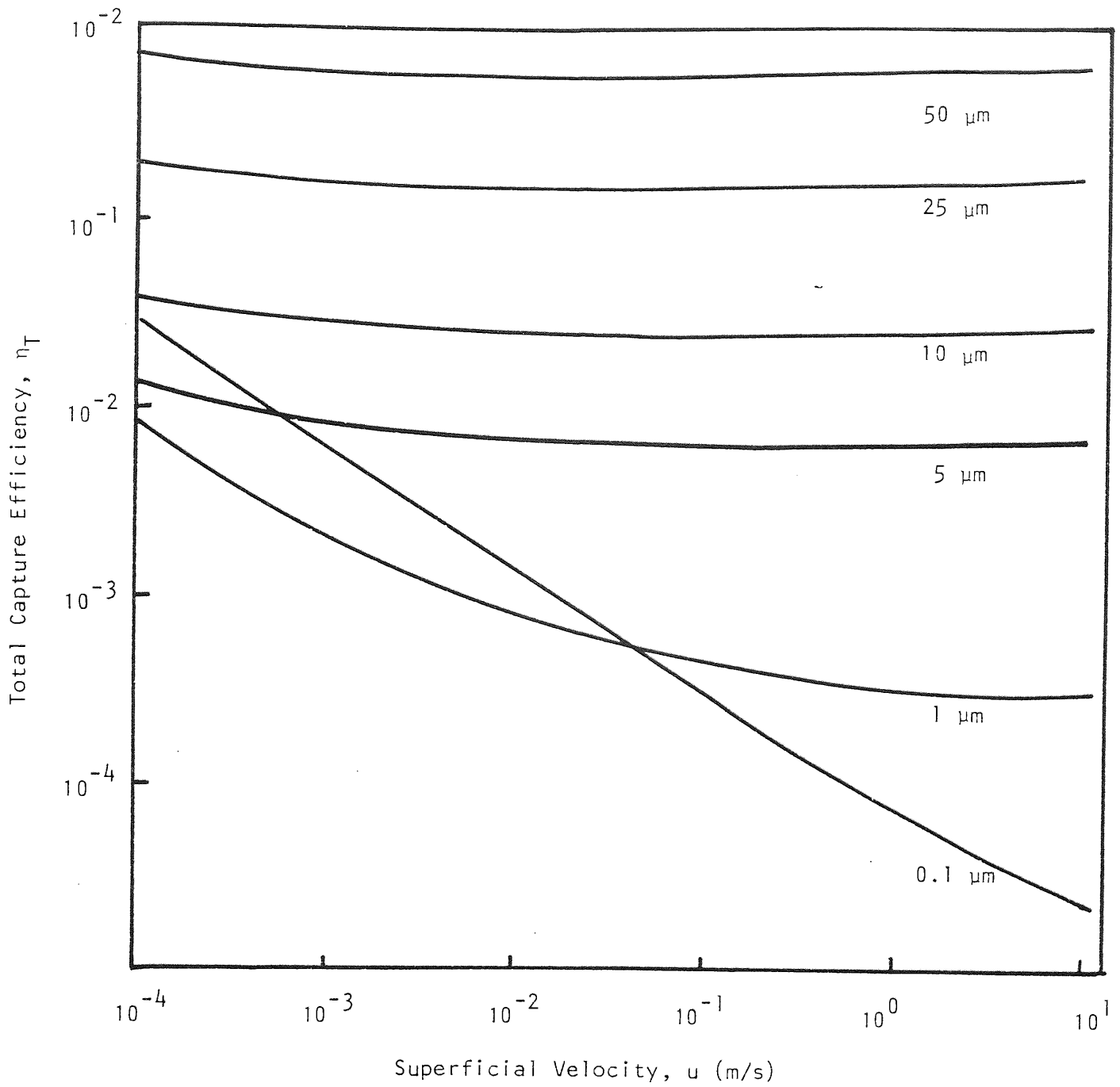


Figure 10.1 Variation of Total Capture Efficiency with Velocity for Different Drop Sizes.

required to determine the constant and exponent, and thus it is of limited use in coalescer design.

This equation predicts $\lambda=0.266 \text{ m}^{-1}$ for similar conditions to those described in Section 10.1.1 and for a drop diameter, $d_p = 25 \text{ }\mu\text{m}$.

10.1.3 Sherony and Kintner Equation

Sherony and Kintner (44) were the first authors to develop a mathematical model of a fibrous bed coalescer and to use it to derive a design equation. It is based on the 'travelling drop' model discussed in Section 5.4.2 and drop capture was assumed to occur by interception and inertial impaction. The final equation was expressed in terms of an overall coalescence efficiency, η_c and the average saturation:

$$\lambda = \frac{0.75}{d_c} \left\{ \frac{\bar{S}_d}{1-\bar{S}_d} \right\} (1-e_1) \left\{ 1 + \frac{d_p}{d_c} \right\} \eta_c \dots\dots\dots (10.4)$$

One serious shortcoming of their model is that it predicts that as the velocity increases the efficiency of the bed increases. This is opposite of what have been observed by all other workers (13,14,58,66,213).

From the correlation between η_c and $\frac{NRe}{e_1}$ given in Sherony's paper, using the data of Table 10.1, $\eta_c=0.37$. Also for a mean saturation of 0.3, equation 10.3 gives $\lambda=154.37 \text{ m}^{-1}$.

10.1.4 Rosenfeld and Wasan Equation

This model (47) also advocates the travelling drop hypothesis but unlike Sherony's model, did not assume that when a drop detaches from a fibre, it is replaced by an identical one and that detachment occurs after a single coalescence event. Furthermore, they assume that drops flow along the streamlines of the fluid and if they come close to a held drop or fibre, they will strike it. Rosenfeld introduced an effective collector diameter, d_{ce} to account for held drops and introduced a factor, β to relate these collision frequency to coalescence efficiency:

$$\lambda = \frac{8\beta(1-e_1)d_p}{\pi^2 d_c^2 e_1 (1-\bar{S}_d)} \left\{ \frac{2d_{ce} + d_p}{d_{ce} + d_p} \right\} \dots\dots\dots (10.5)$$

where $d_{ce} = d_c \left\{ \frac{1-e_1(1-\bar{S}_d)}{1-e_1} \right\}$

Equation 10.5 is only valid at low velocities. At higher velocities a purely empirical extension of equation 10.5 was made to fit the data, including the superficial velocity and the velocity at which the filtration coefficient begins to decrease. This was referred to as the critical velocity and is an adjustable parameter that must be evaluated experimentally, which makes the model unsuitable for design purposes.

A typical value of β was determined by Sherony (44) to be 0.41 which produces a filter coefficient, $\lambda = 147.65 \text{ m}^{-1}$.

The calculated values of the filter coefficient using the above four equations vary over two orders of magnitude for the same operating conditions which alone

illustrates the shortcomings of these models.

In view of the complexity of the coalescence process, the interactions between the operating parameters may account for the discrepancies. Coalescence of secondary dispersions has been studied using different porous media with many systems under an extensive range of operating conditions but several basic principles have evolved. Both filter coefficient and pressure drops depend on the saturation in the bed and so determination of the latter by theoretical or experimental methods is essential. In the following sections, a combined approach is discussed in an attempt to relate these parameters quantitatively.

10.2 THEORETICAL COMPARISON OF CAPTURE MECHANISMS

Although many mechanisms have been suggested for drop capture, it is desirable to determine their relative contributions to the overall capture efficiency under practical operating conditions. This comparison was designed to produce an equation for estimation of the drop capture in a coalescer.

The variables investigated in this experimental study included superficial velocity and drop diameter which both affect theoretical capture efficiency. Drop diameter may be treated as a variable since the inlet dispersion was polydisperse. Drop capture efficiencies due to interception, London-Van der Waal's forces, diffusion and sedimentation were determined employing a basic set of parameters, relevant to the experimental

work presented in Table 10.1. The equations for evaluation of the individual mechanisms were discussed in Section 5.2 and are summarised in Table 10.2. The calculations were performed for a range of values of drop diameter and superficial velocity using a computer program listed with the output in Appendix I. The comparison was made with Happel's cell expression for an assemblage of spheres, A_s , characterising the flow parameter for viscous flow. Direct Interception (pore catchment) was not included in the analysis since the efficiencies cannot be compared directly and this mechanism only becomes significant when the drop size exceeds the effective aperture diameter. Inertial impaction was also excluded since drop density is less than continuous phase density.

The overall efficiency is therefore:

$$\eta_T = \eta_I + \eta_D + \eta_G + \eta_L \dots\dots\dots (10.6)$$

and calculated values of η_T are presented in Table 10.3. The domain associated with each mechanism is also expressed qualitatively in Table 10.4 where its significance is recorded if it contributes greater than an arbitrary 5% of the total efficiency. All four mechanisms investigated were found to be relevant to coalescence of secondary dispersions. Fig. 10.1 shows that the overall efficiency, decreases gradually to an almost constant value over the range studied, the only exception being for 0.1 μm drops when only diffusion and London Van der Waal's forces predominate.

Mechanism	Characteristic Dimensionless Group	Equation for Capture Efficiency.
Interception	Interception number, R	$\eta_I = \frac{3}{2} A_s R^2$
Direct Interception	Direct Interception number, R_D	$\eta_{DI} = (R_D > 1); \eta_{DI} = 0 (R_D < 1)$
Inertial Impaction	Stoke's number, N_{Stk}	$\eta_{II} = \frac{N_{Stk}^3}{N_{Stk}^3 + 0.77 N_{Stk}^2 + 0.22}$
Sedimentation	Gravity number, N_G	$\eta_G = N_G$
London Forces	Adhesion number, N_{Ad}	$\eta_L = 2 A_s R^2 \left[\frac{9}{5} N_{Ad} \right]^{1/3}$
Diffusion	Peclet number, N_{Pe}	$\eta_D = 4.04 A_s^{1/3} N_{Pe}^{-2/3}$

Table 10.2 Dimensionless Groups and Equations used in Capture Mechanisms Evaluation.

Drop Diameter d_p (μm)	Superficial Velocity, u ($\times 10^{-2}$ m/s)						
	0.01	0.1	0.2	0.3	1.0	10	100
0.1	0.0272	0.0059	0.0037	0.0029	0.0013	0.0003	0.00007
1	0.0073	0.0020	0.0015	0.0012	0.0008	0.0004	0.0003
5	0.0122	0.0082	0.0077	0.0074	0.0069	0.0064	0.0062
10	0.0332	0.0273	0.0265	0.0262	0.0254	0.0247	0.0244
25	0.1743	0.1571	0.1554	0.1547	0.1532	0.1518	0.1512
50	0.6685	0.6159	0.6118	0.6102	0.6072	0.6047	0.6038

Table 10.3 Total Capture Efficiency for the Range of Velocities and Drop Diameters encountered in Secondary Dispersion Coalescence (enclosed section describes range of variables encountered in this study).

Drop Diameter d_p (μm)	Superficial Velocity, ($\times 10^{-2}$ m/s)						
	0.01	0.1	0.2	0.3	1.0	10	100
0.1	D	D	D	D	DL	DL	DL
1	DL	DLI	DLI	DLI	LDI	ILD	IL
5	ILD	ILD	IL	IL	IL	IL	IL
10	ILG	IL	IL	IL	IL	I	I
25	ILG	I	I	I	I	I	I
50	IG	I	I	I	I	I	I

Table 10.4 Significance of Different Capture Mechanisms at 5% Contribution Level for Range of Velocities and Drop Diameters encountered in Secondary Dispersion Coalescence (enclosed section describes range of drop diameter and velocity encountered in this study).

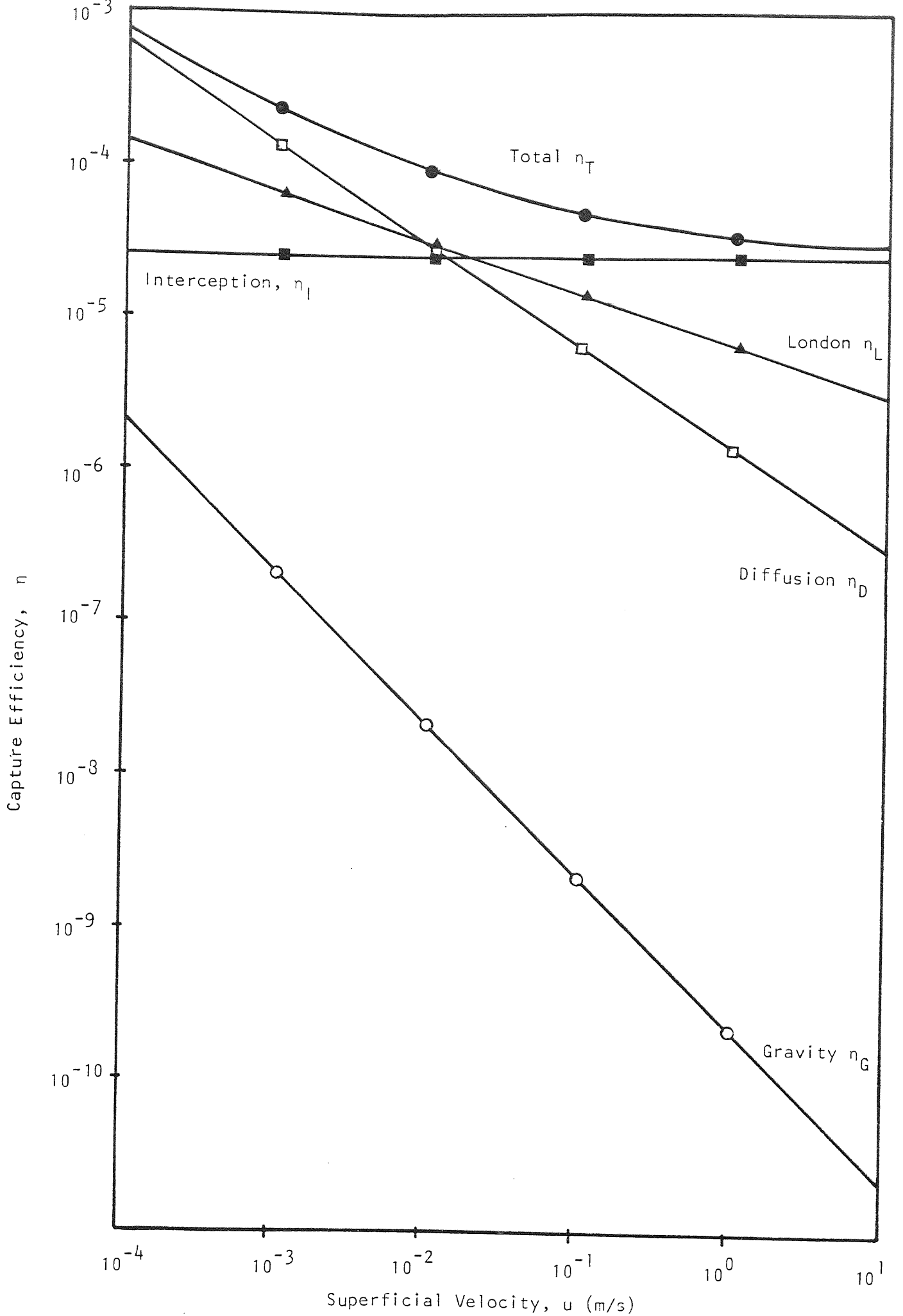


Figure 10.2 Variation of Capture Efficiencies with Velocity at 1 μm.

Selected values of drop size and velocity were taken to illustrate the magnitude of the individual mechanism contributions. Fig. 10.2 indicates that at low velocities, diffusion, London forces and interception predominate whereas, at high velocities, interception is most important. Fig. 10.3 also exhibits a minimum efficiency since diffusion becomes significant for small drops and interception and sedimentation are responsible for the high capture efficiency as the drop size increases.

10.2.1 Screening of Mechanisms

To formulate an expression describing the capture efficiency for the range of variables investigated in this study, the theoretical results were examined further. Firstly, the contribution of diffusion is negligible for drops greater than 1 μm diameter and this mechanism may thus be eliminated. Capture by sedimentation is shown to be significant at low velocities and Fig. 10.3 demonstrates that its contribution increases as the drop size increases, although it remains lower than the contribution by interception and London forces. This mechanism, however, should not be neglected since the coalescence process produces larger drops.

London-Van der Waal's forces are only significant when the overall efficiency is less than 0.025 and for droplets less than 5-10 μm diameter. On Fig. 10.3 it can be seen that London forces contribution to drop capture is higher than that of diffusion and sedimentation and therefore this criteria on its own cannot be used to

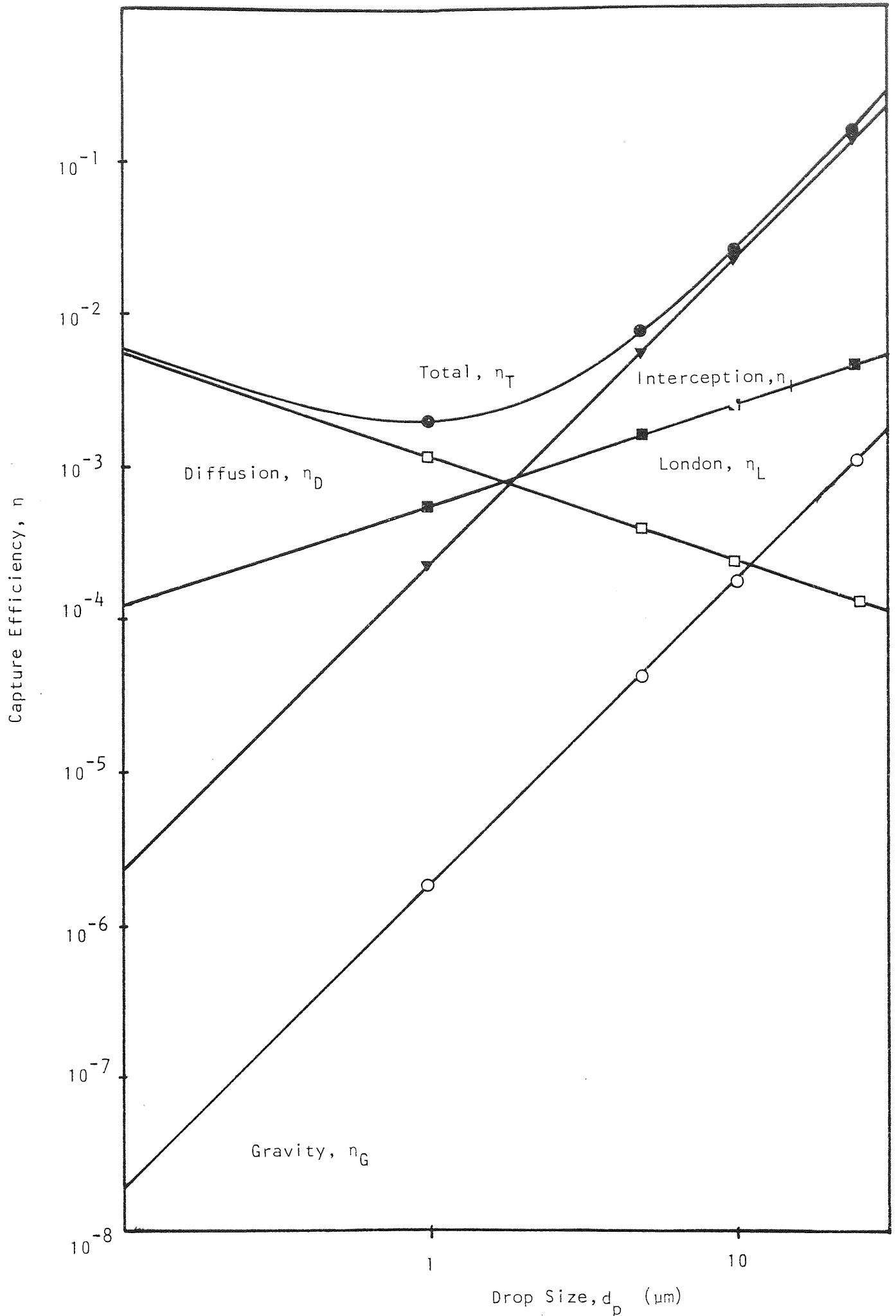


Figure 10.3 Variation of Capture Efficiencies with Drop Size at 0.1×10^{-2} m/s.

neglect the contribution of London forces.

When more than one capture mechanism is important in predicting the total capture efficiency, different formulas have been proposed. For the case of interception and gravity settling, Prieve and Ruckenstein (99) showed that superimposition of the individual contributions of each mechanism was found to yield capture efficiencies sufficiently close to those obtained by rigorous consideration of coupling through trajectory analysis. This implies that the combined effects of sedimentation and interception may be represented by:

$$\eta_{GI} = \eta_G + \eta_I \dots\dots\dots (10.7)$$

Expressions have been derived analytically to account for this particular combination in the context of aerosol filtration where the direction of flow and gravity forces coincide. Emi (214) proposed this equation:

$$\eta_{GI} = \frac{1+R}{1+N_G} \left\{ \frac{1}{2A} \left\{ \frac{1}{(1+R)^2} - 1 + \log_e(1+R) \right\} + N_G \right\} \dots (10.8)$$

where the hydrodynamic function $A = 2 - \log_e N_{Re}$ as proposed by Lamb (78).

Pich (90), who investigated the variation of capture by gravity forces with the angular position of a particle relative to a collector, suggested an alternative form:

$$\eta_{GI} = \eta_I + \eta_G + RN_G \dots\dots\dots (10.9)$$

Sedimentation is predicted to be a significant mechanism for large drop diameters and low velocities, conditions that are outside the range of variables

relevant to this study, and thus the combination of interception and sedimentation as implied in equations 10.7, 10.8 and 10.9 will not be considered.

Spielman and Goren (80) established an equation describing the trajectory of a very small spherical particle in close proximity to a much larger cylindrical or spherical collector subject to hydrodynamic and unretarded London forces. Their equation is intended to describe collection of non-Brownian particles under negligible double layer forces from water. Neglecting the retardation effect, Spielman and Fitzpatrick (98) were able to solve numerically the trajectory equation and calculated the dimensionless filter coefficient as a function of dimensionless Adhesion Group, N_{Ad} , for various dimensionless Gravity Numbers, N_G .

From dimensional considerations, Friedlander (215) studied the case of simultaneous interception and diffusion of both cylindrical and spherical collectors. The efficiency of removal is given by:

$$\eta_{ID}^{RN_{Pe}} = f(A_s^{1/3} R N_{Pe}^{1/3}) \dots \dots \dots (10.10)$$

for particles of diameter which is finite but much smaller than the diameter of the collecting sphere.

Following the procedure of Friedlander (215) Spielman and Goren (80) have also shown that the collection efficiency by simultaneous interception and diffusion is of the form:

$$\eta_{ID}^{RN_{Pe}} = f(N_{Ad}, A_s u_p^3 a_c^2) \dots \dots \dots (10.11)$$

if retardation is neglected. After substitution of

$\mathcal{D} = k'T/6\pi\mu_c a_p$ one can write:

$$\frac{A_S u a_p^3}{\mathcal{D} a_c^2} = \frac{6\pi\mu_c u A_S a_p^4}{k'T a_c^2} = \frac{2}{3} \frac{Q}{k'T} \frac{1}{N_{Ad}} \dots \dots \dots (10.12)$$

and $A_S R^3 N_{Pe} = A_S \frac{a_p^3}{a_c^3} \left(\frac{2a_c u}{\mathcal{D}} \right) = \frac{4}{3} \frac{Q}{k'T} \frac{1}{N_{Ad}} \dots \dots \dots (10.13)$

Equations 10.11 and 10.12 give the following expression:

$$\eta_{ID} R N_{Pe} = F(N_{Ad}, k'T/Q) \dots \dots \dots (10.14)$$

The relation in equation 10.14 is important because the group $(k'T/Q)$ is very nearly constant in most experimental studies so $(\eta_{ID} R N_{Pe})$ should depend on N_{Ad} alone, even when diffusion is significant.

The dimensionless collection efficiency is then

$$\frac{\eta_{ID}}{\eta_I} = \frac{\eta_{ID}}{1.5R^2 A_S} = \frac{\eta_{ID} R N_{Pe}}{1.5 A_S R^3 N_{Pe}} = \frac{F(N_{Ad}, k'T/Q)}{2(Q/k'T) N_{Ad}^{-1}} = G(N_{Ad}, k'T/Q) \dots \dots \dots (10.15)$$

Equation 10.15 suggests a useful method for correlating experimental data by plotting η_{ID}/η_I vs. N_{Ad} at various values of dimensionless $k'T/Q$. If the collection efficiency by London attraction and diffusion can be approximated by the sum of their respective efficiencies, then:

$$\frac{\eta_{LD}}{1.5R^2 A_S} \equiv \frac{\eta_L}{1.5R^2 A_S} + \frac{\eta_D}{1.5R^2 A_S}$$

or $\frac{\eta_{LD}}{\eta_I} = f(N_{Ad}) + 2.22 N_{Ad}^{2/3} \left(\frac{k'T}{Q} \right)^{2/3} \dots \dots \dots (10.16)$

where $\eta_D = 4.04A_S^{1/3}N_{Pe}^{-2/3}$ is the diffusion efficiency and $f(N_{Ad})$ is a universal function of the Adhesion Group N_{Ad} which has been solved numerically by Spielman and Fitzpatrick (98).

Similarly, the theoretical collection efficiency for interception, London and diffusion is approximated by their sum:

$$\frac{\eta_{ILD}}{1.5A_S R^2} \cong \frac{\eta_I}{1.5A_S R^2} + \frac{\eta_L}{1.5R^2 A_S} + \frac{\eta_D}{1.5R^2 A_S}$$

$$\frac{\eta_{ILD}}{\eta_I} = 1 + f_1(N_{Ad}) + 2.22 N_{Ad}^{2/3} \left(\frac{k'T}{Q}\right)^{2/3} \dots (10.17)$$

when $\frac{k'T}{Q} = 0$, the capture efficiency is due to interception and London forces alone or pure interception if the London forces are not being considered.

The different values for equation 10.17 obtained from Spielman and Fitzpatrick's (98) solution are presented in Table 10.5, for $\frac{k'T}{Q}$ calculated at 293°K and the Hamaker constant, Q , as $0.401 \times 10^{-20} \text{J}$ calculated in Appendix C. The results are plotted as $\frac{\eta_{ILD}}{\eta_I}$ vs. N_{Ad} for $\frac{k'T}{Q} = 1.01$ and $\frac{k'T}{Q} = 0$ in Fig. 10.4. The results obtained for the total filter coefficient, η_T , using equation 10.6 were plotted as η_T/η_I vs. N_{Ad} on this figure, and they show close agreement with the curve obtained using Spielman and Fitzpatrick (98) correlation.

For 25 μm inlet drop diameter and $0.1 \times 10^{-2} \text{ m/s}$ velocity and using equation 10.17 and Spielman and Fitzpatrick (98) solution:

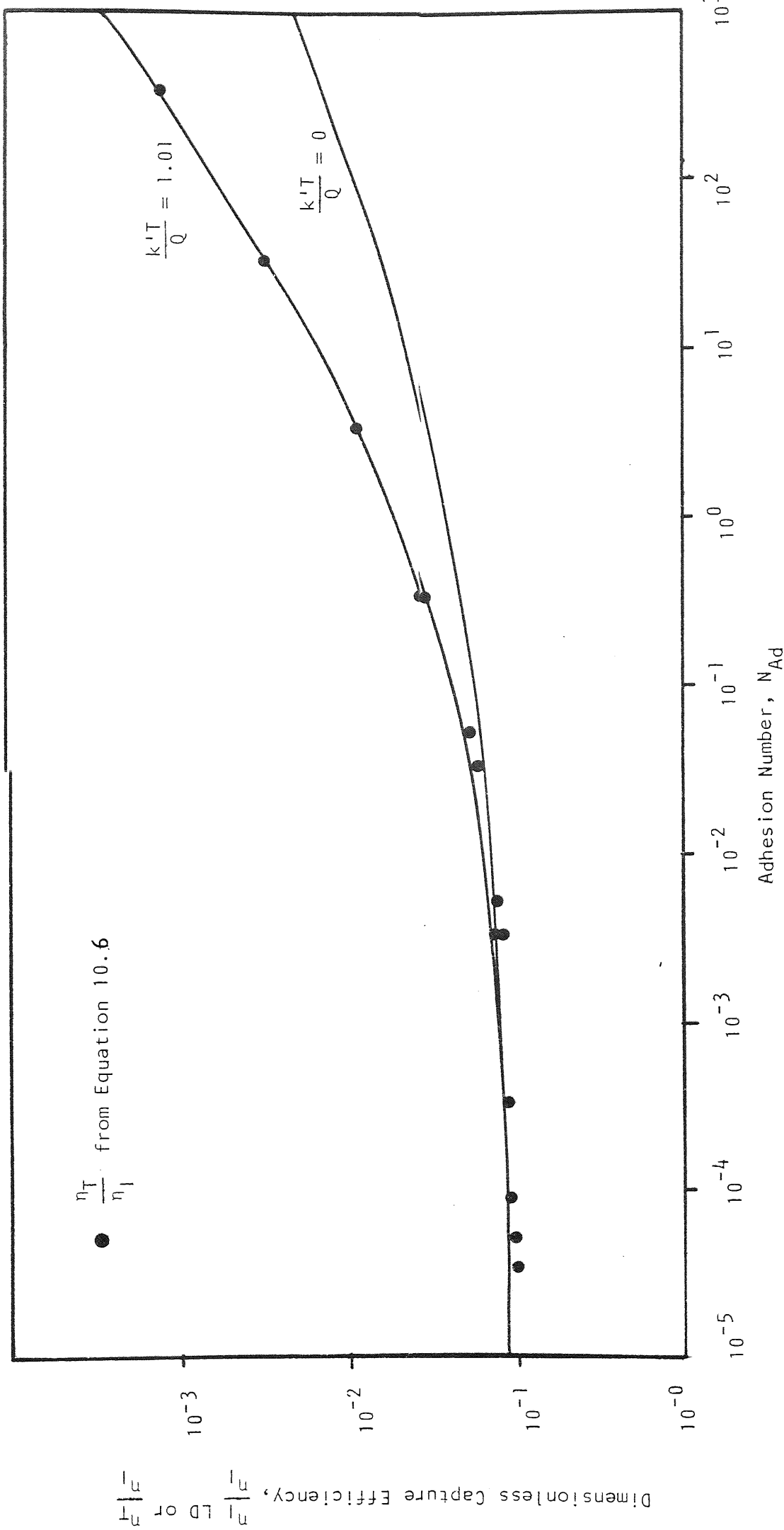


Figure 10.4 Dimensionless Capture Efficiency Vs. Adhesion Number at Different $k'T/Q$ According to Spielman and Fitzpatrick.

$$\frac{\eta_{ILD}}{\eta_I} = 1.120$$

from equation 10.6 $\frac{\eta_T}{\eta_I} = 1.042$

This gives a 7% difference between both methods of calculating the drop capture efficiency and therefore either one could be used to predict the drop capture efficiency.

10.3 RATE OF DROP CAPTURE

Theories of particle capture by assemblages focus on collection by a representative element within the array. For a bed of uniform spherical grains perpendicular to the mean flow, a suspended particle balance over a differential depth of bed dl and containing many grains gives for the differential change dn in suspended particle number concentration:

$$-u \frac{dn}{dl} = j \left(\frac{\alpha}{\frac{4}{3}\pi a_c^3} \right) \dots\dots\dots (10.18)$$

where α is the volume fraction of solids and j is the average rate of particle capture per spherical collector.

For any capture mechanism, the relationship between the dimensionless filter coefficient and dimensionless efficiency is obtained by equating the difference in particle concentration entering and leaving the bed.

Defining the filter coefficient λ by:

$$- \frac{dn}{dl} = \lambda n \dots\dots\dots (10.19)$$

and the dimensionless grain collection efficiency as:

$$\eta = \frac{j}{\pi a_c^2 u_n} \dots\dots\dots (10.20)$$

the relationship between λ and η is then obtained by substituting equations 10.19 and 10.20 into 10.18 as:

$$\lambda = \frac{3}{4} \frac{\alpha}{a_c} \eta \dots\dots\dots (10.21)$$

Integration of equation 10.19 over a depth of bed $0 \rightarrow L$ gives equation 10.1, or

$$\lambda = \frac{-\log_e \left\{ \frac{n_1}{n_0} \right\}}{L}$$

where n_0 and n_1 are the inlet and outlet drop density numbers entering and leaving a depth of bed L . Substituting and rearranging for n_1 in equation 10.21 we obtain:

$$n_1 = n_0 e^{\left(-\frac{3}{4} \frac{\alpha}{a_c} \eta L \right)} \dots\dots\dots (10.22)$$

The inlet drop size distribution curve (Fig. 7.1) was fitted to a distribution function by polynomial regression and the resulting expression employed to calculate the number of drops in each drop diameter interval (2 μ m). The total capture rate, η_T for a given superficial velocity was calculated by application of equations 10.6 or 10.17 as explained in Section 10.2 to each size interval. For a given bed depth, l , between $0 \rightarrow L$ the number of drops, n_1 , leaving the bed interval was obtained by using equation 10.22. Assuming no drop redispersion, n_1 is used as the input of suspended drops to the next interval of bed depth l_2 and a new value of n_1 was obtained.

This calculation procedure was repeated, for a 20×10^{-2} m bed depth using a microcomputer, for superficial velocities 0.1×10^{-2} -10 m/s. The flowsheet for the program and one set of results are presented in Appendix G. A graph, presented on Fig. 10.5 was plotted from the program output, which shows the removal rate of suspended drops as a function of bed depth. Increasing the value of velocity decreases the rate of drop capture but to a minimum after which, any further increase in velocity no longer will imply a decrease in drop capture. As discussed in Section 10.2, at high velocities, interception is the predominant capture mechanism and independent from velocity. Therefore there is a minimum capture efficiency and thus a minimum rate of drop removal. The shape of this profile exhibits a marked resemblance to the experimental data of Spielman and Su (72) obtained under steady state conditions (Fig. 10.7).

The theoretical results were determined for the operation of the coalescer after a period of one second from an initially clean bed and dispersed phase free condition. Due to rapid accumulation of the dispersed phase, this analysis cannot be applied to a coalescer which has been operating even for a few seconds. This is due to held drops effectively reducing the aperture of the interstices, so that capture by direct interception, which does not feature in equations 10.6 or 10.17, increases rapidly as the local saturation increases.

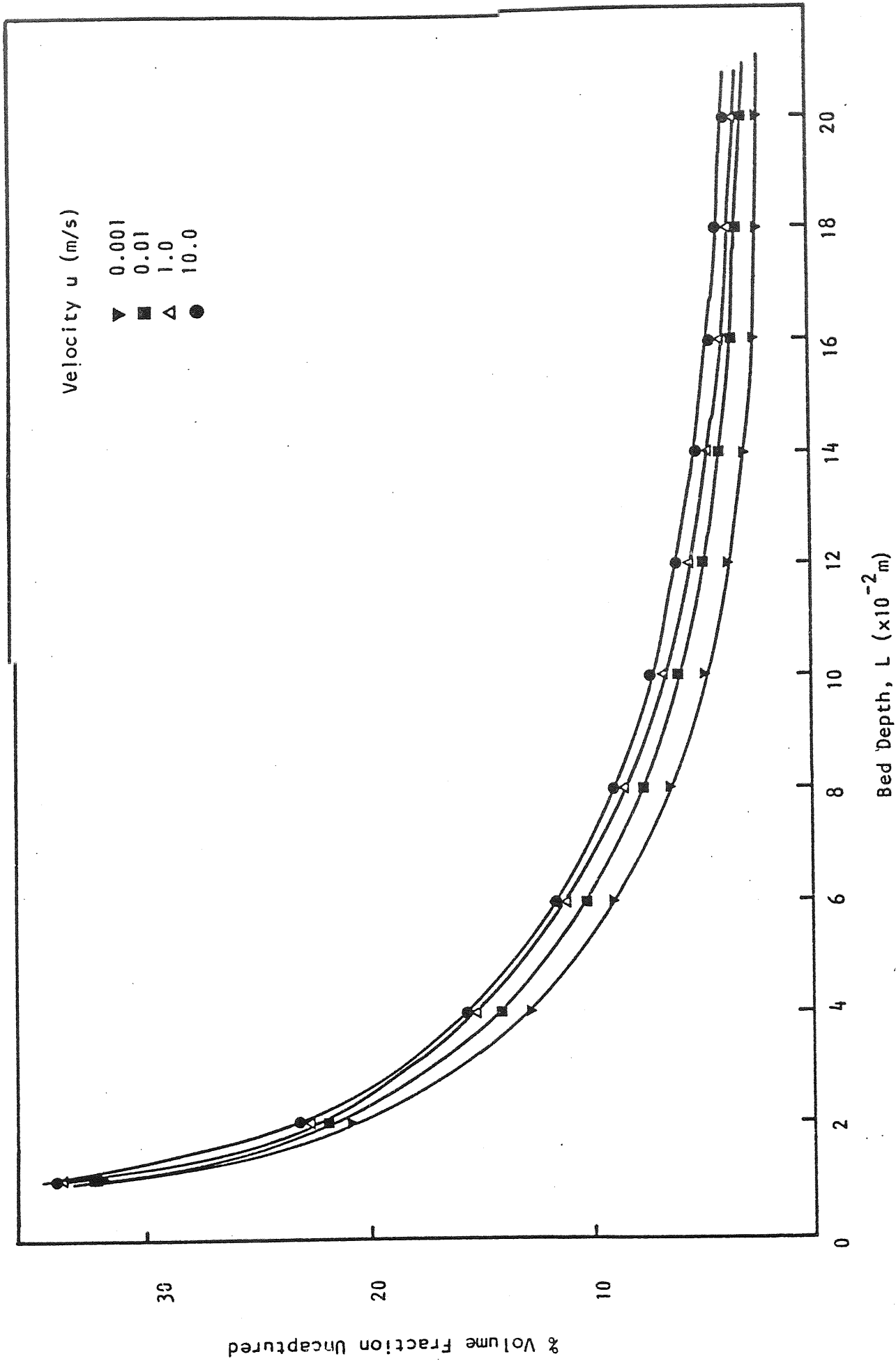


Figure 10.5 Effect of Superficial Velocity on the Variation of Volume Fraction of Dispersed Phase Uncaptured with Bed Depth.

However, this theoretical approach is useful because since the drop capture rate depends on local saturation, after steady state operation has been reached and the drop capture profile developed, it would not be expected to change significantly.

10.4 PHASE SATURATION PREDICTION

10.4.1 Preliminary Consideration

When liquid-liquid dispersions such as the oil/water suspension used in this study are passed through a porous solid, suspended droplets are convected to the solid backing and entrapped at liquid interfaces where they are captured. Oil captured at interfaces exists distinct from capillary-conducted oil until its eventual coalescence into that regime. Spielman and Su (72), after experimental observations of the coalescence process, suggested that three predominantly discernible interstitial regimes of the (coalescing) oil exists simultaneously within the voids. One oil regime is very finely dispersed within a capillary-conducted aqueous phase and consists of droplets considerably smaller than the pores. The second oil-regime is the captured but non capillary-conducted and is maintained by the steady deposition of the finely dispersed oil at solid-liquid and liquid-liquid interfaces. This non-equilibrium oil can be either an agglomeration of uncoalesced droplets or a large coalesced oil globule which fails to form channels to flow. The other regime is capillary-conducted (or equilibrium oil regime) and is maintained by the coalescence of non-equilibrium oil.

At steady state the equilibrium oil drains through the solid matrix under the action of hydrodynamic and surface tension forces; and the deposition rate of finely dispersed droplets into the non-equilibrium regime is equal to the rate at which the non-equilibrium oil coalesces into equilibrium oil. In other words, at steady state the volume flow rate of oil leaving the bed through the capillary-conducted oil regime is equal to the volume rate at which oil is captured from the aqueous suspended regime.

From the preceding discussion, the total oil saturation at any point in a coalescing bed is:

$$S = S''' + S'' + S' \dots\dots\dots (10.23)$$

The relative proportions of these regimes are indicated qualitatively in Fig. 10.6. It was further assumed that the fraction of newly captured drops is negligible, i.e. $S''' \rightarrow 0$ but if the sizes of these source drops are comparable to the pore sizes of the packing then S''' would be expected to increase at the expense of S'' , that is, only a few coalescences have to occur before the diameter of the drop exceeds the pore size, and eventually the drop will be forced into a channel when the continuous phase pressure gradient exceeds the restraining interfacial tension forces.

To evaluate the performance of a coalescer in terms of filter coefficient and pressure drop, it is necessary to combine knowledge of the nature and relative amounts of the local dispersed phase regime with information

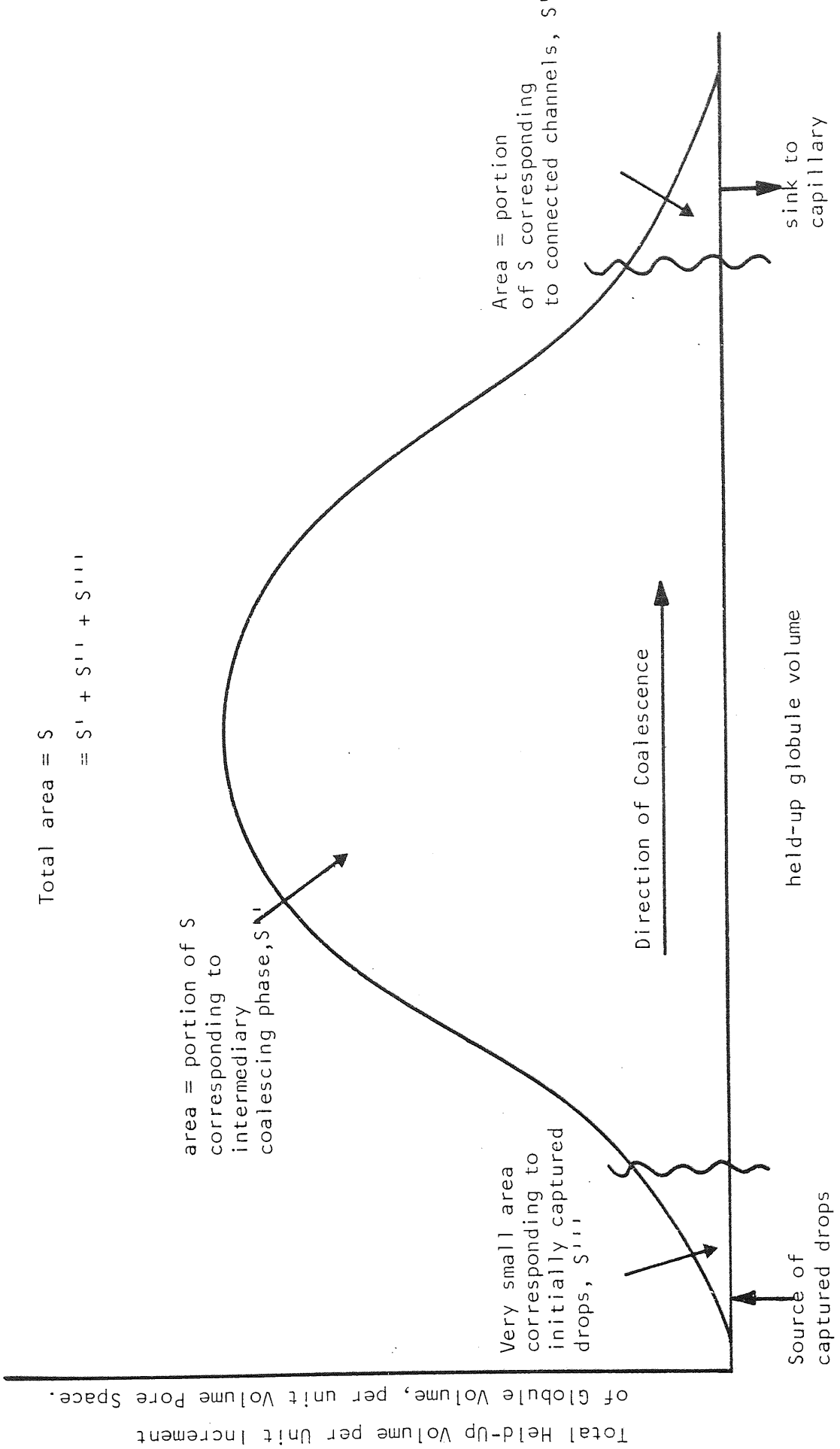


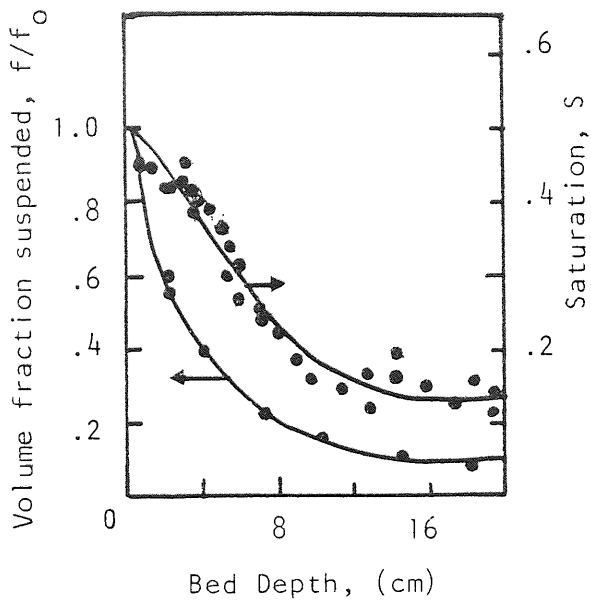
Figure 10.6

Qualitative distribution of the total volume of held-up oil over individual held-up globule volumes. Drops are captured at the left hand of the spectrum. Dispersed phase is transferred to successively larger drops by coalescence eventually leaving the capillary conduction at the right.

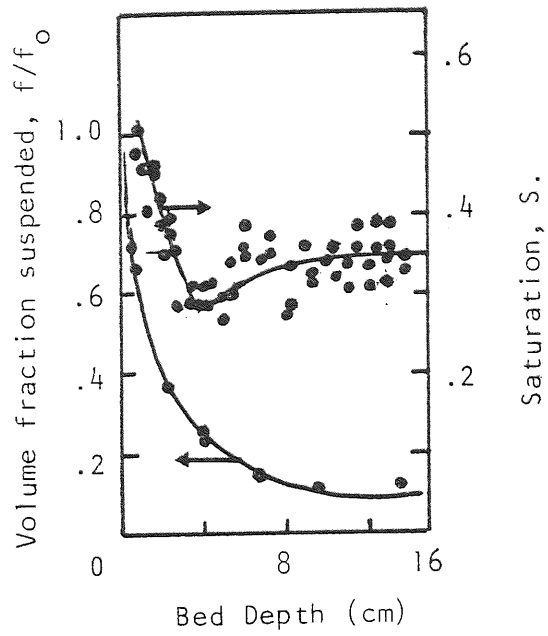
concerning the spatial variation of the total dispersed phase saturation. The existence of saturation profiles has been discussed in Chapter 5 and typical data from a number of studies is presented in Figs. 10.7, 10.8 and 10.9.

Despite the differences between absolute values of local saturation, attributable to different operating parameters of the system and packing media, the shapes of the profiles exhibit several common factors. There is a maximum value of the saturation at the inlet face which appears to have a constant value, independent of superficial velocity, as the bed depth, $l \rightarrow 0$. Secondly, the local saturation decays, with bed depth at a rate which depends on velocity, to a minimum value that remains constant as far as the exit face. The minimum value is also shown experimentally to be a function of velocity. The profiles found by Shalhoub (13) and Bitten (108) indicate a slight increase in local saturation just upstream of the exit face for which no explanation was given.

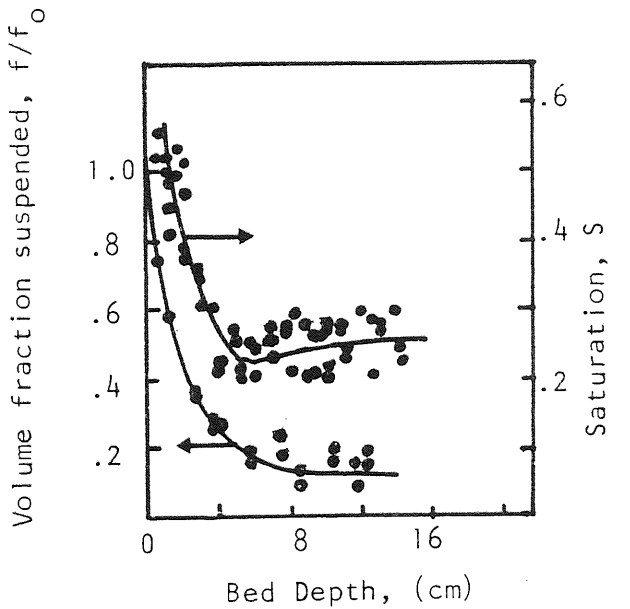
In this experimental study, it was not possible to measure the saturation profile without interfering with the coalescence process, but as presented in Section 9.7.2, by using pressure drop measurements across the bed and relative permeability correlations, the saturation profiles for the system were obtained. These profiles are in excellent agreement with those of previous workers.



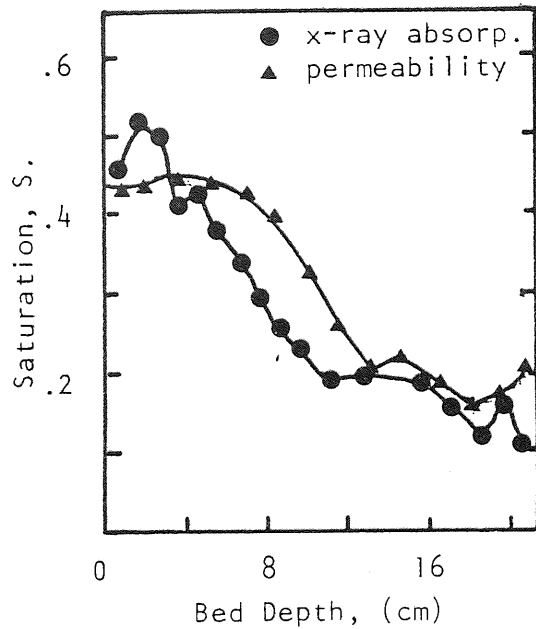
$d_c = 0.5\text{mm}, \mu_d = 50 \text{ cP}$
 $u = 0.3 \text{ cm/s}, f_0 = 2 \times 10^{-4}$



$d_c = 0.36 \text{ mm}, \mu_d = 500 \text{ cP}$
 $u = 0.3 \text{ cm/s}, f_0 = 8 \times 10^{-4}$

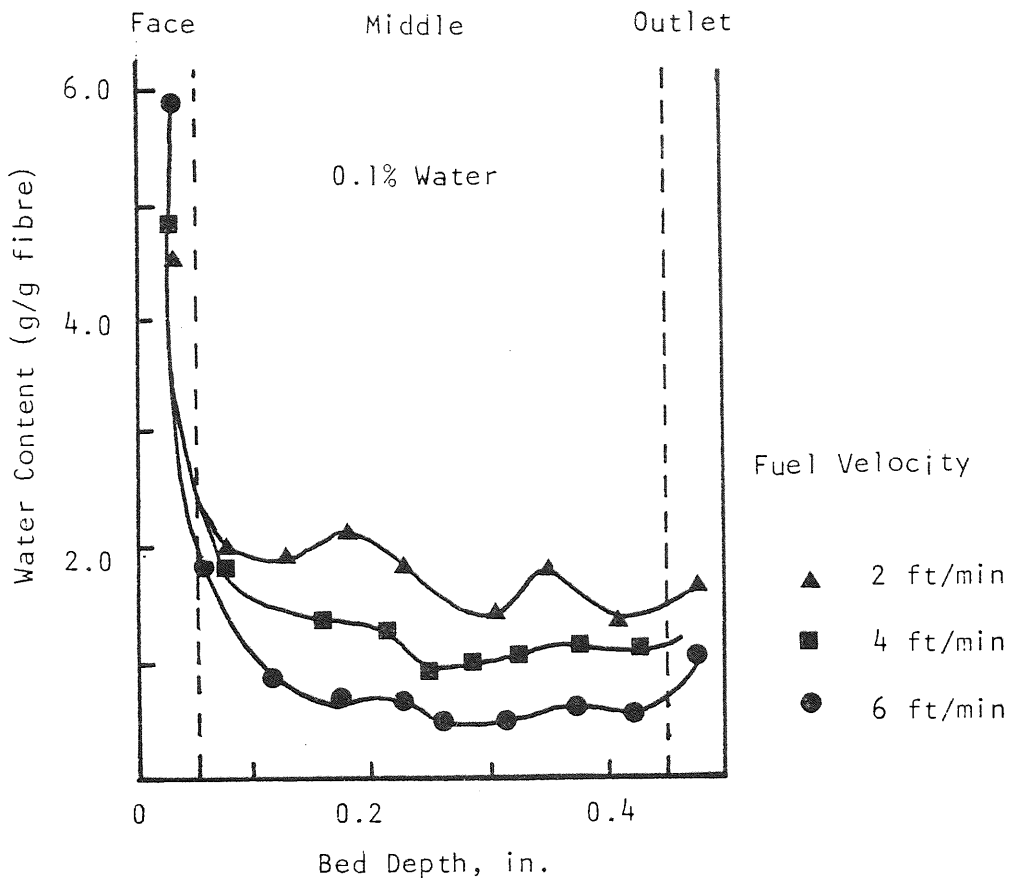


$d_c = 0.36, \mu_d = 500 \text{ cP}$
 $u = 0.3 \text{ cm/s}, f_0 = 2. \times 10^{-4}$

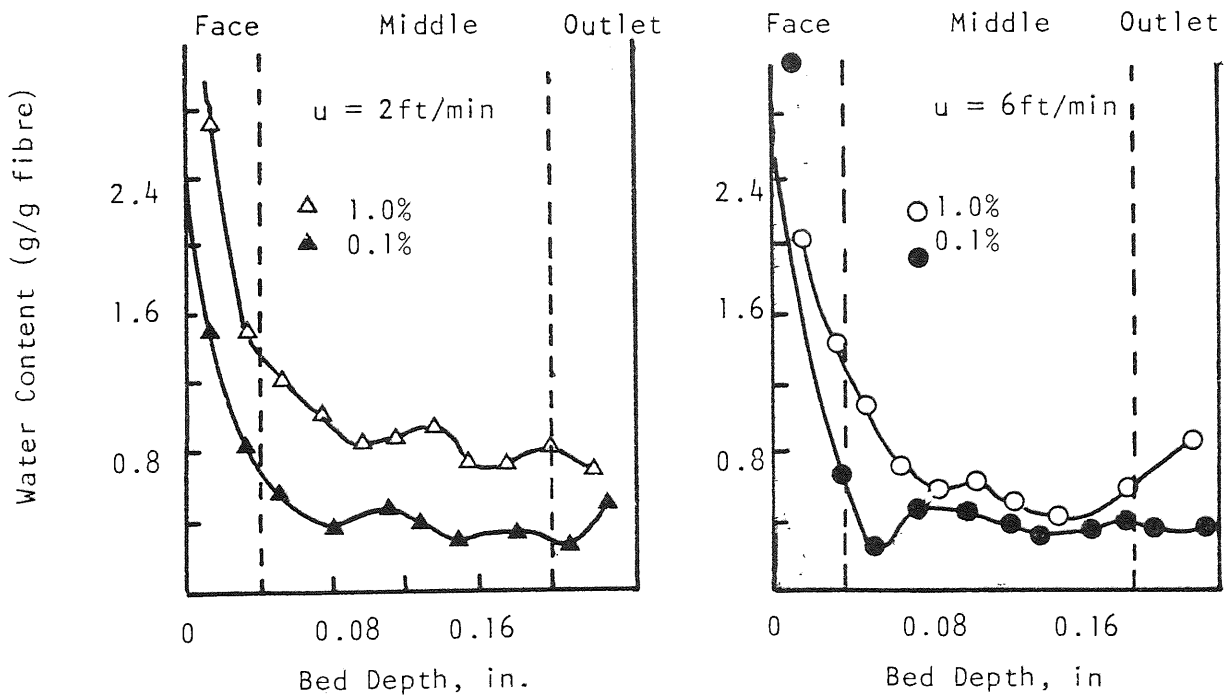


$d_c = 0.36 \text{ mm}, \mu_d = 50 \text{ cP}$
 $u = 0.6 \text{ cm/s}, f_0 = 2 \times 10^{-4}$

Figure 10.7 Variation of Volume Fraction of Suspended Drops and Dispersed Phase Saturation with Bed Depth.
 (Data of Spielman and Su)



(a) $\frac{1}{2}$ inch thick fibreglass coalscrer (6 lb/ft³).



(b) $\frac{1}{2}$ inch thick fibreglass coalscrer (14 lb/ft³)

Figure 10.8 Variation of Hold-Up with Bed Depth.
(Data of Bitten and Fochtman).

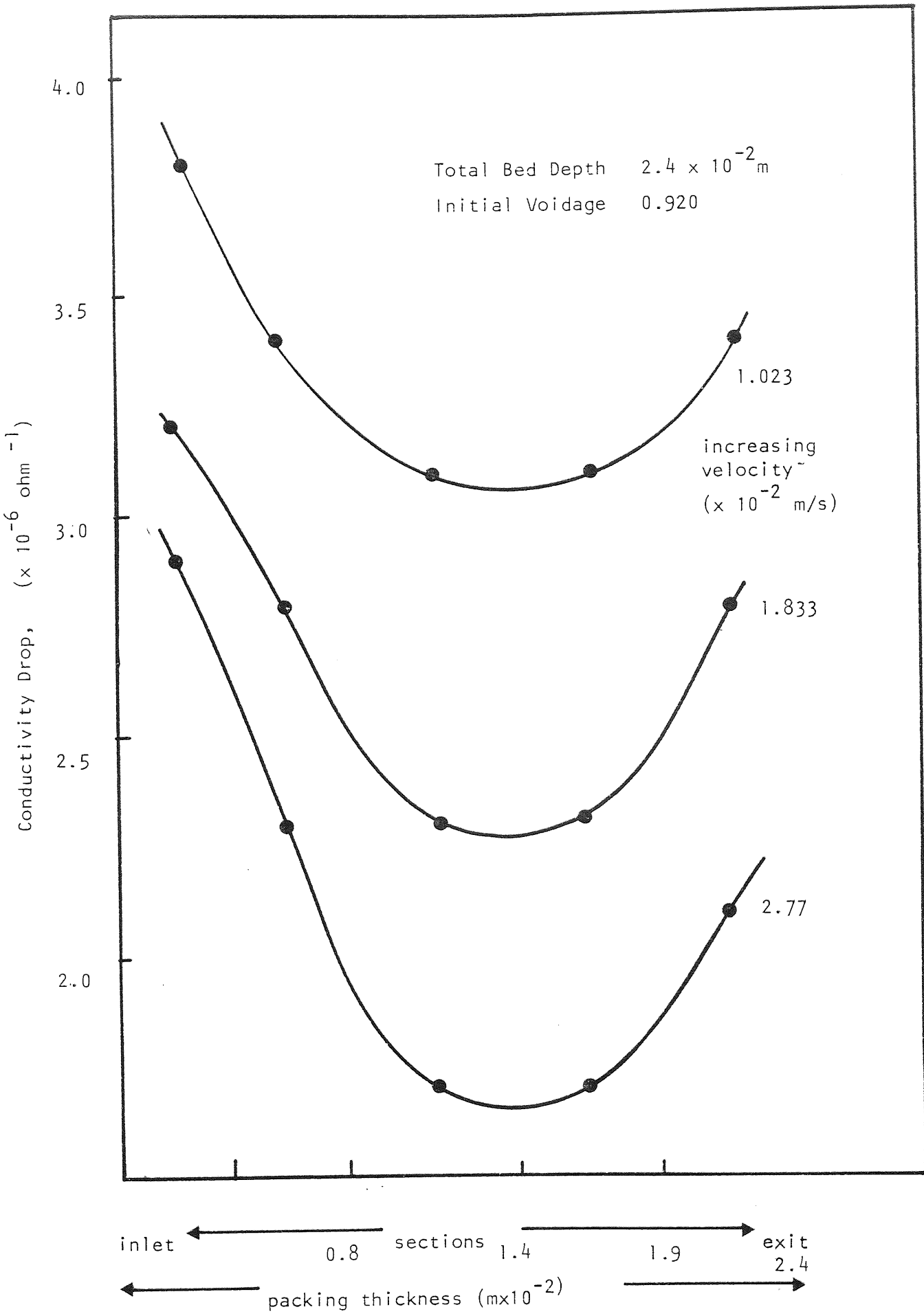


Figure 10.9 Variation of Hold-Up with Superficial Velocity
(Data of Shalhoub)

10.4.2 Mathematical Description of Saturation Profiles

Based on the general trends shown by experimental data, Austin (14) proposed an idealised saturation profile, illustrated in Fig. 10.10. Since the saturation at the inlet face cannot be infinite, a small length, L_I where the saturation has a constant value, S_I , was proposed. S_I was assumed to be independent of velocity. Thereafter, the saturation decays exponentially at a rate characterised by the value of k which is a function of velocity. The decrease continues until a final value of saturation, S_E is attained which is also dependent on velocity.

$$\text{i.e. } S = S_I \quad 0 < \ell \leq L_I$$

$$S = (S_I - S_E)e^{-k(\ell - L_I)} + S_E \quad L_I \leq \ell \leq L \dots \dots (10.24)$$

This expression was fitted to the saturation profiles of this study to find the value of k by regression analysis according to Appendix H. The value of S_E was taken as the lowest value of the saturation before the slight increase in local saturation at the bed exit.

On Figs. 10.11, 10.12, 10.13, 10.14 some of the experimental and predicted saturation profiles are presented. As it can be seen the model can be used to mathematically represent the system, the only drawback being that the inlet saturation, S_I , predicted is always higher than the experimental values obtained. In some cases the predicted saturation is above 80% and as it was proposed in Section 9.7.2, from the relative permeability calculations, the dispersed phase saturation cannot be

higher than 80% due to the presence of irreducible water saturation. To determine the maximum irreducible water saturation for the system, capillary pressure measurements must be carried out.

Since the drop capture rate near the inlet face is high and the inlet drop size distribution is polydispersed, a saturation equivalent to the void fraction of the bed of mixed spheres would be expected. Bear (217) states that typical values of void fraction for this type of media is approximately 0.17 which corresponds to a saturation of 0.83. This is again above the maximum 80% saturation predicted by relative permeability. Brown (118) gives a correlation between void fraction and the diameter ratio, $\frac{d_p}{d_a}$ which for a mean drop size 25 μm and a aperture diameter of 99.6 μm , $\frac{d_p}{d_a} = 0.251$ gives $e_p = 0.437$ corresponding to a saturation of 0.56. This value is in close agreement with the data of Spielman and Su (72) and with the values obtained from relative permeability calculations in this study. This value will be used as a reference when predicting values of S_I .

The experimentally determined profiles all indicate that decay of saturation with bed depth occurs very close to the inlet face implying that L_I is very small. However, since the saturation must be zero at the inlet face, in the absence of flooding, a small finite value of L_I must be assumed. For the experimental saturation curves L_I was fixed at 2 cm from the bed inlet but after a value for the rate of decay, k , has been found, L_I can be taken to be as small as the length of a single

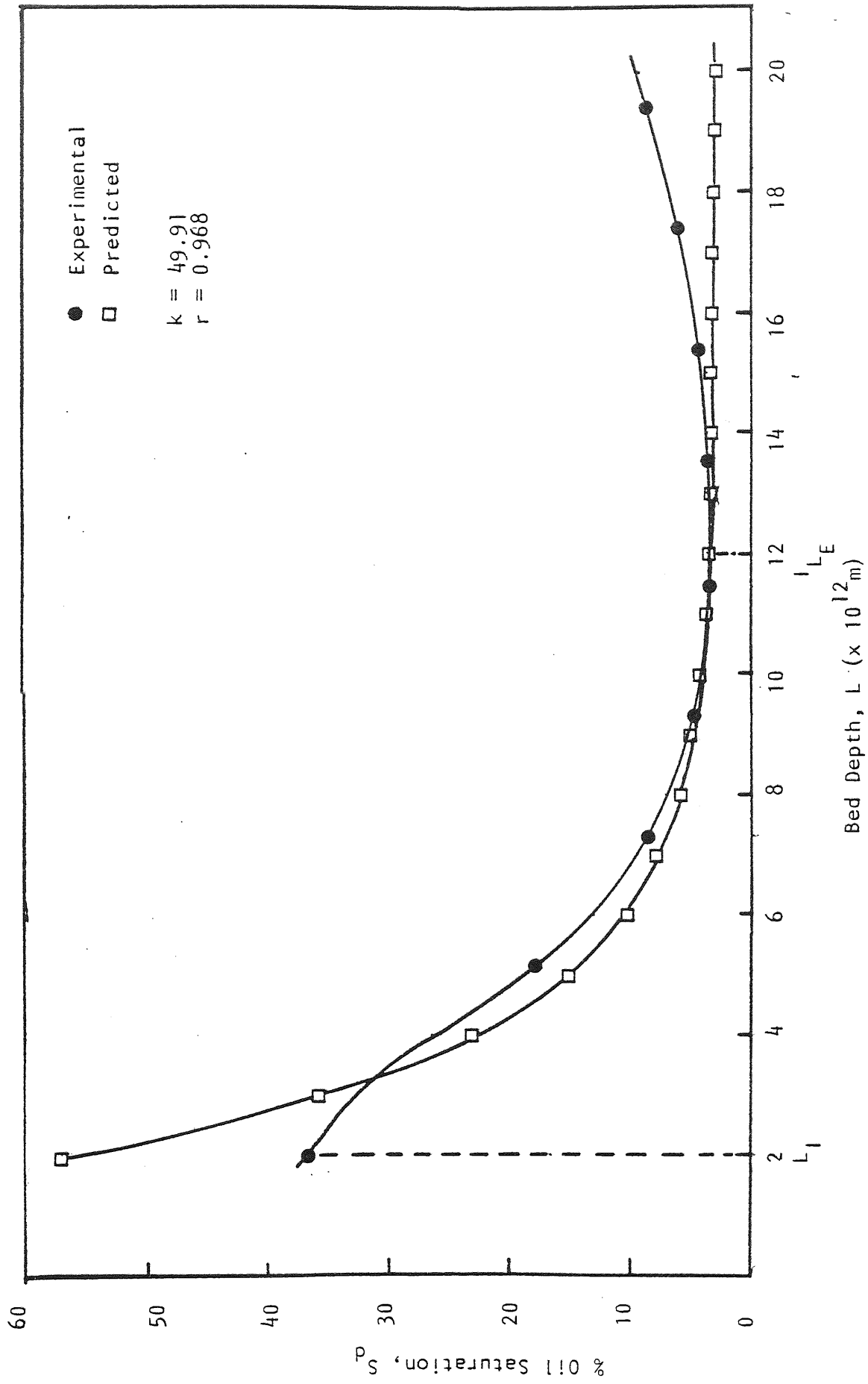


Figure 10.11 Experimental and Predicted Dispersed Phase Saturation Vs Bed Depth for 486 μ m Ballotini 20×10^{-2} m Bed Depth, 0.3×10^{-2} m/s Velocity and 0.2% v/v Dispersed Phase Concentration.

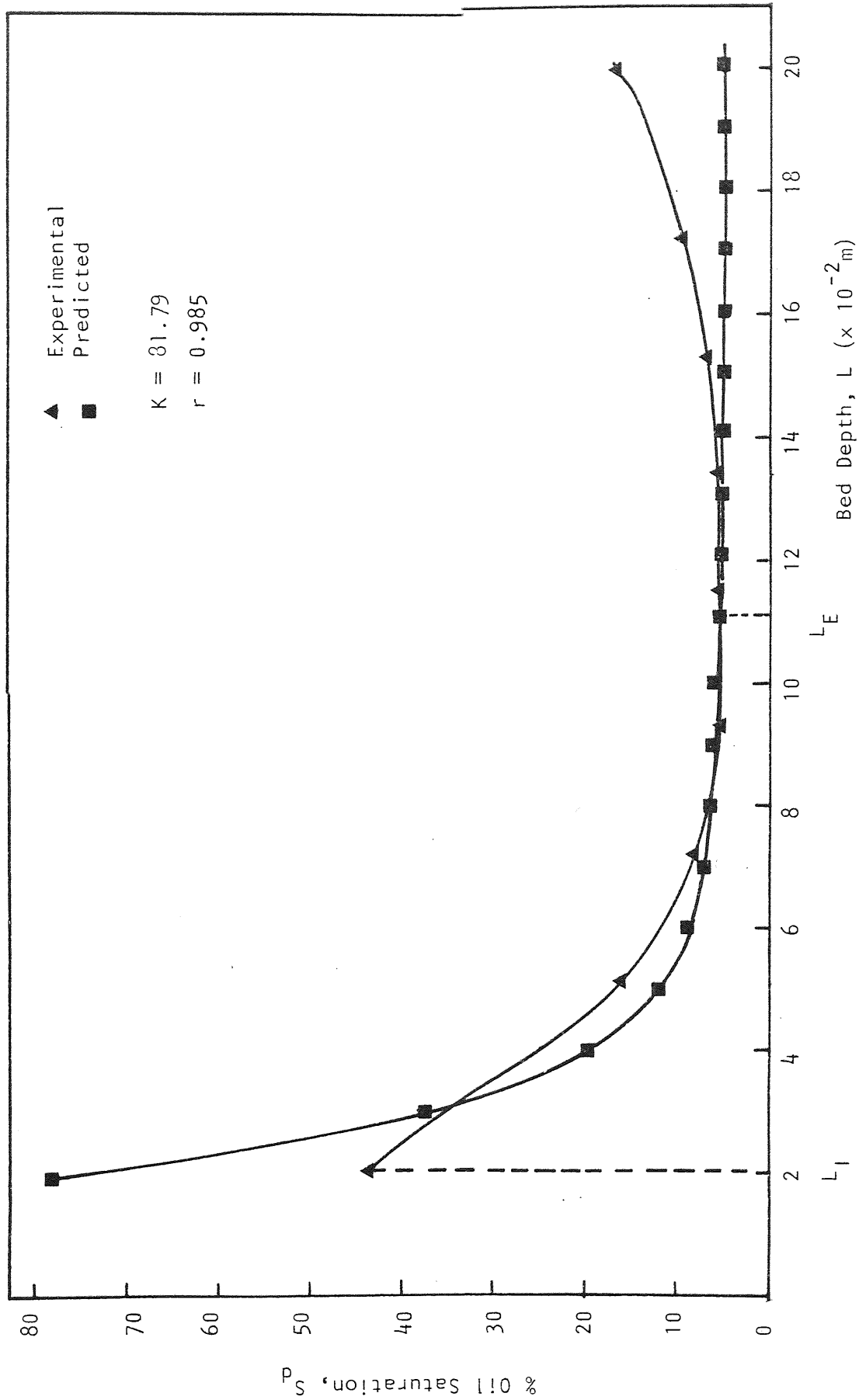


Figure 10.12 Experimental and Predicted Dispersed Phase Saturation Vs Bed Depth for
 486 μm Ballotini 20×10^{-2} m Bed Depth, 0.3×10^{-2} m/s Velocity and 0.4 v/v
 Dispersed Phase Concentration.

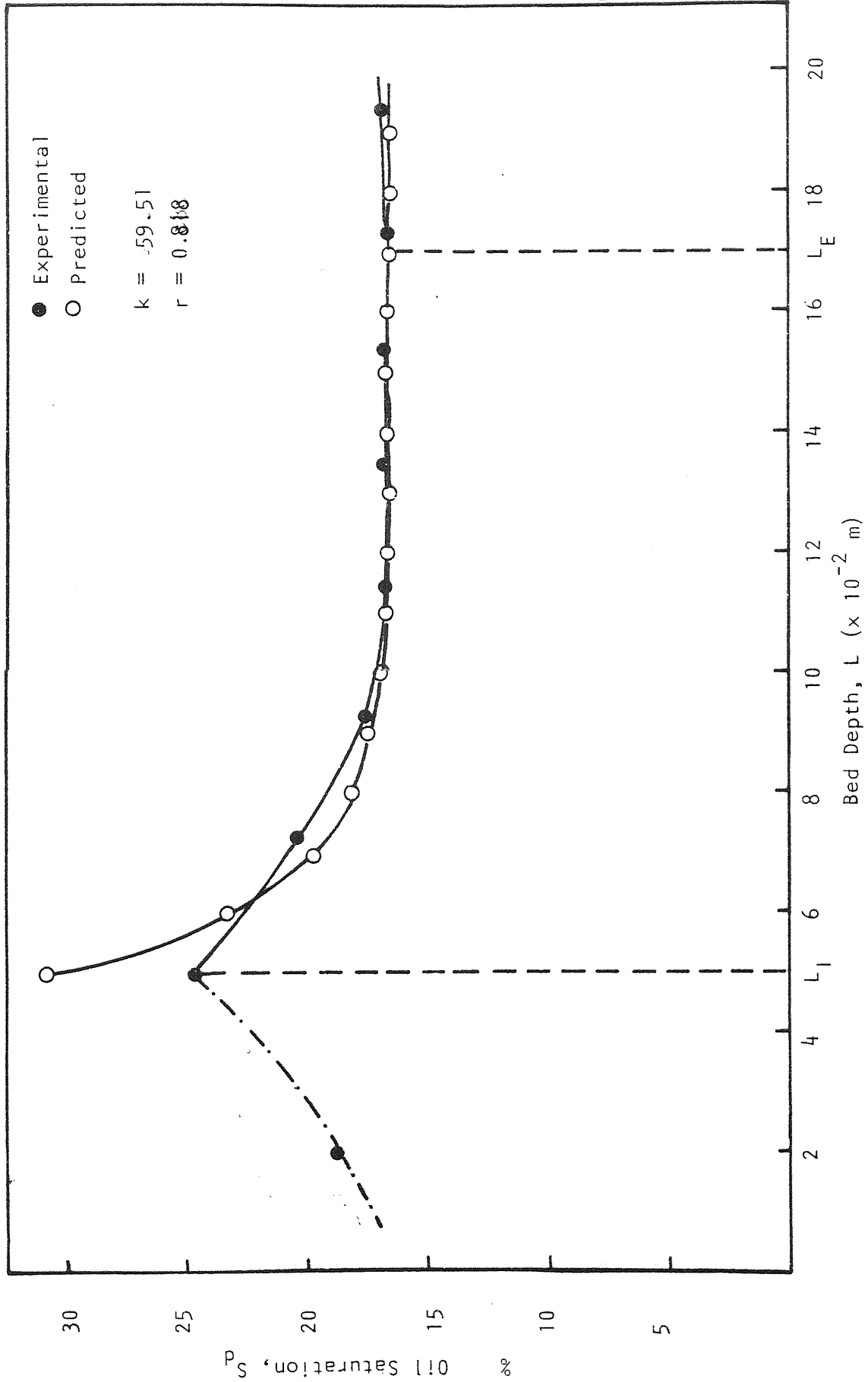


Figure 10.13 Experimental and Predicted Dispersed Phase Saturation Vs Bed Depth for 486 μm Ballotini, 10×10^{-2} Bed Depth, 4.0×10^{-2} m/s Velocity and 0.1% v/v Dispersed Phase Concentration.

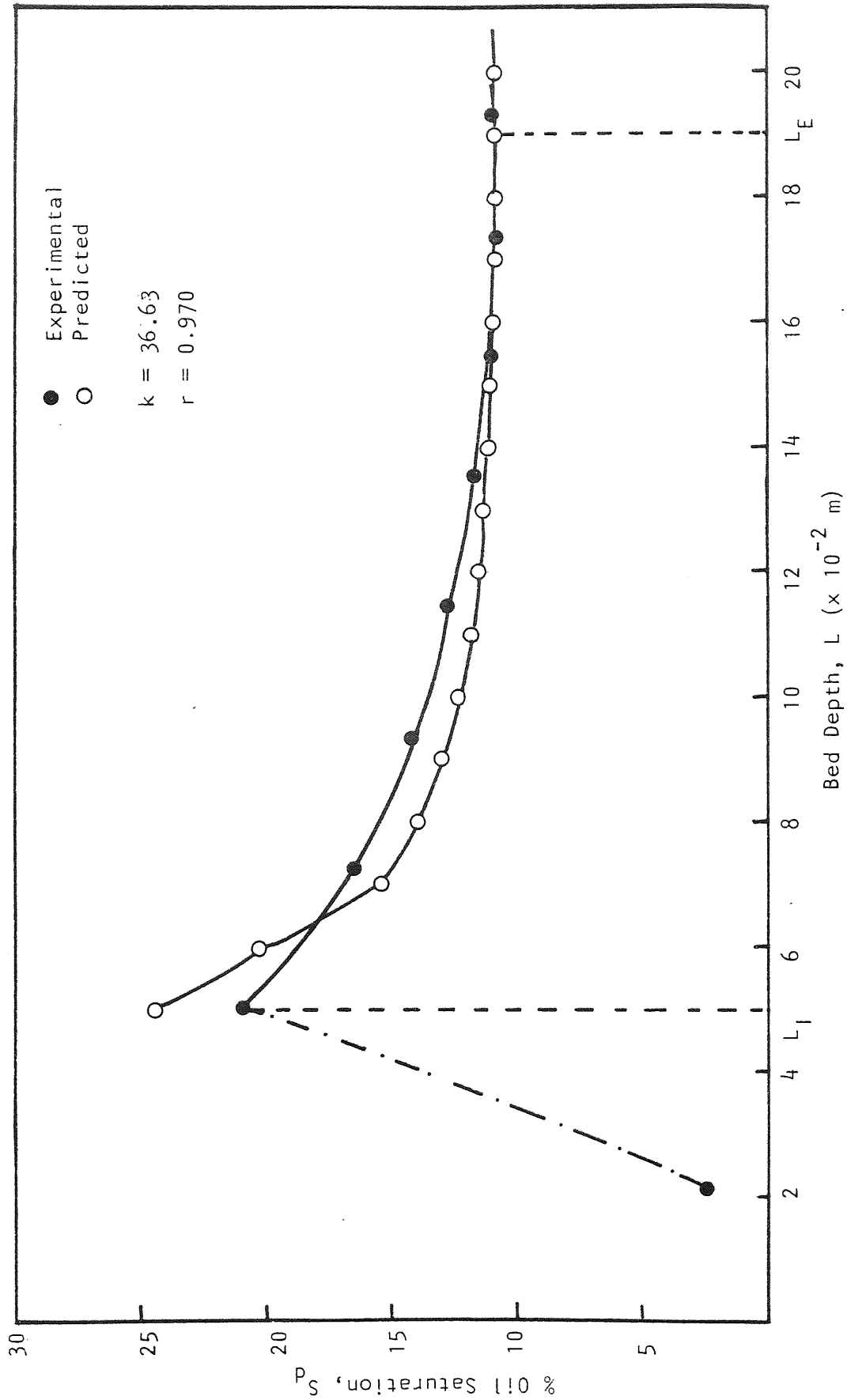


Figure 10.14 Experimental and Predicted Dispersed Phase Saturation Vs Bed Depth for 486 μm , 20×10^{-2} Bed Depth, 5.0×10^{-2} m/s Velocity and 0.1 % v/v Dispersed Phase Concentration.

ballotini layer and assuming the saturation profile is unchanged, a new value of k can be calculated. Although the saturation will increase from 0 to S_I within a very small distance from the inlet face, i.e. $\ll L_I$, omission of this section of the saturation profile from the integration of equation 10.24 will not incur any significant error.

Inspection of equation 10.24 shows that as k increases, then the decay will approximate to a step change in saturation at L_I from S_I to S_E .

In Figs. 10.15 and 10.16, the average value of k obtained has been plotted against superficial velocity for both the low and high velocity experiments. In both cases the value of k decreases with an increase in superficial velocity suggesting that for the two sets of experiments $S_I \rightarrow S_E$ nearer to the inlet of the bed. This may be due to the fact that despite the greater influx of captured drops at higher velocities, the existence of larger hydrodynamic forces causes the drops to progress through the bed more quickly. This factor was not taken into account when the model was formulated.

On Fig. 10.17 the effect of dispersed phase concentration is presented. As it can be seen, the decay factor increases with increasing concentration. This is due to an increased drop capture at the forepart of the bed produced by a higher number of drops in the dispersion which accumulate in the voids making it more difficult for incoming drops to pass through and therefore aiding further capture. This produces a much higher saturation at the inlet of the bed than downstream of the bed, which

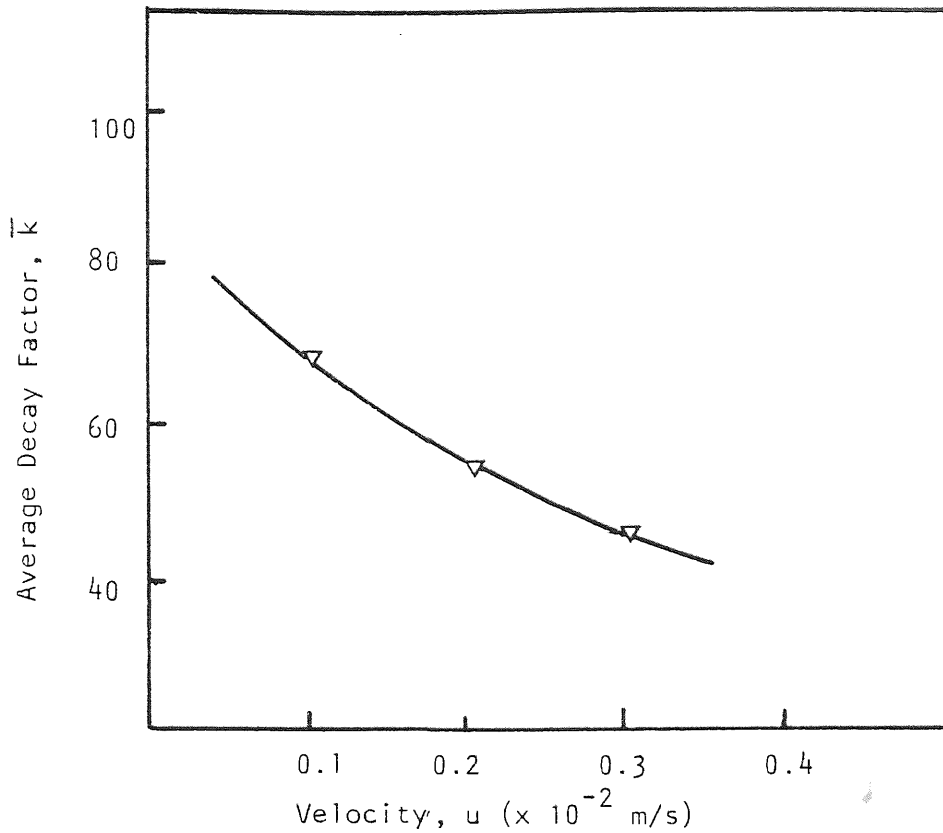


Figure 10.15 Average Decay Factor Vs Low Velocity Range. Ballotini 486 μm , 20×10^{-2} m Bed Depth, 0.1 % v/v Dispersed Phase.

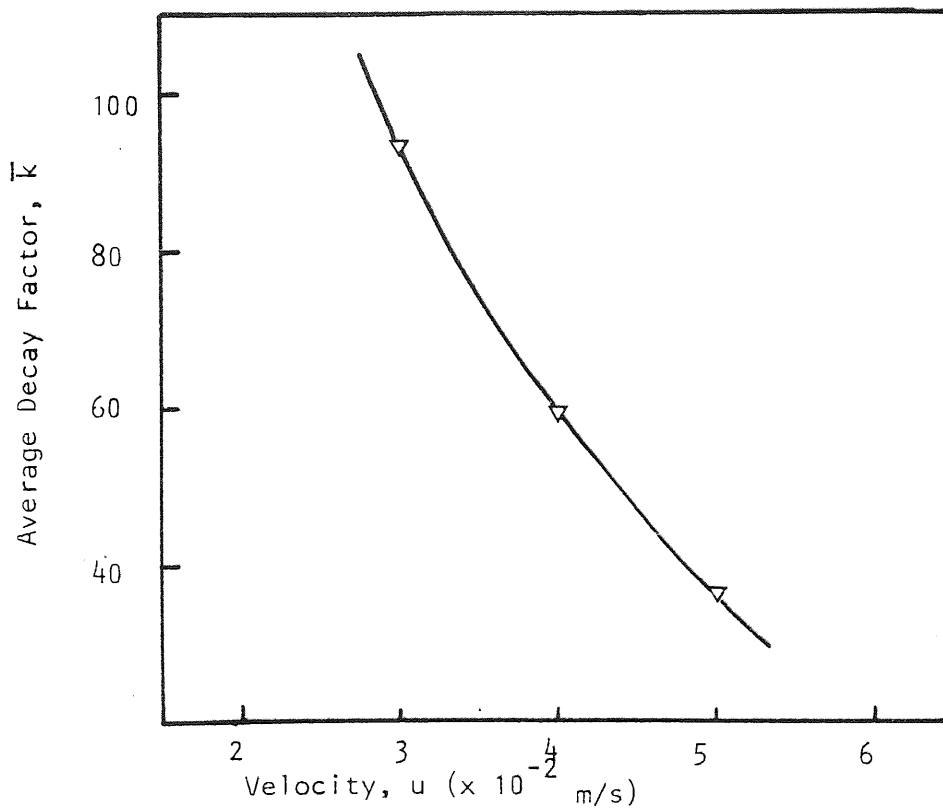


Figure 10.16 Average Decay Factor Vs High Velocity Range. Ballotini 486 μm , 20×10^{-2} m Bed Depth, 0.1 % v/v Dispersed Phase.

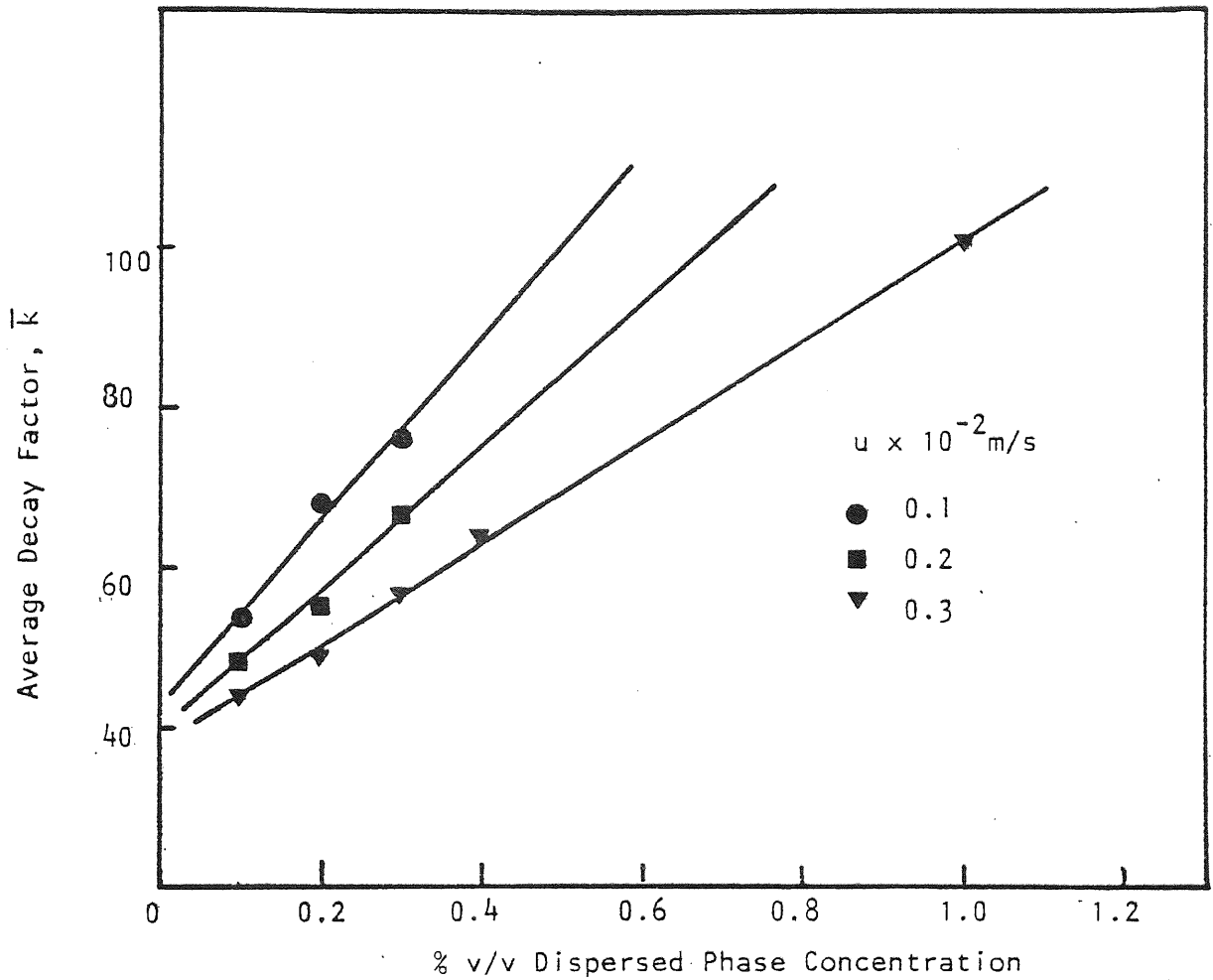


Figure 10.17 Average Decay Factor Vs Dispersed Phase Concentration for Different Superficial Velocities.

may be equivalent to a step change between S_I and S_E . Also the rate of increase of k with increasing dispersing phase concentration is higher with decreasing superficial velocity. This produced a set of curves for the velocity range $0.1-0.3 \times 10^{-2}$ m/s. For the higher superficial velocity range, $3-5 \times 10^{-2}$ m/s, there is little change in the saturation profiles, which suggests that k remains nearly constant with increasing dispersed phase concentration for a fixed value of superficial velocity.

10.5 TWO PHASE PRESSURE DROP PREDICTION

10.5.1 Previous Models

The prediction of pressure drops across a coalescing bed has been attempted only by these workers who advocated the travelling drop model which implies a constant saturation throughout the length of the bed. The equation proposed by Sherony (44) was based on the Blake-Kozeny equation which on rearrangement, may be expressed as,

$$\frac{\Delta P_2}{\Delta P_1} = \frac{\left\{ 1 - e_1 (1 - \bar{S}) \right\}^2}{(1 - e_1)^2 (1 - \bar{S})^3} \dots\dots\dots (10.25).$$

where the saturation, \bar{S} is determined from a curve giving the variation of $\frac{e_1 \bar{S}}{(1 - e_1)}$ with Reynolds Number,

$$N_{Re} = \frac{ud_c \rho_c}{\mu_c} . \text{ Rosenfeld and Wasan (47) suggested a}$$

similar, simplified equation,

$$\frac{\Delta P_2}{\Delta P_1} = \left\{ 1 + \frac{e_1 \bar{S}}{1 - e_1} \right\}^{2/3} \dots\dots\dots (10.26)$$

where \bar{S} may be correlated with superficial velocity using,

$$\bar{S} = \frac{C(1 - e_1)u^n}{e_1} \dots\dots\dots (10.27)$$

Rosenfeld determined the value of the parameter, C and n to be 0.8 and 0.2 respectively when u is measured in ft/min. These models are inadequate representations of experimental data since they predict that the pressure drop ratio is independent of bed depth which is contrary to the variation shown in Figures 9.7, 9.8, 9.9, 9.10, 9.11. An entirely empirical approach was adopted by Euzen (218) who fitted their data to the following type equation,

$$\frac{\Delta P_2}{\Delta P_1} = k^L (uL)^{0.14} \dots\dots\dots (10.28)$$

where the constant k^L depends on the liquid system studied.

10.5.2 Derivation of Proposed Equation

Therefore, generally, the ability of existing equations to predict two phase pressure drop for the operating conditions applied in this study was not acceptable. As the Carman-Kozeny equation proved to be successful for correlating single phase pressure drop, it was used as the basis for this model. However, the Carman Kozeny equation must be modified since during two phase flow, the bed consists of a mixture of 'spheres' of different diameters which possess different values of specific surface, a.

For single phase flow through an element of bed δL ,

$$\frac{\delta P_1}{\delta L} = K\mu_c u (1 - e_1)^2 a_1^2 \dots\dots\dots (10.29)$$

by writing equations 10.29 by analogy for two phase flow,

$$\frac{\delta P_2}{\delta L} = \frac{K\mu_c u (1 - e_2)^2 a_2^2}{e_2^3} \dots\dots\dots (10.30)$$

where $e_2 = e_1 (1 - S)$, $a_1 = \frac{6}{d_c}$

$$a_2 = \frac{\frac{6e_1 S}{d_p} + \frac{6(1-e_1)}{d_c}}{1 - e_1 (1 - S)} \dots\dots\dots (10.31)$$

for a mixture of 'spheres' (see Appendix D). Substituting for e_2 and a_2 into 10.30 and taking the limit as $\delta L \rightarrow 0$.

$$\frac{dP}{dL} = 36 K\mu_c u \frac{\left(\frac{e_1 S}{d_p} + \frac{(1 - e_1)}{d_c} \right)^2}{e_1^3 (1-S)^3} \dots\dots\dots (10.32)$$

The total two phase pressure drop may now be determined by integration of equation 10.32 between the limits of 0 and L.

$$\therefore \Delta P_2 = \frac{36K\mu_c u}{e_1^3} \int_0^L \frac{\left(\frac{e_1 S}{d_p} + \frac{(1 - e_1)}{d_c} \right)^2}{(1 - S)^3} dL \dots (10.33)$$

Similarly from equation 10.29 and substituting for a_1 ,

$$\Delta P_1 = \frac{36 K\mu_c u (1 - e_1)^2 L}{e_1^3 d_c^2}$$

then,
$$\frac{\Delta P_2}{\Delta P_1} = \frac{d_c^2}{(1 - e_1)^2 L} \int_0^L f(S) dl \dots\dots\dots (10.34)$$

where $f(S) = \frac{\left(\frac{e_1 S}{d_p} + \frac{(1 - e_1)}{d_c} \right)^2}{(1 - S)^3} \dots\dots\dots (10.35)$

by letting $b = \frac{1}{d_p}$ and $c = \frac{1}{d_c}$, the right hand side of equation 10.35 becomes,

$$f(S) = \frac{b^2 e_1^2 S^2 + 2 b c e_1 S(1 - e_1) + (1 - e_1)^2 c^2}{(1 - S)^3} \dots (10.36)$$

introducing the following constant to simplify the coefficients,

let $d = b^2 e_1^2$; $f = 2 b c e_1 (1 - e_1)$; $i = (1 - e_1)^2 c^2$

equation 10.36 is given by,

$$f(S) = \frac{dS^2 + fS + i}{(1 - S)^3} \dots\dots\dots (10.37)$$

considering equation 10.34, the integration of $f(S)$ cannot be performed in one stage since discontinuity appears in the mathematical description of the saturation profile. When $0 < \ell < L_I$, $S = S_I$ and is independent of ℓ , therefore,

$$\int_0^{L_I} f(S) dl = \frac{(dS_I^2 + f S_I + i) L_I}{(1 - S_I)^3} \dots\dots\dots (10.38)$$

When $L_I < \ell < L$, $S_I = (S_I - S_E) e^{-k(\ell - L_I)} + S_E$

Letting, $g = (S_I - S_E)$; $h = S_E$

and substituting,

$$v = g e^{-k(\ell - L_I)} + h$$

$$\frac{dv}{d\ell} = -k g e^{-k(\ell - L_I)}$$

$$= k(v - h)$$

$$\text{or } d\ell = \frac{dv}{k(v-h)}$$

also when, $\ell = L_I$, $v = g + h$

$\ell = L$, $v = g e^{-k(L - L_I)} + h$

$$\begin{aligned} \therefore \int_{L_I}^L f(S) d\ell &= \int_{g+h}^{g e^{-k(L-L_I)} + h} f(v) \left(-\frac{dv}{k(v-h)} \right) \\ &= \frac{1}{k} \int_{g e^{-k(L-L_I)} + h}^{g+h} \left(\frac{f(v)}{(v-h)} \right) dv \\ &= \frac{1}{k} \int_{g e^{-k(L-L_I)} + h}^{g+h} \left(\frac{dv^2 + fv + i}{(v-h)(1-v)^2} \right) dv \dots\dots (10.39) \end{aligned}$$

Evaluation of the integral given by equation 10.39 is fairly straight forward but tedious and so has been completed in Appendix E.

The total pressure drop across the bed will therefore be predicted using,

$$\frac{\Delta P_2}{\Delta P_1} = \frac{d_c^2}{(1-e_1)^2 L} \left\{ \int_0^{L_I} f(S) dl + \int_{L_I}^L f(S) dl \right\} \quad (10.40)$$

where $\int_0^{L_I} f(S) dl$ is determined using equation 10.38,

and $\int_{L_I}^L f(S) dl$ is determined using equation 10.39.

10.6 TESTING THE MODEL

10.6.1 Evaluation of Parameters from Saturation Data

As presented in Section 10.4.2, the experimental saturation can be successfully predicted by using the proposed model. By taking the experimental values of S_I , S_E , L_I and L_E and the calculated decay value k , equation 10.40 will be used to predict the two phase pressure drop ratio.

10.6.2 Comparison with Experimental Data

Equation 10.40 was used to predict the pressure drop ratios for the saturation Vs bed depth graphs on Figures 10.11, 10.12, 10.13, 10.14.

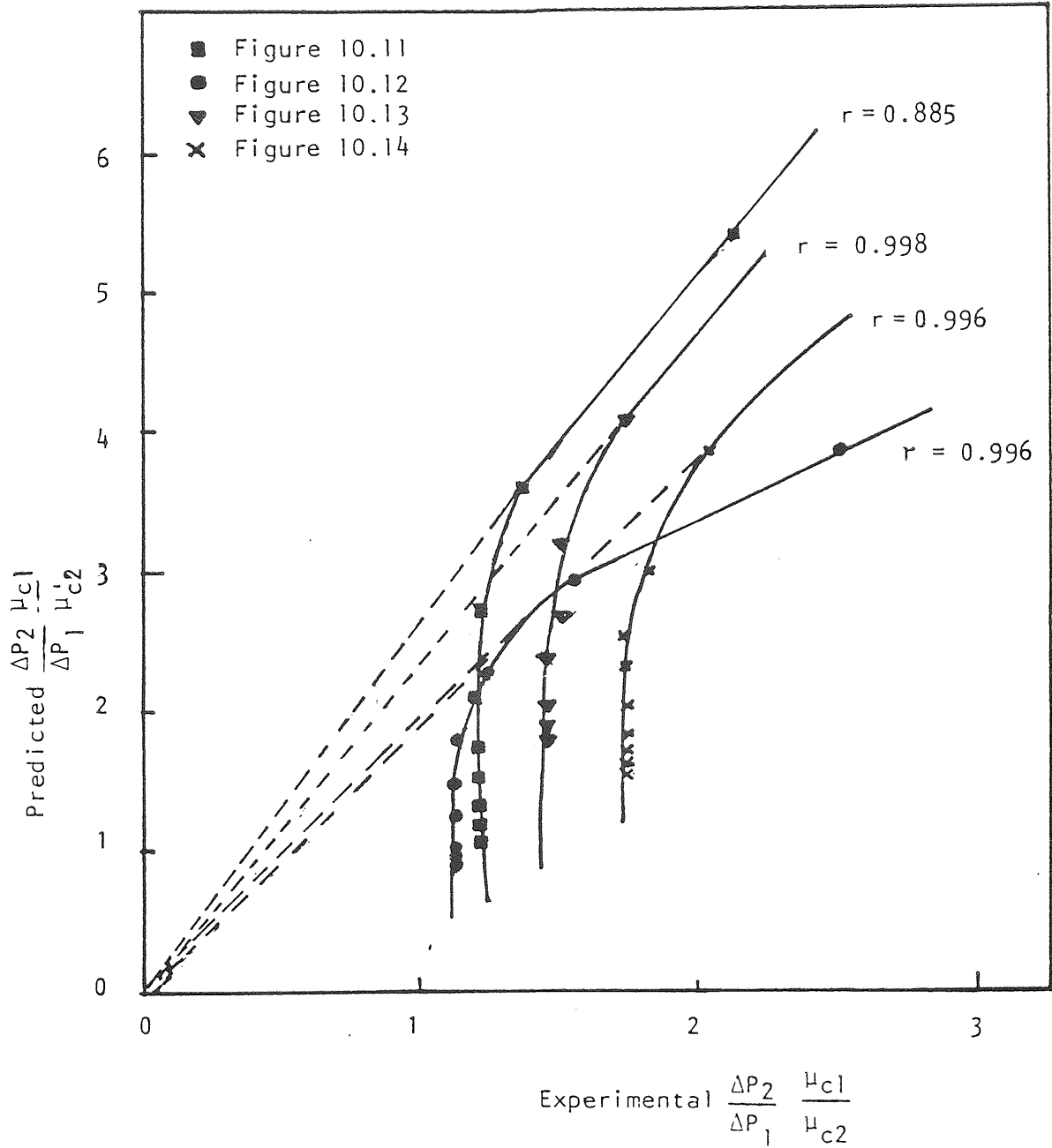


Figure 10.18 Predicted Vs. Experimental Pressure Drop Ratio

The parameters used are those obtained by regression analysis of the experimental saturation profiles as shown on these figures.

The predicted ratios were then plotted against the experimental values from Appendix J.

Although some of the data points are well represented by the model, shown on Figure 10.18, the overall fit is not particularly good. The best fit was obtained for the higher superficial velocities considered. This is most likely due to the fact that for high velocities, the saturation profiles approximate the idealised model presented in Section 10.4.2 whereas at low velocities there is a slight increase of dispersed phase saturation at the exit of the bed which is not included in the model. Also, the values used for S_I were those predicted by the saturation model, and as previously discussed they can be much higher than the experimental value.

An alternative means of empirically fitting the pressure drop data would be to manipulate the value of the inlet saturation S_I , and /or the constant saturation length L_I . Also, inclusion of the increase in local dispersed phase saturation at the bed exit should improve the data fit.

10.7 PREDICTION OF EXIT DROP SIZE

10.7.1 Preliminary Considerations

In Sections 8.3 and 9.7 the flow of the coalesced dispersed phase through fixed channels was considered. In this section the flow between mutually tangential parallel circular cylinders on equilateral triangular pitch will be used as the basis for the model.

This follows an investigation into interstitial flow through foam (219). Such flow occurs through capillaries (Plateau borders). In one limiting case, the walls of such a capillary are rigid and in the shape of tangential circular arcs as shown by the heavy solid curves of Fig. 10.19a. This cross-section is obviously identical with that of the free space between tangential parallel congruent circular cylinders. Although in packed bed of spheres the channels for flow are periodically constricted it will be assumed that the channels have constant longitudinal cross sectional areas as shown on Fig. 10.19b. The dispersed phase is incompressible and with steady longitudinal laminar flow. The area for flow is shown on Fig. 10.19b and the shaded area is in sixfold symmetry within the channel.

From geometric considerations

$$A_{\text{cap}} = \left(3\sqrt{3} - \frac{3\pi}{2}\right)b^2 + 3bh + \frac{\sqrt{3}}{4}h^2 \dots\dots\dots (10.41)$$

Since $b \gg h$ normally, and $a_c = b\sqrt{3}$, equation 10.41 reduces to equation (219):

$$\begin{aligned} A_{\text{cap}} &= 0.1612 a_c^2 + 1.732 a_c h \\ &\approx 0.1612 a_c^2 \end{aligned}$$

The rate of flow through the channels is (220)

$$u_{\text{cap}} = \frac{d_H^2}{2K\mu} \frac{\Delta P}{\Delta L} \dots\dots\dots (10.42)$$

where the hydraulic mean diameter, $d_H = 0.205 a_c$ and $K = 6.43$. Then the volumetric flowrate $q_d = u_{\text{cap}} A_{\text{cap}}$ that is:

$$q_d = \frac{0.0065 a_c^4}{12.86} \frac{\Delta P}{\Delta L}$$

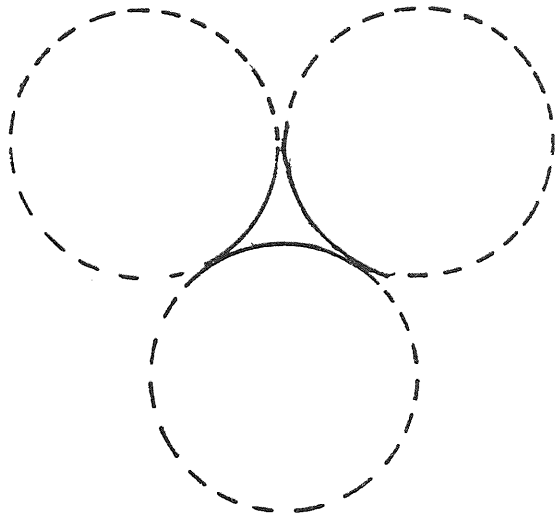
Then

$$\text{No. of capillaries} = \frac{\text{Total flowrate of dispersed phase}}{\text{Flowrate through capillary}}$$

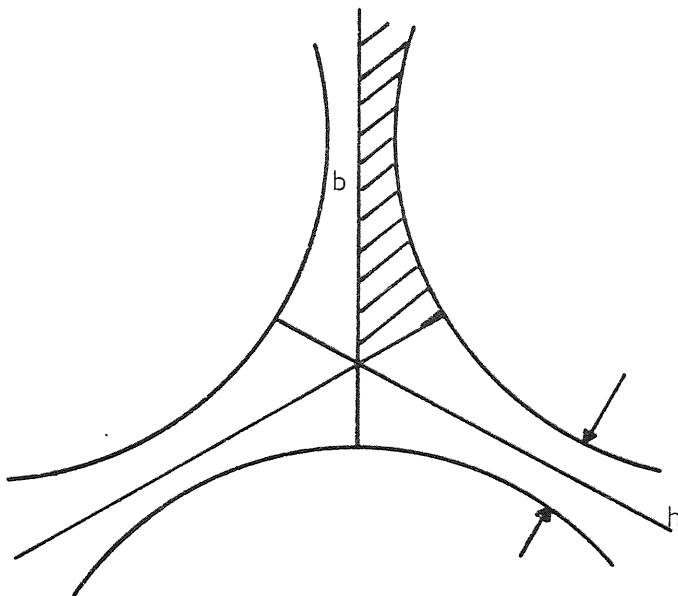
From a knowledge of the velocity through the capillary, volumetric flowrate, physical properties of the system and using Meister-Scheele's (221) correlation for predicting the drop volume, the exit drop diameter, d_{pe} , can be calculated.

A set of results is presented on Appendix K as an example. The predicted Vs experimental drop sizes are plotted on Fig. 10.20. This shows that all data points are well represented by the model.

This approach could be developed further by calculating the rate of discharge of dispersed phase. By taking cine-films of the flow of dispersed phase through the bed, the residence time could be obtained and the effective flow path, L_e , evaluated. This may aid the modelling of the coalescence process by means of the "queuing theory" approach.



a) Schematic Representation of Capillary



b) Area for Capillary Flow with Sixfold Geometry.

Figure 10.19 Schematic Representation of the Capillary Area

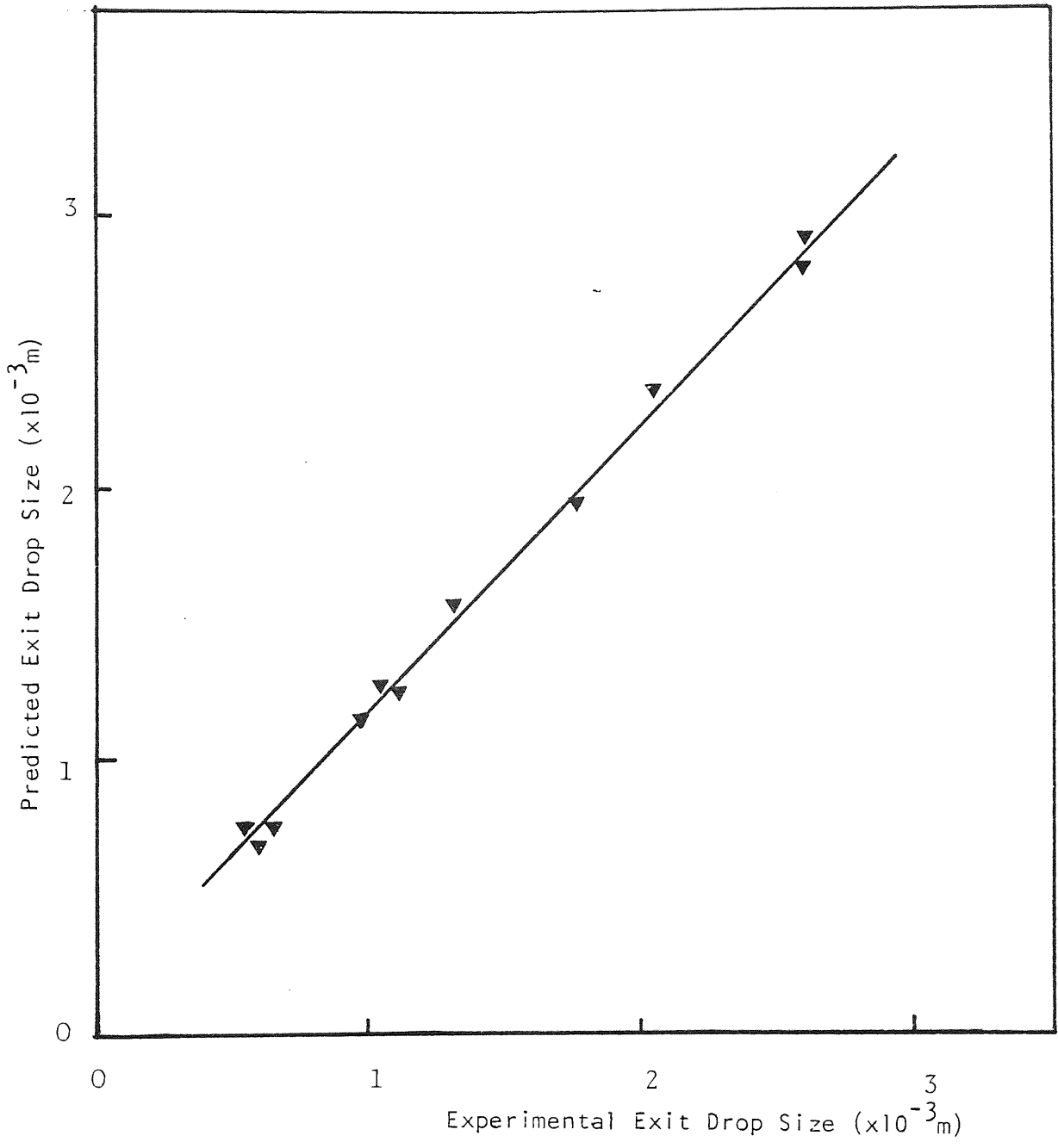


Figure 10.20 Predicted Vs Experimental Exit Drop Size

CONCLUSIONS

CONCLUSIONS

1. Packings, consisting of varying sizes of monosized glass ballotini and different bed depths, provided a suitable media for investigation of the effects of operating conditions and bed properties on the coalescence of secondary dispersions.
2. Measurements of separation efficiency and coalesced drop sizes indicated the existence of a critical velocity above which breakthrough of the dispersion occurred. This velocity was found to be approximately 2.0×10^{-2} m/s. Also there is a maximum bed depth above which drop redispersion occurs. For the range of ballotini sizes used this maximum height varied between 7.5×10^{-2} m and 25×10^{-2} m.
3. Using relative permeability correlations, the dispersed phase saturation was determined from experimental pressure drop data. The saturation profiles obtained confirm the spatial variation of saturation with bed depth. There is an increase of saturation at the bed inlet decreasing exponentially thereafter to a constant value for the remainder of the bed. Also there is a slight increase of the saturation at the exit face of the bed; this is due to an accumulation of dispersed phase prior to drop release due to a resultant of interfacial forces existing at the bed exit attempting to retain the drops. The highest values obtained

for the inlet and exit bed saturations are 0.54 and 0.14 respectively.

4. A theoretical comparison of drop capture mechanisms demonstrated that direct and indirect interception are most significant under operating conditions encountered in this study but diffusion and London-Van der Waals forces may predominate for drops of less than 25 μm diameter. The drop capture efficiency, for beds initially free from dispersed phase, may be estimated using:

$$\frac{\eta_T}{\eta_I} = 1 + f(N_{Ad}) + 2.22 N_{Ad}^{2/3} \left(\frac{k'T}{Q}\right)^{2/3}$$

where $f(N_{Ad})$ is obtained from Spielman and Fitzpatrick's correlation at different values of N_G .

Application of this equation to typical operating conditions show that the drop capture rate is likely to be highest in the forepart of the bed.

5. The single phase pressure drop results were satisfactorily correlated by the Carman-Kozeny equation:

$$\left\{\frac{\Delta P_1}{\mu_c}\right\} \left\{\frac{e_1^3 d_c^2}{(1-e_1)^2 36L}\right\} = K_u$$

From theoretical considerations this value of the Kozeny constant, K , was taken as 5.0. This value is in good agreement with those obtained experimentally.

6. An expression, based on the Carman-Kozeny equation, was derived to predict the two phase pressure drop

from knowledge of the saturation profiles:

$$\frac{\Delta P_2}{\Delta P_1} = \frac{d_c^2}{(1-e_1)^2 L} \int_0^L f(s) dl$$

A model was postulated from inspection of the calculated saturation profiles from pressure drop data and from other studies in which the local saturation decays exponentially from a constant value near the inlet face to a constant value in the downstream part of the bed:

$$S = S_I \quad 0 < l < L_I$$

$$S = (S_I - S_E) e^{-k(l-L_I)} + S_E \quad L_I < l < L$$

The decay factor, k , was evaluated for various superficial velocities and dispersed phase concentrations. The predicted and experimental saturation profiles are in excellent agreement and thus, providing the correct value of the decay factor is used, the saturation profiles can be successfully predicted using the proposed equation.

The different parameters of this model were used in the evaluation of $\int_0^L f(S) dl$, and for a given superficial velocity and dispersed phase concentration produced good agreement between the predicted and experimental pressure drop.

7. Using an analogy to flow through non-cylindrical channels, the prediction of exit drop size and dispersed phase rate of flow through the bed has been attempted. From a mass balance over the

coalescer the number of channels of flow can be obtained. Although refinement of the model and further experimental testing is necessary, this novel approach is concluded to be valuable in the prediction of exit drop size based on the rate of flow of the dispersed phase through the bed. Therefore at steady state operation it could be possible to determine the rate at which coalescence takes place from knowledge of inlet and exit drop size, rate of dispersed phase discharge and residence time within the bed.

8. Based on this theoretical and experimental study, a mechanism of coalescence of secondary dispersion is proposed:

Drops are captured by direct and indirect interception, primarily in the forepart of the bed. The drops reside in the bed either attached to the packing or intercepted by pores, where coalescence occurs until they attain such a size when hydrodynamic forces exceed the restraining interfacial tension and adhesion forces. The drops are then squeezed through the packing interstices into a dispersed phase continuum. Hence, a dispersed phase front is seen to propagate from inlet to outlet, in a zig-zag fashion within fixed channels of flow, with a maximal local dispersed phase saturation fixed at a critical value which depends on the flowrate and capillary pressure.

RECOMMENDATIONS FOR FURTHER WORK

RECOMMENDATIONS FOR FURTHER WORK

1. This study has been restricted to investigation of the effects of superficial velocity, bed depth, ballotini diameter and dispersed phase concentration. It is recommended that the range of values employed for ballotini diameter and thus aperture diameter be extended to determine the optimum conditions where large drops are formed with a high separation efficiency. Since high drop capture efficiencies are released using small ballotini diameters and large drops are produced by larger ballotini diameters, it would be useful to perform experiments where the ballotini diameter increases through the bed. The effects of system properties should also be investigated using other suitable dispersed phases.
2. An experimental study, combining variation of liquid system properties for different ballotini materials, would be desirable to elucidate the relationship existing between wetting effects and the coalescence parameters, pressure drop and filter coefficients. A more fundamental study is necessary to determine how wettability may be characterised for two phase flow in packed beds when coalescence occurs simultaneously. By chemical treatment the packing could be rendered hydrophobic or hydrophilic and its effect on the coalescence process should be tested.

3. More accurate determination of saturation profiles can be achieved by setting pressure taps closer to each other. Experimental determination of capillary pressure for drainage and imbibition will give the minimum saturation required for capillary flow and the maximum saturation that could be attained with a particular system.
4. Setting of sample ports along the bed for the measuring of drop number density and size at different bed depth intervals, should be tested. It will provide values for the filter coefficient and rate of drop capture during operation, and the effect of held up oil on drop capture, and how this compares with the theoretical rate of drop capture obtained for clean beds after one second operating time.
5. Since granular media may be easily fluidized or backflushed for regeneration, the effect of particle matter suspended in the continuous phase should be studied.

APPENDICES

APPENDIX A

PHYSICAL PROPERTIES OF LIQUID SYSTEM

As temperature changes were inevitable during operation of the coalescer, the physical properties of the liquid system were determined as a function of temperature. The temperature coefficient of density for both continuous and dispersed phases is low and in the temperature range between 10°C and 30°C, it is sufficient to take one value,

$$\text{Density of Water, } \rho_c = 998 \pm 2 \text{ kg/m}^3 \dots\dots (222)$$

$$\text{Density of Toluene, } \rho_d = 867 \pm 3 \text{ kg/m}^3 \dots\dots (222)$$

The remaining relevant properties are presented as a function of temperature in Figs. A.1, A.2 and A.3. Viscosity and mutual solubility data were extracted from the literature (223) but since interfacial tension is sensitive to the purity of the two phases, this was measured with a Du Nouy Tensiometer. Interfacial tension was found to remain constant over the operational temperature range as shown in Fig. A.2.

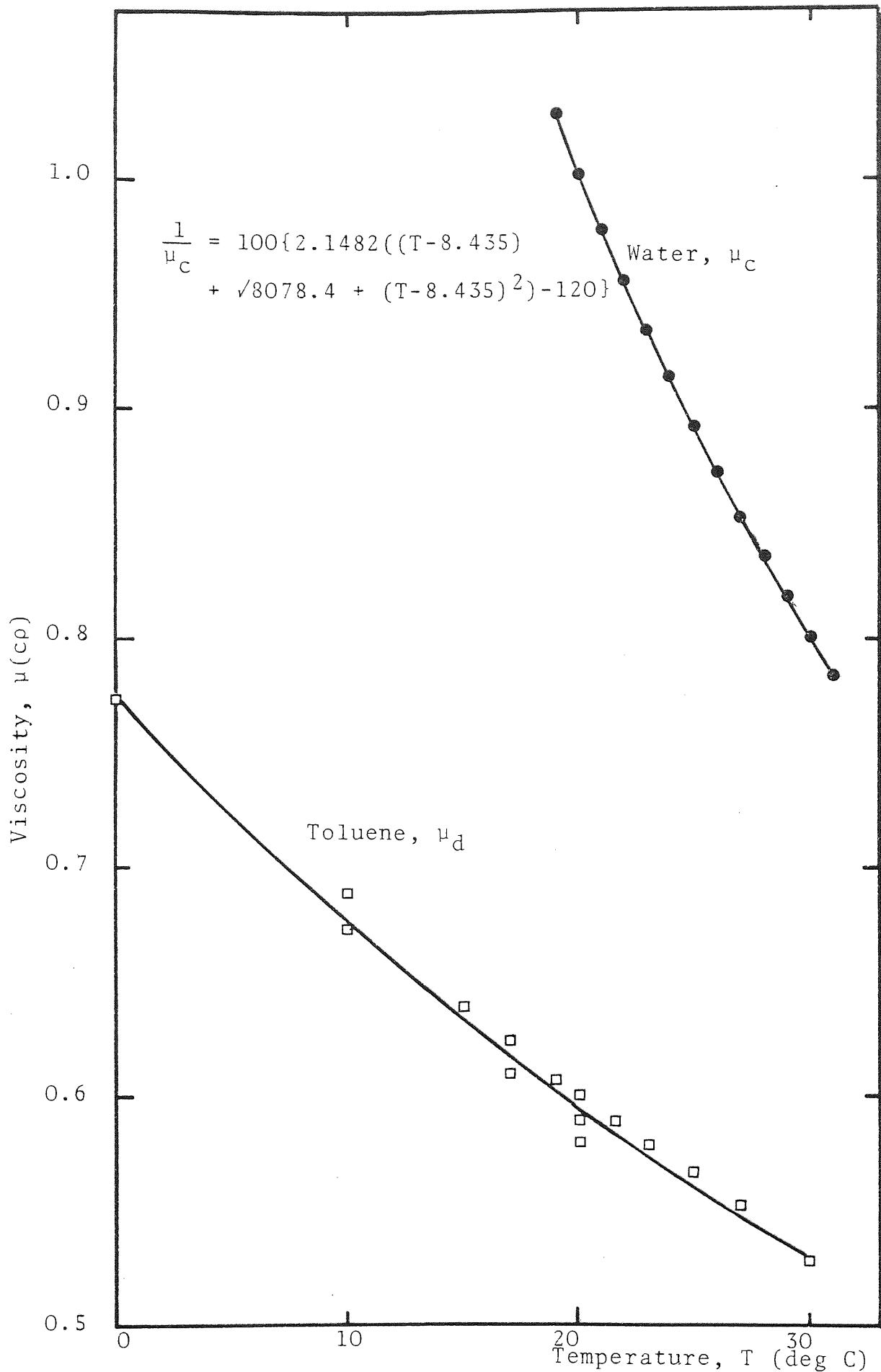


FIG. A.1 Phase Viscosities as a Function of Temperature

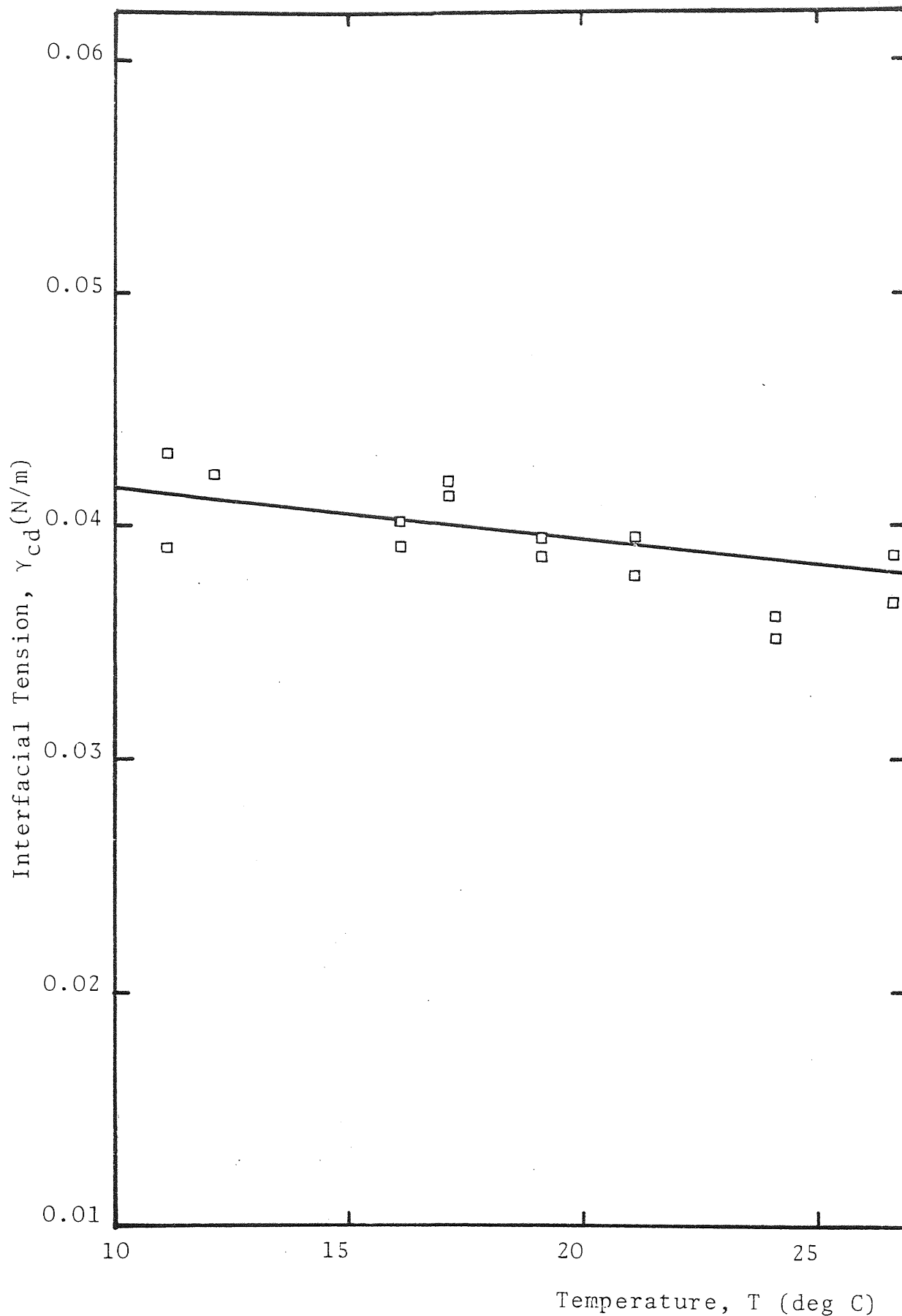


Fig. A.2 Interfacial Tension for Toluene/Water System as a Function of Temperature

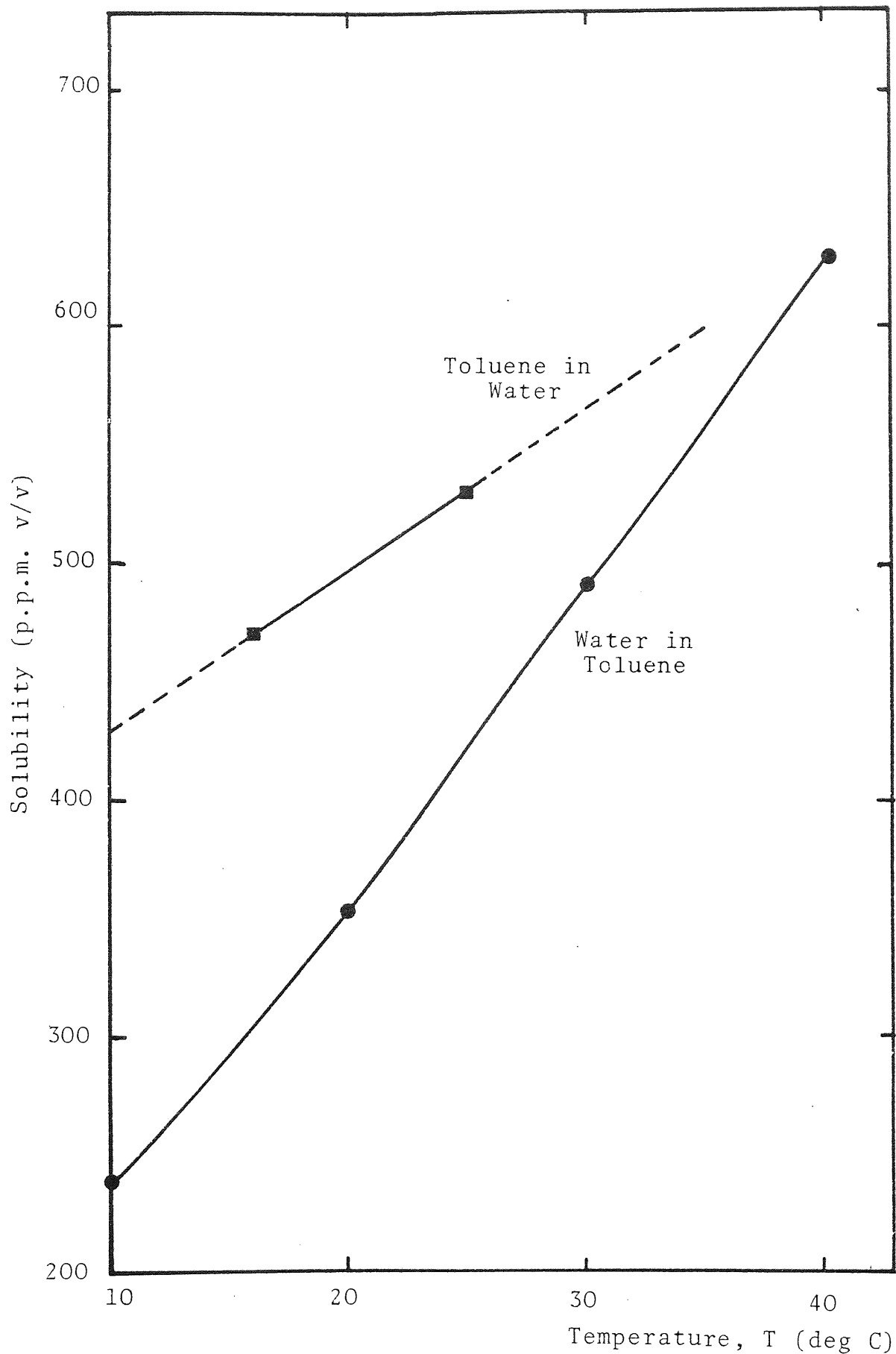


Fig. A.3 Mutual Solubility of Toluene/Water System as Function of Temperature

APPENDIX B

BED VOIDAGE DETERMINATION

Packing thickness: 5×10^{-2} m

Datum Reading: 28.13

Volume Collected $\times 10^{-6} \text{ m}^3$	New Reading $\times 10^{-2} \text{ m}$	Distance Drop $\times 10^{-2} \text{ m}$
50	23.76	4.37
50	19.37	4.39
50	15.02	4.35
50	10.64	4.38
50	4.27	6.37

∴ Distance drop per $50 \times 10^{-6} \text{ m}^3$ above the packing =

$$\frac{4.37 + 4.39 + 4.35 + 4.38}{4} = 4.37 \times 10^{-2} \text{ m}$$

$6.37 \times 10^{-2} - 5.0 \times 10^{-2} = 1.37 \times 10^{-2} \text{ m}$. This contains
 $15.62 \times 10^{-6} \text{ m}^3$ water.

But water collected: $50 \times 10^{-6} \text{ m}^3$

∴ Hold up of water = $50 \times 10^{-6} - 15.62 \times 10^{-6} = 34.38 \times 10^{-6} \text{ m}^3$

Volume of packing: $57 \times 10^{-6} \text{ m}^3$

∴ Packing voidage $e_1 = \frac{57 - 34.38}{57} = 0.397$

This was repeated three more times to obtain the average value of e_1 for $50 \times 10^{-2} \text{ m}$. The same procedure was repeated for the different bed depths and ballotini sizes used. The average voidages obtained are presented in Table 9.3.

APPENDIX C

DETERMINATION OF THE HAMAKER CONSTANT

An equation for calculating Hamaker's constant for a system of two immiscible liquids and a solid is presented by Sherony and Kintner (225). This equation is:

$$Q = 6\pi r_{22}^2 (\sqrt{\sigma_d^d} - \sqrt{\sigma_c^d}) (\sqrt{\sigma_s^d} - \sqrt{\sigma_c^d})$$

where r_{22} is the intermolecular distance, and σ_c^d , σ_d^d , and σ_s^d are the London-Van der Waal's component to the surface tensions of the continuous, dispersed, and solid phases, respectively.

Fowkes (224) estimates that $6\pi r_{22}^2$ is equal to $1.44 \times 10^{-18} \text{ m}^2$ for water and hydrocarbon systems.

$$\text{for glass, } \sigma_s^d = 0.0780 \text{ N/m}$$

$$\text{for water, } \sigma_c^d = 0.0218 \text{ N/m}$$

$$\text{for toluene, } \sigma_d^d = 0.0285 \text{ N/m}$$

$$\therefore Q = 1.44 \times 10^{-18} (\sqrt{0.0285} - \sqrt{0.0218}) (\sqrt{0.0780} - \sqrt{0.0218})$$

$$\underline{\text{Hamaker constant, } Q = 0.401 \times 10^{-20} \text{ J}}$$

APPENDIX D

EVALUATION OF SPECIFIC SURFACE FOR COALESCER CONTAINING DROPS OF DISPERSED PHASE

Specific Surface -

$$a = \frac{(\text{surface area of drops} + \text{surface area of spheres})}{(\text{volume of drops} + \text{volume of spheres})}$$

let the number of drops per unit volume of bed = N_p

$$\text{then surface area} = N_p \Pi d_p^2$$

$$\text{Volume} = N_p \Pi \frac{d_p^3}{6}$$

let the number of grains per unit volume of bed = N_c

$$\text{then surface area} = N_c \Pi d_c^2$$

$$\text{Volume} = N_c \Pi \frac{d_c^3}{6}$$

if void fraction of sphere = e_1

$$\text{then } N_c = \frac{6(1-e_1)}{\Pi d_c^3}$$

if void fraction of drops = e_p

$$N_p = \frac{6(1-e_p)}{\Pi d_p^3}$$

also two phase effective voidage, $e_2 = (e_p + e_1) - 1$

$$\text{then } e_p = (e_2 - e_1) + 1$$

but saturation, $S = 1 - \frac{e_2}{e_1}$

$$\text{or } e_2 = e_1(1-S)$$

$$\therefore a = \frac{\left\{ \frac{6}{d_p} (e_1 - e_2) + \frac{6}{d_c} (1 - e_1) \right\}}{(1 - e_2)}$$

$$a = \frac{\left\{ \frac{6}{d_p} e_1 S + \frac{6}{d_c} (1 - e_1) \right\}}{\{1 - e_1(1 - S)\}}$$

APPENDIX E

INTEGRATION OF PRESSURE DROP EQUATION

In Section 10.5 solution of the equation describing the two phase pressure drop ratio was reduced to the problem of integration of the following polynomial expression,

$$\int_{L_I}^L f(S) dl = \frac{1}{k} \int_{L_I}^{g+h} e^{-k(L-L_I)} + h \frac{(dv^2 + fv + i)}{(v-h)(1-v)^3} dv \dots E.1$$

Integration is performed by partial fractions

i.e.

$$\frac{dv^2 + fv + i}{(v-h)(1-v)^3} = \frac{A}{(1-v)} + \frac{B}{(1-v)^2} + \frac{C}{(1-v)^3} + \frac{D}{(v-h)} \dots E.2$$

or

$$\begin{aligned} dv^2 + fv + i &= A(1-v)^2(v-h) + B(1-v)(v-h) + C(v-h) + D(1-v)^3 \\ &= A\{v^3 - v^2(2+h) + v(1+2h) - h\} \\ &\quad + B\{-v^2 + v(h+1) - h\} + C\{v-h\} \\ &\quad + D\{-v^3 + 3v^2 - 3v + 1\} \end{aligned}$$

equating coefficients,

$$v^3: 0 = A - D$$

$$v^2: d = -(2+h)A - B + 3D$$

$$v: f = (1+2h)A + (h+1)B + C - 3D$$

$$v^0: i = -hA - hB - hC + D$$

Solution to this four simultaneous equations gives,

$$A = D = \frac{dh^2 + fh + i}{(h^2 - 2h + 1)(1-h)} \dots E.3$$

$$B = \frac{(f+2d)h - d + i}{(h^2 - 2h + 1)} \dots E.4$$

$$C = \frac{(d+f+i)(1-h)}{(h^2 - 2h + 1)} \dots E.5$$

Since the above expressions are independent of v , it is possible to integrate equation E.2 in its simple form,

$$\begin{aligned}
 & \int_{ge^{-k(L-L_I)+h}}^{g+h} \frac{(dv^2 + fv + i)}{(v-h)(1-v)^3} dv \\
 &= \{-A \log_e(1-v) + \frac{B}{(1-v)} + \frac{C}{2(1-v)^2} \\
 & \quad + D \log_e(v-h)\} \int_{ge^{-k(L-L_I)+h}}^{g+h} \\
 & \dots\dots\dots E.6
 \end{aligned}$$

where the constants A and D, B and C are given by equations E.3, E.4 and E.5 respectively.

APPENDIX F
CALCULATION OF EXPERIMENTAL ERROR IN
PRESSURE DROP MEASUREMENT

(a) Error in time. The error in the value of time is $\Delta t \pm 10$ seconds, since it takes at least 15 seconds to note the pressure drop and temperature. The object is, however, to observe pressure drop changes with time, and also the fluctuations of ΔP occur over times much greater than 10 seconds, then this error in the measurement of time will not be significant.

(b) Temperature coefficient of manometer fluid density.

Conversion factor for Nm^{-2}

$$\text{at } 12^{\circ}\text{C } \rho_{\text{CCl}_4} = 1.6023 \text{ g cm}^{-3} \pm 0.001$$

then conversion factor $C = 157.1 \pm 0.1$ at 24°C

$$\rho_{\text{CCl}_4} = 1.5948 \text{ g cm}^{-3} \pm 0.001$$

then the conversion factor = 156.4 ± 0.1

Conversion factor used = 156.7

Maximum error $\Delta c = \pm 0.5 \text{ g cm}^{-3}$

$$\therefore \text{Error} = \frac{\Delta c}{c} = \frac{0.5}{156.7} = 0.0032$$

(c) Variation in density of manometer fluid, i.e. impurities. This error is $\Delta \rho = \pm 0.001 \text{ g cm}^{-3}$ and was accounted for in the evaluation of (b).

(d) Reading error of each manometer limb. During the experiment, fluctuations are infrequent enough to remain constant effectively during measurements and therefore

the error will be taken as $\Delta l \pm 0.1$ cm on each limb.

For a mean reading of 30.0 cm, the error, $\frac{\Delta l}{l} = \frac{0.2}{30} = 0.00666$.

(e) Absolute error in rotameter calibration

(i) Error in coalescer area is, effectively 0.

(ii) Error in 'volume collector', $\Delta V = \pm 10 \text{ cm}^3$.

(iii) Error in 'time', $\Delta t = \pm 1$ s.

(iv) Error in tube reading, $\Delta r = \pm 0.1$ cm.

For rotameter 75 and taking the middle of both ranges, at 15 cm.

error in volume, $\frac{\Delta V}{V} = \frac{10}{800} = 0.0125$

error in time, $\frac{\Delta t}{t} = \frac{1}{89} = 0.0112$

error in volumetric flowrate, $\frac{\sigma_1}{Q} = \left\{ \left(\frac{\Delta V}{V} \right)^2 + \left(\frac{\Delta t}{t} \right)^2 \right\}^{\frac{1}{2}}$

$$\frac{\sigma_1}{Q} = 0.017$$

Volumetric flowrate = 0.539 l/min

\therefore Standard deviation, $\sigma_1 = 0.539 \times 0.017$

$$\sigma_1 = \pm 0.009 \text{ l/min}$$

With reference to the calibration curve, this produces a standard deviation, σ_2 , in the tube reading equal to 0.3 cm.

$$\sigma_2 = \pm 0.3 \text{ cm}$$

However this value does not take into account any variation of the tube reading for a given flowrate due to temperature changes - a previous analysis showed this effect to be only slightly significant. Therefore it is assumed that the effect may be compensated for by increasing the value of σ_1 .

i.e. assume $\sigma_1' = \pm 0.015$ l/min

which corresponds to $\sigma_2' = \pm 0.5$ cm

Repeating this calculation for the 14 S rotameter taking the middle of the range.

at 15 cm

$$\text{error in volume} = \frac{\Delta V}{V} = \left(\frac{10}{2300}\right) = 0.00434$$

$$\text{error in time} = \frac{\Delta t}{t} = \left(\frac{1}{50}\right) = 0.020$$

$$\therefore \text{error in volumetric flowrate } \frac{\sigma_3}{Q} = \left\{ \left(\frac{\Delta V}{V}\right)^2 + \left(\frac{\Delta t}{t}\right)^2 \right\}^{\frac{1}{2}}$$

Volumetric flowrate, $Q = 2.75$ l/min

$$\sigma_3 = \pm 0.0565 \text{ l/min}$$

Correcting for temperature fluctuations

$$\sigma_3' = \pm 0.085 \text{ l/min}$$

and from the calibration graph, the standard deviation of tube reading $\sigma_4' = \pm 0.6$ cm.

(f) Velocity fluctuations.

By careful experimentation it is possible to control the rotameter readings to ± 0.3 cm. For the 7S rotameter, this produces a velocity fluctuation of $\Delta u = \pm 0.01$ cm/s.

Velocity in the middle of the range (15 cm tube reading)

$$u = 0.788 \text{ cm/s}$$

$$\text{Then error in velocity } \frac{\Delta u}{u} = \frac{0.01}{0.788} = 0.0127$$

For the 14 S rotameter, ± 0.3 cm rotameter reading error produces an error in velocity

$$\Delta u = \pm 0.13 \text{ cm/s}$$

Velocity in the middle of the range (15 cm tube reading)

$$u = 4.75 \text{ cm/s}$$

$$\text{Then error in velocity, } \frac{\Delta u}{u} = \frac{0.13}{4.75} = 0.0273$$

Taking the largest error, $\frac{\Delta u}{u} = 0.0273$

If a linear relationship between ΔP and u is assumed, then the error in ΔP are:

$$\frac{\delta \Delta P}{\Delta P} = \left\{ \left(\frac{\Delta c}{c} \right)^2 + \left(\frac{\Delta l}{l} \right)^2 + \left(\frac{\Delta u}{u} \right)^2 \right\}^{\frac{1}{2}}$$

Since the pressure drop data is presented as $\frac{\Delta P}{\mu_c}$, the error in the continuous phase viscosity, μ_c , should be taken into account.

Since the viscosity vs. temperature values were obtained from a polynomial fit given in the literature (223), any error in temperature measurement will be negligible compared to the accuracy of the polynomial fit. Therefore the deviations of the published data will be used as an estimate of the errors.

$$\Delta \mu_c = \pm 0.003 \text{ cp}$$

and for 25°C , $\mu_c = 0.8904 \text{ cp}$

$$\therefore \frac{\Delta \mu_c}{\mu_c} = \frac{0.003}{0.8904} = 0.0033$$

$$\Delta T = \pm 0.1^\circ\text{C} \quad \therefore \frac{\Delta T}{T} = \frac{0.1}{25} = 0.004$$

and thus the total error in pressure drop measurement is:

$$\frac{\delta \Delta P}{\Delta P} = \left\{ \left(\frac{\Delta c}{c} \right)^2 + \left(\frac{\Delta l}{l} \right)^2 + \left(\frac{\Delta u}{u} \right)^2 + \left(\frac{\Delta \mu_c}{\mu_c} \right)^2 + \left(\frac{\Delta T}{T} \right)^2 \right\}^{\frac{1}{2}}$$

$$\frac{\delta \Delta P}{\Delta P} = (8.267 \times 10^{-4})^{\frac{1}{2}}$$

$$\frac{\delta \Delta P}{\Delta P} = 0.0287$$

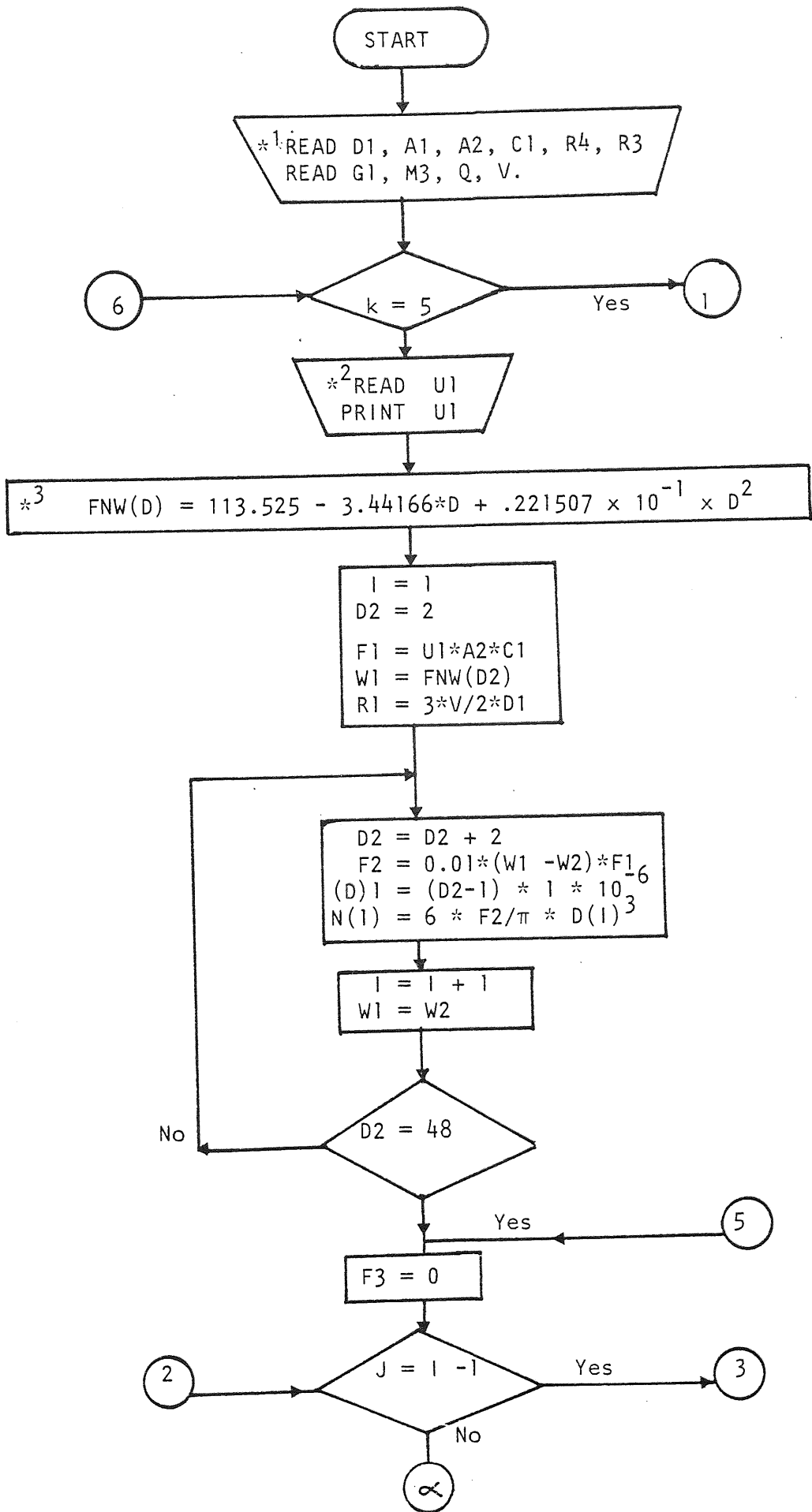
Take for example total pressure drop at $0.3 \times 10^{-2} \text{ m/s}$:

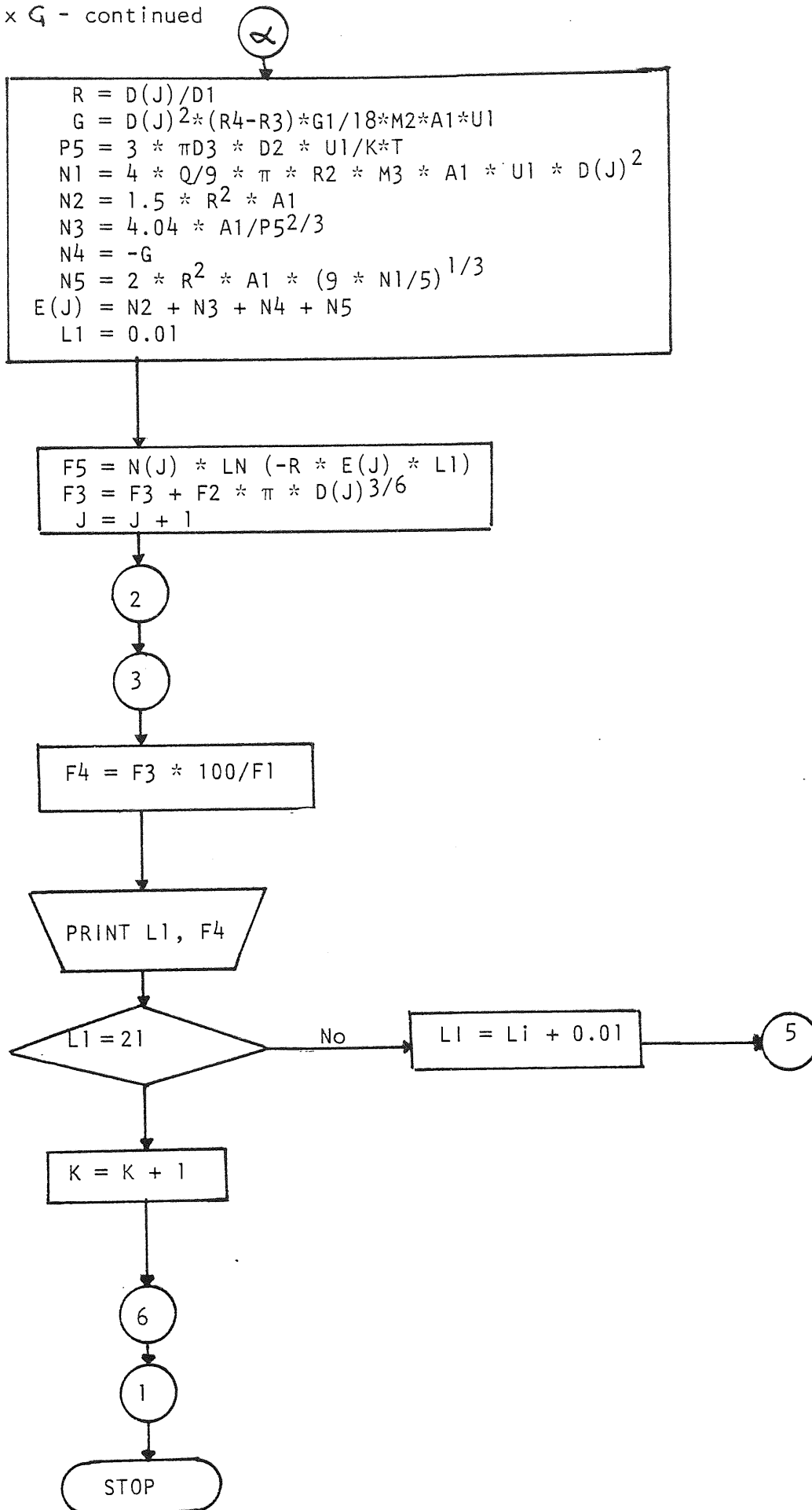
$$\frac{\Delta P}{\mu_c} = \frac{3165.34 \text{ Nm}^{-2}}{1.027 \times 10^{-5} \text{ Nm}^{-2}\text{s}} = 3.082 \times 10^6 \text{ s}^{-1}$$

∴ σ_5 , standard deviation due to fluctuations during an experiment:

$$\sigma_5 = \pm 0.884 \times 10^5 \text{ s}^{-1}$$

APPENDIX G - COMPUTER FLOWSHEET FOR CALCULATION OF RATE OF DROP CAPTURE.





Appendix G - continued

List of Variables

- *¹ D1 = Ballotini Diameter
- A1 = Happel's Cell Hydrodynamic Functions
- A2 = Coalescer Area
- C1 = Dispersed Phase Concentration
- R4 = Dispersed Phase Density
- R3 = Continuous Phase Density
- G1 = Acceleration of Gravity
- M3 = Continuous Phase Viscosity
- Q = Hamaker's Constant
- V = Volume of Solids
- *² U1 = Superficial Velocity
- *³ FNW(D) = Polynomial Fit of Inlet Drop Size Distribution

I	D2	FNW (D2)	D(I) × 10 ⁻⁶	N(I) × 10 ³	N6
1	2	106.703	3	5.336 × 10 ⁴	0.287 × 10 ⁻²
2	4	100.112	5	1.121 × 10 ⁴	0.693 × 10 ⁻²
3	6	93.672	7	3.975 × 10 ³	0.129 × 10 ⁻²
4	8	87.409	9	1.817 × 10 ³	0.207 × 10 ⁻²
5	19	81.323	11	9.666 × 10 ²	0.306 × 10 ⁻²
6	12	75.414	13	5.680 × 10 ²	0.423 × 10 ⁻²
7	14	69.683	15	3.583 × 10 ²	0.559 × 10 ⁻²
8	16	64.129	17	2.383 × 10 ²	0.715 × 10 ⁻²
9	18	58.751	19	1.650 × 10 ²	0.890 × 10 ⁻²
10	20	53.552	21	1.180 × 10 ²	0.108
11	22	48.529	23	86.714	0.129
12	24	43.683	25	65.054	0.153
13	26	39.015	27	49.681	0.178
14	28	34.524	29	38.513	0.205
15	30	30.210	31	30.234	0.234
16	32	26.074	33	23.990	0.265
17	24	22.114	35	19.208	0.298
18	26	18.332	37	15.496	0.333
19	28	14.727	39	12.582	0.370
20	40	11.299	41	10.269	0.408
21	42	8.049	43	8.416	0.449
22	44	4.975	45	6.920	0.491
23	46	2.079	47	2.897	0.536
24	48				

$$F1 = 1.140 \times 10^{-8}$$

TABLE G.1 Example of set of data obtained using the computer program based on the accompanying flowchart for $U1 = 1 \times 10^{-2}$ m/s. The values have been presented to the third decimal figure and only few intervals of bed depth, L1, have been used to illustrate this example.

D(J) $\times 10^{-6}$	$L1 \times 10^{-2}$					
	1	2	4	10	14	20
3	7.153×10^{-10}	6.782×10^{-10}	6.097×10^{-10}	4.429×10^{-10}	3.580×10^{-10}	2.601×10^{-10}
5	"	5.680 "	4.394 "	2.034 "	1.217×10^{-10}	5.637×10^{-11}
7	"	4.427 "	2.745 "	6.545×10^{-11}	2.516×10^{-11}	6.000×10^{-12}
9	"	3.211 "	1.486 "	1.475 "	3.160×10^{-13}	3.135×10^{-13}
11	"	2.168 "	6.579×10^{-11}	2.327 "	1.116×10^{-14}	8.041×10^{-15}
13	"	1.361 "	2.838 "	2.570×10^{-13}	3.139×10^{-16}	1.011×10^{-16}
15	"	7.959×10^{-11}	1.000 "	1.986×10^{-14}	-	-
17	"	4.327 "	3.054×10^{-12}	1.074×10^{-15}	-	-
19	1.38×10^{-11}	2.188 "	8.077×10^{-13}	4.062×10^{-17}	-	-
21	7.677 "	1.029 "	1.850 "	-	-	-
23	4.987 "	4.502×10^{-12}	3.669×10^{-14}	-	-	-
25	3.122 "	1.831 "	6.301×10^{-15}	-	-	-
27	1.883 "	6.926 "	1.022 "	-	-	-
29	1.094 "	2.435 "	-	-	-	-
31	6.127×10^{-12}	7.959×10^{-14}	-	-	-	-
33	3.303 "	2.417 "	-	-	-	-
35	1.715 "	6.825×10^{-15}	-	-	-	-
37	8.577×10^{-13}	1.789 "	-	-	-	-
39	4.127 "	4.359×10^{-16}	-	-	-	-
41	1.911 "	-	-	-	-	-
43	8.518×10^{-14}	-	-	-	-	-
45	3.650 "	-	-	-	-	-
47	7.640×10^{-15}	-	-	-	-	-
F3	3.675×10^{-9}	2.522×10^{-9}	1.584×10^{-9}	7.295×10^{-10}	5.083×10^{-10}	3.228×10^{-10}
F4	32.235	22.126	13.859	6.398	4.589	2.831

TABLE 9.2 Rate of Drop Capture with Bed Depth.

APPENDIX H

Regression Analysis used in the evaluation of the Decay Factor k.

From equation 10.24 the saturation profile is

$$S = (S_I - S_E)^{-k(1-L_I)} + S_E \dots\dots\dots (H.1)$$

Rearranging and linearising

$$\log_e(S - S_E) = \log_e(S_I - S_E) - k(1-L_I) \dots\dots\dots (H.2)$$

$$\text{Equal } \log_e y = \log_e a + bx \dots\dots\dots (H.3)$$

The following statistics are computed:

1. Coefficients a, b

$$b = \frac{\sum x_i \log_e y_i - \frac{1}{n} (\sum x_i) (\sum \log_e y_i)}{\sum x_i^2 - \frac{1}{n} (\sum x_i)^2} \dots\dots\dots (H.4)$$

$$a = \exp\left(\frac{\sum \log_e y_i}{n} - b \frac{\sum x_i}{n}\right) \dots\dots\dots (H.5)$$

2. Coefficient of determination

$$r^2 = \frac{\{\sum x_i \log_e y_i - \frac{1}{n} \sum x_i \sum \log_e y_i\}^2}{\{\sum x_i^2 - \frac{(\sum x_i)^2}{n}\} \{\sum (\log_e y_i)^2 - \frac{(\sum \log_e y_i)^2}{n}\}}$$

From the saturation vs. bed depth graph obtained from relative permeability calculations the experimental values of S_I , S_E and changing S with L are obtained and used in the program to obtain the coefficients of equation H.3.

APPENDIX I

COMPUTER PROGRAM FOR EVALUATION OF
CAPTURE MECHANISM CONTRIBUTIONS

```

10 REM          EVALUATION OF CAPTURE MECHANISM CONTRIBUTIONS
11 REM          FOR TOLUENE-WATER SYSTEM
20 DIM F(7),N(7),P(7)
30 READ D1,D3,A1
40 READ K3,M3,R4
50 READ K,T,C,G1
60 FOR L=1,7
70 READ F(L)
80 NEXT L
81 FOR M=1,7: READ P(M): NEXT M
90 FOR M=1,7
100 READ V
101 PRINT "VELOCITY=",V,"M/S"
102 PRINT "DROP SIZE          TOTAL          SIGNIFICANT          %REL"
103 PRINT "(MICRON)          EFFICIENCY          MECHANISM          CONTR"
110 FOR L=1,6
120 D2=F(L)*.1E-05
125 REM          CALCULATION OF DIMENSIONLESS GROUPS
130 R=D2/D3
140 G=(D2*.2*(R4-R3)*G1)/(18*M3*A1*V)
180 P5=(3*3.14159*D3*D2*V*M3)/(K*T)
190 N1=4*C/(9*3.14159*K*.2*M3*A1*V*D2*.2)
195 REM          CALCULATION OF CAPTURE EFFICIENCIES
200 N(1)=1.5*R*.2*A1
210 N(2)=4.04*A1*.33333/P5*.66667
220 N(3)=-G
230 N(4)=2*R*.2*A1*(9*N1/5)*.33333
240 N6=N(1)+N(2)+N(3)+N(4)
250 PRINT F(L),N6
260 FOR I=1,4
270 C=INT(N(1)*100/N6)
280 IF C<1 THEN 300
290 IF I=1 THEN PRINT TAB(30);"INTERCEPTION",TAB(46);C
291 IF I=2 THEN PRINT TAB(30);"DIFFUSION",TAB(46);C
292 IF I=3 THEN PRINT TAB(29);"SEDIMENTATION",TAB(46);C
293 IF I=4 THEN PRINT TAB(29);"LONDON FORCES",TAB(46);C
300 NEXT I
305 PRINT
310 NEXT L
315 FOR I=1,P(M): PRINT : NEXT I
320 NEXT M
330 STOP : END : FINISH
500 DATA .995E-04,.486E-03,37.98
510 DATA 1000,.1E-02,866.9
520 DATA .138048E-22,293,.401E-20,9.81
530 DATA .1,1,5,10,25,50,100
535 DATA 1,1,1,1,7,6,20
540 DATA .1E-03,.1E-02,.2E-02,.3E-02,.1E-01,.1,10

```


VELOCITY=	. 1E-03	M/S		
DROP SIZE (MICRON)	TOTAL EFFICIENCY	SIGNIFICANT MECHANISM	%RELATIVE CONTRIBUTION	
. 1	. 272154E-01	DIFFUSION LONDON FORCES	99 1	
1	. 734511E-02	INTERCEPTION DIFFUSION LONDON FORCES	3 79 17	
5	. 122432E-01	INTERCEPTION DIFFUSION SEDIMENTATION LONDON FORCES	49 16 4 30	
10	. 332351E-01	INTERCEPTION DIFFUSION SEDIMENTATION LONDON FORCES	72 4 6 18	
25	. 174334	INTERCEPTION SEDIMENTATION LONDON FORCES	86 7 6	
50	. 668534	INTERCEPTION SEDIMENTATION LONDON FORCES	90 7 2	

VELOCITY=	. 1E-02	M/S		
DROP SIZE (MICRON)	TOTAL EFFICIENCY	SIGNIFICANT MECHANISM	%RELATIVE CONTRIBUTION	
. 1	. 593249E-02	DIFFUSION LONDON FORCES	98 2	
1	. 208860E-02	INTERCEPTION DIFFUSION LONDON FORCES	11 60 29	
5	. 824655E-02	INTERCEPTION DIFFUSION LONDON FORCES	73 5 21	
10	. 273443E-01	INTERCEPTION LONDON FORCES	88 10	
25	. 157180	INTERCEPTION LONDON FORCES	96 3	
50	. 615944	INTERCEPTION LONDON FORCES	98 1	

VELOCITY=	. 2E-02	M/S		
DROP SIZE (micron)	TOTAL EFFICIENCY	SIGNIFICANT MECHANISM	%RELATIVE CONTRIBUTION	
.1	.375914E-02		DIFFUSION	97
			LONDON FORCES	2
1	.150225E-02		INTERCEPTION	16
			DIFFUSION	52
			LONDON FORCES	31
5	.770525E-02		INTERCEPTION	78
			DIFFUSION	3
			LONDON FORCES	18
10	.265789E-01		INTERCEPTION	91
			LONDON FORCES	8
25	.155479		INTERCEPTION	97
			LONDON FORCES	2
50	.611856		INTERCEPTION	98
			LONDON FORCES	1

VELOCITY=	. 3E-02	M/S		
DROP SIZE (micron)	TOTAL EFFICIENCY	SIGNIFICANT MECHANISM	%RELATIVE CONTRIBUTION	
.1	.288057E-02		DIFFUSION	97
			LONDON FORCES	3
1	.125567E-02		INTERCEPTION	19
			DIFFUSION	47
			LONDON FORCES	33
5	.745877E-02		INTERCEPTION	80
			DIFFUSION	2
			LONDON FORCES	16
10	.262296E-01		INTERCEPTION	92
			LONDON FORCES	7
25	.154747		INTERCEPTION	97
			LONDON FORCES	2
50	.610235		INTERCEPTION	99

VELOCITY=	. 1E-01	M/S		
DROP SIZE (MICRON)	TOTAL EFFICIENCY	SIGNIFICANT MECHANISM	%RELATIVE CONTRIBUTION	
.1	.131191E-02		DIFFUSION	95
			LONDON FORCES	4
1	.787109E-02		INTERCEPTION	30
			DIFFUSION	34
			LONDON FORCES	35
5	.693829E-02		INTERCEPTION	87
			DIFFUSION	1
			LONDON FORCES	11
10	.254799E-01		INTERCEPTION	94
			LONDON FORCES	5
25	.153263		INTERCEPTION	98
			LONDON FORCES	1
50	.607243		INTERCEPTION	99

VELOCITY=	. 1	M/S		
DROP SIZE (MICRON)	TOTAL EFFICIENCY	SIGNIFICANT MECHANISM	%RELATIVE CONTRIBUTION	
.1	.299348E-03		DIFFUSION	90
			LONDON FORCES	9
1	.427540E-03		INTERCEPTION	56
			DIFFUSION	13
			LONDON FORCES	30
5	.643543E-02		INTERCEPTION	93
			LONDON FORCES	5
10	.247297E-01		INTERCEPTION	97
			LONDON FORCES	2
25	.151864		INTERCEPTION	99
50	.604788		INTERCEPTION	99

APPENDIX J

TABULATED EXPERIMENTAL RESULTS

All results are presented for the steady state operation. The pressure drop ratio is tabulated for the length of the bed at the following intervals: 2, 5.12, 7.27, 9.35, 11.45, 13.5, 15.5, 17.35, 19.4, 21.35 ($\times 10^{-2}$ m). One set of transient pressure drop ratio is presented in the results of Experiment Number 35. The experimental results for small bed depths, say $L = 5 \times 10^{-2}$ m, are not included. It was not possible to calculate saturation profiles as they predict constant saturation with bed depth (only one measurement of pressure drop was possible).

Ballotini: 486 μ m, Velocity, 0.3×10^{-2} m/s, Concentration, 0.15 % v/v, Bed Depth 20×10^{-2} m							
Run No	Temperature (°C)	Pressure Drop Ratio $\frac{\Delta P_2}{\Delta P_1} \frac{\mu C_1}{\mu C_2}$	Saturation (%)	Separation Efficiency (%)	Effluent Drop Size (μ m)	Coalesced Drop Size (mm)	
27	22.0	1.92	19.5	41.0	22.0	1.27	
		1.64	15.25				
		1.48	12.25				
		1.35	9.5				
		1.32	8.75				
		1.31	8.5				
		1.31	8.5				
29	21.5	1.32	8.75	43.8	27.0	-	
		1.35	9.5				
		3.11	31.5				
		2.85	29.5				
		1.42	11.0				
		1.12	3.75				
		1.10	3.0				
33	23.0	1.07	2.25	39.0	-	1.38	
		1.07	2.25				
		1.10	3.25				
		4.75	1.16				
		1.76	17.25				
		1.59	14.25				
		1.39	10.5				
1.24	7.0						
1.20	6.0						
1.19	5.75						
1.20	6.0						
1.23	6.75						
1.25	7.25						

Ballotini: 267 μ m Velocity: 0.3 x 10 ⁻² m/s Concentration: 0.1 % v/v, Bed Depth: 20x10 ⁻² m							
Run No	Temperature (°C)	Pressure Drop Ratio $\frac{\Delta P_2}{\Delta P_1} \frac{\mu c_1}{\mu c_2}$	Saturation (%)	Separation Efficiency (%)	Effluent Drop Size (μ m)	Coalesced Drop Size (mm)	
60	24.0	4.87	41.0	51.0	21.0	1.32	
		1.30	8.50				
		1.23	6.75				
		1.20	6.0				
		1.18	5.5				
		1.22	6.5				
61	23.8	1.25	7.25	48.0	-	0.90	
		1.3	8.38				
		4.4	39.0				
		1.36	9.7				
		1.20	6.0				
		1.15	4.5				
64	23.5	1.15	4.5	57.3	19.0	-	
		1.22	6.5				
		1.29	8.3				
		1.31	8.7				
		7.01	47.75				
		1.33	9.0				
1.21	6.25						
1.16	5.0						
1.16	5.0						
1.14	4.25						
1.18	5.5						
1.23	6.75						
1.34	9.25						

Ballotini: 486 μm , Velocity, 0.3×10^{-2} m/s, Concentration 1% v/v, Bed Depth, 20×10^{-2} m						
Run No	Temperature (°C)	Pressure Drop Ratio $\frac{\Delta P_2}{\Delta P_1} \frac{\mu\text{C}_1}{\mu\text{C}_2}$	Saturation (%)	Separation Efficiency (%)	Effluent Drop Size (μm)	Coalesced Drop Size (mm)
93	24.5	10.27	54.0	90.5	30.0	3.44
		1.22	6.5			
		1.14	4.25			
		1.10	3.0			
		1.12	3.75			
		1.17	5.0			
		1.34	9.25			
1.42	11.0					
1.61	14.75					
94	23.0	7.32	48.5	91.0	-	2.16
		1.72	16.5			
		1.47	12.0			
		1.43	11.25			
		1.47	12.0			
		1.45	11.75			
		1.51	12.75			
1.57	14.0					
1.70	16.25					
98	25.5	7.01	47.75	-	-	1.04
		1.59	14.25			
		1.33	9.0			
		1.20	6.0			
		1.15	4.5			
		1.16	4.75			
		1.22	6.5			
1.31	8.5					
1.42	11.0					

Ballotini: 486 μ m Velocity: 4.0 x 10⁻²m/s, Concentration: 0.1 % v/v Bed Depth 20 x 10⁻² m

Run No	Temperature (°C)	Pressure Drop Ratio $\frac{\Delta P_2}{\Delta P_1} \frac{\mu c_1}{\mu c_2}$	Saturation (%)	Separation Efficiency (%)	Effluent Drop Size (μ m)	Coalesced Drop Size (mm)
57	20.0	1.90	19.25	40.5	37.0	0.36
		2.37	25.0			
		2.03	21.0			
		1.76	17.25			
		1.76	17.25			
		1.78	17.5			
		1.76	17.25			
1.76	17.25					
1.75	17.0					
58A	21.5	1.87	18.90	44.0	42.0	0.26
		2.32	24.52			
		1.57	14.0			
		1.75	17.0			
		1.80	18.0			
		1.75	17.0			
		1.75	17.0			
1.92	19.6					
1.20	5.9					
60A	21.0	2.02	21.0	41.0	-	0.50
		2.20	23.1			
		1.90	19.2			
		1.78	17.5			
		1.75	17.0			
		1.72	16.5			
		1.75	17.0			
1.90	19.25					
1.69	16.0					

Ballotini: 486 μ m Velocity, 0.3×10^{-2} m/s Concentration: 0.4 % v/v, Bed Depth $2\sigma \times 10^{-2}$ m						
Run No	Temperature (°C)	Pressure Drop Ratio $\frac{\Delta P_2}{\Delta P_1} \frac{\mu C_1}{\mu C_2}$	Saturation (%)	Separation Efficiency (%)	Effluent Drop Size (μ m)	Coalesced Drop Size (mm)
51	23.2	7.01	47.75	68.0	22.0	1.32
		2.17	22.75			
		1.33	9.0			
		1.26	7.25			
		1.16	4.75			
		1.15	4.5			
49	23.7	1.17	5.0	73.0	-	2.30
		1.22	6.5			
		1.63	15.0			
		3.91	36.5			
		1.35	9.5			
		1.22	6.5			
53	22.9	1.17	5.0	70.0	-	1.26
		1.16	4.75			
		1.13	4.0			
		1.11	3.5			
		1.14	4.25			
		1.23	6.75			
53	22.9	4.00	37.0	70.0	-	1.26
		2.15	22.5			
		1.36	9.75			
		1.21	6.25			
		1.19	5.62			
		1.18	5.5			
53	22.9	1.22	6.5	70.0	-	1.26
		1.26	7.5			
53	22.9	1.36	9.75	70.0	-	1.26
		1.26	7.5			

Ballotini: 486 μ m, Velocity: 5.0×10^{-2} m/s, Concentration: 0.1 % v/v, Bed Depth: 20×10^{-2} m						
Run No	Temperature (°C)	Pressure Drop Ratio $\frac{\Delta P_2}{\Delta P_1} \frac{\mu c_1}{\mu c_2}$	Saturation (%)	Separation Efficiency (%)	Effluent Drop Size (μ m)	Coalesced Drop Size (mm)
47	17.5	1.08	2.5	41.0	-	0.32
		2.03	21.0			
		1.69	16.0			
		1.64	15.25			
		1.53	13.25			
		1.48	12.25			
		1.43	11.25			
		1.42	11.0			
50	19.0	1.15	4.5	44.0	62.0	0.42
		2.03	21.0			
		1.36	9.8			
		1.65	15.37			
		1.53	13.0			
		1.59	14.32			
		1.54	13.5			
		2.0	20.6			
52A	18.3	1.36	9.8	47.5	74.0	-
		1.10	3.25			
		1.92	19.5			
		1.67	15.75			
		1.65	15.37			
		1.60	14.5			
		1.57	14.0			
		1.63	15.0			
1.75	17.0					
1.24	7.0					

Ballotini: 486 μ m, Velocity, 0.3×10^{-2} m/s, Concentration 0.3 %v/v Bed Depth: 20×10^{-2} m							
Run No	Temperature (°C)	Pressure Drop Ratio $\frac{\Delta P_2}{\Delta P_1} \frac{\mu c_1}{\mu c_2}$	Saturation (%)	Separation Efficiency (%)	Effluent Drop Size (μ m)	Coalesced Drop Size (mm)	
40	22.7	3.25	32.5	76.0	-	1.76	
		2.98	30.5				
		1.23	6.75				
		1.13	4.0				
42	24.0	1.10	3.25	71.5	27.0	1.81	
		1.07	2.25				
		1.07	2.25				
		1.09	2.75				
43	23.5	1.13	4.0	-	31.0	-	
		3.11	31.5				
		2.88	29.75				
		1.42	11.0				
43	23.5	1.20	6.0	-	31.0	-	
		1.16	4.75				
		1.13	4.0				
		1.16	4.75				
43	23.5	1.22	6.5	-	31.0	-	
		1.27	7.75				
		2.98	30.25				
		2.74	28.5				
43	23.5	1.20	6.0	-	31.0	-	
		1.04	1.25				
		1.02	0.75				
		1.02	0.75				
43	23.5	1.03	1.0	-	31.0	-	
		1.10	3.25				
		1.16	4.75				

Ballotini: 486 μ m, Velocity 0.3×10^{-2} m/s Concentration 0.2% v/v Bed Depth: 20×10^{-2} m						
Run No	Temperature (°C)	Pressure Drop Ratio $\frac{\Delta P_2}{\Delta P_1} \frac{\mu C_1}{\mu C_2}$	Saturation (%)	Separation Efficiency (%)	Effluent Drop Size (μ m)	Coalesced Drop Size (mm)
34	19.2	3.56	34.5	-	-	2.34
		1.31	8.5			
		1.23	6.75			
		1.16	4.75			
		1.15	4.5			
		1.17	5.0			
		1.20	6.0			
35	23.0	1.23	6.75	64.0	18.0	1.54
		1.24	7.0			
		3.11	31.5			
		1.60	14.5			
		1.55	13.5			
		1.47	12.0			
		1.47	12.0			
22.5		1.48	12.25	65.5	-	2.0
		1.51	12.75			
		1.57	14.0			
		1.61	14.75			
		3.15	31.75			
		1.60	14.5			
		1.55	13.5			
1.47	12.0					
1.45	11.75					
1.48	12.25					
1.51	12.75					
1.56	13.75					

Ballotini: 486 μ m, Velocity: 3.0×10^{-2} m/s, Concentration 0.1% v/v, Bed Depth: 20×10^{-2} m

Run No	Temperature (°C)	Pressure Drop Ratio $\frac{\Delta P_2}{\Delta P_1} \frac{\mu c_1}{\mu c_2}$	Saturation (%)	Separation Efficiency (%)	Effluent Drop Size (μ m)	Coalesced Drop Size (mm)
30	16.0	2.03	21.0	40.5	35.0	0.28
		2.47	26.0			
		2.32	24.5			
		2.30	24.25			
		2.32	24.5			
		2.35	24.75			
		2.35	24.75			
31	18.0	2.37	25.0	42.0	-	0.38
		2.49	26.25			
		2.1	21.91			
		2.4	25.31			
		2.2	23.11			
		2.45	25.82			
		2.42	25.56			
44	16.5	2.45	25.82	45.0	-	0.52
		2.38	25.10			
		2.4	25.31			
		2.53	26.61			
		2.10	22.0			
		2.37	25.0			
		2.35	24.75			
2.41	25.5					
2.46	26.0					
2.46	26.0					
2.52	26.5					
2.52	26.5					
2.57	27.0					

Ballotini: 57.5 μ m Velocity: 0.1 x 10 ⁻² m Concentration: 0.1% v/v Bed Depth: 20x10 ⁻² m							
Run No	Temperature (°C)	Pressure Drop Ratio $\frac{\Delta P_2}{\Delta P_1} \frac{\mu c_1}{\mu c_2}$	Saturation (%)	Separation Efficiency (%)	Effluent Drop Size (μ m)	Coalesced Drop Size (mm)	
21A	23.2	4.87	41.0	45.5	7.0	2.6	
		1.32	8.75				
		1.23	6.75				
		1.20	6.0				
		1.17	5.07				
		1.20	6.0				
		1.23	6.75				
		1.26	7.5				
27A	21.0	1.31	8.5	49.5	9.5	3.22	
		5.85	44.5				
		1.34	9.2				
		1.19	5.7				
		1.15	4.5				
		1.11	3.5				
		1.10	3.0				
		1.11	3.5				
1.20	6.0						
28	19.0	1.24	7.0	48.75	-	2.98	
		5.06	41.75				
		1.33	9.0				
		1.03	1.1				
		1.01	0.33				
		1.01	0.33				
		1.007	0.25				
		1.07	0.25				
1.007	0.25						
1.0	0						

Ballotini: 486 μm Velocity: 0.1×10^{-2} m/s Concentration: 0.1% v/v Bed Depth: 20×10^{-2} m							
Run No	Temperature (°C)	Pressure Drop Ratio $\frac{\Delta P_2}{\Delta P_1} \frac{\mu\text{C}_1}{\mu\text{C}_2}$	Saturation (%)	Separation Efficiency (%)	Effluent Drop Size (μm)	Coalesced Drop Size (mm)	
20A	24.7	3.60	34.75	77.5	3.5	1.64	
		1.39	10.5				
		1.34	9.25				
		1.24	7.0				
		1.25	7.25				
		1.24	7.0				
19A	25.2	1.32	8.75	79.5	4.0	2.32	
		1.35	9.5				
		1.42	11.0				
		3.81	36.0				
		1.49	12.5				
		1.42	11.0				
17	23.8	1.31	8.5	72.5	-	3.94	
		1.20	6.0				
		1.15	4.5				
		1.15	4.5				
		1.26	7.5				
		1.35	9.5				
		3.18	32.0				
		1.35	9.5				
		1.25	7.2				
		1.17	5.0				
1.15	4.5						
1.13	4.0						
1.20	6.0						
1.32	8.75						
1.37	10.0						

Run No. 35.

Ballotini 486 μm , Velocity, $0.3 \times 10^{-2} \text{m}$
 Concentration: 0.2 % v/v, Bed Depth, $20 \times 10^{-2} \text{m}$
 Effluent Drop Size: 18.0 μm ,
 Coalesced Drop Size: 1.54 mm
 Separation Efficiency: 64.0%

Temperature ($^{\circ}\text{C}$)	Time (hrs)	Pressure Drop Ratio $\frac{\Delta P_2}{\Delta P_1} \frac{\mu C_1}{\mu C_2}$	Saturation (%)
17.5	0.5	1.35 1.07 1.02	9.50 2.25 0.5
19.7	0.75	1.66 1.20 1.09 1.05 1.02 1.01	15.5 6.0 2.75 1.50 0.5 0.25
20.0	1.0	1.76 1.34 1.22 1.15 1.10 1.07 1.05 1.03	17.25 9.25 6.5 4.5 3.0 2.25 1.5 1.0
20.3	1.5	2.05 1.42 1.31 1.22 1.21 1.19 1.17 1.18 1.18	21.25 11.0 8.5 6.5 6.15 5.75 5.0 5.38 5.25
21.0	2.0	2.68 1.61 1.38 1.33 1.32 1.29 1.33 1.39 1.38	28.0 14.75 10.25 9.0 8.75 8.05 9.0 10.50 10.25
23.0	2.5	3.11 1.6 1.55 1.47 1.47 1.48 1.51 1.57 1.61	31.5 14.5 13.5 12.0 12.0 12.25 12.75 14.0 14.75

APPENDIX K

PREDICTION OF EXIT DROP SIZE

The following steps were used in determining the exit drop size for Run No. 35. The data used is:

$$\begin{aligned} a_c &= 243 \times 10^{-6} & u &= 0.3 \times 10^{-2} \text{ m} \\ k &= 6.43 & L &= 0.2 \text{ m} \\ \mu &= 9.399 \times 10^{-4} \text{ Nsm}^{-2} & \rho_c &= 998 \text{ kg m}^{-3} \\ \gamma &= 0.02291 \text{ Nm}^{-1} & \rho_d &= 867 \text{ Kg m}^{-3} \\ D &= 3.81 \times 10^{-2} \text{ m} & g &= 9.80 \text{ m s}^{-2} \\ C &= 0.2\% \text{ v/v} \end{aligned}$$

The value of ΔP used is the overall value of two phase pressure drop less the overall single phase pressure drop, i.e., only the concentration of the held up dispersed phase is used, $\therefore \Delta P = 1781.007 \text{ Nm}^{-2}$

From Equation 10.41,

$$\begin{aligned} A_{\text{cap}} &= 0.1612 a_c^2 = 9.52 \times 10^{-9} \text{ m}^2 \\ d_H &= 0.205 a_c = 4.98 \times 10^{-5} \text{ m} \end{aligned}$$

Equation 10.42 gives,

$$u_{\text{cap}} = \frac{d_H^2}{2k_u} \times \frac{\Delta P}{\Delta L} = 1.83 \times 10^{-3} \text{ m/s}$$

$$Q = \frac{\pi D^2}{4} \times C \times u = 6.84 \times 10^{-9} \text{ m}^3/\text{s}$$

$$q = A_{\text{cap}} \times u_{\text{cap}} = 1.74 \times 10^{-11} \text{ m}^3/\text{s}$$

$$\text{No. of capillaries} = \frac{Q}{qd} = 393 \text{ capillaries}$$

Using Meister and Scheele's correlations (221) to predict the volume of the exist drop, we have

$$V_{pe} = F \frac{\pi \gamma d_H}{g \Delta \rho} + \frac{20 \mu q_d d_H}{d_{pe}^2 g \Delta \rho} - \frac{4 \rho_d q_d u_{cap}}{3 g \Delta \rho}$$

$$+ 4.5 \frac{q_d^2 d_H^2 \rho_d \gamma}{(g \Delta \rho)^2}^{1/3}$$

where V_{pe} is the volume of the exit drop, d_{pe} the diameter of the exit drop and F is the Harkins-Brown correction factor. The term including d_{pe} is negligible when the continuous phase viscosities is less than $1 \times 10^{-2} \text{ Nm/s}^2$. $\therefore V_{pe} = 2.812 \times 10^{-9} \text{ m}^3$

From Harkins-Brown correlation $F = 1.0$

$\therefore V_{pe} = 2.812 \times 10^{-9} \text{ m}^3$ and the predicted drop diameter $d_{pe} = 1.75 \text{ mm}$. The experimental drop diameter is 1.54 mm .

NOMENCLATURE

NOMENCLATURE

Symbols have the following meanings except where specifically indicated in the text.

a	specific surface area (m^2/m^3)
a_c	collector radius (m)
a_p	drop radius (m)
A	flow parameter (-)
A_c	surface area of container per unit volume of bed (m^2/m^3)
A_{cap}	area of capillary available for flow (m^2)
A_F	Happel's cell flow parameter for assemblage of cylinders (-)
A_S	Happel's cell flow parameter for assemblage of spheres (-)
b	width of capillary (m)
C	fractional concentration of dispersion (-)
d	channel diameter (m)
d_a	aperture diameter (m)
d_c	collector diameter (m)
\bar{d}_c	average collector diameter (m)
d_{ce}	effective collector diameter (m)
d_H	hydraulic radius (m)
d_p	drop diameter (m)
d_{pc}	critical drop diameter for release (m)
d_{pe}	exit drop size (m)
	molecular diffusion coefficient (m^2/s)
D	diameter of coalescing bed (m)

e	voidage fraction (-)
f_p	friction factor (-)
f_w	correction factor for wall effect (-)
F_{AD}	adhesion force (N)
F_{DL}	double layer force (N)
F^*	dimensionless drag force (-)
g	acceleration due to gravity = 9.81 (m/s ²)
h	drop/collector separation (m)
	film thickness for capillary flow (m)
H	dimensionless separation between drop and collector = h/a_p (-)
H^*	dimensionless separation at reaf stagnation poin
I	mass capture rate (m ² /s)
j	rate of particle capture per unit sphere length (n_o/m s)
k	relative permeability (-)
	saturation profile parameter characterizing rate of decay (-)
k'	Boltzman constant
K	Kozeny constant (-)
K_o	shape factor (-)
l	distance into coalescing bed from inlet face (m)
L	bed depth (m)
L_e	effective path length (m)
L_E	length of bed near exit face having constant saturation value (m)
L_I	length of bed near inlet face having constant saturation value (m)
n	number of drops (-)
n_o	number of drops entering interval l from inlet face (-)

n_1	number of drops leaving interval 1 from inlet face (-)
N_{AD}	adhesion number = $\frac{4Q}{9\pi R^2 A} \cdot \frac{1}{\mu_c u d_p^2}$ (-)
N_{DL}	double layer group $\frac{\kappa d_p}{2}$ (-)
N_{E2}	electrokinetic group = $\frac{2 p c}{(\frac{2}{p} + \frac{c}{c^2})}$ (-)
N_G	gravity number = $\frac{d_p^2 (\rho_d - \rho_c) g}{18 \mu_c u A}$ (g)
N_{Pe}	Peclet number = $\frac{d_c u}{\mu_c}$ (-)
N_{Re}	Reynolds number = $\frac{d_c u \rho_c}{\mu_c}$ (-)
N_{Re}'	Reynolds number = $\frac{d_p u \rho_c}{\mu_c}$ (-)
N_{Stk}	Stoke's number = $\frac{d_p^2 \rho_c u}{9 \mu_c d_c}$ (-)
ΔP	pressure drop (N/m ²)
q_i	flowrate of phase i (m ³ /s)
Q	Hamaker constant (J)
	Total volumetric flowrate (m ³ /s)
r	distance from centre of cylinder or sphere (m)
r_{22}	intermolecular distance (m)
R	interception number = $\frac{d_p}{d_c}$ (-)
R_d	direct interception number = $\frac{d_p}{d_a}$ (-)
S	local saturation of dispersed phase (-)
\bar{S}	average saturation of dispersed phase (-)
S_c	local saturation of continuous phase (-)
S_d	local saturation of dispersed phase when used in conjunction with S_c (-)
S_E	saturation near exit face of bed (-)
S_I	saturation near inlet face of bed (-)
t	time (s)
T	temperature (°K)
	tortuosity factor (-)

u	superficial velocity (m/s)
u_1	aqueous superficial velocity for single phase (m/s)
u_2	aqueous superficial velocity for two phase flow (m/s)
u_{cap}	interstitial velocity (m/s)
X	cross sectional area (m^2)

Greek Letters

α	volume of solids in the bed = $1 - e_1$ (-)
γ	interfacial tension (N/m)
ϵ	dielectric constant of continuous phase
σ	surface tension (N/m)
η	drop capture efficiency (-)
η_c	coalescence efficiency (-)
μ	viscosity (Ns/m^2)
ρ	density (kg/m^3)
λ	theoretical filter coefficient (m^{-1})
ν	kinematic viscosity (m^2/s)
ψ	streamline function for drop/collector system (-)
θ	polar coordinate for drop/collector system (rad)
ϕ_i	i th particle shap parameter (-)
κ	reciprocal Debye length

Subscripts

1	single phase flow
2	two phase flow
c	continuous phase
d	dispersed phase
f	bed of fibres
s	bed of spheres

d dispersed phase
f bed of fibres
s bed of spheres
D diffusion
D direct interception
G gravity sedimentation
I interception
II inertial impaction
L London forces
T total

REFERENCES

REFERENCES

1. Science Research Council (U.K.), Science Board, Chemistry Committee, "Report on the Science of Colloidal Dispersions", Jan., (1972).
2. Bikerman, J.J., Ind.Eng.Chem., 57, (1), pp59-62, (1965).
3. Rumscheidt, F.D., and Mason, S.G., J. Colloid Sci., 16, 238 (1961).
4. Carroll, B.J., Lucassen, J., "Theory and Practice of Emulsion Technology" Symp., Soc.Chem.Ind., Brunel Univ., pp29-41 (1974).
5. Taylor, G.I., Proc.Roc.Soc., (London, A138, 47 (1932).
6. Timotika, S., Proc.Roy.Soc. (London), A153, 302 (1936).
7. Sherman, P., "Emulsion Science", Academic Press, London (1968).
8. Selker, A.H., Sleicher, C.A., Can.Jl.Chem.Eng., 43, pp298-301 (1965).
9. Rower, E.L., Jl. Pharm.Sci., 54, (2), pp260-265 (1965).
10. Becher, P., Jl.Coll.Interfac.Sci., 24, pp91-96 (1967).
11. Narasinga, E.V.L., Kumar, R., Kuloor, N.R., Chem.Eng. Sci., 21, pp867-880 (1966).
12. Polichronakis, C., M.Sc. Thesis, University of Aston, October (1972).
13. Shalhoub, N.G., Ph.D. Thesis, University of Aston, Birmingham, (1975).
14. Austin, D.g., Ph.D. Thesis, University of Aston, Birmingham (1979).
15. Elgar, C., B.Sc. Project Report, University of Aston, Birmingham (1977).
16. Ullman, J.M., B.Sc. Project Report, University of Aston, January (1974).
17. Alexander, P., Paint Manuf., 21, pp157-175 (1951).
18. Meissner, H.P., Chertow, B., Ind.Eng.Chem., 38(8), 856, (1946).
19. Wilkinson, M.J., B.Sc. Project Report, January (1974), University of Aston.

20. Hermanie, P.H.J., van der Waarden, M., J1.Coll.Interfac. Sci., 21, pp513-521 (1966).
21. Hayes, J.G. et al., Chem.Eng.Prog., 45, 235 (1949).
22. Chillingar, G.V., Beeson, C.M., "Surface Operations in Petroleum Production", Elsevier, New York, (1969).
23. Matijevec, E., "Surface and Colloid Science", Vol.9, John Wiley & Sons, New York, 1976.
24. Lissant, K.J., J1.Coll.Interfac.Sci., 22, pp462-468 (1966).
25. Allak, A.M.A., Ph.D. Thesis, University of Aston, (1973).
26. Waterman, L.C., Chem.Eng.Prog., 61 (10), 51, (1965).
27. Truter, E.V., "Woolwax", pp117-131, Interscience Publishers, New York, 1956.
28. Outlook - 'Waste Water Treatment with Air Flotation', Process Engineering, 7, (11), 996 (1973).
29. Sallabanks, L.G.A., 'Treating Ballast Water Oily Waste', I.Ch.E. Meeting, University of Surrey, Guildford, 28th May (1975).
30. Clayton, R., Hiebenthal, D., Illmer, M., 'The Applications of the Dissolved Air Flotation Process for Waste Water Treatment', I.Ch.E. Symposium: Separation of Liquid Dispersions, Manchester, 3rd November, (1977).
31. Franklin, J.S., Effl.Water Treat.J1., October, pp655-657 (1973).
32. Douglas, E., Elliott, I.G., Trans.Inst.Marine Eng., 74, (5), 164 (1962).
33. Farley, R., Valentin, F.H.H., A.I.Ch.E. - I.Chem.E. Symposium Series No.1, pp1:39-1:48 (1965).
34. Chambers, D.B., 'Oil Water Separation using Fibrous Materials', I.Ch.E. Symposium: Separation of Liquid Dispersions, Manchester, 3rd November, 1977.
35. Gammon, H., Filtration and Separation, 409, July/August (1973).
36. Gabriel, J.C., Parry, G., Filtration and Separation, 253, May/June (1977).
37. Jordan, G.V., Trans.A.S.M.E., 393, April (1955).

38. Treybal, R.E., 'Liquid Extraction', McGraw Hill, New York (1963).
39. Sareen, S.S. et al., A.I.Ch.E.Jl., 12 (6), 1045, (1966).
40. Langdon, W.H. et al., Petro/Chem.Engng. Nov., 34 (1963).
41. Redmon, O.C., Chem.Eng.Progr., 59, 87 (1963).
42. Fowkes, F.M. et al., Eng.Sci.Technol., 4, 510 (1970).
43. Sherony, D.F., Ph.D. Thesis, Illinois Institute of Technology, Chicago (1969).
44. Sherony, D.F., Kintner, R.C., Can.Jl.Chem.Eng., 49, 314, (1971).
45. Spielman, L.A., Goren, S.K., Ind.Eng.Chem., 62, 10(1970).
46. Rosenfeld, J.I., Ph.D. Thesis, Illinois Institute of Technology, Chicago (1973).
47. Rosenfeld, J.I., Wasan, D.T., Can.Jl.Chem.Eng., 52, 3 (1974).
48. Osterman, J.W., Filt. & Sep., March/April, 127, (1966).
49. Burtis, T.A., Kirkbride, C.G., Trans. A.I.Ch.E., 42, 413 (1946).
50. Hayes, J.G., Hays, L.A., Wood, H.S., Ch.Eng.Progr., 45, 235 (1949).
51. Voyutskii, S.S. et al., Doklady Akad. Nauk., S.S.S.R., 91, 1155 (1953) (C.A.49, 12053d(1955)).
52. Gudesen, R.C., M.Sc. Thesis, Illinois Institute of Technology, Chicago (1964).
53. Graham, R.J., M.Sc. Thesis, University of California, Berkeley (1962).
54. Sweeney, W.F., M.Sc. Thesis, University of California, Berkeley (1964).
55. Davies, G.A., Jeffreys, G.V., Filt. and Sep., July/Aug., 349 (1965).
56. Langdon, W.M. et al., Envirom.Sci. and Tech., 6 (10), 905 (1972).

57. Hazlett, R.N., Carhart, H.W., Filt. and Sep., July/Aug., 456 (1972).
58. Vinson, C.G., Churchill, S.W., The Ch.Eng.Jl., 1, 110 (1970).
59. Voyutskii, S.S. et al., Izv. Vysshikh Uchebn., Zavedenii, Khim. ikhim. Tekhnol., 2, 190 (1958) (C.A. 52, 19266a (1958)).
60. Bartle, J.W., Filtration and Separation, Sept/Oct., 1 (1966).
61. Rose, P.R., M.Sc. Thesis, Illinois Institute of Technology, Chicago (1963).
62. Lindenhofen, H.E., Filtration & Separation, July/Aug., 317 (1968).
63. Lindenhofen, H.E., Filtration & Separation, Sept./Oct., 567 (1969).
64. Harkins, W.D., 'The Physical Chemistry of Surface Films', Reinhold, New York (1952).
65. Huang, W.S., Ph.D. Thesis, Illinois Institute of Technology, Chicago (1968).
66. Bitten, J.F., Jl. Coll. and Interfac. Sci., 33 (2), 265 (1970).
67. Ghosh, M.M., Brown, W.P., Jl. Water Pollution Control Fed., 47 (8), 2101 (1975).
68. Sherony, D.F., M.Sc. Thesis, Illinois Institute of Technology, Chicago (1967).
69. Hazlett, R.N., Ind.Eng.Chem.Fundam., 8 (4), 625 (1969).
70. Rosenfeld, J.I., Wasan, D.T., Proc. I.S.E.C. 74, Lyons, 319 (1974).
71. Spielman, L.A., Goren, S.L., Ind.Eng.Chem.Fundam., 11 (1), 66 (1972).
72. Spielman, L.A., Su, Y.P., Ind.Eng.Chem.Fundam., 16 (2), 272 (1977).
73. Happel, J., A.I.Ch.E.J., 5, 174 (1959).
74. Kuwabara, S., J.Phys.Soc.Jpn., 14 (4), 527 (1959).
75. Happel, J., Brenner, H., "Low Reynolds Number Hydrodynamics", Prentice-Hall, pp533, Englewood Cliffs, New Jersey (1965).

76. Yao, K., Habibian, M.T., O'Melia, C.R., *Envirom.Sci. Technol.*, 5, 1105 (1971).
77. Chang, D.P.Y., Ph.D. Thesis, California Inst. Technol., Pasadena, California (1973).
78. Lamb, H., "Hydrodynamics", Cambridge University Press, Cambridge, 6th Edition, 788 pp (1932).
79. Langmuir, I., Office of Technical Service, Washington D.C., OSRD Report NO. 865 (1942).
80. Spielman, L.A., Goren, S.L., *Envirom.Sci. & Tech.*, 4 (2), 135 (1970).
81. Rajagopalan, R., Tien, C., *Can.Jl.Ch.E.*, 55, 246 (1977).
82. Hogg, R. et al., *Trans. Faraday Soc.*, 62, 1638 (1966).
83. Wilkinson, D., Mumford, C.J., Jeffreys, G.V., *A.I.Ch.E.Jl.*, 21 (5), 910 (1975).
84. Albrecht, F., *Phys. Z.*, 32, 48 (1931).
85. Langmuir, I., Brodgett, K.B., Army Air Forces, Technical Report, 5418 (1946).
86. Brun, R. et al., *Nate. Advis. Comm. Aeronaut. Rep.*, p1215 (1955).
87. Chen, C.Y., *Chem.Rev.*, 55, 595 (1955).
88. Herne, H., 'Aerodynamic Capture of Particles', E.G. Richardson, Pergamon, New York (1960).
89. Fuchs, N.A., 'The Mechanics of Aerosols', Pergamon, Oxford, pp408 (1964).
90. Pich, J., 'Aerosol Science', Academic Press, Chapter 9,10, New York (1966).
91. Dorman, R.G., 'Filtration', in *Aerosol Science*, C.N. Davies, Academic Press, New York (1966).
92. Bradie, J.K., Ph.D. Thesis, Heriot Watt, Edinburgh (1969).
93. Stechkina, I.B., Fuchs, N.A., *Ann. Occup. Hyg.*, 9, 59 (1966).
94. Fitzpatrick, J.A., Ph.D. Thesis, Harvard University, Cambridge, Mass. (1972).
95. Hamaker, H.C., *Physica*, 4, 1058 (1937).

96. Natanson, G., Dokl. Akad. Nauk., SSSR, 112 (4), 696 (1957).
97. Aveyard, R., Haydon, D.A., 'Introduction to the Principles of Surface Chemistry', University Press, Cambridge (1973).
98. Spielman, L.A., Fitzpatrick, J.A., J1.Coll. and Interfac. Sci., 42 (3), 607 (1973).
99. Prieve, D.C., Ruckenstein, E., A.I.Ch.E. J1., 20 (6), 1178 (1974).
100. Einstein, A., 'Investigations of the Theory of Brownian Movement', New York: Dover, 119 pp,(1926).
101. Friedlander, S.K., A.I.Ch.E. J1., 3, 43 (1957).
102. Hillstad, J.G., Rushton, J.H., 59th Annual A.I.Ch.E. Meeting, Columbus, Ohio, May (1966).
103. Howarth, W.J., I.A.Ch.E. J1., 13, 1007 (1967).
104. Sprow, F.B., A.I.Ch.E. J1. 13, 995 (1967).
105. Wilkinson, D., Ph.D. Thesis, University of Aston in Birmingham (1974).
106. Lawson, G.B., Chem. and Proc.Eng., 45, May (1967).
107. Brown, R., 'A Microphotographic Study of Water Coalescence', U.S. Army film RF 1916, Fort Belvior, Virginia (1966).
108. Bitten, J.F., Fochtman, E.G., J1. Coll. and Interfac. Sci., 37 92), 312 (1971).
109. Richardson, J.G. et al., Trans. A.I.M.E., 195, 187 (1952).
110. Collins, R.E., 'Flow of Fluids Through Porous Materials, Reinhold, New York (1961).
111. Hazlet, R.N., Ind.Eng.Chem.Fundam., 9 (3), 520 (1970).
112. Attarzadeh, G.R., Ph.D. Thesis, University of Aston in Birmingham, (1979).
113. Singhal, A.K., Dranchuk, P.M., Can.J1.Ch.Eng., 53, 3 (1975).
114. Shah, B.S., M.Sc. Thesis, Illinois Institute of Technology, Chicago, 111 (1975).
115. Mason, G., J1.Coll., Interfac.Sci., 35, 286 (1971).

116. Houghley, D.P. and Beverlidge, G.S.G., Chem.Eng. Sci., 22, 715 (1967).
117. Ridgeway, K. and Jarbuck, K.J., Brit., Chem., Eng., 12, 384 (1967).
118. Brown, G.G., 'Unit Operations', John Wiley, New York (1950).
119. Verman, L.C. and Barnerjee, S., Nature, 157, 584 (1946).
120. Thomas, R.J., Mumford, C.J., Int. solvent Extraction Conf., Hague, Vol.1, 400 (1971).
121. Hittit, H.A., Ph.D. Thesis, University of Aston, Birmingham (1972).
122. Calibration Data, 'Metric Series Rotameters', G.E.C., Elliott Automation Group (1975).
123. Fattah, A.F.M., Ph.D. Thesis, University of Aston, Birmingham (1975).
124. Davies, R., Ind.Eng.Chem., 62 (12), 87 (1970).
125. Lloyd, N.E., J1. Coll. Sci., 14, 441 (1959).
126. Weissberger, A., 'Techniques of Chemistry', Vol.1, Part IIIA, Wiley Interscience (1972).
127. Coulter Electronics, L.T.D. Coulter Counter Model ZB Instruction Manual, Dunstable, England (1980).
128. Zinky, W.R., Ann. N.Y. Acad. Sci., 158, 741 (1969).
129. Malvern Electronics - Malvern Particle Sizer 2200, Instruction Manual-, Malvern, England (1981).
130. Irani, R.R., Callis, C.F., 'Particle Size: measurement, Interpretation and Application', John Wiley (1963).
131. Kahn, A., Lewis, D.R., J.Phys.Chem., 58, 801 (1954).
132. Benoit, H., Ann. Phys., 6, 561 (1951).
133. O'Konski, C.I., Zimm, B., Science, 11, 113 (1950).
134. Smith, T.N., Chem.Eng.Sci., 29, 583 (1974).
135. Private Communication, Coulter Electronics, Malvern, England, July 1980.
136. Matthews, B.A., Can.J1.Pharm.Soc., 6 (2), 89 (1971).

137. Mumford, C.J., Ph.D. Thesis, University of Aston, Birmingham (1970).
138. Ibrahim, S.Y., M.Sc., University of Aston, Birmingham (1981).
139. Tonna, J.A., B.Sc. Project Report, University of Aston, Birmingham (1977).
140. Spielman, L.A., Ph.D. Thesis, University of California, Berkeley, California (1968).
141. Baez, S., Unpublished Report, University of Aston, Birmingham (1979).
142. Mumford, C.J. and Al Hemeri, A.A.A., I.S.E.C. Hague, Vol.2, 1591 (1974).
143. Dullien, F.A.L., 'Porous Media', Academic Press, London (1979).
144. Coulson, J.M. and Richardson, J.F., "Chemical Engineering", Vol.2, Pergamon Press, Oxford (1965).
145. Slichter, C.S., U.S. Geol.Surv., 19th Annu. Rep., Part II, 295 (1899).
146. Rumpf, H. and Gupte, A.R., Chem.Ing.Tech., 43, 367 (1971).
147. Morrow, N.R., Huppler, J.D., Simmons, A.B. III, J. Sediment. Pet., 39, 312 (1969).
148. Berg, R.R., Annu. Gulfcoast Assoc. Geol. Soc. Meeting, 20th, Streve Port, Lousiana, Oct. 20, 303 (1970).
149. Pryor, W.A., 46th Ann. Fall Meeting Soc. Pet.Eng. A.I.M.E., Oct. 3-6, New Orleans, Lousiana (1971).
150. Davies, C.N., Proc.Inst.Mech.Eng., 1B, 185 (1952).
151. Kyan, C.P., Wasan, D.T., Kintner, R.C., Ind.Eng.Chem. Fund., 9, 596 (1970).
152. Scheidegger, A.E., "The Physics of Flow through Porous Media", 3rd Ed., University of Toronto Press, Toronto (1960).
153. Macdonald, I.F. et. al., Ind.Eng.Chem.Fundam. 18, 199 (1979).
154. Chilton, T.H. and Colburn, A.P., Trans.Am.Inst., Chem.Eng., 26, 178 (1931).
155. Morcom, A.R., Trans.Inst.Chem.Eng., 24, 30 (1946).

156. Ergun, S., Chem.Eng.Prog., 48, 98 (1952).
157. Gupte, A.R., Ph.D. Thesis, University of Karlsruhe Germany (1970).
158. Dudgeon, C.R., Houille Blanche, I, 785 (1966).
159. Fancher, G.H., Lewis, J.A., Ind.Eng.Chem., 25, 1140 (1933).
160. Pahl, M.H., Ph.D. Thesis, University of Karlsruhe, Germany (1975).
161. Doering, E., Allg. Warmetech., 4, 82 (1955).
162. Matthies, H.J., VDI-Forschungsh, 454 (1956).
163. Luther, H. et al., Chem.Ing.Tech., 6, 376 (1971).
164. Carman, P.C., Trans.Inst.Chem.Eng., 15, 150 (1937).
165. Kozeny, J., Royal Acad. of Science, Proc. Class I, 136, 271, Vienna (1927).
166. Childs, E.C. and Collis-George, N., Proc.Roy.Soc. (London), Ser. A201, 392 (1950).
167. Marshall, T.J., J. Soil Sci., 9, 1 (1958).
168. Millington, R.J., Quirk, J.P., Trans. Faraday Soc., 57, 1200 (1961).
169. Brutsaert, W., Soil Sci., 101, 85 (1966).
170. Brutsaert, W., Water Resource Res., 4, 425 (1968).
171. Haring, R.E. and Greenkom, R.A., A.I.Ch.E.Jl., 16, 477 (1970).
172. Payatakes, A.C., et al., A.I.Ch.E.Jl., 19, 58, 67 (1973).
173. Azzam, M.I.S., Ph.D. Thesis, University of Waterloo, Canada (1975).
174. Runchal, A.K. et. al., Phys. Fluids Suppl., 12, 21, (1969).
175. Christiansen, E.B. et. al., A.I.Ch.E.Jl., 18, 372 (1972).
176. Azzam, M.I.S. and Dullien, F.A.L., I.E.C. Fundam., 15, 281 (1976).
177. Slattery, J.C., "Momentum, Energy and Mass Transfer in Continua", McGraw-Hill, New York (1972).

178. Forchheimer, P.H., Z. Ver. Deutsch.Ing., 45, 1781 (1901).
179. Ahmed, N. and Sunada, D.K., J.Hyd.Div.Proc. A.S.C.E., 95 (HY6), 1947 (1969).
180. Heller, J.P., Procc. Symp. Fundamentals Transport Phenomenon Porous Media, 2nd, IAHR-ISSS Vol. 1, 1, University of Guelph, Ontario, Canada (1972).
181. Scheidegger, A.E., "The Physics of Flow Through Porous Media", University of Toronto Press, Toronto (1974).
182. Brinkman, H.C., Appl.Sci.Res., A1, 27, 81 : A2, 190 (1949).
183. Phillip, J.R., Jl. Appl. Math. Phys., 23, 353 (1972).
184. Lundgren, T.S., J. Fluid Mech., 51, 273 (1972).
185. Brenner, H., "Transport Processes in Porous Media", McGraw-Hill, New York (1983).
186. Rose, W.D. and Bruce, W.A., Trans.Am.Inst. Mining Met. Engrs., 186, 127 (1949).
187. Coulson, J.M., Trans.Inst.Chem.Eng., 27, 237 (1949).
188. Thornton, O.F., Trans.Am.Inst.Mining.Met.Engrs., 186, 328 (1949).
189. Wyllie, M.R.J., Rose, W.D., Ind.Eng.Chem., 189, 105 (1950).
190. Cornell, D., Katz, D.L., Ind.Eng.Chem., 45, 2145 (1952).
191. Winsauer, W.O. et. al., Bull.Am.Assoc. Petroleum Geol., 36, 253 (1952).
192. Carman, P.C., Jl.Agr.Sci., 29, 262 (1939).
193. Wyllie, M.R., Gregory, A.R., Ind.Eng.Chem., 41, 1379 (1955).
194. Wiggs, P.K.C, 'The Structure and Properties of Porous Materials' (D.H. Everett and F.S. Stone eds.), p.183 Academic Press, New York (1958).
195. Johnson, M.F.L., Stewart, W.E., J.Catal., 4, 248 (1965).
196. Dullien, F.A.L., A.I.Ch.E.J., 21, 299 (1975).
197. Bartell, F.E., Osterhof, H.J., J.Phys.Chem., 32, 1553 (1928).

198. Hitchcock, D.I., J.Gen.Physiol., 9, 755 (1926).
199. Davies, S.J., White, C.M., Engineering, 128, 69 and 98 (1929).
200. Piercy, N.A.V., Hooper, M.S., Winny, H.F., Phil.Mag., 15 (7), 647 (1933).
201. Fair, G.M., Hatch, G.B., Trans.Amer.Wat.Wks.Assn., 25, 1551 (1933).
202. Rose, H.E., Rizk, A.M.A., Proc.Inst.Mech.Engrs., 160, 493 (1949).
203. Sullivan, R.R., Hertel, K.L., Advances in Colloid Science, 1, 37 (1942).
204. Muskat, M., Botser, H.G., Physics, 1, 27 (1931).
205. Saraf, D.N., Fatt, I., Soc.Petrol.Eng.J., 7, 235 (1967).
206. Josendal, V.A., Sandiford, B.B., Wilson, J.W., Trans. A.I.M.E., 195, 65 (1952).
207. Osoba, J.S., Richardson, J.G., Hafford, J.A., and Blair, P.M., Trans.A.I.M.E. 192, 47 (1951).
208. Leverett, M.C., Trans., A.I.M.E., 132, 149 (1939).
209. Jones, P.J., World Oil, 129, (2), 170 (1949)
210. Carpenter, C.W. Jr., Bail, P.T., Bobek, J.E., Soc.Petrol. Eng. Jnl. March 9 (1962).
211. Hazlet, R.N., Ind.Eng.Chem.Fundam., 8, (4), 633 (1969).
212. Tan, C.B., M.Sc Thesis, Illinois Institute of Technology, Chicago(1968).
213. Spielman, L.A., Goren, S.L., Ind.Eng.Chem. Fundam, 11, 73 (1972).
214. Emi, H., Okuyama, K., Yoshioka, N., J1.Ch.Eng. Japan, 6, (4), 349 (1973).
215. Friedlander, S.K., J1.Colloid Interface.Sci., 23, 157 (1967).
216. Levich, V.G., 1962.'Physicochemical Hydrodynamics' Prentice Hall, New Jersey, (1962).
217. Bear, J.'Dynamics of Fluids in Porous Media', American Elsevier, New York, (1972).
218. Euzen, J.P. et al., Proc.I.S.E.C, 5, 130, Lyons, September (1974)

219. Leonard, R.A., and Lemlich, R., A.I.Ch.E.J.,
11, 18 (1965).
220. Leonard, R.A., and Lemlich, R., Chem. Eng. Sci.,
20, 790 (1965).
221. Scheele, G.F., Meister, B.J., A.I.Ch.E.J.,
14, (1), 9 (1968)
222. Perry, R.H., Chilton, C.H., 'Chemical Engineers
Handbook', 5th Edition, McGraw Hill, Tokyo, (1973).
223. Chemical Rubber Co., 'Handbook of Chemistry and
Physics', 58th Edition., Editor Weast, R.C.,
C.R.C. Press, Cleveland (1980).
224. Fowkes, F.M., Ind. Eng. Chem. 56, (12), 40 (1964)
225. Sherony, D.F., Kintner, R.C., A.I.Ch.E. Jnl.
17, (21), 291 (1971).